Advanced Materials Research Laboratory

Department of Mechanical & Aerospace Engineering

University of Strathclyde

Friction Stir Welding (FSW) of Dissimilar Metals and Alloys

Gihad Karrar

A thesis submitted in fulfilment of the requirements

for the degree of Doctor of Philosophy

August 2023

Abstract

This thesis presents a comprehensive investigation into the Friction Stir Welding (FSW) process of dissimilar materials, specifically aluminium and copper. The research employed a combination of experimental and numerical methods to evaluate the weld quality through metallurgical and mechanical analyses. Finite Element (FE) methods were utilised as an auxiliary tool, supplementing the experimental work to simulate the FSW process and facilitating the prediction of IMCs formation.

The study begins with a literature review emphasising the importance of placing copper on the advancing side (AS) to achieve defect-free dissimilar aluminium to copper FSW joints. However, tool offsetting on the retreating side (RS) or AS was found impractical for industrial applications due to varying tool offsets. Alternatively, researchers achieved defect-free joints by placing aluminium on the AS without tool offset. However, limited research has focused on this configuration, despite its benefits for joint mechanical properties. Further investigation is needed to understand the relationship between intermetallic compound microstructure and mechanical properties.

To address these gaps, the research focused on dissimilar FSW between AA5083 aluminium and copper, exploring the influence of tool rotational and traverse speeds on joint quality without introducing tool offsetting. The findings revealed successful weld joints between the dissimilar materials using specific parameter combinations, including rotational speed levels of 1000 rpm (at welding speeds of 100 and 120 mm/min), 1200 rpm (at 80 mm/min), and 1400 rpm (at welding speeds of 80 and 120 mm/min). An inhomogeneous microstructure was observed within the weld, with the predominant intermetallic compounds (IMCs) identified as Al_2Cu and Al_4Cu_9. The

volume fraction of IMCs increased with higher tool rotational speeds, leading to improved ultimate tensile strength (UTS) and joint efficiency.

Additionally, the study employed a novel approach to predict and validate the formation of IMCs during FSW of AA6061 aluminium to copper. The use of a Coupled Eulerian Lagrangian (CEL) model, combined with a modified friction law, provided good agreement with experimental data. The predicted IMCs, including AlCu, Al_2Cu, and Al_4Cu_9, were confirmed through the comparison of temperature distribution, Al-Cu phase diagram, and elemental concentration. The research demonstrated that defect-free joints could be achieved at specific rotational speeds and traverse speed, where the softer material (AA6061) was placed on the AS.

Furthermore, the research focused on optimising the FSW parameters for dissimilar joints between AA5083 and copper using the Taguchi design of experiments (DoE) method. By considering tool rotational speed, welding speed, and FSW tool design, the study successfully identified the significant parameters affecting joint mechanical strength. The optimised parameter combinations resulted in enhanced UTS, and flexure stress compared to the initial parameter sets. Linear regression analysis further confirmed the agreement between predicted and actual values of UTS and flexure stress.

Finally, the study investigated the influence of different aluminium grades (AA5083 and AA6061) on dissimilar FSW of aluminium to magnesium AZ31B. Placing the softer material (AZ31B) on the AS consistently produced defect-free joints, and the joint mechanical strength improved when AZ31B was joined to the harder aluminium grade (AA6061). The presence of intermetallic compounds, such as Al_3Mg_2 and

$Al_{12}Mg_{17}$, contributed to higher hardness values in the weld nugget, resulting in improved joint mechanical efficiency.

The findings of this research have advanced the understanding of dissimilar materials FSW and provided insights into optimising the FSW process parameters for enhanced joint quality. The conclusions drawn from this study offer valuable guidance for future research and advancements in the field of dissimilar materials FSW process.

Dedications

I dedicate this thesis first and foremost to all Sudanese engineers, scientists, researchers, and scholars. My thoughts particularly extend to those of the post-2019-revolution era, who have been bravely and tirelessly maintaining the momentum of progress and production amidst formidable challenges. Your tenacity, resilience, and undying spirit of inquiry are a beacon of inspiration and have profoundly influenced this work. This is a humble tribute to your commitment and passion for science and innovation.

Secondly, this work is a heartfelt dedication to my late uncle, Professor Ahmed Elagib (1932-2020). As the venerated father of mechanical engineering in Sudan, his life and works have been a beacon that guided my path. He was an individual of unparalleled wisdom and dedication, whose life journey is an enduring source of inspiration. His legacy will forever be treasured, and the impact he made will continue to guide aspiring engineers in our homeland. This thesis is an effort to perpetuate his ideals and commemorate his immense contribution to the field of mechanical engineering.

Finally, I wish to dedicate this work to the late John Anderson (1726 – 1796). As the posthumous founder of Anderson’s College, his vision gave birth to what eventually became the esteemed University of Strathclyde. His pioneering efforts towards shaping the future of education, particularly in the field of engineering and sciences, laid the groundwork that has enabled countless scholars, including myself, to contribute to the enrichment of global knowledge. This thesis is an homage to his legacy, a symbol of gratitude for the knowledge imparted, and the opportunities provided by the institution he envisioned.

Acknowledgements

Foremost, I express my sincere thanks to my supervisors, Professor Alex Galloway and Dr Athanasios Toumpis. Their vast expertise, diligent guidance, and unwavering support have been the linchpin of my doctoral research. Professor Galloway's insightful perspectives on the engineering industry and academia provided me with invaluable tools to navigate the university landscape effectively. Dr Toumpis, with his meticulous approach and relentless pursuit of quality, instilled in me the diligence and precision required in research. His effective project management skills were key in sharpening the standard of my work.

I must also acknowledge the crucial role played by the members of the Advanced Materials Research Laboratory - Dr Tiziana Marrocco, Dr Maider Olasolo, and Dr Fiona Sillars. Their expertise, skill, and amicability were pivotal to my Ph.D. completion. I am grateful for their patience, humour tolerance, and unwavering support in experimental technique, the intricacies of postgraduate study, and life's broader aspects. Their mentorship has undeniably shaped me as a young professional, and I am in their debt.

Mr James Kelly of the Department of Mechanical & Aerospace Engineering deserves a special mention. His friendship, mentorship, and unrivalled technical knowledge in metallurgical, microstructural, and Glaswegian matters have enriched my understanding and equipped me to become a better materials engineer.

I owe a debt of gratitude to the workshop staff of the Department of Mechanical & Aerospace Engineering, particularly Mr Drew Irvine and Mr James Gillespie, for their relentless assistance with manufacturing and testing. Their diligence and expertise underpinned my experimental work.

The efficient running of the Department of Mechanical & Aerospace Engineering Central Services is a testament to its diligent administrative and managerial staff. I am appreciative of their behind-the-scenes efforts in ensuring smooth operations and efficient communication.

My gratitude extends across continents to Professor Hongjun Li and his research group at the Faculty of Mechanical Engineering and Automation, Zhejiang Sci-Tech University, Hangzhou, China. Their generosity in providing technical support and resources was instrumental to my research.

My friends and colleagues at Strathclyde University, with their continuous encouragement and camaraderie, made this journey enjoyable and meaningful.

My heartfelt gratitude goes out to my parents, Mrs Nagwa Eljelani and Mr Mohamed Karrar. Their unwavering love and moral support have been my bedrock, enabling me to grow not only academically but also personally. I am thankful to my brothers Ali and Anis, and my sister Buthania, for their encouragement and belief in me.

And last but far from least, my deepest appreciation is for my wife, Mrs Romiesa Abdalhaleem, whose ceaseless inspiration, patience, and support are my guiding light. To my beloved children, Ibrahim, Ahmed, and Owais – you give the true meaning to my life. This thesis is as much a testament to your love as it is to my research.

To all mentioned and the many more unmentioned, your contributions are reflected in each page of this thesis. I am, and always will be, profoundly grateful.

Declaration of Authenticity and Author's Rights

This thesis is the result of the author's original research. It has been composed by the author and has not been previously submitted for examination which has led to the award of a degree.

Signed:

Date:

Research outputs

During my PhD studies, I have consistently sought to contribute to our understanding of the FSW process, particularly with respect to dissimilar materials. My research output includes a series of peer-reviewed journal articles and conference papers, and the supervision of master's theses that stem from my work. My endeavours have also been recognised in the form of several prestigious awards.

Journal Articles

1. Karrar, G., Galloway, A., Toumpis, A., Li, H., & Al-Badour, F. (2020). Microstructural characterisation and mechanical properties of dissimilar AA5083-copper joints produced by friction stir welding. Journal of Materials Research and Technology, 9(5), 11968-11979. **Based on Chapter 4**
2. Li, H., Qu, X., Gao, J., Karrar, G., Toumpis, A., & Galloway, A. (2021). Microstructure and mechanical performance of FSWed joint of T2 copper and AA 1061. Science and Technology of Welding and Joining, 26(2), 91-98. **Based on Chapter 4**
3. Karrar, G., Galloway, A., Toumpis, A., Al-Badour, F., & Li, H. (2021). Prediction and validation of intermetallic compound formation during friction stir welding of AA6061 to commercially pure copper. Science and Technology of Welding and Joining. **Based on Chapter 5**

Conference Papers

1. Karrar, G., Galloway, A., Toumpis, A., & Li, H. (2022). Optimisation of Friction Stir Welding Parameters Using the Taguchi Technique for Dissimilar Joining of AA5083 to Copper. Presented at Joint International Symposium on

Friction Stir Welding and Processing (ISFSWP), Leuphan University of Lüneburg, Germany. **Based on Chapter 6.**

2. Karrar, G., Galloway, A., Toumpis, A., & Li, H. (2022). Influence of Aluminium Alloy Grade on Dissimilar Friction Stir Welding of Aluminium to AZ31B. Presented at Joint International Symposium on Friction Stir Welding and Processing (ISFSWP), Leuphan University of Lüneburg, Germany. **Based on Chapter 7.**

Supervised Master's Theses based on my PhD Work

1. Iain Lind, "Computational Analysis of the Friction Stir Welding Process", University of Strathclyde, 2020.
2. Abdurrehman Desai, "Experimental and Numerical Investigation of the FSSW Process for Dissimilar Materials", University of Strathclyde, 2021.

Awards

1. Winner of JEOL SEMple Microscopy Competition, Scotland, UK (2020).
2. Recipient of the Alan Hendry Travel Scholarship (2022).
3. Recipient of the PGR Travel Award (2022).

Journal Articles under review

1. Karrar, G., Galloway, A., Toumpis, A., & Li, H. Development of processing window for dissimilar aluminium to copper joints produced by FSW. **Based on Chapter 4.**
2. Karrar, G., Galloway, A., Toumpis, A., & Li, H. Parametric optimisation of Friction Stir Welding Parameters Using the Taguchi Technique for Dissimilar Joining of AA5083 to Copper. **Based on Chapter 5.**

Preface

The work presented within this thesis encapsulates the culmination of a four-year journey (June 2018 – June 2022) of dedicated and intensive research, followed by a year of writing up, carried out while I was serving as a research fellow. The project involved collaboration between the Advanced Materials Research Laboratory (AMRL) at the University of Strathclyde, UK, and the Faculty of Mechanical Engineering and Automation at Zhejiang Sci-Tech University, China. It builds upon my Master's degree from King Fahd University of Petroleum and Minerals (KFUPM), Saudi Arabia. The thesis focuses on investigating FSW of dissimilar metals, specifically aluminium to copper joints.

These four years were marked by global events, notably the COVID-19 pandemic. Government responses like lockdowns, closures of schools, and travel restrictions significantly impacted this research's progression. Yet, despite such challenges, the pursuit of academic excellence remained unwavering.

The findings within these pages extensively involves both experimental and numerical investigations, aiming to evaluate weld quality via detailed metallurgical and mechanical analyses. The Finite Element Method (FEM) was employed to simulate the FSW process, providing an in-depth understanding of the effect of varying process parameters on the characteristics of the dissimilar materials' welds.

I aspire that this thesis, and its related publications, will make a valuable contribution to the advancement of FSW technology, inspiring continued growth and innovation within the sphere of mechanical engineering.

Table of Contents

Nomenclature

Symbol	Description
$P_{contact}$	Contact Pressure (MPa)
$\varepsilon_{predicted}$	Predicted S/N Ratio Parameter
σ_0	Yield Stress (MPa)
CO_2	Carbon Dioxide
ABS	American Bureau of Shipping
Al	Aluminium
ALE	Arbitrary Lagrangian-Eulerian
ANOVA	Analysis of Variance
AS	Advancing Side
AWS	American Welding Society
BM	Base Metal
CCT	Continuous Cooling Transformation Curves
CEL	Coupled Eulerian Lagrangian
CFD	Computational Fluid Dynamics
Cu	Copper
D	FSW Tool Diameter
d0	Tool Offset (mm)
DoE	Design of Experiments
D_p	Pin Diameter (mm)
D_s	Shoulder Diameter (mm)
EBSD	Electron Backscatter Diffraction

EBW	Electron Beam Welding
EDS	Energy Dispersive Spectroscopy
FEM	Finite Element Method
FSW	Friction Stir Welding
FSP	Friction Stir Processing
FSSW	Friction Stir Spot Welding
FSWT	FSW Tool Design
GTAW	Gas Tungsten Arc Welding
h	Convention Coefficient (W/m^2.K)
HAZ	Heat Affected Zone
HV	Vickers Hardness
ICE	Internal Combustion Engine
IMCs	Intermetallic Compounds
ipm	Inches per Minute
K	Thermal Conductivity Coefficient (W/m.K)
B	Larger Shoulder Design
LBW	Laser Beam Welding
Load	Tensile Load or Tensile Force(kN)
Mg	Magnesium
MIG	Metal Inert Gas
Nd	Neodymium
Nr	Tool Rotational Speed (rpm)
OA	Orthogonal Array
OFHC	Oxygen-Free High Conductivity Copper

RS	Retreating Side
RSM	Response Surface Methodology
S/N	Signal-to-Noise Ratio
S	Simple Tool Design
SEM	Scanning Electron Microscopy
SZ	Stir Zone
T	Tapered Pin Tool Design
t	Thickness of the Workpiece (mm)
TMAZ	Thermo-Mechanically Affected Zone
TWI	The Welding Institute
UTS	Ultimate Tensile Strength (MPa)
v	Traverse Speed (mm/min)
XRD	X-ray Diffractometry
Y	Yttrium
ε	Emissivity Factors
μ	Friction Coefficient
ν	Tool Welding Speed in (mm/min)
τ_{max}	Maximum Shear Stress (MPa)
ω/ν	Tool Rotational Speed to the Welding Speed

Table of Figures

Table of Tables

1. Introduction

1.1. Background

1.1.1. Friction stir welding

The Friction Stir Welding (FSW) technique, as a form of a solid-state joining process, has emerged as a highly technological advancement over the past thirty years, facilitating the joining of an array of metallic materials across a broad spectrum [1.1]. The initial patent for the technology was filed by Thomas et al. [1.2] in 1991, following which the Welding Institute (TWI) embarked on its development, culminating in the year 1994 [1.3] when the first successful implementation of the technology was demonstrated. Conceptually, the FSW process utilises a rotating shouldered tool with a profiled pin, both in contact with clamped workpiece [1.4]. The solid-state joining process – FSW - is accompanied by a number of advantages over conventional welding techniques [1.5, 1.6]. These include the absence of shielding gas, filler wire, and welder or process qualification. Additionally, FSW results in low distortion in long metal workpieces, and is applicable to metals that are typically difficult to weld, including dissimilar metals [1.7]. Furthermore, the FSW process yields higher mechanical strength of joints and does not produce fumes, porosity, or spatter. Moreover, FSW is amenable to automation and has a low environmental impact [1.4-1.9]. For all the aforementioned advantages, this advanced joining technique is of interest to be used in the field of automotive, aerospace, shipbuilding, and military domains [1.10, 1.11].

Nevertheless, it is noteworthy that the FSW technique does possess certain limitations [1.12], including:

- The magnitude of clamping force that must be exerted by the non-consumable tool to ensure proper fixation of the workpiece.
- The reduction in the workpiece thickness resulting from the lack of filler material, requires an included margin in the FSW joint design to ensure accurate compliance with specific requirements.

The FSW process is typically categorised into four primary steps [1.13, 1.14], which comprises:

- **Plunging Step:** the FSW pin tool penetrates into the workpiece while rotating. Frictional heat is generated, elevating the temperature of the workpiece to a level below its melting point, inducing material plasticisation. The plunging action concludes when the tool shoulder makes contact with the upper surface of the workpiece, resulting in the introduction of an additional heat source arising from the plastic deformation energy of the workpiece.
- **Dwell step:** the FSW tool undergoes continuous rotation to promote sufficient frictional heat, thereby plasticising the process zone of the workpieces.
- **Welding step:** Subsequent to the plasticisation of the workpiece material, the FSW tool initiates its traversing motion along the welding direction or seam. As a result of the complete contact between the FSW tool and the workpiece, heat is continuously produced through friction and plastic deformation. The plasticised material flows from the advancing side (AS) to the retreating side (RS), aided by the FSW pin and shoulder, while the FSW tool shoulder encapsulates the underlying material.

- **The retraction step:** By the end of the welding seam, the FSW tool exits the produced joint leaving a keyhole that indicates the end welding position.

Throughout all of the FSW steps, the workpieces are firmly clamped to a bottom (backing) plate, thereby preventing longitudinal, vertical, or lateral movement. From a manufacturing perspective, it is widely acknowledged that FSW can be regarded as a forging/extrusion process [1.15]. The terminologies associated with FSW, and its four distinct steps are illustrated in Figures 1.1 and 1.2, respectively.

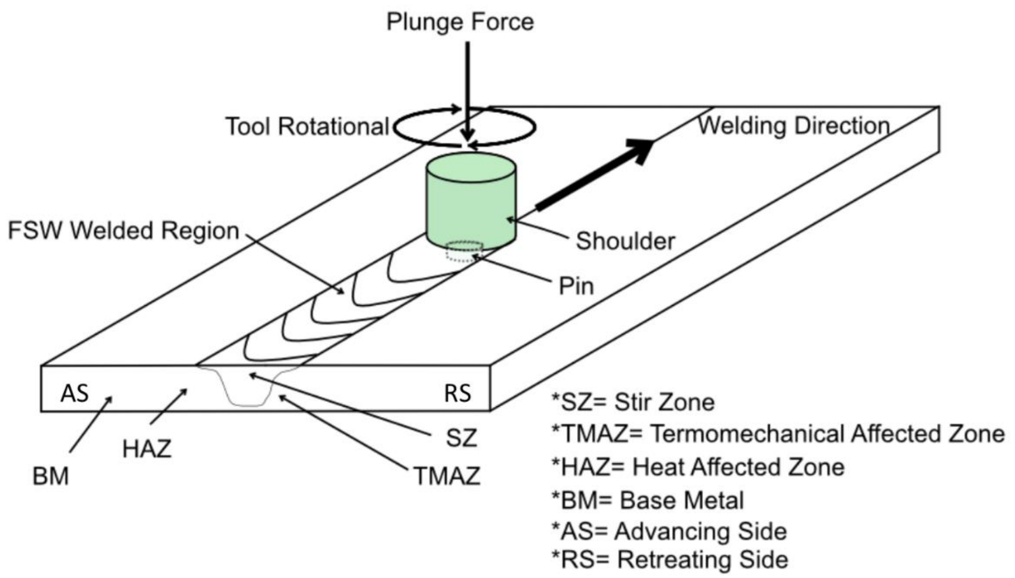

Fig. 1.1 Schematic illustration of FSW process

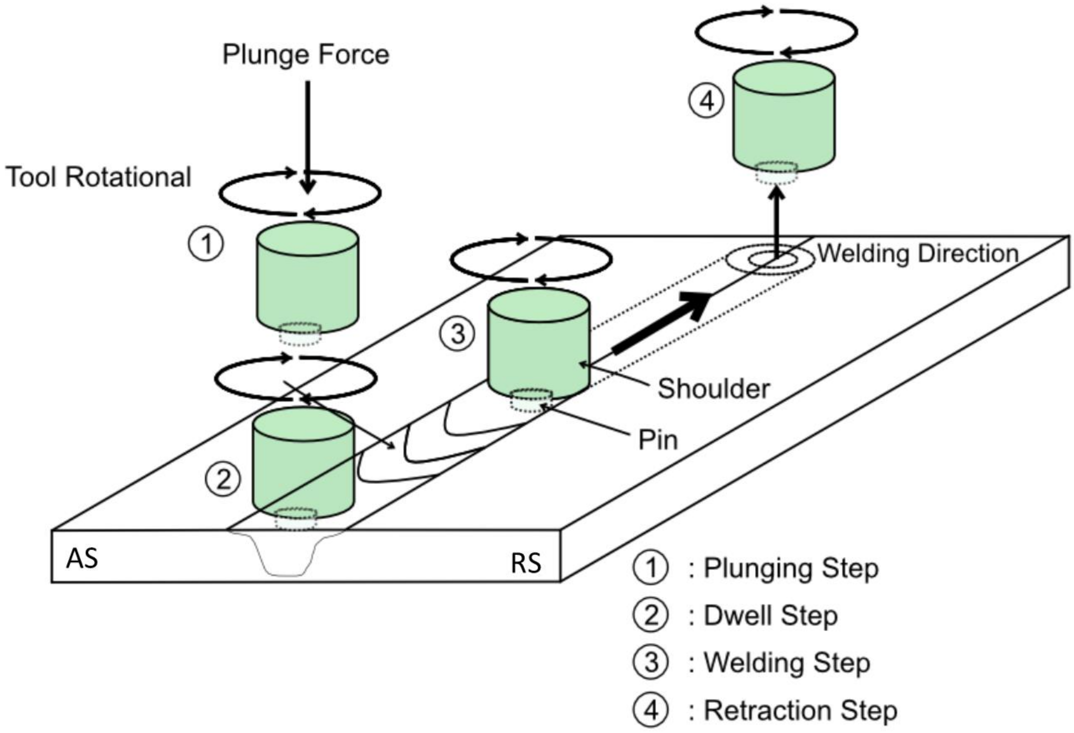

Fig. 1.2 FSW primary steps.

1.1.2. Metals and alloys dissimilar joining processes

The wide variation in physical and mechanical properties among different grades of metals and alloys provides designers with a range of options for selecting suitable material combinations to meet specific design requirements [1.16, 1.17]. Dissimilar material joints are typically used in situations where it is advantageous to replace similar joint materials for specific engineering applications. Examples of such applications include the use of combinations of austenitic to ferritic steels in power systems [1.18], dissimilar joints of copper-nickel to steel in the oil and gas industry [1.19], the application of copper to steel joints in shipbuilding engineering industries, and dissimilar joints of aluminium to steel in automotive and aerospace fields [1.20, 1.21].

The rapid demand for joints with a high strength-to-weight ratio, particularly in the transportation and aerospace industries, has led to an increased need for defect-free joints that possess high mechanical properties and low energy consumption. Dissimilar joints have become favoured due to their ability to improve product performance while meeting the functional requirements of the component. However, the use of dissimilar joints presents several technical challenges [1.22]. Conventional joining techniques for dissimilar materials include fusion welding, adhesive bonding, diffusion bonding, brazing, glazing, riveting, laser roll welding, friction welding, clinching, and mechanical attachment, depending on the joint requirements and materials combinations [1.23, 1.24]. The success of dissimilar joints is usually dependent on the joining process and its associated process parameters. Despite its limitations, fusion welding remains the most commonly used joining process for dissimilar metals and alloys [1.25].

In circumstances where there is a need to join a combination of dissimilar metals and/or alloys using the conventional fusion welding processes, significant challenges emerge as a result of the differences in chemical compositions and the mismatch in the physical and mechanical properties of each metal [1.26, 1.27]. For example, the mismatch in thermal expansion can result in the formation of residual stresses that impair joint mechanical strength [1.28]. Moreover, excessive heat input during the fusion welding process can negatively alter the microstructure and mechanical properties of the dissimilar joints [1.29]. In contrast, FSW technology has the potential to replace conventional joining methods due to its ability to produce defect-free welds on dissimilar metals and alloys [1.30].

1.1.3. Modelling of the FSW process

The growing interest in FSW applications has resulted in an increased demand for accurate numerical analysis and prediction of the final weld quality. Developing robust and validated FSW models has become essential as they facilitate the development of new tool designs and provide information on the optimum process parameters for a new joint design and materials [1.31]. Furthermore, numerical models can also be utilised to study the role of the intermetallic compound (IMCs) formation in improving dissimilar joint mechanical performance, and thus reduce the experimental costs associated with dissimilar FSW's. Advanced FSW models can also predict the conditions under which flaws or defects may arise [1.32, 1.33].

It is widely acknowledged that the FSW process can be considered as a multi-physical problem, which encompasses the combined material deformation, mass flow, and heat flow processes [1.34]. Consequently, the current FSW models can be broadly classified into four categories: thermal-based models [1.35], thermo-mechanical-based models [1.36], material flow-based models [1.37], and microstructure evaluation-based models [1.38]. Overall, these models have been developed to predict various aspects of the FSW process, including material flow, thermal and residual stresses, and reaction forces on the FSW tool [1.39].

1.2. Problem statement and objectives

The disparity in physical and mechanical properties between two dissimilar materials, such as aluminium and copper, presents significant technological challenges when considering fusion welding joining processes [1.40]. Therefore, FSW technology can replace conventional joining methods, due to its ability to produce defect-free dissimilar joints of metals and alloys, which exhibit better joint quality [1.41-1.45]. This study presents the successful butt welding results of dissimilar materials using the FSW process.

The primary objective of the present study is to develop a process using FSW for welding both similar and dissimilar materials. The specific aims of this research include:

- Identification of the FSW process parameters that consistently produce defect-free FSW butt joints.
- Evaluating the impact of the FSW parameters on weldment quality, using metallurgical, analytical, and mechanical techniques.
- Development of a finite element model to simulate the FSW process, with a primary focus on understanding the effects of welding parameters on temperature as part of thermal simulation. Stress and strain, although initially considered, were not the central subjects of numerical modelling in this study.
- Establishment of a robust optimisation process for dissimilar FSW parameters that requires the minimum number of experiments and is less sensitive to other uncontrolled parameters, such as environmental conditions and user input.

1.3. Research approach

This investigation utilises both experimental and numerical modelling techniques to achieve its objectives. Specifically, the FSW process will be employed to create butt welds between various similar metal combinations including copper-to-copper, aluminium-to-aluminium, and magnesium-to-magnesium, as well as dissimilar combinations such as copper-to-aluminium and aluminium-to-magnesium. The weldment quality will be assessed through the use of metallurgical and mechanical analysis techniques. Finite element modelling will be utilised to simulate the joining process and investigate the impact of process parameters on the weld characteristics. The results of both the experiments and the numerical simulations will be used in conjunction with phase diagrams of metallic alloys to predict the evolution of intermetallic phases and elemental composition in different areas of the weldment.

Design of experiments (DoE) techniques will be implemented to ascertain the key parameters influencing the mechanical strength of FSW joints and to minimise the number of experiments needed to optimise joint efficiency. The impact of tool rotational speed, welding speed, material placement, and tool geometry will be comprehensively evaluated to establish a process window that ensures consistently high joint mechanical performance.

1.4. Thesis structure

This thesis is divided into seven further chapters. Chapter 2 presents a comprehensive literature review of the state of the art knowledge associated with the FSW process, as well as the challenges involved in performing similar and dissimilar FSW of metals and alloys.

Chapter 3 outlines the experimental procedures employed to achieve similar and dissimilar FSW butt joints using various selected metals, including aluminium, copper, and magnesium alloy. A comprehensive description of the characterisation methods employed to critically evaluate the FSW butt joints is also presented. This includes metallographic examination, compositional analysis, and phase identification, which were accomplished using energy dispersive spectroscopy (EDS), X-ray diffractometry (XRD), and electron backscatter diffraction (EBSD). The chapter also delves into the mechanical assessment approach of the joints. Moreover, Chapter 3 also provides details on the numerical modelling techniques employed to simulate the FSW process, including different solution methods for partial differential equations and various domain discretisation techniques such as Lagrangian, Eulerian, and Coupled Eulerian Lagrangian (CEL).

Chapter 4 presents an analysis and discussion of the results obtained from similar and dissimilar FSW butt welding joints. The first part of the chapter focuses on the presentation of the optimal process parameters that produce defect-free joints for copper-to-copper and aluminium-to-aluminium. Subsequently, the chapter discusses the results of obtaining defect-free joints of dissimilar FSW between aluminium and copper. The experiments involved welding of aluminium grades AA5083 and AA1061 to copper, with different tool rotational speeds (ω) and traverse speeds (v) - (ω/v) ratios - to identify the optimal process parameters that result in higher joint mechanical strength.

Chapter 5 focuses on the results obtained from the dissimilar FSW of AA6061 to copper, including the optimal process parameters identified to achieve defect-free joints. The chapter also details the results of the numerical modelling approach using the coupled Eulerian-Lagrangian (CEL) method, along with the validation procedure used for the dissimilar FSW of AA6061 to copper. Moreover, the chapter presents a robust prediction method for IMCs formation during dissimilar FSW welding of aluminium to copper.

Chapter 6 details the outcomes of optimising the dissimilar FSW process parameters of aluminium grade AA5083 to copper. The impact of welding speed, tool rotational speed, material placement, and tool design on the joint properties is explored in detail throughout the chapter. The Taguchi DoE approach is adopted to determine the key parameters that significantly affect the dissimilar FSW joints' mechanical strength while reducing the number of experiments required for optimal joint efficiency. Statistical analysis methods such as the analysis of variance (ANOVA) technique are employed to validate that the identified process parameters have a significant impact on the mechanical properties of the dissimilar FSW joints.

Chapter 7 details the investigation of the influence of aluminium alloy grade on dissimilar FSW of aluminium to the magnesium alloy, AZ31B. The impact of using two different aluminium alloys on the joint quality of dissimilar Al to Mg grades (AZ31B) is also assessed. The optimal process parameters for achieving defect-free joints are explored by examining the joints' macro and microstructure, as well as assessing the presence and distribution of the IMCs. Additionally, the chapter discusses the combined impact of joint microstructure and IMCs formation on the dissimilar Al to Mg joint mechanical strength.

Finally, Chapter 8 contains the research conclusions and provides recommendations for future work.

1.5. References

[1.1] L. E. Murr, "A review of FSW research on dissimilar metal and alloy systems," J. Mater. Eng. Perform., vol. 19, no. 8, pp. 1071–1089, Feb. 2010. https://doi.10.1007/s11665-010-9598-0.

[1.2] T. Wayne, N. Edward, and N. James: European Patent No. Ep 0615480 B1, 1994.

[1.3] O. T. Midling, E. James and A. Sandvik "Friction Stir Welding" United State Patent No. Us 5,813,592, 1998.

[1.4] R.S. Mishra and M. Mahoney: Friction Stir Welding and Processing, ASME International, 2007. https://doi.10.1016/j.mser.2005.07.00.

[1.5] Y. Uematsu, K. Tokaji, Y. Tozaki, T. Kurita, S. Murata "Effect of Re-Filling Probe Hole on Tensile Failure and Fatigue Behaviour of Friction Stir Spot Welded Joints in Al–Mg–Si Alloy" International Journal of Fatigue 30, (2008) 1956–1966. https://doi.org/10.1016/j.ijfatigue.2008.01.006.

[1.6] R.S. Mishra and Z.Y. Ma "A Review: Friction Stir Welding and Processing" Materials Science and Engineering R 50 (2005) 1–78. https://doi.org/10.1016/j.mser.2005.07.001.

[1.7] R. Nandan, T. Debroy and H. K. D. H. Bhadeshia "Recent Advances in Friction Stir Welding – Process, Weldment Structure and Properties" Progress in Materials Science 53 (2008) 980-1023, 2017. http://dx.doi.org/10.1016/j.pmatsci.2008.05.001.

[1.8] P. Cavaliere, R. Nobile, F.W. Panella, A. Squillace "Mechanical and Microstructural Behavior of 2024–7075 Aluminum Alloy Sheets Joined by Friction Stir Welding" International Journal of Machine Tools & Manufacture 46, 588–594, 2006. http://www.archivesmse.org.

[1.9] W.Gan, K.Okamoto, S.Hirano, K.Chung and C.Kim "Properties of Friction-Stir Welded Aluminium Alloys 6111 and 5083" Journal of Engineering Materials and Technology Vol. 130, 2008. https://doi.org/10.14445/22315381/IJETT-V10P231.

[1.10] C.D. Sorensen, T.W. Nelson “Friction stir welding of ferrous and nickel alloys”, Friction stir Weld. Process., ASM International, p. 111–2, 2007.

[1.11] P. Cavaliere, G. Campanile, F. Panella, A. Squillace “Effect of Welding Parameters on Mechanical and Microstructural Properties of AA 6056 Joints Produced by Friction Stir Welding” Journal of Materials Processing Technology, 180, pp. 263–270, 2006. https://doi.org/10.1016/j.jmatprotec.2006.06.015.

[1.12] N. Sharma, Z. A. Khan, and A. N. Siddiquee, “Friction stir welding of aluminium to copper an overview”, The Transactions of Nonferrous Metals Society of China (English Ed., vol. 27, no. 10, pp. 2113–2136, 2017. https://doi.org/10.1016/S1003-6326(17)60238-3.

[1.13] I. Galvão, A. Loureiro & D. M. Rodrigues, “Critical review on friction stir welding of aluminium to copper”, Science and Technology of Welding and Joining, 21:7, 523-546, 2016. http://dx.doi.org/10.1080/13621718.2015.1118813.

[1.14] M.A. Gharacheh, A.H. Kokabi, G.H. Daneshi, B. Shalchi, R. Sarrafi “The Influence of the Ratio of ‘‘Rotational Speed/Traverse Speed’’ (O/V) on Mechanical Properties of Az31 Friction Stir Welds” International Journal of Machine Tools & Manufacture, 46, pp. 1983–1987, 2006. https://doi.org/10.1016/j.ijmachtools.2006.01.007.

[1.15] M. B. Uday, M. N. Ahmad Fauzi, H. Zuhailawati & A. B. Ismail, “Advances in friction welding process: a review”, Science and Technology of Welding and Joining, 15:7, 534-558, 2010. https://doi.org/10.1179/136217110X12785889550064.

[1.16] J. Ouyang, E. Yarrapareddy, and R. Kovacevic, “Microstructural evolution in the friction stir welded 6061 aluminium alloy (T6-temper condition) to copper”, Journal of Materials Processing Technology, vol. 172, no. 1, pp. 110–122, 2006. https://doi.org/10.1016/j.jmatprotec.2005.09.013.

[1.17] P. Xue, D. R. Ni, D. Wang, B. L. Xiao, and Z. Y. Ma, “Effect of friction stir welding parameters on the microstructure and mechanical properties of the dissimilar Al–Cu joints”, Materials Science and Engineering: A, vol. 528, no. 13–14, pp. 4683–4689, 2011. https://doi.org/10.1016/j.msea.2011.02.067.

[1.18] T. Watanabe, H. Takayam, and A. Yanagisaw “Joining of Aluminium Alloy to Steel by Friction Stir Welding” Journal of Materials Processing Technology Vol.178 (2006) pp. 342–349. https://doi.org/10.1016/j.jmatprotec.2006.04.117.

[1.19] N. Kumar, W. Yuan, and R. S. Mishra, “Introduction,” Friction Stir Welding of Dissimilar Alloys and Materials, A volume in Friction Stir Welding and Processing, pp. 1–13, 2015. https://doi.org/10.1016/C2014-0-01707-8.

[1.20] A. A. Naumov, F. Y. Isupov, O. V Panchenko, and E. N. Rylkov, “Dissimilar Welding of Cu and Al Alloys by Friction Stir Welding and Impulse Friction Stir Welding”, Twenty-eighth International Ocean and Polar Engineering Conference, Japan, pp. 166–171, 2018.

[1.21] M.N. James, D.G. Hattingh and G.R. Bradley “Weld Tool Travel Speed Effects on Fatigue Life of Friction Stir Welds in 5083 Aluminium” International Journal of Fatigue, vol. 25, pp. 1389–1398, 2003. https://doi.org/10.1016/S0142-1123(03)00061-6.

[1.22] O. Lorrain, V. Favier, H. Zahrouni, D. Lawrjaniec "Understanding the Material Flow Path of Friction Stir Welding Process Using Unthreaded Tools" Journal of Materials Processing Technology, PP. 603–609, 2010. https://doi.org/10.1016/j.jmatprotec.2009.11.005.

[1.23] L. Cederqvist, and T.O¨. Berg "Reliability Study of Friction Stir Welded Copper Canisters Containing Sweden's Nuclear Waste" Reliability Engineering and System Safety 93 1491–1499, 2008. https://doi.org/10.1016/j.ress.2007.09.010.

[1.24] G. Buffa, G. Campanile, L. Fratini, and A. Prisco "Friction Stir Welding of Lap Joints: Influence of Process Parameters on The Metallurgical and Mechanical Properties" Materials Science and Engineering A 519 19–26, 2009. https://doi.org/10.1016/j.msea.2009.04.046.

[1.25] I. B. Goldberg, M.W. Mahoney, W.H. Bingel, and C.S. Hollingsworth "Feasibility of Fabricating Microwave Waveguide Using Friction Stir Welding" Review of Scientific Instruments Vol. 77, 116115, 2006. https://doi.org/10.1063/1.2387887.

[1.26] I. Galvão, R. M. Leal, D. M. Rodrigues, and A. Loureiro, "Influence of tool shoulder geometry on properties of friction stir welds in thin copper sheets", Journal of Materials Processing Technology, vol. 213, pp. 129–135, 2013. https://doi.org/10.1016/j.jmatprotec.2012.09.016.

[1.27] Z. Feng, R. Steel, S. Packer, and S.A. David "Friction Stir Welding of API Grade X65 Steel Pipes" Report Oak Ridge National Laboratory U. S. Department of Energy 2005.H. W.

[1.28] L. Dubourg, A. Merati, M. Jahazi “Process Optimization and Mechanical Properties of Friction Stir Lap Welds of 7075-T6 Stringers on 2024-T3 Skin” Materials and Design 31 3324–3330.218, 2010. https://doi.org/10.1016/j.matdes.2010.02.002.

[1.29] K. J. Colligan and R.S. Mishra “A Conceptual Model for The Process Variables Related to Heat Generation In Friction Stir Welding of Aluminium” Scripta Materialia 58 327–331, 2008. https://doi.org/10.1016/j.scriptamat.2007.10.015.

[1.30] N. Rajamanickam, V. Balusamy, G.M. Reddy, K. Natarajan “Effect of Process Parameters on Thermal History and Mechanical Properties of Friction Stir Welds” Materials and Design 30, pp. 2726–2731, 2009. https://doi.org/10.1016/j.matdes.2008.09.035.

[1.31] X. He, F. Gu, and A. Ball, “A review of numerical analysis of friction stir welding,” Progress in Materials Science, vol. 65, pp. 1–66, 2014. https://doi.org/10.1016/j.pmatsci.2014.03.003.

[1.32] Zhang and Z. Zhang, “A fully coupled thermo-mechanical model of friction stir welding”, International Journal of Advanced Manufacturing Technology, vol. 37, pp. 279–293, 2008. https://doi.org/10.1007/s00170-007-0971-6.

[1.33] G. Buffa, J. Hua, R. Shivpuri, and L. Fratini, “A continuum based fem model for friction stir welding—model development”, Materials Science and Engineering: A, vol. 419, no. 1–2, pp. 389–396, 2006. https://doi.org/10.1016/j.msea.2005.09.040.

[1.34] B. Meyghani, M. Awang, S. S. Emamian, M. K. Mohd Nor, and S. R. Pedapati, “A Comparison of Different Finite Element Methods in the Thermal Analysis of

Friction Stir Welding (FSW)", Metals (Basel)., vol. 7, no. 11, pp. 450, 2017. https://www.mdpi.com/2075-4701/7/10/450#.

[1.35] S.N. Pandyaa, D.J. Menghani, "Optimum heat source position offset in welding of dissimilar Al-Cu metals using a theoretical approach", Materials Today: Proceedings 5, pp.26974–26980, 2018. https://doi.org/10.1016/j.matpr.2018.08.187.

[1.36] F. Al-Badour, N. Merah, A. Shuaib, and A. Bazoune, "Coupled Eulerian Lagrangian finite element modelling of friction stir welding processes", Journal of materials processing technology, vol. 213, no. 8, pp. 1433–1439, 2013. https://doi.org/10.1016/j.jmatprotec.2013.02.014.

[1.37] R. Nandan, G. G. Roy, T. J. Lienert, and T. Debroy, "Three-dimensional heat and material flow during friction stir welding of mild steel", Acta Materialia, vol. 55, no. 3, pp. 883–895, 2007. https://doi.org/10.1016/j.actamat.2006.09.009.

[1.38] Y. He, D.E. Boyce, P.R. Dawson, "Three-Dimensional Modelling of Void Growth in Friction Stir Welding of Stainless Steel" Proceedings of The 9th International Conference on Numerical Methods in Industrial Formation Processing, PP. 25–34, 2007. https://doi.org/10.1063/1.2740787.

[1.39] H. Li, D. Liu "Simplified Thermo-Mechanical Modelling of Friction Stir Welding with a Sequential FE Method". Int J Model Optimum 2014; 4:410–6. doi:10.7763/IJMO, V4.409, 2014.

[1.40] M.M. Attallah, H.G. Salem "Friction Stir Welding Parameters: A Tool for Controlling Abnormal Grain Growth During Subsequent Heat Treatment" Materials

Science and Engineering A, pp. 391 51–59, 2005. https://doi.org/10.1016/j.msea.2004.08.059.

[1.41] P. Cavaliere, A. De Santis, F. Panella, A. Squillace "Effect of Welding Parameters on Mechanical and Microstructural Properties of AA 6082 Joints Produced by Friction Stir Welding" Journal of Materials Processing Technology 200, 364–372220, 2008. https://doi.org/10.1016/j.matdes.2008.05.044.

[1.42] M.N. James, D.J. Hughes, D.G. Hattingh, G. Mills, P.J. Webster "Residual Stress and Strain in MIG Butt Welds in 5083-H321 Aluminium: As-Welded and Fatigue Cycled" International Journal of Fatigue 31, 28–40, 2009. https://doi.org/10.1016/j.ijfatigue.2008.04.010.

[1.43] H. Lombard, D.G. Hattingh, A. Steuwer, and M.N. James "Optimizing FSW Process Parameters to Minimize Defects and Maximize Fatigue Life in 5083-H321 Aluminium Alloy" Engineering Fracture Mechanics 75, 341–354, 2008. https://doi.org/10.1016/j.engfracmech.2007.01.026.

[1.44] C. Vidal, V. Infante, and P. Vilaça "Assessment of Improvement Techniques Effect on Fatigue Behaviour of Friction Stir Welded Aerospace Aluminium Alloys" Procedia Engineering 2, 1605–1616, 2010. https://doi.org/10.1016/j.proeng.2010.03.173.

[1.45] V. Balasubramanian "Relationship Between Base Metal Properties and Friction Stir Welding Process Parameters" Materials Science and Engineering A 480, pp.397–403, 2008. https://doi.org/10.1016/j.msea.2007.07.048.

2. Literature review

The literature concerning the experimental and numerical challenges related to the dissimilar friction stir welding (FSW) of metals and alloys is examined in the subsequent chapter. In terms of experimentation, the chapter provides a critical evaluation of the key findings and limitations associated with the application of FSW to join dissimilar materials, such as aluminium, copper, and magnesium alloys. Whereas the numerical content discusses the available modelling methods developed for simulating the FSW process.

In addition, this chapter discusses FSW tool design and material, process parameters, defect formation, and current optimisation methods of FSW process parameters.

2.1. FSW versus conventional welding processes

In current engineering applications, there is a growing trend towards using dissimilar metal joints, due to their inherent advantages in partially substituting different metals and alloys. Examples include copper combined with aluminium alloys in electrical connectors, heat exchanger tubes, transformer foil conductors, and capacitor foil windings [2.1] . Additionally, the dissimilar aluminium joints used in the aerospace and transportation industries [2.3]. With an increased demand for high strength-to-weight ratio components, particularly in the aerospace and transportation sectors, there is a pressing need to produce defect-free joints that exhibit higher mechanical properties. However, conventional fusion processes such as Gas Tungsten Arc Welding (GTAW) and Metal Inert Gas (MIG) welding suffer from various limitations, including the presence of porosity, solidification cracking, oxidation, and high joint distortion, which significantly impair the mechanical performance of dissimilar joints [2.4–2.6]. In addition, fusion welding processes adversely affect the alloy concentration at the fusion zone and the material adjacent to the weld pool due to the diffusion process [2.7].

These challenges mean that various metals and alloys are deemed unweldable or difficult to weld using conventional welding processes, including a wide range of aluminium series such as 2xxx and 7xxx, which are commonly used in the transportation industry [2.2]. The aluminium series of alloys are often categorised as difficult-to-weld metals due to the following reasons when considering a conventional welding process [2.1, 2.8]:

- Impaired solidified microstructure, which can negatively affect the joint's mechanical properties, reducing its overall strength and durability.
- Solidification shrinkage, almost twice that of ferrous alloys.
- Wider solidification temperature ranges.
- Presence of oxide layers.
- High thermal conductivity.
- High coefficient of thermal expansion.
- Voids formation.

Voids or gas porosity defects are common in most metals and alloys, especially in heat treatable aluminium alloys such as the 2xxx, 6xxx, and 7xxx series, which are more prone to crack initiation [2.9, 2.10]. Further, metals that have been subjected to heat treatment, thermo-mechanical processes, and/or chemical precipitates also tend to exhibit lower joint mechanical strength relative to the base metal [2.11, 2.12].

In contrast to fusion welding, the solid-state joining technique known as FSW has the potential to replace conventional joining methods due to its ability to produce defect-free welds on dissimilar metals and alloys [2.13]. As a solid-state joining technique, FSW generates minimal distortion, thereby enabling the creation of superior welds with excellent mechanical properties [2.14]. Presently, FSW applications are not limited to aluminium alloys and can be applied to a wide range of soft and hard-to-weld metals and alloys such as nickel, magnesium, copper, and steel alloys [2.14–2.18]. Several studies have demonstrated the feasibility of the FSW process to produce relatively robust, high-quality welds on dissimilar joints [2.16–2.20]. Table 2.1 provides insight into the various dissimilar friction stir welds and their equivalent industrial applications.

It's worth mentioning that the classification given in Table 2.1 is based on solubility, which reveals how two metals interact during welding. The "severe-interfacial reaction" between Aluminium (Al) and Magnesium (Mg) points to intense metallurgical interactions, often introducing welding complexities [2.28–2.30]. This can be attributed to Mg typically having a higher solubility in Al than Aluminium's solubility in Steel [2.21–2.24] . Conversely, the "medium-interfacial reaction" observed with Aluminium (Al) and Steel indicates a moderated level of interaction. In essence, solubility plays a pivotal role in determining the outcome and quality of the weld.

Table 2.1 Typical examples of dissimilar FSW welds and the industrial applications

Dissimilar FSW materials	FSW joint classification	Joint application	Ref.
Aluminium/ mild steel	Medium-interfacial reaction	Automotive industry i.e., Engine cradles (Honda Motor Co.), Marine industry i.e., decks to hulls. Gasketed joints and vessels.	[2.21–2.24]
Aluminium / aluminium	Severe-interfacial reaction	Fabrication of aircraft structures, ship structures (electronic parts), transport structures (parts of the internal combustion engine, ICE) and bodywork.	[2.9–2.27]
AZ31B/AA6061	Severe-interfacial reaction	Automotive, aerospace electronics, transportation, cathodic protectors, ship building, offshore, power generation, and railway industry.	[2.28–2.30]
Al-Si/ pure titanium	Medium-interfacial reaction	Automobile and aircraft industries.	[2.30–2.32]
Al reinforced/ SiC matrix	New-dissimilar materials	Aerospace, motor sport and automotive industrial fields.	[2.33]
AA5083/copper	Medium-interfacial reaction	Electrical connectors, heat exchangers tubes, transformer’s foil, conductors, and capacitor windings.	[2.34–2.38]

On a commercial scale, the FSW process has been adopted by Eclipse Aviation, Ford, and Mazda Motors as a partial replacement for certain fusion welding applications [2.18, 2.39]. Additionally, the FSW process has been developed to manufacture steel pipes [2.40, 2.41], and copper barrels for nuclear waste applications, resulting in longer lifetimes and defect-free welds [2.34, 2.42]. From a research perspective, the FSW process has been extensively investigated as a means of surpassing fusion welding processes and has been considered as an alternative to brazing for fabricating waveguide structures [2.14]. Recently, FSW has emerged as a competitive alternative to conventional joining processes for producing plastic and polymer parts at relatively higher welding speeds [2.43, 2.44].

In general, research on the FSW process has led to the advancement of modelling approaches to simulate thermo-mechanical processes. This progress has enabled the development of new FSW tool designs, allowed for the consideration of further dissimilar material systems, and improved the FSW optimisation process [2.45, 2.46]. It is noteworthy that the FSW technique has given rise to several sub-processes, such as Friction Stir Processing (FSP), developed by Mishra et al. [2.1]. It is -the FSP- an advanced method that precisely modifies the microstructure of metals, improving their mechanical and thermal attributes while preserving the essential characteristics of the bulk material. This solid-state surface-modification technique -FSP- offers numerous processing capabilities such as eliminating casting defects, refining microstructures, improving strength and ductility, increasing fatigue resistance, enhancing formability, and improving corrosion resistance. Friction Stir Spot Welding (FSSW) can also be considered a sub-process of the FSW technology. Several promising research findings indicate that FSSW can compete against conventional resistance spot welding in the automotive industry, with lower energy consumption and process costs [2.18, 2.47]. Ultimately, the FSW process can also be considered environmentally friendly due to its lower energy requirements compared to fusion and other conventional welding processes. The potential for reduced energy usage in FSW, without compromising joint integrity or mechanical properties, underscores its suitability as a green manufacturing process and aligns with global efforts to promote cleaner production technologies [2.1]and [2.48].

Zhao et al. [2.49] conducted a comprehensive comparative study on aluminium alloys to examine and evaluate the mechanical and microstructural characteristics of joints fabricated via the FSW process and conventional MIG and TIG welding methods.The study's findings indicated that joints produced using the FSW process exhibited relatively consistent higher mechanical strength and fatigue life compared to those produced using conventional fusion welding techniques. Furthermore, the microstructures of the parent metal were usually preserved after the FSW process, whereas the fusion processes had a negative impact on the parent metal microstructure [2.49, 2.50]. Fig. 2.1 provides a comparison of the tensile strength performance of the FSW and conventional welding processes.

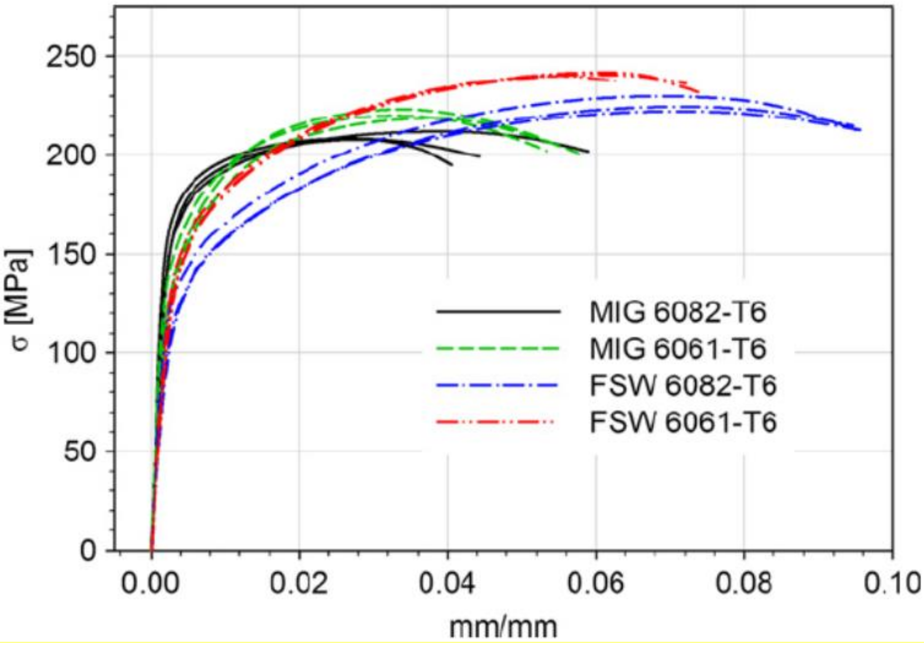

Fig 2.1 AA6082 and AA6061 joints mechanical strength produced by FSW and MIG welding process [2.49].

2.2. Similar and dissimilar FSW of aluminium alloys

The FSW process has been utilised in the early stages to join materials classified as difficult to weld by conventional fusion welding processes, especially similar and dissimilar aluminium alloys [2.51]. Numerous investigations [2.2, 2.45, and 2.46] have been conducted using the FSW technology to join aluminium materials of different grades, with the aim of identifying the optimum welding parameters that result in defect-free joints and enhanced mechanical performance.

In their pioneering work, Murr et al. [2.2], summarised the extensive research advancements made in this area over a decade and a half. Their review report comprised 18 FSW reference systems with similar materials and 25 distinct FSW systems involving dissimilar materials. The report established the optimum FSW parameters for similar and dissimilar aluminium alloys, such as tool design and material, tool rotational speed, and traverse speed. Based on Murr et al.'s [2.2] findings, similar and dissimilar aluminium alloy joint systems are no longer difficult to weld since the process window for achieving defect-free FSW joints has been clearly identified.

2.3. FSW of copper

Copper and its alloys, which are relatively difficult to weld, have been widely considered for several engineering applications due to their high electrical and thermal conductivity properties. Copper applications include shell and tube heat exchangers, electrical connections such as capacitor windings, and transformer conductors [2.52]. Moreover, the application of copper has recently been extended to include structural materials that require multi-manufacturing processes, such as welding techniques, owing to its superb corrosion resistance properties [2.53,]. However, several factors limit the weldability of copper and its alloys when using the fusion welding process, such as the alloying elements, thermal conductivity, shielding gas, type of current used during welding, joint design, welding position, surface condition, and cleanliness [2.54].

The high thermal conductivities of commercial copper and its alloys necessitate the consideration of selected types of current and shielding gas to apply an appropriate heat input that is as high as possible to counteract the steep heat dissipation that occurs around the localised weld zone (welding pool) [2.55]. In addition, certain copper alloys require a preheating process to achieve defect-free joints [2.56]. Overall, it is widely recognised that copper alloy joints produced by the fusion welding process typically exhibit unavoidable residual stresses and hot shortness [2.57]. To overcome the aforementioned challenges that arise when considering conventional fusion joining processes, solid-state joining processes such as FSW technology have been extensively investigated. These investigations have involved both experimental and numerical approaches to achieve high FSW joint efficiency [2.36-2.58].

In their work, Sakthivel et al. [2.58] successfully produced defect-free FSW butt joints of commercially pure copper with a sheet thickness of 2 mm. A relatively lower welding speed of 30 mm/min and high rotational speed of 1000 rpm were utilised, and the resulting joint achieved up to 85% mechanical joint efficiency relative to the parent material. Subsequently, Sun et al. [2.59] identified a process window for achieving defect-free FSW joints of commercially pure copper, which included tool rotational speed, tool welding speed, and tool load. The authors [2.59] also investigated the influence of FSW welding parameters on both the joint mechanical performance and microstructure. Based on this work [2.59], it was found that FSW of commercially pure copper is more sensitive to the applied tool load than the tool rotational or welding speed. Increasing the applied tool load directly enhances the joint's mechanical strength.

Building on the work of Sakthivel et al. [2.58] and Sun et al. [2.59], Shen et al. [2.60] investigated the trade-off point between FSW joint microstructure, in terms of stir zone grain size, and ultimate tensile strength. It was reported that the ultimate tensile strength increases -unconditionally - by decreasing the grain size of the stir zone microstructure. However, the stir zone grain size was found to initially increase and then decrease with an increase in the tool welding speed, which led to a decrease in the joint ultimate tensile strength after reaching a certain peak point (as shown in Fig. 2.2). The authors [2.60] also emphasised that the tool welding speed has a relatively lower effect on the joint's mechanical strength within the range of 25-150 mm/min.

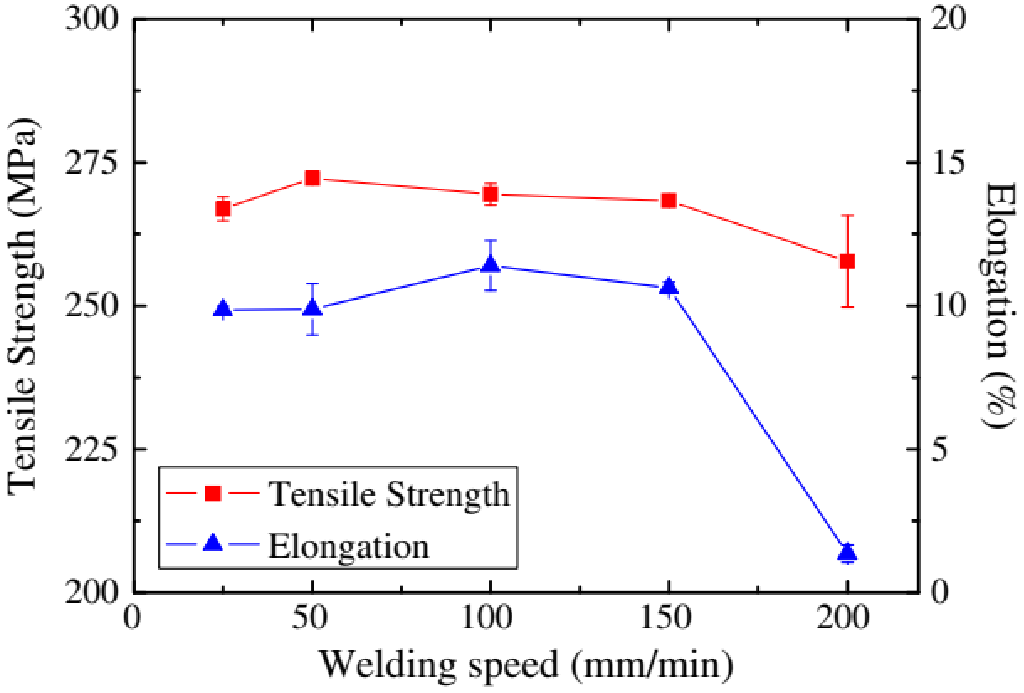

Fig. 2.2 Mechanical performance of commercial pure copper FSW joints at different welding speeds [2.60].

Based on the findings of Shen et al. [2.60], Zadeh et al. [2.61] developed an analytical model that enabled them to predict the mechanical properties of butt joints produced using FSW on commercially pure copper. In their analytical model, the response surface methodology (RSM) was applied at five levels and 31 runs of four different FSW parameters (tool rotational speed, welding speed, forging force, and tool design) with the aid of design expert software. It was claimed [2.61] that joint mechanical strength in FSW of commercial copper is proportionally affected by the tool rotational speed, welding speed, and forging force. According to their model, the maximum joint efficiency can be achieved at a tool rotational speed of 942 rpm, a welding speed of 84 mm/min, and an axial force of 1.62 KN. Zadeh et al. [2.61] also concluded that increasing the tool rotational speed, welding speed, and axial force increases the joint ultimate tensile strength (UTS) up to a trade-off value before it starts to decrease.

More recently, Jabbari et al. [2.62] successfully simulated the grain growth behaviour during the FSW of commercially pure copper. The predicted temperature from a pre-developed thermal model was used to trace the grain growth behaviour at different FSW zones with a constant welding speed and various rotational speeds. This was achieved by incorporating the predicted temperature into a microstructural model to determine grain size variations throughout the welding process. Such a detailed simulation provides valuable insights into the microstructural dynamics of FSW, contributing significantly to the understanding of material behaviour under different welding conditions. The authors observations [2.62] supported the findings of Zadeh et al. [2.61], where the ultimate joint tensile strength was achieved at 900 rpm. This was mainly attributed to the proportional relationship between the stir zone grain size and tool rotational speed.

2.4. Similar and dissimilar FSW of magnesium alloys

There is an increasing research interest in the joining of lightweight metals, such as magnesium-based alloys, due to their potential applications in various fields, including automotive, aerospace, and electronics [2.16]. This interest is fuelled by several attractive properties, including low density, high damping behaviour, reliable electromagnetic coating, high specific strength, and stable formability behaviour at higher temperatures [2.16-2.63]. Additionally, the casting of magnesium alloys is relatively less expensive and often recyclable [2.64]. Further, the properties of magnesium alloys make them an ideal candidate for use in nuclear reactors, as they exhibit excellent resistance to carbon dioxide (CO_2) and can serve as fuel cladding and structural components in nuclear power plants [2.1, 2.18]. Furthermore, magnesium alloy applications have expanded to include the biomaterials industry due to their good biocompatibility behaviour. However, magnesium alloys possess some adverse properties such as poor formability and ductility at room temperature, limited mechanical strength, low fatigue behaviour, and low creep resistance [2.16, 2.28].

It is widely acknowledged that methods such as grain refinement, recrystallisation, and the addition of rare-earth elements like Yttrium (Y) and Neodymium (Nd), can significantly enhance the mechanical properties of magnesium alloys [2.16-2.64]. As such, the FSW technology can effectively replace conventional joining methods by producing defect-free welds of magnesium-based alloys while maintaining the desired level of grain refinement arising from higher strain rates. FSW of magnesium alloys has been found to prevent the formation of coarse grains, brittle intermetallic compounds (IMCs), porosity, solidification cracking, oxidation, and joint distortion, which are commonly associated with fusion welding processes [2.65].

Several research works have been carried out to evaluate the potential of FSW technology in enhancing the joint mechanical performance of magnesium alloys by improving the joint microstructure. A summary of these reports is presented in Table 2.2.

Table 2.2 An overview of research on FSW joints for magnesium-based alloys

Magnesium alloy	Welding parameters	Mechanical properties	Remarks/Conclusions	Ref.
AZ31/AZ91	N (1400-1800) rpm, v (25-100) mm/min	UTS up to 183 MPa	Defect-free joints were achieved by optimising the process parameters, resulting in the absence of hot cracking defects.	[2.65]
AZ61A	N (1200 rpm), v (90 mm/min), and 3-7 kN tool axial force.	UTS up to 224 MPa.	A tool rotational speed of 1200 rpm, a tool welding speed of 90 mm/min (equivalent to a 13 ω/v ratio), and an axial force of 5 kN led to a joint efficiency of 83%.	[2.66]
AZ31	N (800-1600) rpm, v (120 mm/min)	UTS up to 225 MPa.	Higher joint mechanical strength was obtained at a tool rotational speed of 1200 rpm, corresponding to a 10 ω/v ratio.	[2.30]
AZ31B	N 600 rpm, v (200 mm/min)	UTS up to 216 MPa.	The use of CO_2 as a cooling medium in the process has been observed to refine the joint microstructure and promote a high dislocation density. As a result, a significant number of twins and second-phase particles have been detected.	[2.63]

In general, the FSW of magnesium-based alloys is highly dependent on the welding process parameters, as reported in various studies [2.16-2.67]. Thus, the current research is aimed to optimising the FSW parameters to leverage the full potential of this solid-state joining technology and overcome the limitations associated with the fusion processes. Furthermore, the exact influence of FSW welding parameters on joint mechanical performance has yet to be accurately predicted and validated.

2.5. Dissimilar FSW of aluminium alloys to copper

Dissimilar welding of aluminium to copper provides an attractive solution for engineering systems that require partial replacement of copper with aluminium to benefit from the latter's lower cost and lightweight properties while maintaining the electrical properties of the former. Such systems include shell and tube heat exchangers, electrical connections, capacitor windings, and transformer conductors [2.68 –2.70]. However, dissimilar aluminium to copper welding presents challenges due to the differences in thermal, chemical, and metallurgical properties of the two metals. The solid-state FSW process was developed to join difficult-to-weld metals and alloys and offers advantages over fusion welding techniques in dissimilar welding. These benefits include reduced environmental impact, elimination of solidification problems such as cracking and porosity formation, lower heat input, and less distortion [2.14].

Nevertheless, challenges emerge when joining aluminium to copper, particularly the formation of IMCs at the interface and weld nugget zones as well as the mismatch in their melting points temperature. Several attempts have been made to predict and control IMCs formation. Mishra et al. [2.71] proposed the first approach for predicting the IMCs in such cases. The authors [2.71] made use of a simplified material volume under the FSW tool and demonstrated -qualitatively- that the formation of IMCs could be predicted through the use of a phase diagram, provided that the tool offset was carefully controlled. However, as Mishra et al. approach [2.71] took no account of the thermo-mechanical effect during the FSW process, the ability to accurately predict the IMCs formation is questioned. Additionally, the material volume beneath the FSW tool is known to form a simple parallelepiped shape which was not accounted for [2.71]. More recently, Shailesh et al. [2.72] advanced the work of Mishra et al. [2.71] by assuming a cylindrical material volume under the FSW tool. Although the derived equations of Shailesh et al. [2.72] were valid and logically accepted to represent the material volume under the FSW tool, there was again an absence of accurate thermo-mechanical data to fully support their method.

In addition to the above-mentioned predictive approaches, some attempts have been conducted to comprehend the formation of IMCs and their impact on the joint's mechanical strength. Ouyang et al. [2.8] studied the microstructural evolution during FSW of AA6061-T6 to copper, where the dissimilar weld nugget exhibited several IMCs, such as Al_2Cu, AlCu and Al_4Cu_9. In this work [2.8], thermocouples were positioned at 2 mm, 4 mm, and 6 mm from the pin area and towards the aluminium (the retreating side (RS)). It was found [2.8] that the measured temperature of the AA6061 reached 580°C, which is greater than the melting temperature at the eutectic composition of an Al-Cu binary alloy. The authors [2.8] proposed that these IMCs evolved on the basis of two different phenomena, these being the constitutional liquation that governs the formation of aluminium-rich phases (Al/Al_2Cu eutectics, Al_2Cu and AlCu), which is due to their solidified morphology, and the relatively lower melting temperature of aluminium-rich phases. In contrast, the solid-state diffusion phenomenon was claimed to control the formation of the copper-rich IMCs in the weld zone (Cu(Al) and Al_4Cu_9). The latter phenomena can be attributed to the thermo-mechanical effect of FSW at the weld nugget, where the melting temperature of Al_4Cu_9 (1030°C) is higher than the peak temperature during FSW. It was concluded [2.8] that the existence of these brittle IMCs created a high level of disparity in the mechanical properties of the weld. In their work [2.8], there was an absence of the resultant high strain rate effect in the evolution of the relatively lower melting temperature IMCs (Al_2Cu and AlCu), as the thermo-mechanical effect of FSW can also explain the formation of these IMCs.

More recently, Galvao et al. [2.73] claimed that the IMCs formation in dissimilar FSW of aluminium to copper can only be explained by the thermo-mechanically activated solid state diffusion phenomenon. Unlike the approach of Ouyang et al. [2.8], Galvao et al. [2.73], proved the absence of solidification structures in both the aluminium and copper rich sides, and reported that the resultant high strain rate during the FSW process facilitates the formation of Al_2Cu, AlCu and Al_4Cu_9, an approach that has also been supported in other recent publications [2.34-2.37]. Further, Xue et al. [2.74] and Galvao et al. [2.75], investigated the influence of process parameters on the evolution of IMCs during FSW of aluminium to copper. It has been claimed [2.74, 2.75] that the tool rotational speed to the welding speed (ω/v ratio) has a significant effect on the IMCs formation and subsequently the joint mechanical strength. Other published work [2.37, 2.76] demonstrated that the thin and continuous IMCs layer in aluminium to copper could significantly improves the mechanical properties of the joint in which the predominant IMCs in the weld nugget were Al_2Cu and Al_4Cu_9, and that their presence resulted in a tensile strength equating to 80% of the aluminium base alloy.

An additional key factor that affects the joint mechanical properties in FSW of aluminium to copper is the placement of each workpiece [2.19–2.77]. Numerous studies noted that defect-free butt joints between aluminium to copper could be produced by placing the harder material (copper) on the AS [2.73–2.81]. According to these studies [2.73–2.81], placing the copper on the AS leads to suitable mixing between aluminium and copper since it is easier for the softer material (aluminium) to flow. However, tool offsetting towards either the retreating or advancing side was usually required to achieve defect-free joints [2.70]. The various ranges reported for the tool offsets resulted in this method being impractical for industrial use.

In contrast, other researchers reported that defect-free joints can be obtained by placing the softer material (aluminium) on the AS [2.17–2.82]. For example, Tan et al. [2.82], successfully joined 3 mm thick 5A02 aluminium to commercially pure copper by placing the aluminium on the AS and negligible tool offset towards the advancing/retreating sides. A tool rotational speed of 1100 rpm and a 20 mm/min tool traverse speed were the welding parameters that resulted in high UTS of 130 MPa (75.6% joint efficiency relative to the aluminium base metal). According to their findings [2.82], the presence of a thin and continuous layer of IMCs was observed at the aluminium/copper interface. The formation of these IMCs was also detected inside the stir zone and resulted in an inhomogeneous hardness distribution across the weld. Additionally, Tan et al. [2.82] argued that, placing the softer material (aluminium) on the AS facilitates the formation of a composite-like structure at the stir zone (as shown in Fig. 2.3). This is a structure which was found to considerably enhancing the joint mechanical strength. Further, the authors [2.82] noted a development of channel defect at higher tool traverse speed of 40 mm/min.

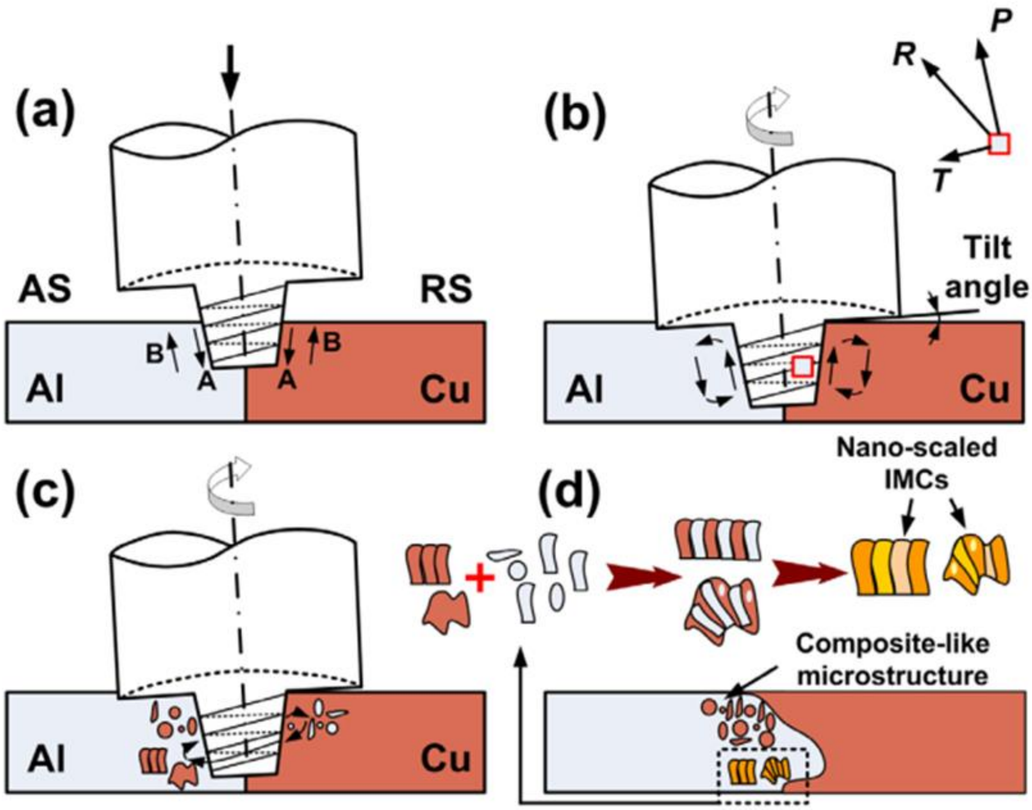

Fig. 2.3 Composite-like structure and IMCs Formation mechanism during FSW: (a) tool was plunged into workpiece, (b) material flowed when tool rotated, (c) fragments and particles were transported into each side and (d) formation of composite-like structure and nano-scaled microstructure [2.82].

Likewise, Karrar et al. [2.17], reported on the advantages of placing the softer material on the AS. Their work established the validity of placing the softer material (AA5083) on the AS to achieve relatively higher mechanical properties, i.e., 94.8% joint efficiency, which agreed with the work of Tan et al. [2.82]. Although Karrar et al. [2.17] qualitatively identified the direct benefit of the combined presence of IMCs and the composite-like microstructure on the joint mechanical strength, there was a lack in quantifying these IMCs as well as predicting their presence relative to the FSW parameters, i.e. ω/v ratio. Overall, researchers [2.17, 2.82] have not definitively demonstrated the negative or positive role played by the IMCs particles.

2.6. Dissimilar FSW of aluminium alloys to magnesium

It is vital in some engineering applications to replace aluminium alloys with certain magnesium alloys, since the latter provides efficient cost and weight reduction benefits compared to the former, while maintaining similar electrical and thermal properties [2.28, 2.83]. Section 1.5 of this thesis highlighted the limitations of fusion welding processes in achieving defect-free joints of dissimilar metals. However, it is important to note that dissimilar fusion welding of aluminium to magnesium alloys commonly results in relatively larger brittle IMCs and coarse grains at the weldment zone. In addition, the reflectivity of aluminium and magnesium alloys poses a challenge for certain welding processes such as electron beam welding (EBW), laser beam welding (LBW), and gas tungsten arc welding (GTAW) [2.16]. This is due to the lower energy efficiency of LBW, the evaporation of magnesium and zinc during EBW, and the wider weld seam resulting from the high heat exchange rate in GTAW [2.83].

The FSW technology has been expanded to include dissimilar joints of aluminium to magnesium alloys, as it has shown outstanding capability in joining a wide spectrum of hard-to-weld metals and alloys and can overcome the aforementioned limitations of conventional welding processes. Luo et al. [2.84] emphasised that tool offset is necessary to achieve defect-free joints, as cracks were consistently observed at zero mm tool offset. In a subsequent study, Khodir et al. [2.85] argued that defect-free joints of dissimilar AA2024-T3 to AZ31 magnesium alloy can only be obtained by placing the harder material (AA2024-T3) on the AS. However, Kostka et al. [2.86], refuted this claim in their work [2.86], producing defect-free joints of AA6064 and AZ31 magnesium alloy by positioning the softer material (AZ31B) on the AS.

Furthermore, dissimilar FSW of aluminium to magnesium alloys is also affected by other welding parameters, including tool rotational speed, tool welding speed, and tool shoulder design such as the ratio of the diameter of the welding tool (D) to the thickness of the workpiece (T) (D/T ratio) [2.16, 2.65]. Fig. 2.4 demonstrates the significant influence of the ω/v ratio on the mechanical strength of dissimilar butt welds of aluminium to magnesium alloys [2.87]. It is important to note that a wider process window can be achieved by placing the softer material (magnesium) on the AS and offsetting the tool towards the magnesium side. In contrast to FSW of aluminium to aluminium or magnesium to magnesium, a D/T ratio of 3 is not suitable for dissimilar FSW of aluminium to magnesium alloys. Malarvizhi et al. [2.28] reported that joint efficiency of up to 89% (192 MPa tensile strength) can be achieved with a 3.5 D/T ratio. The authors [2.28] argued that the relatively high D/T ratio increases the frictional heat, which in turn stimulates the dynamic recrystallisation rate, resulting in a composite-like microstructure and higher mechanical performance.

On the other hand, it is widely acknowledged that the combination of low diffusion rate and chemical reaction during FSW of dissimilar aluminium to magnesium alloys can improve joint mechanical strength by preventing the formation of brittle IMCs, which cannot be avoided with conventional fusion processes [2.16-2.29]. Similarly, other researchers have noted that the relatively lower joining temperature profile during FSW initially limits the formation of IMCs, and subsequently ensures a homogeneous distribution of the evolved IMCs due to the dual action of high strain rate and severe plastic deformation at the weldment zones [2.16, 2.29, and 2.87].

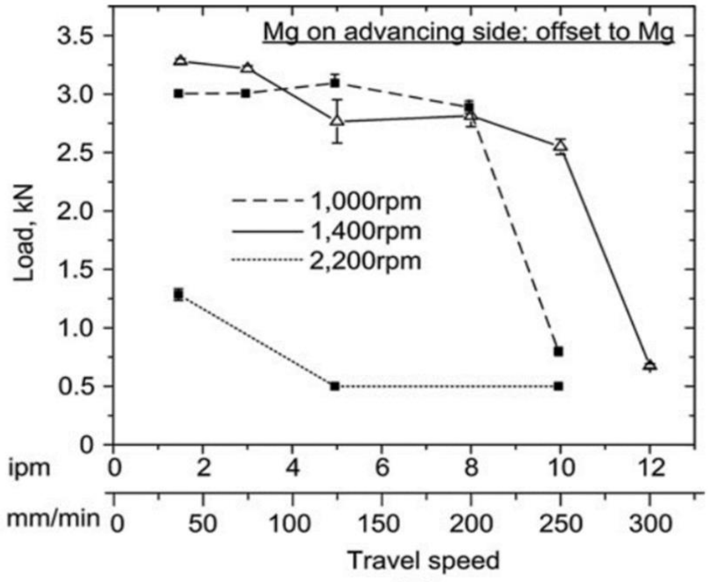

(a)

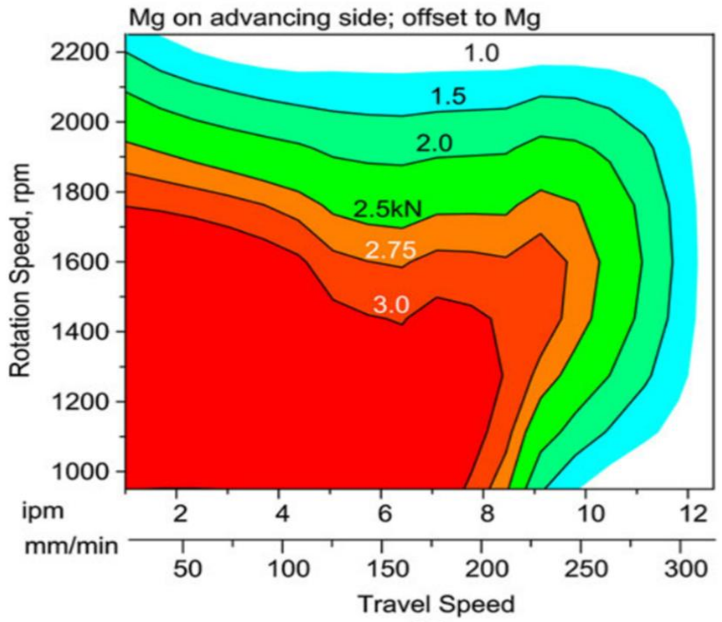

(b)

*ipm≡ inches per minute. *Load (kN)≡ tensile load or tensile force.

Fig. 2.4 The influence (ω/v) of on the joint mechanical strength in dissimilar FSW of aluminium to magnesium (AS) and offset to magnesium side. (a) plot and (b) contour relationship [2.87].

2.7. Modelling of the FSW process

Since the inception of FSW technology in 1991, researchers have made significant efforts to develop a numerical understanding of the thermo-mechanical phenomenon of the FSW process, these efforts have been in addition to ongoing experimental investigations [2.1-2.90]. These investigations have led to the development of various modelling techniques and the application of different computational modelling approaches to accurately explain the mechanisms that govern material behaviour during the FSW process. Ultimately, these efforts aim to reduce the cost of experimental work.

Initially, the primary focus of simulating the FSW process was placed on thermal models, where researchers [2.91-2.93] aimed to elucidate the heat transfer and thermal behaviour of the process. These thermal models could only predict the temperature distribution at different FSW zones. For example, Song et al. [2.91] developed a 3-D heat transfer FSW model, considering a moving coordinate system. In their model, the analytical finite difference method (FDM) was used to numerically predict Navier Stock's energy equations. While the heat transfer during the FSW process was reasonably well simulated, Song et al.'s. [2.91] model was unable to calculate the temperature distribution around the FSW zones.

Cho et al. [2.92] made advancements on Song et al.'s [2.91] model by presenting a 3D model capable of predicting both thermal gradients and material flow during the FSW process. The ANSYS FLUENT computational fluid dynamics software was employed to run the model [2.92]. The FSW workpiece material - aluminium - was considered as an incompressible non-Newtonian fluid, where convection/conduction boundary conditions were applied along with temperature-dependent properties of the workpiece.

In their work, Cho et al. [2.92] assumed that plastic heat generation, which is the heat generated by the frictional forces between the FSW tool and the workpiece, is mainly originated from the sticking boundary conditions between the FSW tool and the workpiece.

Material flow is widely recognised as a crucial factor that affects FSW joint properties [2.90]. Several parameters, including tool design, can affect and complicate material flow during the FSW process. For instance, a threaded conical tool pin can stimulate the stirring process and decrease the applied load. Material flow during the FSW process is highly dependent on the nature of the workpiece material (including its thermal and physical properties), and it, in turn, affects the selection of optimum welding parameters. Numerical visualisation of material flow during the FSW process has always been considered valid to optimise FSW tool design and achieve high joint performance [2.43, 2.63]. In a pioneering study, Colegrove et al. [2.93], successfully visualised material flow during the FSW process through a 3-D computational fluid dynamics (CFD) model, considering a simple shoulder and threaded pin tool profile. Colegrove et al. [2.93] aimed to comprehend the impact of various FSW parameters on the material flow around a complex threaded pin FSW tool. It was found [2.93] that the plasticised material that flowed in line with the deformation zone was swept around the RS of the pin. Colegrove et al. [2.93] also noted that the amount of this swept plasticised material around the pin increases at a location close to the shoulder. However, it was observed [2.93] that the deformation zone size was relatively larger than the experimentally observed zone size, indicating a limitation of this model to fully visualise the thermo-mechanical phenomenon during the FSW process.

Although the numerical models mentioned above [2.91–2.93] were valid in visualising material flow and/or predicting the temperature profile around FSW zones, there was a lack of evaluation of stress and strain during the FSW process and, therefore, the resultant reaction forces on the tool, such as the axial force. To overcome the limitations of the thermal models, researchers [2.94, 2.95] developed thermo-mechanical models of the FSW process. These models were based on two methods: (a) ignoring metal flow for non-flow-based models, or (b) assuming a flow-based thermomechanical modelling approach, such as Arbitrary Lagrangian-Eulerian (ALE) models.

Non-flow-based FSW models are capable of predicting both the residual stresses resulting from thermal strain and the applied axial force - a key parameter that has been argued to influence the mechanical performance of FSW joints [2.91, 2.94]. For instance, Rajesh et al [2.94] successfully calculated the resultant residual stresses during FSW by assuming a 3-D thermo-mechanical analytical model of the stir zone around the tool pin. In their model [2.94], the force due to friction was neglected at the steady state of the FSW process, an assumption attributed to the fact that the plasticised material in the stir zone is plastically deformed rather than inducing friction on the FSW tool. The authors [2.94] argued that the calculated longitudinal residual stress component could reach up to 24% higher than the yield strength of the parent metal. Additionally, Rajesh et al. [2.94] claimed a symmetrical pattern of the residual stress distribution along the FSW sides, i.e., AS and RS sides. This pattern was attributed to the equivalent symmetrical pattern of the plasticised material along the FSW joint sides.

In contrast, Buffa et al. [2.95] developed a robust 3-D Lagrangian implicit finite element model (FEM) of the FSW process, based on a combined rigid visco-plastic nature between the workpiece and the FSW tool. This continuum-based model was validated using acquired experimental data of the FSW tool forces and workpiece temperature. Unlike previous studies [2.94], Buffa et al. [2.95] reported asymmetric thermal behaviour during the FSW process, along with a detailed description of FSW tool forces at different welding parameters. It was concluded [2.95] that the temperature distribution around the FSW tool implies an asymmetric strain distribution around the stir zone. Additionally, it was found [2.95] that temperature and the resultant thermal strain decrease at different weldment zones by increasing the welding speed. Furthermore, Buffa et al. [2.95] noted that the asymmetric behaviour of material flow around the stir zone was dominantly affected by the tool rotational and welding speeds.

Nevertheless, accurately formulating the interaction between the rotating FSW tool and the workpiece remained a challenge. It has been widely emphasised that a fully coupled thermo-mechanical finite element approach should be applied to numerically model the FSW process [2.96]. This technique was adopted by Grujicic et al. [2.97], who developed an Arbitrary Lagrangian Eulerian (ALE) model that was not only robust in simulating the FSW process, but also capable of overcoming the severe mesh distortion that limits the previously mentioned FSW models [2.91–2.95]. In their model [2.97], the adaptive remeshing technique was applied to fully capture the free surfaces material and the material evolution in the weldment zone. Moreover, the modified Johnson-Cook material model was used to formulate the variation in dynamic recrystallisation relative to the plasticised material around the stir zone. Overall, Grujicic et al. [2.97] ALE-based predictive model showed good agreement with the experimental results.

The coupled Eulerian Lagrangian (CEL) technique has recently been widely reported as the most appropriate modelling solution for the FSW process [2.98]. Unlike the ALE models which require continuous application of the remeshing technique, the CEL technique captures severe plastic deformation by avoiding the distortion of the mesh during the process, as the material flows through a stationary mesh in the Eulerian domain. Using the Abaqus Explicit Solver environment, Al-Badour et al. [2.99] presented a CEL FSW model capable of predicting the welding parameters that are more likely to generate void defects during FSW of aluminium alloys (Fig. 2.5). In their model [2.99], the FSW workpiece was considered as an Eulerian domain where the FSW tool was modelled as a Lagrangian domain. The Coulomb's friction contact model was assumed to formulate the interaction between the Lagrangian (FSW tool) and the Eulerian (workpiece) domains. To model the plasticity of the workpiece material, Johnson-Cook’s constitutive model was employed, whereby the material flow/yield stress was described as a function of plastic strain, strain rate, and temperature profile. It was found [2.99] that the void formation, considering the CEL model, is highly affected by the applied coefficient of friction, with lower friction coefficients resulting in a higher tendency for void formation. The authors [2.99] also reported that a force control method at lower tool welding speeds results in relatively smaller void defects and wider TMAZ, a condition that leads to higher joint mechanical performance.

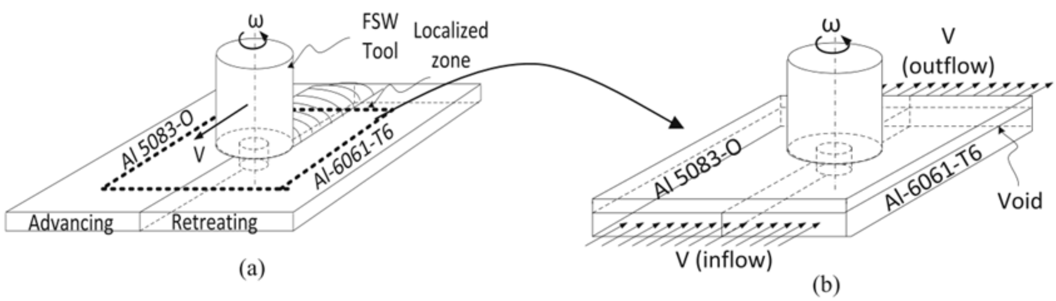

Fig. 2.5 (a) The CEL schematic representation of FSW of dissimilar AA6061-T6 to AA5083-O butt joint. (b) localised FSW zone idealisation model [2.99].

More recently, Karrar et al. [2.42] further improved on the CEL method by introducing a novel approach in which the FSW tool rotates and traverses along the Eulerian domain instead of the in/out flow model proposed by Al-Badour et al. [2.99]. The authors [2.42] incorporated the modified friction law described by Shokri et al. [2.100] to model the interaction between the Lagrangian (tool) and Eulerian (aluminium and copper) domains, which can involve both sticking and slipping conditions.

2.8. FSW tool Design and process parameters

2.8.1. FSW tool profile effect

The FSW tool design has received increasing attention from researchers [2.1, 2.10, 2.18] since the introduction of the solid-state joining process. This is largely due to the crucial role that the FSW tool design plays in achieving better joint efficiency. It has been widely acknowledged that the upper part of the FSW tool (shoulder) not only generates enough frictional heat to plasticise the workpiece material, but also ensures the necessary forging force for FSW joint consolidation [2.9, 2.101]. Conversely, the FSW tool pin profile stirs the plasticised material and enhances the mixing process [2.10, 2.96]. In general, FSW tool design can be divided into two main aspects: (a) the FSW joint type and (b) the thickness of the workpiece [2.101]. Table 2.3 outlines the functions and effects of various FSW tool feature parameters on joint configuration [2.18].

Table 2.3 Functions and impacts of FSW tool features on joint configuration

Parameter	Function	Dimensional impact
Shoulder feature	Stirring, and mixing the plasticised materials in the joint surface.	The complex the shoulder feature the better the material flow.
Shoulder diameter	Heat generation, material swept, and plastic deformation.	The amount of heat generated during the FSW process increases with an increase in the shoulder diameter.
Shoulder angle	Forging and joint consolidation.	A concave shoulder angle promotes material accumulation, whereas a convex shoulder angle promotes flash formation.
Pin feature	Stirring and mixing the swept material around the pin.	The complex the pin features the better the material flow.
Pin angle	Swept the plasticised material along the workpiece thickness.	Material flow is enhanced by increasing the pin angle.
Pin diameter	Partially, generating heat and thus, ensures the plasticised flow.	Material flow is decreased by increasing the pin diameter.
Pin length	Forging and stirring action.	The forging and stirring actions are improved by increasing the pin length, thereby reducing the tendency for defect formation.

Scialpi et.al [2.102] investigated the impact of different shoulder designs on the mechanical strength of FSW butt joints of 1.5 mm thick AA6082-T6 aluminium alloy. The study [2.102] examined three shoulder designs (Fig. 2.6), including fillet, scroll/fillet, and cavity/fillet, and was conducted at 1800 rpm and 460 mm/min tool rotational and welding speed, respectively. It was revealed [2.102] that the cavity/fillet shoulder design was the most appropriate geometry for the FSW butt joint, as it produced better crown -the raised portion in the centre of the welded joint- and root quality. While the three designs showed no significant differences in terms of joint transverse and tensile strengths, the cavity/fillet shoulder design was found to enhance longitudinal tensile strength [2.102]. This difference was attributed to the dual action of the cavity/fillet geometry, which improved joint strength and elongation. Therefore, the study [2.102] highlighted the importance of FSW tools with fillet and cavity shoulder designs for producing better joint crown surface and higher longitudinal strength.

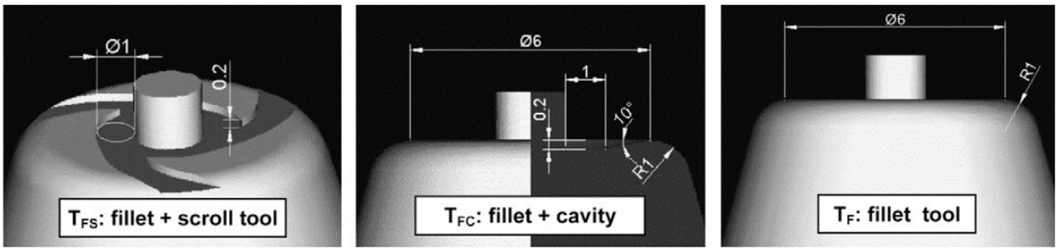

Fig. 2.6 Tools employed for the experimentation and their primary dimensions in mm [2.102].

A recent study by Elangovan et al. [2.103] comprehensively investigates the effects of FSW tool shoulder diameter and pin profile on the formation of the friction stir weldment zones of aluminium AA6061 alloy. The study [2.103] considers three different shoulder designs and five unique tool pin profiles (straight cylindrical, tapered cylindrical, threaded cylindrical, triangle, and square). The produced FSW joints are characterised to observe the shape, height, and width of the weldment process zones (SZ, HAZ, and TMAZ). The authors [2.103] conclude that the shape of the weldment zones and the production of defect-free joints can be attributed to the combined effects of the FSW tool shoulder diameter and pin profile.

In general, it is widely acknowledged that the material flow during the FSW process is primarily influenced by the tool pin profile. For instance, Lorrain et al. [2.104] conducted a study on the influence of FSW pin shape on the material flow path during the FSW process by considering two different pin profiles; feature and featureless (threaded and unthreaded) cylindrical and tapered pin profiles. In their investigation [2.104], the FSW tool shoulder was kept the same for the two designs (concave type), and a 2.5° tilt angle was applied to ensure an additional tool compression force on the workpiece. To ascertain the flow patterns, both cross-sectional and longitudinal sections of the welds were meticulously examined. This investigation was enhanced through the application of material markers (MM), which allowed for a more precise observation of the material's movement. It's important to note that these flow pattern differences were analysed through experimental means rather than numerical simulations, providing direct empirical evidence of the effects of pin geometry on material flow during the FSW process. The authors [2.104] suggested that the material flow during the FSW process is less affected by the pin feature, with threaded and unthreaded tool pins exhibiting almost similar material flow behaviour around the weldment zones.

2.8.2. The influence of FSW process parameters

Overall, the parameters of the FSW process can be divided into two categories: independent (controlled) and dependent parameters. The controlled parameters mainly refer to the FSW tool conditions, such as tool rotational and welding speeds, while the dependent factors include the applied forces (forging forces), torque, and resultant temperature. In more complex configurations, such as robotic FSW, the axial (forging) force can also be considered an independent factor [2.1-2.105]. Technically, there are two common approaches to implementing the FSW process: force control method and torque control method. The latter approach (torque control) is widely recommended during the process for its robust sensitivity to the plunging depth [2.106].

Mishra et al. [2.107] proposed a conceptual model that qualitatively describes the correlation between the independent and dependent FSW process parameters and their influence on heat generation and dissipation. The primary objective of the model was to distinguish between the contributions of plastic deformation and friction work to the heat generation process. Fig. 2.7 illustrates the effect of the controlled parameter, FSW tool rotational speed, on various FSW dependent parameters. The model also shed light on the role of friction coefficient in the different process parameters.

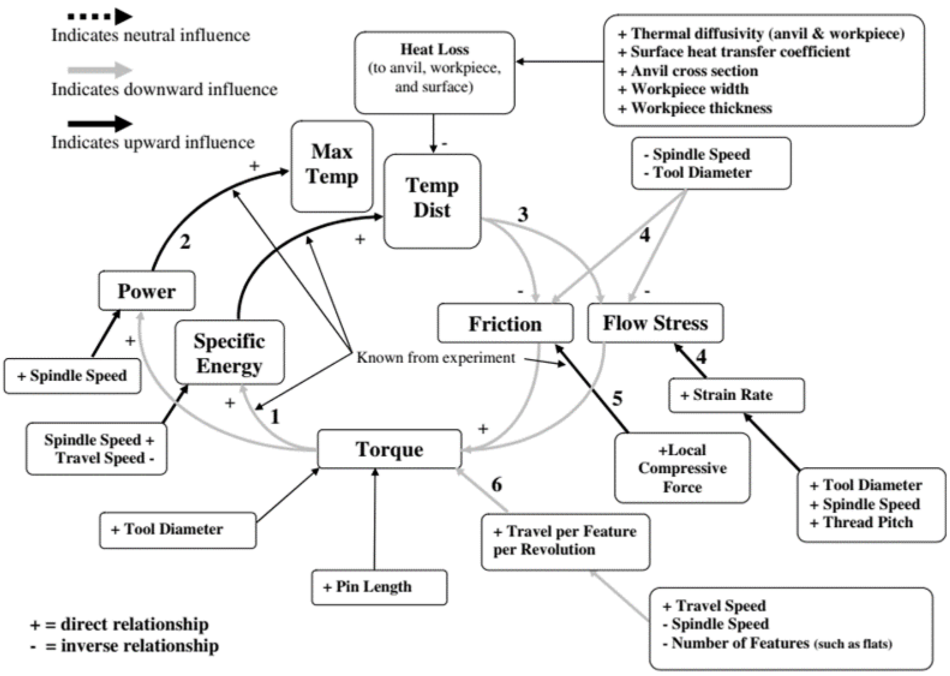

Fig. 2.7 The relationships between FSW variables and the tool rotational speed [2.107].

Researchers [2.108-2.110] have further developed Mishra et al.'s [2.107] conceptual model by investigating the effect of FSW process parameters on joint mechanical performance, including UTS, microhardness, fracture toughness, fatigue crack growth rate, and residual stresses. For example, Cederqvist et al. [2.108] have successfully identified the optimal process parameters that result in high mechanical performance of dissimilar AA2024-T3 to AA7075-T6 FSW butt joints. Their model used a robust optimisation approach based on defect detection using non-destructive testing methods such as ultrasonic and radiography.

Other studies [2.109, 2.110] have investigated the effect of controlled FSW variables on different FSW dependent process parameters, such as axial force, torque, transverse force, longitudinal force, and temperature distribution. It has been widely reported that increasing the tool rotational speed results in higher temperature and lower applied forces [2.12-2.34]. Conversely, increasing the tool welding speed leads to lower temperature and higher applied loads, which is attributed to the material plasticisation at higher heat input [2.10-2.101]. However, there is still a lack of understanding regarding the combined impact of tool rotational and welding speeds on FSW joint mechanical performance. Higher rotational speed can impair the joint mechanical strength within certain ranges of tool welding speeds, and a similar effect can also be observed on joint fatigue life [2.12].

In a related study, Gharacheh et al. [2.111] examined the joint macro/microstructure and mechanical performance of AZ31B magnesium alloy FSW, focusing on the combined effect of tool rotational and welding speed, specifically the ω/v ratio. The authors [2.111] found that defect-free joints were obtained at relatively high ω/v ratios, which resulted in a wider weld nugget zone. However, they also observed that the presence of a magnesium oxide layer between the SZ and TMAZ severely impaired the mechanical strength of the FSW joint.

2.8.3. Defect formation during the FSW process

Detecting defects in a produced FSW joint is a crucial inspection factor, which involves identifying both flow and geometric defect types across the joint configuration. Improper plunging depth may cause geometric defect types, such as root defects, due to the lack of penetration. Flow defects, on the other hand, may result from either excessive or insufficient heat input [2.27-2.112]. Excessive heat input can cause sticky contact conditions between the FSW tool and the workpiece, leading to excessive material flow and the development of undesirable defects, such as surface flash, surface galling, and nugget collapse [2.30, 2.113]. Insufficient heat input, however, can impede the flow of plasticised material by imposing slip conditions at the interface zones, resulting in several flow defects, including lack of fill, wormholes, and lack of consolidation defects on the AS [2.98, 2.114]. The most common reported FSW defect types are summarised in Fig. 2.8.

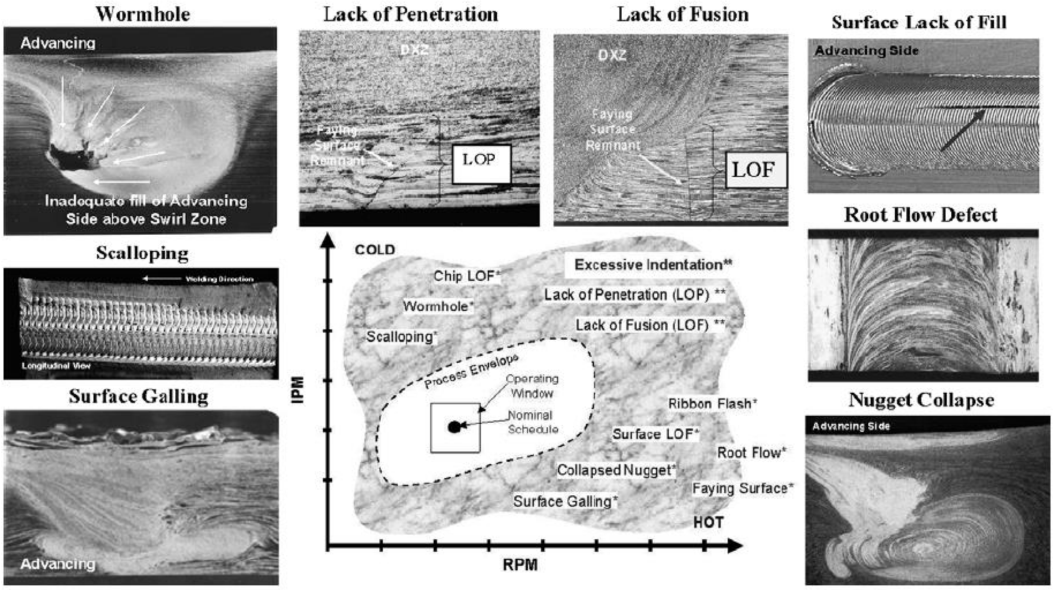

Fig. 2.8 Characteristic friction stir welds defect types [2.115].

The wide variety of FSW defects has led to a debate over whether this relatively new joining process can completely replace traditional fusion processes. This debate is largely due to the lack of robust industrial standards and specifications for the FSW process [2.114-2.116]. To address this issue, the American Welding Society (AWS) has attempted to establish consistent specifications for FSW of aluminium alloys that are commonly used in aerospace applications [2.114]. The American Bureau of Shipping (ABS) has further advanced this effort by publishing a peer-reviewed FSW bulletin for aluminium alloys [2.116]. However, most FSW user guide specifications are currently applied internally and individually for specific FSW joint configurations.

2.8.4. FSW optimisation process

Achieving defect-free joints and high mechanical performance can only be possible through the optimisation of FSW process parameters, by considering the key factors that lead to better joint mechanical strength. Optimum weld parameters can be determined by evaluating the macro/microstructural FSW zones, which can be further supported by utilising various mechanical testing methods such as hardness, tensile strength, shear strength, and fatigue life performance [2.34-2.117].

Furthermore, optimising the FSW process requires a comprehensive analysis of multiple input parameters in various directions. The FSW tool design, for instance, must consider tool dimensions, tool profile, tool tilt angle, required fixture position, and machine rigidity. To reduce the cost of the optimisation process, researchers have utilised various analytical methods to initially investigate the quality of FSW joints at different process parameters. [2.26-2.96].

Analytical models that consider the FSW process parameters typically focus on two primary factors: the tool rotational speed and the tool welding speed. A process window for the FSW can be identified by varying the ω/ν ratio, as shown in Fig. 2.9. It has been reported [2.118] that a wider range of optimal process window can be achieved with higher plunging forces.

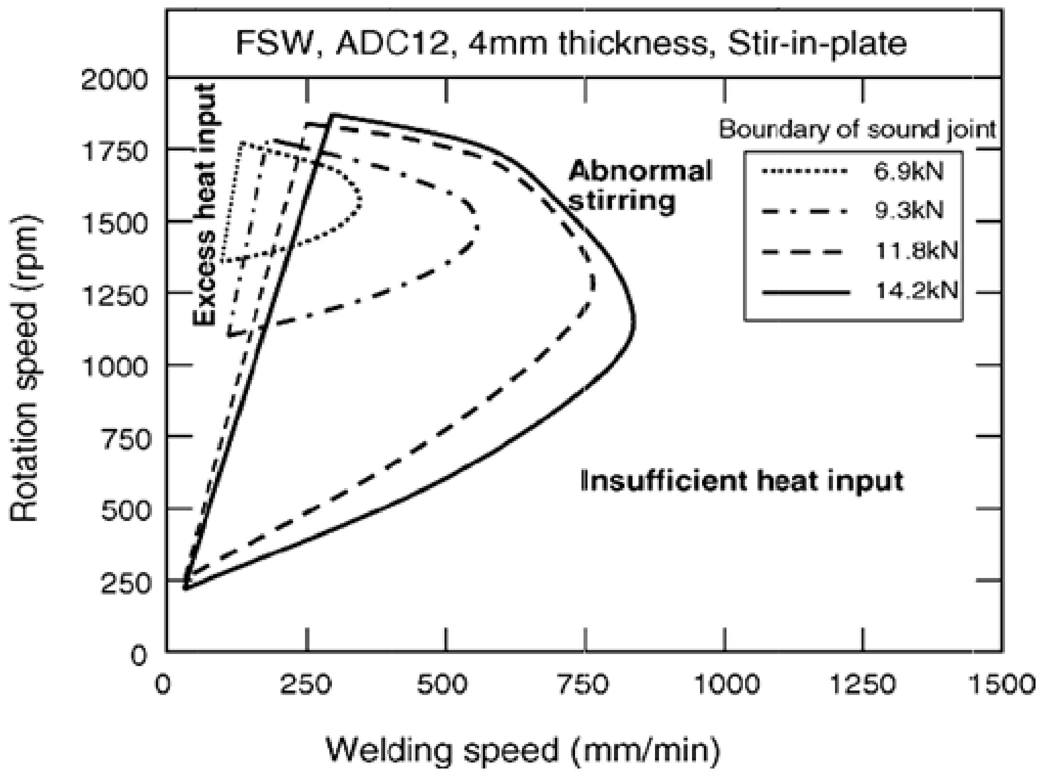

Fig. 2.9 An instance of the range of optimal FSW conditions corresponding to each tool plunging force, as developed for the aluminium die casting alloy [2.118].

Overall, optimising the FSW process parameters is crucial for predicting various FSW output variables such as temperature profile, resultant plastic strain, strain rate, and residual stresses. For example, Kim et al. [2.118] and Zhang et al. [2. 119] were able to predict joint plastic strain by optimising the tool welding speed. According to Kim et al. [2.118], joint plastic strain is inversely proportional to the tool welding speed, where an increase in welding speed results in joint volumetric defects (voids) due to low plastic strain. However, a FSW optimisation process using finite element (FE) methods is computationally expensive and, in most cases, numerical results cannot be solely guaranteed without robustly validated experimental results.

2.9. Current status

The previous literature survey emphasises the scarcity of utilising the FSW technology as an alternative approach for creating dissimilar aluminium-to-copper or aluminium-to-magnesium alloy joints. In the present study, the FSW process has been refined to produce defect-free butt joints for aluminium-to-copper and aluminium-to-magnesium alloys. Finite element models have also been established to simulate the FSW process and examine the impact of its parameters on weld characteristics. Additionally, analytical models have been employed to enhance the FSW optimisation process and attain superior joint mechanical strength.

Although placing the softer material on the AS offers potential benefits, there has been limited research focusing on this configuration. Moreover, the combined relationship between the IMCs microstructure and mechanical properties necessitates additional investigations. In this study, the effect of tool rotation and travel speed on dissimilar metals joint quality has been assessed with the softer material on the AS, without introducing tool offset and its related complexities. Utilising this setup, various combinations of rotational and traverse speeds were examined to investigate the relationship between microstructure and mechanical properties.

Furthermore, this research aims to address the knowledge gap regarding IMCs evolution during the FSW process and provide a quantitative analysis of IMCs formation within the weldment zones. By systematically establishing these factors, this work enhances the current understanding and provides a robust framework for achieving defect-free FSW joints of dissimilar materials. The absence of tool offset in this approach simplifies the FSW process without compromising joint integrity, offering a significant stride forward in both academic and practical applications of FSW technology.

Ultimately, this study seeks to achieve superior and consistent weld quality by controlling the formation of IMCs during the FSW process for dissimilar materials. The preceding review demonstrated that the formation of IMCs during FSW is inherently dependent on a thermo-mechanical phenomenon, influenced by the combined effects of temperature and plastic deformation. As a result, predicting the evolution of IMCs during FSW of dissimilar materials necessitates the use of precise numerical thermo-mechanical data in conjunction with phase diagram information. Therefore, a novel approach for accurately predicting the formation of IMCs in FSW of dissimilar materials is presented and examined throughout this research.

The coupled Eulerian Lagrangian (CEL) model is utilised to simulate the FSW process. As previously stated within this chapter, and due to the multiple layers of complexity in formulating the FSW process, the CEL model approach is regarded as the most suitable modelling solution. The CEL model accounts for extreme plastic deformation by avoiding mesh distortion during the FSW process, wherein the material flows through a stationary mesh in the Eulerian domain. Moreover, the modified friction law has also been taken into account, coupling the interaction between the Lagrangian (tool) and Eulerian (workpiece) domains, while incorporating both sticking and slipping conditions.

It is worth noting that this numerical work is considered alongside the primary goal of identifying the process parameters for successful dissimilar FSW joints of aluminium to copper to introduce a novel approach for predicting the IMCs formation. This innovative method combines experimental data with the numerical modelling provided by the CEL approach. While the experimental work establishes the parameters for defect-free welding, the numerical model offers predictions on IMC formation, enhancing the depth of the research with its predictive insights.

This combination of experimental and numerical work not only confirms the practical findings but also extends the scope of the study, providing a broader understanding of the effects of the FSW parameters on the development of IMCs. Thus, the research contributes a comprehensive view of the FSW process, from setting the right parameters to understanding the resulting material behaviour.

2.10. References

[2.1] R. S. Mishra and Z. Y. Ma, "Friction stir welding and processing," Mater. Sci. Eng. R Reports, vol. 50, no. 1–2, pp. 1–78, Aug. 2005. https://doi.org/10.1016/j.mser.2005.07.001.

[2.2] L. E. Murr, "A review of FSW research on dissimilar metal and alloy systems," J. Mater. Eng. Perform., vol. 19, no. 8, pp. 1071–1089, Feb. 2010. https://doi.10.1007/s11665-010-9598-0.

[2.3] I. Galvão, R. M. Leal, A. Loureiro, and D. M. Rodrigues, "Material flow in heterogeneous friction stir welding of aluminium and copper thin sheets," Sci. Technol. Weld. Join., vol. 15, no. 8, pp. 654–660, 2010. https://doi.org/10.1179/136217110X12785889550109.

[2.4] K.-T. Huang, T.-S. Lui, and L.-H. Chen, "Effect of microstructural feature on the deterioration of tensile properties and vibration fracture resistance of FSW 5052-

H34 alloy," Mater. Trans., vol. 45, no. 11, pp. 3216–3222, 2004. https://doi.org/10.2320/matertrans.45.3216.

[2.5] V. Soundararajan, "Thermo-mechanical and microstructural issues in joining similar and dissimalr metals by friction stir welding," PhD Thesis, Southern Methodist University, December 9, 2006.

[2.6] C. B. Fuller, "Friction stir tooling: tool materials and designs," Frict. Stir Weld. Process., pp. 7–35, 2007.

[2.7] H. S. Bang, H. S. Bang, G. H. Jeon, I. H. Oh, and C. S. Ro, "Gas tungsten arc welding assisted hybrid friction stir welding of dissimilar materials Al6061-T6 aluminum alloy and STS304 stainless steel," Mater. Des., vol. 37, pp. 48–55, 2012. https://doi.org/10.1016/j.matdes.2011.12.018.

[2.8] J. Ouyang, E. Yarrapareddy, and R. Kovacevic, "Microstructural evolution in the friction stir welded 6061 aluminum alloy (T6-temper condition) to copper," J. Mater. Process. Technol., vol. 172, no. 1, pp. 110–122, Feb. 2006. https://doi.org/10.1016/j.jmatprotec.2005.09.013.

[2.9] D. J. Franke, J. D. Morrow, M. R. Zinn, N. A. Duffie, and F. E. Pfefferkorn, "Experimental determination of the effective viscosity of plasticized aluminum alloy 6061-T6 during friction stir welding," Procedia Manuf., vol. 10, pp. 218–231, 2017. https://doi.org/10.1016/j.promfg.2017.07.050.

[2.10] S.-W. Kang and B.-S. Jang, "Friction stir welding analysis based on equivalent strain method using neural networks," J. Ocean Eng. Technol., vol. 28, no. 5, pp. 452–465, 2014.

[2.11] S. Tan, F. Zheng, J. Chen, J. Han, Y. Wu, and L. Peng, "Effects of process parameters on microstructure and mechanical properties of friction stir lap linear welded 6061 aluminum alloy to NZ30K magnesium alloy," J. Magnes. Alloy., vol. 5, no. 1, pp. 56–63, 2017. https://doi.org/10.1016/j.jma.2016.11.005.

[2.12] R. I. Rodriguez, J. B. Jordon, P. G. Allison, T. Rushing, and L. Garcia, "Low-cycle fatigue of dissimilar friction stir welded aluminum alloys," Mater. Sci. Eng. A, vol. 654, pp. 236–248, 2016. https://doi.org/10.1016/j.msea.2015.11.075.

[2.13] H. Lombard, D. G. Hattingh, a. Steuwer, and M. N. James, "Optimising FSW process parameters to minimise defects and maximise fatigue life in 5083-H321 aluminium alloy," Eng. Fract. Mech., vol. 75, no. 3–4, pp. 341–354, Feb. 2008. https://doi.org/10.1016/j.engfracmech.2007.01.026.

[2.14] N. Sharma, Z. A. Khan, and A. N. Siddiquee, "Friction stir welding of aluminum to copper—An overview," Trans. Nonferrous Met. Soc. China (English Ed., vol. 27, no. 10, pp. 2113–2136, 2017. https://doi.org/10.1016/S1003-6326(17)60238-3.

[2.15] T. Peat, A. Galloway, A. Toumpis, P. McNutt, and N. Iqbal, "The erosion performance of particle reinforced metal matrix composite coatings produced by co-deposition cold gas dynamic spraying," Appl. Surf. Sci., vol. 396, no. October, pp. 1623–1634, 2017. https://doi.org/10.1016/j.apsusc.2016.10.155.

[2.16] F. Badkoobeh, H. Mostaan, M. Rafiei, H. R. Bakhsheshi-Rad, and F. Berto, "Friction stir welding/processing of mg-based alloys: A critical review on advancements and challenges," Materials (Basel)., vol. 14, no. 21, 2021. https://doi.org/10.3390/ma14216726.

[2.17] G. Karrar, A. Galloway, A. Toumpis, H. Li, and F. Al-Badour, "Microstructural characterisation and mechanical properties of dissimilar AA5083-copper joints produced by friction stir welding," J. Mater. Res. Technol., vol. 9, no. 5, pp. 11968–11979, 2020. https://doi.org/10.1016/j.jmrt.2020.08.073.

[2.18] X. Meng, Y. Huang, J. Cao, J. Shen, and J. F. dos Santos, "Recent progress on control strategies for inherent issues in friction stir welding," Prog. Mater. Sci., vol. 115, no. December 2018, p. 100706, 2021. https://doi.org/10.1016/j.pmatsci.2020.100706.

[2.19] P. Xue, B. L. Xiao, D. R. Ni, and Z. Y. Ma, "Enhanced mechanical properties of friction stir welded dissimilar Al-Cu joint by intermetallic compounds," Mater. Sci. Eng. A, vol. 527, no. 21–22, pp. 5723–5727, 2010. https://doi.org/10.1016/j.msea.2010.05.061.

[2.20] K. Raza, M. Shamir, M. K. A. Qureshi, A. S. Shaikh, and M. Zain-ul-abdein, "On the friction stir welding, tool design optimization, and strain rate-dependent mechanical properties of HDPE–ceramic composite joints," J. Thermoplast. Compos. Mater., vol. 31, no. 3, pp. 291–310, 2018. https://doi.org/10.1177/0892705717697779.

[2.21] M. Pourali, A. Abdollah-zadeh, T. Saeid, and F. Kargar, "Influence of welding parameters on intermetallic compounds formation in dissimilar steel/aluminum friction stir welds," J. Alloys Compd., vol. 715, pp. 1–8, 2017. https://doi.org/10.1016/j.jallcom.2017.04.272.

[2.22] Z. Boumerzoug and Y. Helal, "Friction Stir Welding of Dissimilar Materials Aluminum AL6061-T6 to Ultra Low Carbon Steel," Metals (Basel)., vol. 7, no.

2, p. 42, 2017. https://doi.org/10.3390/met7020042.

[2.23] H. Xia, C. Tan, L. Li, and N. Ma, “In situ SEM Observations of fracture behavior of laser welded–brazed Al/Steel dissimilar joint,” J. Mater. Eng. Perform., vol. 27, no. 3, pp. 1047–1057, 2018. https://doi.org/10.1007/s11665-018-3227-8.

[2.24] X. Lyu, M. Li, X. Li, and J. Chen, “Double-sided friction stir spot welding of steel and aluminum alloy sheets,” Int. J. Adv. Manuf. Technol., no. February, 2018. https://doi.org/10.1007/s00170-018-1710-x.

[2.25] M. Koilraj, V. Sundareswaran, S. Vijayan, and S. R. Koteswara Rao, “Friction stir welding of dissimilar aluminum alloys AA2219 to AA5083 – Optimization of process parameters using Taguchi technique,” Mater. Des., vol. 42, pp. 1–7, Dec. 2012. https://doi.org/10.1016/j.matdes.2012.02.016.

[2.26] Z. Y. Ma, A. H. Feng, D. L. Chen, and J. Shen, “Recent advances in friction stir welding/processing of aluminum alloys: microstructural evolution and mechanical properties,” Crit. Rev. Solid State Mater. Sci., vol. 8436, pp. 1–65, 2017. https://doi.org/10.1080/10408436.2017.1358145.

[2.27] M. Muthu Krishnan, J. Maniraj, R. Deepak, and K. Anganan, “Prediction of optimum welding parameters for FSW of aluminium alloys AA6063 and A319 using RSM and ANN,” Mater. Today Proc., vol. 5, no. 1, pp. 716–723, 2018. https://doi.org/10.1016/j.matpr.2017.11.138.

[2.28] S. Malarvizhi and V. Balasubramanian, “Influences of tool shoulder diameter to plate thickness ratio (D/T) on stir zone formation and tensile properties of friction stir welded dissimilar joints of AA6061 aluminum–AZ31B magnesium alloys,” Mater. Des., vol. 40, pp. 453–460, Sep. 2012. https://doi.org/10.1016/j.matdes.2012.04.008.

[2.29] B. Fu, G. Qin, F. Li, X. Meng, J. Zhang, and C. Wu, “Friction stir welding process of dissimilar metals of 6061-T6 aluminum alloy to AZ31B magnesium alloy,” J. Mater. Process. Technol., vol. 218, pp. 38–47, 2015. https://doi.org/10.1016/j.jmatprotec.2014.11.039.

[2.30] U. Singarapu, K. Adepu, and S. R. Arumalle, “Influence of tool material and rotational speed on mechanical properties of friction stir welded AZ31B magnesium alloy,” J. Magnes. Alloy., vol. 3, no. 4, pp. 335–344, 2015. https://doi.org/10.1016/j.jma.2015.10.001.

[2.31] S. M. Manladan, F. Yusof, S. Ramesh, M. Fadzil, Z. Luo, and S. Ao, A review on resistance spot welding of aluminum alloys, vol. 90, no. 1–4. 2017. https://doi.org/10.1007/s00170-016-9225-9

[2.32] L. Wu, H. Zhang, X. Zeng, P. Xue, B. Xiao, and Z. Ma, “Achieving superior low temperature and high strain rate superplasticity in submerged friction stir welded Ti-6Al-4V alloy,” vol. 61, no. November 2017, pp. 417–423, 2018. https://doi.org/10.1007/s40843-017-9145-4.

[2.33] H. Uzun, “Friction stir welding of SiC particulate reinforced AA2124 aluminium alloy matrix composite,” Mater. Des., vol. 28, no. 5, pp. 1440–1446, 2007. https://doi.org/10.1016/j.matdes.2006.03.023.

[2.34] H. Bisadi, A. Tavakoli, M. Tour Sangsaraki, and K. Tour Sangsaraki, “The influences of rotational and welding speeds on microstructures and mechanical properties of friction stir welded Al5083 and commercially pure copper sheets lap joints," Mater. Des., vol. 43, pp. 80–88, 2013. https://doi.org/10.1016/j.matdes.2012.06.029.

[2.35] M. Iordache, G. Sicoe, D. Iacomi, E. Niţu, and C. Ducu, "Analysis of microstructure and mechanical properties of aluminium-copper joints welded by FSW process," IOP Conf. Ser. Mater. Sci. Eng., vol. 227, no. 1, 2017. https://doi. 10.1088/1757-899X/227/1/012065.

[2.36] S. Siddharth, T. Senthilkumar, and M. Chandrasekar, "Development of processing windows for friction stir spot welding of aluminium Al5052 /copper C27200 dissimilar materials," Trans. Nonferrous Met. Soc. China (English Ed., vol. 27, no. 6, pp. 1273–1284, 2017. https://doi.org/10.1016/S1003-6326(17)60148-1.

[2.37] M. F. X. Muthu and V. Jayabalan, "Tool travel speed effects on the microstructure of friction stir welded aluminum-copper joints," J. Mater. Process. Technol., vol. 217, pp. 105–113, 2015. https://doi.org/10.1016/j.jmatprotec.2014.11.007.

[2.38] M. P. Mubiayi and E. T. Akinlabi, "Characterization of the intermetallic compounds in aluminium and copper friction stir spot welds," Mater. Today Proc., vol. 4, no. 2, pp. 533–540, 2017. https://doi.org/10.1016/j.matpr.2017.01.054.

[2.39] W. Kyffin, P. Threadgill, H. Lalvani, and B. Wynne, "Progress in FSSW of DP 800 high strength automotive steel",6th Int. Symp.,May 2006.

[2.40] A. Toumpis, A. Galloway, L. Molter, and H. Polezhayeva, "Systematic investigation of the fatigue performance of a friction stir welded low alloy steel," Mater. Des., vol. no. 80, June 2016, pp. 116–128, 2015. https://doi.org/10.1016/j.matdes.2015.04.046.

[2.41] D. Micallef, D. Camilleri, A. Toumpis, A. Galloway, and L. Arbaoui, "Local heat generation and material flow in friction stir welding of mild steel assemblies", Proc. Inst. Mech. Eng. Part L J. Mater. Des. Appl., vol. 230, no. 2, pp. 586–602, 2015. https://doi.org/10.1177/1464420715583163.

[2.42] G. Karrar, A. Galloway, A. Toumpis, F. Al-Badour & H. Li, "Prediction and validation of intermetallic compound formation during friction stir welding of AA6061 to commercially pure copper", Science and Technology of Welding and Joining, 27:5, 374-387,2022, https://doi: 10.1080/13621718.2022.2055289.

[2.43] Z. C. Nik, M. Ishak, and N. H. Othman, "The effect of tool pin shape of friction stir welding (FSW) on polypropylene," IOP Conf. Ser. Mater. Sci. Eng., vol. 238, no. 1, 2017. https://doi.org/10.1088/1757-899X/238/1/012003.

[2.44] P. Kah, R. Suoranta, J. Martikainen, and C. Magnus, "Techniques for joining dissimilar materials: Metals and polymers", Rev. Adv. Mater. Sci., vol. 36, no. 2, pp. 152–164, 2014.

[2.45] R. Jain, S. K. Pal, and S. B. Singh, "Numerical modeling methodologies for friction stir welding process", Computational Methods and Production Engineering, vol. (1), pp.125-169, 2017. https://doi.org/10.1016/B978-0-85709-481-0.00005-7.

[2.46] B. Meyghani, M. Awang, S. S. Emamian, M. K. Mohd Nor, and S. R. Pedapati, "A comparison of different finite element methods in the thermal analysis of friction stir welding (FSW)", Metals (Basel)., vol. 7, no. 11, p. 450, 2017. https://doi.org/10.3390/met7100450.

[2.47] M. P. Mubiayi and E. T. Akinlabi, "Friction stir spot welding of dissimilar materials : an overview," vol. II, no. January, pp. 22–24, 2014.

[2.48] Kulkarni, Nilesh, Rajiv S. Mishra, and Wei Yuan. "Friction stir welding of dissimilar alloys and materials. Butterworth-Heinemann, pp. 1–13, 2015. https://doi.org/10.1016/C2014-0-01707-8.

[2.49] J. Zhao, F. Jiang, H. Jian, K. Wen, L. Jiang, and X. Chen, "Comparative investigation of tungsten inert gas and friction stir welding characteristics of Al – Mg – Sc alloy plates," Mater. Des., vol. 31, no. 1, pp. 306–311, 2010. https://doi.org/10.1016/j.matdes.2009.06.012.

[2.50] P. M. G. P. Moreira, T. Santos, S. M. O. Tavares, V. Richter-trummer, P. Vilaça, and P. M. S. T. De Castro, "Mechanical and metallurgical characterization of friction stir welding joints of AA6061-T6 with AA6082-T6," vol. 30, pp. 180–187, 2009. https://doi.org/10.1016/j.matdes.2008.04.042.

[2.51] P. T. Summers et al., "Overview of aluminum alloy mechanical properties during and after fires," Fire Sci. Rev., vol. 4, no. 1, 2015. https://doi.org/10.1186/s40038-015-0007-5.

[2.52] J. R. Davis, "Copper and copper alloys",A. H. ASM International Specialty Handbook, , 2002. https://www.scribd.com/document/370020448/Copper-and-

Copper-Alloys.

[2.53] P. Agostinetti et al., “Investigation of the thermo-mechanical properties of electro-deposited copper for ITER,” J. Nucl. Mater., vol. 417, no. 1–3, pp. 924–927, 2011. https://doi.org/10.1016/j.jnucmat.2011.01.084.

[2.54] A. Heidarzadeh, T. Saeid, H. Khodaverdizadeh, a. Mahmoudi, and E. Nazari, “Establishing a mathematical model to predict the tensile strength of friction stir welded pure copper joints,” Metall. Mater. Trans. B, vol. 44, no. 1, pp. 175–183, Oct. 2012. https://doi.org/10.1007/s11663-012-9755-y.

[2.55] M. M. Hailat, A. Mian, Z. A. Chaudhury, G. Newaz, R. Patwa, and H. J. Herfurth, “Laser micro-welding of aluminum and copper with and without tin foil alloy,” Microsyst. Technol., vol. 18, no. 1, pp. 103–112, 2012. https://doi.org/10.1007/s00542-011-1378-8.

[2.56] B. Dong, Z. Pan, C. Shen, Y. Ma, and H. Li, “Fabrication of copper-rich Cu-Al alloy using the wire-arc additive manufacturing Process,” Metall. Mater. Trans. B Process Metall. Mater. Process. Sci., vol. 48, no. 6, pp. 3143–3151, 2017. https://doi.org/10.1007/s11663-017-1071-0.

[2.57] I. Galvão, R. M. Leal, D. M. Rodrigues, and A. Loureiro, “Influence of tool shoulder geometry on properties of friction stir welds in thin copper sheets”, Journal of Materials Processing Technology, vol. 213, pp. 129–135, 2013. https://doi.org/10.1016/j.jmatprotec.2012.09.016.

[2.58] T. Sakthivel and J. Mukhopadhyay, “Microstructure and mechanical properties of friction stir welded copper,” J. Mater. Sci., vol. 42, no. 19, pp. 8126–8129, Jun. 2007. https://doi.org/10.1007/s10853-007-1666-y.

[2.59] Y. F. Sun and H. Fujii, “Investigation of the welding parameter dependent microstructure and mechanical properties of friction stir welded pure copper,” Mater. Sci. Eng. A, vol. 527, no. 26, pp. 6879–6886, Oct. 2010. https://doi.org/10.1016/j.msea.2010.07.030.

[2.60] J. J. Shen, H. J. Liu, and F. Cui, “Effect of welding speed on microstructure and mechanical properties of friction stir welded copper,” Mater. Des., vol. 31, no. 8, pp. 3937–3942, 2010. https://doi.org/10.1016/j.matdes.2010.03.027.

[2.61] H.P. Zadeh, J. Teimournezhad, and A. Masoumi, “Numerical investigation on the mechanical, thermal, metallurgical and material flow characteristics in friction stir welding of copper sheets with experimental verification,” Mater. Des., vol. 55, pp. 619–632, Mar. 2014. https://doi.org/10.1016/j.matdes.2013.09.028.

[2.62] M. Jabbari, “Elucidating of rotation speed in friction stir welding of pure copper: Thermal modeling,” Comput. Mater. Sci., vol. 81, pp. 296–302, Jan. 2014. https://doi.org/10.1016/j.commatsci.2013.08.040.

[2.63] S. Ramaiyan, S. Kumar, V. Santhanam, P. Muthuguru, and T. Pin, “Effect of Scroll Pin Profile and Tool Rotational Speed on Mechanical Properties of Submerged Friction Stir Processed AZ31B Magnesium Alloy,” 2018. https://doi.org/10.1590/1980-5373-MR-2017-0769.

[2.64] A. D. G.R.Ebrahimi, A.R. Maldar, REbrahimi, “The effect of homogenization on microstructure and hot ductility behaviour of AZ91 magnesium alloy,” Kov.

Mater., no. 48, pp. 277–284, 2010.

[2.65] U. K. Singh and A. K. Dubey, “Study of weld characteristics in friction stir welding of dissimilar Mg-Al-Zn magnesium alloys under varying welding conditions,” J. Mater. Eng. Perform., vol. 30, no. 10, pp. 7690–7703, 2021. https://doi.org/10.1007/s11665-021-05893-z.

[2.66] A. Razal Rose, K. Manisekar, and V. Balasubramanian, “Effect of axial force on microstructure and tensile properties of friction stir welded AZ61A magnesium alloy,” Trans. Nonferrous Met. Soc. China (English Ed., vol. 21, no. 5, pp. 974–984, 2011. https://doi.org/10.1016/S1003-6326(11)60809-1.

[2.67] S. Sharma, A. Handa, S. S. Singh, and D. Verma, “Effects of tool rotation speeds on morphological and mechanical properties of friction stir processed AZ31Mg-MWCNT-Graphene hybrid nanocomposite,” J. Magnes. Alloy., no. xxxx, pp. 1–14, 2019.

[2.68] H. Bang, H. Bang, G. Jeon, I. Oh, and C. Ro, “Gas tungsten arc welding assisted hybrid friction stir welding of dissimilar materials Al6061-T6 aluminum alloy and STS304 stainless steel,” Mater. Des., vol. 37, pp. 48–55, 2012. https://doi.org/10.1016/j.matdes.2011.12.018.

[2.69] H. J. Liu, J. J. Shen, L. Zhou, Y. Q. Zhao, C. Liu, and L. Y. Kuang, “Microstructural characterisation and mechanical properties of friction stir welded joints of aluminium alloy to copper,” no. January, 2011. https://doi.org/10.1179/1362171810Y.0000000007.

[2.70] D. Aravindkumar, “A review on friction stir welding of dissimilar materials between aluminium alloys to copper,” Int. J. Latest Res. Eng. Technol., vol. 2, no. 2, pp. 9–15, 2016.

[2.71] R. Mishra, P. Sarathi De, and N. Kumar, "Friction stir welding of magnesium alloys." Friction Stir Welding and Processing: Science and Engineering, 149-187, (2014). https://doi.org/10.1007/978-3-319-07043-8_6.

[2.72] N. Shailesh and J. Menghani, “Optimum heat source position offset in welding of dissimilar Al-Cu metals using a theoretical approach,” Mater. Today Proc., vol. 5, no. 13, pp. 26974–26980, 2018. https://doi.org/10.1016/j.matpr.2018.08.187.

[2.73] I. Galvão, J. Oliveira, A. Loureiro, and D. Rodrigues, “Formation and distribution of brittle structures in friction stir welding of aluminium and copper: influence of process parameters,” Sci. Technol. Weld. Join., vol. 16, no. 8, pp. 681–689, 2011. https://doi.org/10.1179/1362171811Y.0000000057.

[2.74] P. Xue, D. R. Ni, D. Wang, B. L. Xiao, and Z. Y. Ma, “Effect of friction stir welding parameters on the microstructure and mechanical properties of the dissimilar Al–Cu joints,” Mater. Sci. Eng. A, vol. 528, no. 13–14, pp. 4683–4689, May 2011. https://doi.org/10.1016/j.msea.2011.02.067.

[2.75] I. Galvão, A. Loureiro, D. Verdera, D. Gesto, and D. M. Rodrigues, “Influence of tool offsetting on the structure and morphology of dissimilar aluminum to copper friction-stir welds,” Metall. Mater. Trans. A, vol. 43, no. 13, pp. 5096–5105, Aug. 2012. https://doi.org/10.1007/s11661-012-1351-x.

[2.76] P. K. Sahu, S. Pal, and S. K. Pal, “Al/Cu dissimilar friction stir welding with Ni, Ti, and Zn Foil as the interlayer for flow control, enhancing mechanical and metallurgical properties," Metall. Mater. Trans. A Phys. Metall. Mater. Sci., vol. 48, no. 7, pp. 3300–3317, 2017. https://doi.org/10.1007/s11661-017-4093-y.

[2.77] H. J. Liu, J. J. Shen, L. Zhou, Y. Q. Zhao, C. Liu, and L. Y. Kuang, "Microstructural characterisation and mechanical properties of friction stir welded joints of aluminium alloy to copper," Sci. Technol. Weld. Join., vol. 16, no. 1, pp. 92–98, 2011. https://doi.org/10.1179/1362171810Y.0000000007.

[2.78] E. Akinlabi, D. Madyira, and S. Akinlabi, "Effect of heat input on the electrical resistivity of dissimilar friction stir welded joints of aluminium and copper," Africon, 2011, no. September, pp. 13–15, 2011. https://doi.10.1109/AFRCON.2011.6071973.

[2.79] G. Karrar, N. Merah, A. N. Shuaib, F. Al-Badour, and A. Bazoune, "Experimental and numerical investigations of friction stir welding of aluminum to copper." Applied Mechanics, Behavior of Materials, and Engineering Systems: Selected contributions to the 5th Algerian Congress of Mechanics, CAM2015, El-Oued, Algeria, October 25–29. Springer International Publishing, 2017.. https://doi:10.1007/978-3-319-41468-3_10.

[2.80] N. Eslami, Y. Hischer, A. Harms, D. Lauterbach, and S. Böhm, "Optimization of process parameters for friction stir welding of aluminum and copper using the taguchi method," Metals (Basel)., vol. 9, no. 1, pp. 6–10, 2019. https://doi.org/10.3390/met9010063.

[2.81] K. P. Mehta and V. J. Badheka, "Influence of tool design and process parameters on dissimilar friction stir welding of copper to AA6061-T651 joints," Int. J. Adv.

Manuf. Technol., vol. 80, no. 9–12, pp. 2073–2082, 2015. https://doi.org/10.1007/s00170-015-7176-1.

[2.82] C. W. Tan, Z. G. Jiang, L. Q. Li, Y. B. Chen, and X. Y. Chen, "Microstructural evolution and mechanical properties of dissimilar Al-Cu joints produced by friction stir welding," Mater. Des., vol. 51, pp. 466–473, 2013. https://doi.org/10.1016/j.matdes.2013.04.056.

[2.83] K. Singh, G. Singh, and H. Singh, "Review on friction stir welding of magnesium alloys," J. Magnes. Alloy., vol. 6, no. 4, pp. 399–416, 2018. https://doi.org/10.1016/j.jma.2018.06.001.

[2.84] T. Luo et al., "Low-temperature superplasticity of nugget zone of friction stir welded Al-Mg alloy joint," Mater. Sci. Eng. A, vol. 727, no. May, pp. 177–183, 2018. https://doi.org/10.1016/j.msea.2018.05.003.

[2.85] S. A. Khodir and T. Shibayanagi, "Dissimilar friction stir welded joints between 2024-T3 aluminum alloy and AZ31 magnesium alloy", vol. 48, no. 9, pp. 2501–2505, 2007. https://doi.org/10.2320/matertrans.MRA2007093.

[2.86] A. Kostka, R. S. Coelho, and A. R. Pyzalla, "Microstructure of friction stir welding of aluminium alloy to magnesium alloy," Scr. Mater., vol. 60, no. 11, pp. 953–956, 2009. https://doi.org/10.1016/j.scriptamat.2009.02.020.

[2.87] V. Firouzdor and S. Kou, "Al-to-Mg friction stir welding : effect of material position , travel Speed , and rotation Speed", Metallurgical and Materials Transactions A, vol. 41A, pp. 2914, 2010. https://doi.org/10.1007/s11661-010-0340-1.

[2.88] S. MD and A. K. Birru, "Mechanical and metallurgical properties of friction stir welded dissimilar joints of AZ91 magnesium alloy and AA 6082-T6 aluminium alloy," J. Magnes. Alloy., vol. 7, no. 2, pp. 264–271, 2019. https://doi.org/10.1016/j.jma.2018.09.004.

[2.89] H. Schmidt and J. Hattel, "Modelling heat flow around tool probe in friction stir welding," Sci. Technol. Weld. Join., vol. 10, no. 2, pp. 176–186, 2005. https://doi.org/10.1179/174329305X36070.

[2.90] M. Awang, "Simulation of friction stir spot welding (FSSW) process : study of friction phenomena," no. March 2016, pp. 1–147, 2007.

[2.91] M. Song and R. Kovacevic, "Thermal modeling of friction stir welding in a moving coordinate system and its validation," Int. J. Mach. Tools Manuf., vol. 43, no. 6, pp. 605–615, May 2003. https://doi.org/10.1016/S0890-6955(03)00022-1.

[2.92] H.-H. Cho et al., "Three-dimensional numerical and experimental investigation on friction stir welding processes of ferritic stainless steel," Acta Mater., vol. 61, no. 7, pp. 2649–2661, Apr. 2013. https://doi.org/10.1016/j.actamat.2013.01.045.

[2.93] P. a. Colegrove and H. R. Shercliff, "3-Dimensional CFD modelling of flow round a threaded friction stir welding tool profile," J. Mater. Process. Technol., vol. 169, no. 2, pp. 320–327, Nov. 2005. https://doi.org/10.1016/j.jmatprotec.2005.03.015

[2.94] R.S. Rajesh et al., "Numerical determination of residual stress in friction stir weld using 3D-analytical model of stir zone," J. Mater. Process. Technol., vol. 187–

188, pp. 224–226, Jun. 2007. https://doi.org/10.1016/j.jmatprotec.2006.11.205

[2.95] G. Buffa, J. Hua, R. Shivpuri, and L. Fratini, “A continuum based fem model for friction stir welding—model development,” Mater. Sci. Eng. A, vol. 419, no. 1–2, pp. 389–396, Mar. 2006. https://doi.org/10.1016/j.msea.2005.09.040.

[2.96] B. Meyghani, M. Awang, and S. Emamian, “A comparative study of finite element analysis for friction stir welding application,” ARPN J. Eng. Appl. Sci., vol. 11, no. 22, 2016.

[2.97] M. Grujicic, B. Pandurangan, C. F. Yen, and B. A. Cheeseman, “Modifications in the AA5083 Johnson-Cook material model for use in friction stir welding computational analyses,” J. Mater. Eng. Perform., vol. 21, no. 11, pp. 2207–2217, 2012. https://doi.org/10.1007/s11665-011-0118-7.

[2.98] X. Zhou, “Friction stir welding simulation , optimization and design”, University of Strathclyde, Department of Mechanical and Aerospace Engineering, Thesis, 2013.

[2.99] F.A. Al-Badour, “Friction Stir Welding Of Tube-Tube Sheet Joints,” King Fahd University of Petroleum and Minerals,Thesis, 2012.

[2.100] V. Shokri, A. Sadeghi, and M. H. Sadeghi, “Thermomechanical modeling of friction stir welding in a Cu-DSS dissimilar joint,” J. Manuf. Process., vol. 31, pp. 46–55, 2018. https://doi.org/10.1016/j.jmapro.2017.11.004.

[2.101] M. B. Durdanovic, M. M. Miljajlovic, D. S. Milcic, and D. S. Stamenkovic, “Heat Generation During Friction Stir Welding Process,” Tribol. Ind., vol. 31, no. 1, pp. 8–14, 2009.

[2.102] A. Scialpi, L. a. C. De Filippis, and P. Cavaliere, "Influence of shoulder geometry on microstructure and mechanical properties of friction stir welded 6082 aluminium alloy," Mater. Des., vol. 28, no. 4, pp. 1124–1129, Jan. 2007. https://doi.org/10.1016/j.matdes.2006.01.031.

[2.103] K. Elangovan and V. Balasubramanian, "Influences of pin profile and rotational speed of the tool on the formation of friction stir processing zone in AA2219 aluminium alloy," Mater. Sci. Eng. A, vol. 459, no. 1–2, pp. 7–18, Jun. 2007. https://doi.org/10.1016/j.msea.2006.12.124.

[2.104] O. Lorrain, V. Favier, H. Zahrouni, and D. Lawrjaniec, "Understanding the material flow path of friction stir welding process using unthreaded tools," J. Mater. Process. Technol., vol. 210, no. 4, pp. 603–609, Mar. 2010. https://doi.org/10.1016/j.jmatprotec.2009.11.005

[2.105] L. Zhou, R. X. Zhang, G. H. Li, W. L. Zhou, Y. X. Huang, and X. G. Song, "Effect of pin profile on microstructure and mechanical properties of friction stir spot welded Al-Cu dissimilar metals," J. Manuf. Process., vol. 36, no. September, pp. 1–9, 2018. https://doi.org/10.1016/j.jmapro.2018.09.017.

[2.106] B. T. Gibson et al., "Friction stir welding : Process , automation , and control," J. Manuf. Process., vol. 16, no. 1, pp. 56–73, 2014. https://doi.org/10.1016/j.jmapro.2013.04.002

[2.107] R. S. Mishra and K. J. Colligan, "A conceptual model for the process variables related to heat generation in friction stir welding of aluminum," Scr. Mater., vol. 58, no. 5, pp. 327–331, 2008. https://doi.org/10.1016/j.scriptamat.2007.10.015

[2.108] L. Cederqvist et al., "Improved process stability during friction stir welding of 5 cm thick copper canisters through shoulder geometry and parameter studies Improved process stability during friction stir welding of 5 cm thick copper canisters through shoulder geometry and parameter studies," vol. 1718, 2013. https://doi.org/10.1179/136217109X400420.

[2.109] P. Niu, W. Li, X. Yang, and A. Vairis, "Effects of microstructural asymmetries across friction stir welded AA2024 joints on mechanical properties," Sci. Technol. Weld. Join., vol. 23, no. 1, pp. 58–62, 2018. https://doi.org/10.1080/13621718.2017.1328765.

[2.110] K. Fraser, L. Kiss, L. St-Georges, and D. Drolet, "Optimization of Friction Stir Weld Joint Quality Using a Meshfree Fully-Coupled Thermo-Mechanics Approach," Metals (Basel)., vol. 8, no. 2, p. 101, 2018. https://doi.org/10.3390/met8020101.

[2.111] M. A. Gharacheh, A. H. Kokabi, G. H. Daneshi, B. Shalchi, and R. Sarrafi, "The influence of the ratio of "" rotational speed / traverse speed "" (o / v) on mechanical properties of AZ31 friction stir welds," vol. 46, pp. 1983–1987, 2006. https://doi.org/10.1016/j.ijmachtools.2006.01.007.

[2.112] E. Hiteh, M. Divandari, and M. Gholami, "Effect of preheating temperature on thickness and interfacial microstructure of Aluminum-Copper bimetal composite produced by vertical centrifugal," vol. 4(4), pp.391-398, February 2016. https://doi.org/10.22068/jstc.2018.25629.

[2.113] Awang, Mokhtar, ed. "The advances in joining technology", Berlin/Heidelberg, Germany: Springer, 2019.

[2.114] A. J. Leonard and S. A. Lockyer, “Flaws in Friction Stir Welds,” 4th Int. Symp. Frict. Stir Weld., no. May, pp. 14–16, 2003.

[2.115] R. Zettler, T. Vugrin, and G. Aerospace, “Effects and defects of friction stir welds 9,” pp. 245–276, 2003. https://doi.org/10.1533/9781845697716.2.245.

[2.116] American Bureau of Shipping (ABS), “Guide for: the approval of friction stir welding in aluminium”, October 2011.

[2.117] R. M. F. Paulo, P. Carlone, V. Paradiso, R. A. F. Valente, and F. Teixeira-Dias, “Prediction of friction stir welding effects on AA2024-T3 plates and stiffened panels using a shell-based finite element model,” Thin-Walled Struct., vol. 120, no. August, pp. 297–306, 2017. https://doi.org/10.1016/j.tws.2017.09.009

[2.118] Y. G. Kim, H. Fujii, T. Tsumura, T. Komazaki, and K. Nakata, “Three defect types in friction stir welding of aluminum die casting alloy,” vol. 415, pp. 250–254, 2006. https://doi.org/10.1016/j.msea.2005.09.072.

[2.119] H. W. Zhang and Z. Zhang, “A fully coupled thermo-mechanical model of friction stir welding,” Int. J. Adv. Manuf. Technol., vol. 37, pp. 279–293, 2008. https://doi.org/10.1007/s00170-007-0971-6.

3. Experimental and numerical methodology

The following discussion provides a comprehensive account of the experimental procedures for achieving dissimilar FSW butt joints on various metals, such as aluminium, copper, and magnesium-based alloys. It also outlines the characterisation methods used to evaluate the joints critically, including metallographic examination, compositional analysis, and phase identification through techniques such as energy dispersive spectroscopy (EDS) and X-ray diffraction (XRD). Additionally, the chapter discusses the implementation and use of the Topas Rietveld XRD refinement method to examine the developed phases and quantify the amount of IMCs in the weld zone. The mechanical characterisation approach for the joints is also thoroughly described.

Furthermore, Chapter 3 offers insight into the numerical modelling techniques developed to simulate the FSW process. It explores the various methods used to numerically solve the partial differential equations that describe the FSW process, including domain discretisation techniques such as Lagrangian, Eulerian, and Coupled Eulerian Lagrangian (CEL).

3.1. Experimental programme

3.1.1. Experimental setup

A fully instrumented HT-JM16X8/2 static gantry FSW machine was used to butt weld 150 x 50 x 3 mm, resulting in an overall welded sheet width of 100 mm. The machine was equipped with sensors for monitoring and controlling the welding process via computer numerical control, programmed using M- and G-codes, and offered three plunging control modes: force control, position control, and position with deflection compensation control. Despite these features, there were challenges in accurately collecting force data during the experiments. This limitation was primarily due to difficulties in data extraction from the FSW welder machine. Nevertheless, force was monitored and managed during each welding operation to ensure the integrity and quality of the welds, aligning with the primary objective of achieving defect-free joints between the selected dissimilar materials. Fig. 3.1 displays a photograph of the HT-JM16X8/2 in use at the Mechanical Engineering Department Laboratory, Zhejiang Sci-Tech University, Hangzhou, China.

To prevent welding defects caused by relative movement between the workpiece and the machine working table during the FSW experiments, the workpieces were clamped and supported in all directions (x, y, z), as shown in Fig. 3.1. The FSW experiments employed a steel base (backing plate) to support the workpieces, clamps, and screws. Fig. 3.1 also illustrates the temperature measurement setup, which was utilised to verify the numeric temperature outputs gathered from the developed finite element model. Two K-type thermocouples recorded the temperature at the AS and two at the RS at four distinct locations. Section 3.1.2. provides additional information regarding the thermocouples' placement.

The FSW tool was constructed from high-strength tool steel with a hardness of 50-70 HRC. The tool had an 18 mm (featureless) shoulder diameter (Ds), a 4.5 mm (featureless) pin diameter (Dp), and a pin length of 2.7 mm. Subsequently, the effect of various FSW welding tool designs on the mechanical performance of the joints was examined. This included investigating the impact of relatively larger tool Ds and tapered pin types on the joint's integrity. Fig. 3.2 depicts a schematic diagram of the FSW tool geometries. Both the simple tool design (S) (Fig. 3.2 (a)) and the tapered tool pin design (T) (Fig. 3.2 (b)) were equipped with shoulders of 18 mm in diameter and 2.7 mm plunging depth. The relatively larger tool design (B) (Fig. 3.2 (c)) featured a shoulder of 22 mm in diameter and a similar simple tool pin design.

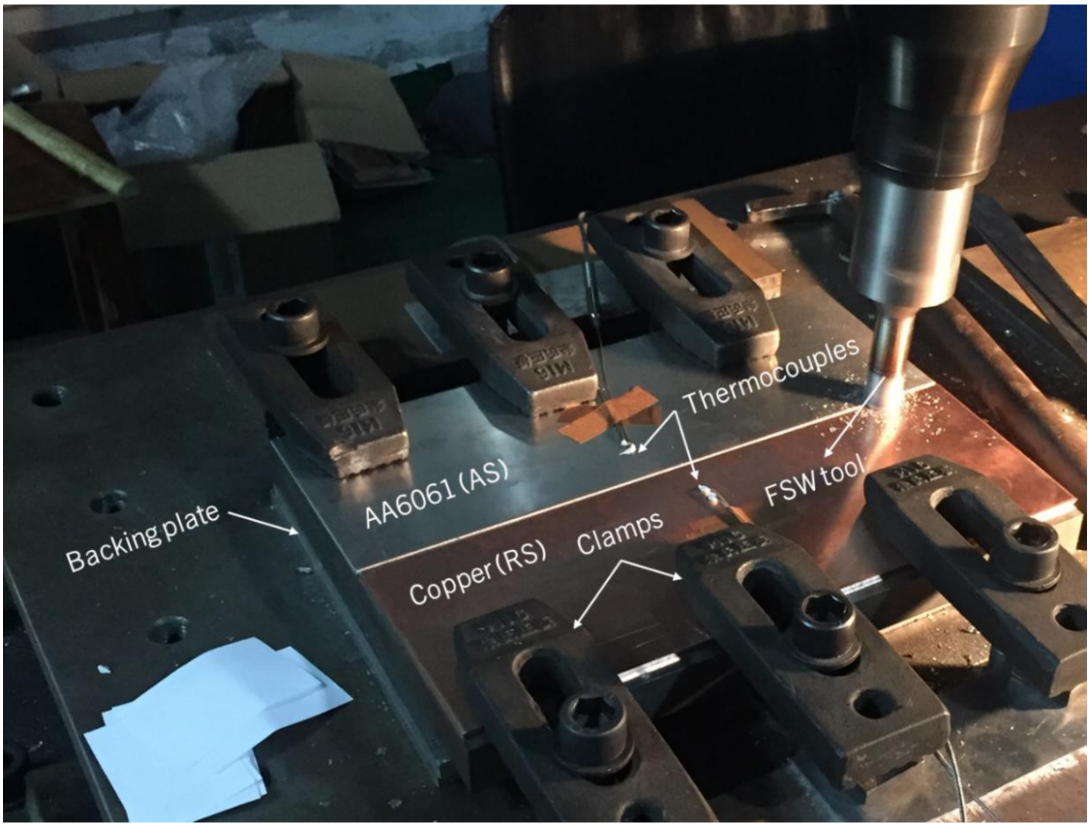

Fig. 3.1 The experimental set-up of dissimilar AA6061 to copper FSW process.

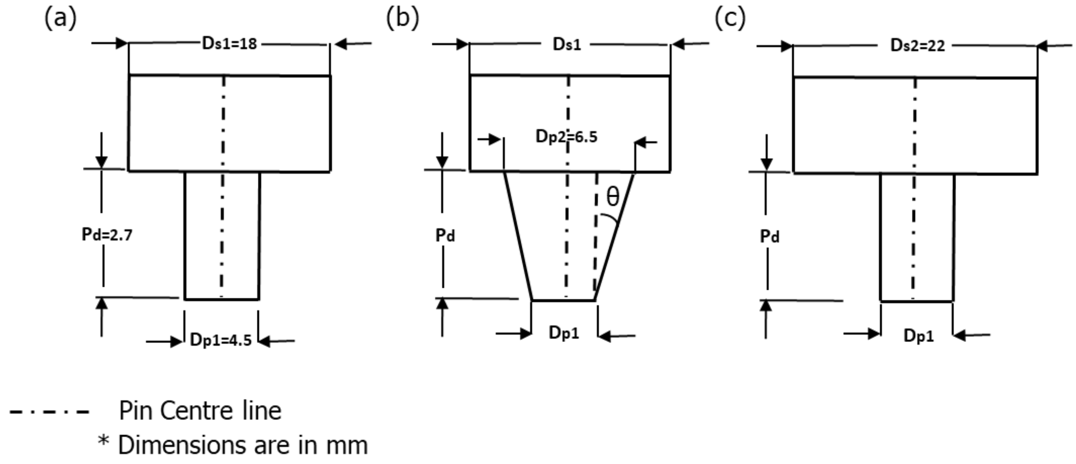

Fig. 3.2 Schematic diagrams of different FSW tool designs: (a) simple tool design (S), (b) tapered pin design (T), and (c) larger shoulder design (B).

3.1.2. Materials and FSW process details

The study considered a range of metals and alloys commonly utilised in industrial applications, which are often challenging to weld using fusion welding methods. The investigation included similar and dissimilar FSW of various aluminium grades, magnesium alloy, and commercially pure copper to evaluate the effectiveness of FSW joining process in producing superior weld joints compared to conventional welding processes. Tables 3.1 and 3.2 provide details on the chemical composition and mechanical properties of the aluminium alloys (AA1061, AA5083, and AA6061), the magnesium alloy type AZ31B, and the commercially pure copper, respectively.

Table 3.1 Chemical composition (in wt.%) of AA1061, AA5083, AA6061, commercially pure copper, and AZ31B as Measured

Al grade	**Si**	**Mg**	**Cu**	**Mn**	**Zn**	**Cr**	**Fe**	**Ti**
AA1061 (wt. %)	0.25	0.03	0.04	0.03	0.05	-	0.3	0.03
AA5083 (wt. %)	0.98	4.0	0.10	0.70	0.25	0.10	0.40	0.15
AA6061 (wt. %)	0.6	1.0	0.3	0.15	0.25	0.10	0.7	
AZ31B (wt. %)	**Al**	**Mg**	**Si**	**Mn**	**Zn**	**Cu**	**Fe**	**Ni**
	3.0	Bal.	0.03	0.4	1.1	0.003	0.02	0.005
Copper (wt. %)	**Ag**	**Fe**	**Bi**	**Sb**	**As**	**Pb**	**S**	
	0.035	0.05	0.001	0.002	0.002	0.005	0.005	

Table 3.2 Mechanical properties of base metals as Measured

Materials	**Yield strength (MPa)**	**UTS (MPa)**	**Young's Modulus (GPa)**	**Avg. HV**
AA1061	151.78	165.50	35.50	50
AA5083	163.97	225.66	67.57	70
AA6061	276	310	68.90	105
AZ31B	217	240	14.0	70
Copper	257.26	273.66	114.14	90

It's worth mentioning that the chemical compositions of these parent materials were determined using Energy Dispersive Spectroscopy (EDS) analysis. The mechanical properties, specifically hardness, were evaluated using the Vickers hardness test, providing an average value for each base material. Further, to explore the mechanical strength of as received base-metals, sub-size specimens from each sample were tested in accordance with ASTM-E8 standards. A minimum of three samples were considered to ensure a comprehensive investigation, thereby enhancing the reliability and accuracy of the results presented.

Several studies [3.4–3.9]. have indicated that the FSW process is greatly influenced by the positioning of materials, where the relative placement of dissimilar materials in relation to the tool's rotational and traverse speeds plays a crucial role in determining the integrity of the resulting joint. The present study examines the validity of placing the softer material (i.e., aluminium for dissimilar aluminium to copper joints or AZ31B magnesium alloy for dissimilar aluminium to magnesium joints) on the AS while centring the FSW tool on the seam line, as shown in Fig. 3.3 (a). Throughout the present study, it was determined that placing the softer material at the AS eliminated the need to offset the tool to either the AS or the RS, a technique that has previously been recommended for producing defect-free joints [3.10–3.14].

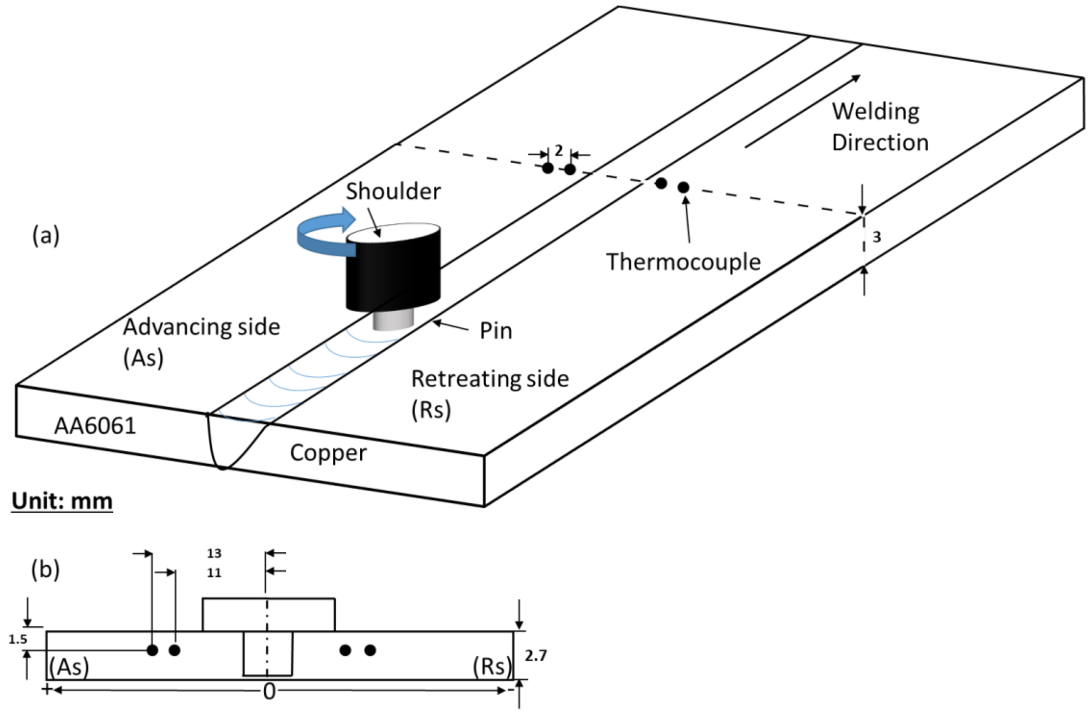

Fig. 3.3 (a) Weld configuration and experimental set-up AA6061 to copper (300 x 50 x 3 mm^3). (b) The measurement positions of thermocouples imbedded into AA6061 (As) and copper (Rs).

As previously mentioned, this study also considered the current thermo-mechanical simulation techniques of the FSW process (a detailed description of the CEL model is provided in section 3.2). The thermal outputs from the developed CEL model were validated against the experimental temperature results measured by K-type thermocouples situated at different positions (11-13 mm) from the joint line, i.e., 2-4 mm from the shoulder surface. To facilitate the development of steady-state FSW conditions, a series of 1.5 mm diameter holes were drilled from the side of AA6061 (AS) and the side of copper (RS), as illustrated in Fig. 3.3 (a) and (b). These holes were positioned in the mid-region of the plate length (i.e., 150 mm from the starting point).

It's worth noting that K-type thermocouples were securely affixed using a specialised adhesive into allocated holes on the workpieces, be it aluminium or copper. This was done to ensure full contact between the thermocouples and the material surface, crucial for accurate thermal readings. Prior to welding, a calibration test was conducted to verify this surface-to-surface contact, ensuring the reliability of the temperature measurements.

Furthermore, the thermocouples were strategically positioned as close as possible to the periphery of the FSW tool's shoulder, specifically at a distance of 2mm from the shoulder diameter. This positioning is critical as placing them any closer would risk melting the thermocouples during the welding process. The careful placement and securing of these thermocouples were essential to gather precise data on the thermal conditions experienced during FSW, contributing significantly to the accuracy of the study's findings. Additionally, Figs. 3.4 (a) and 3.4 (b) depict a transverse cross-section and a top view of the relative location of the FSW tool at 0 mm and d mm tool offset, respectively.

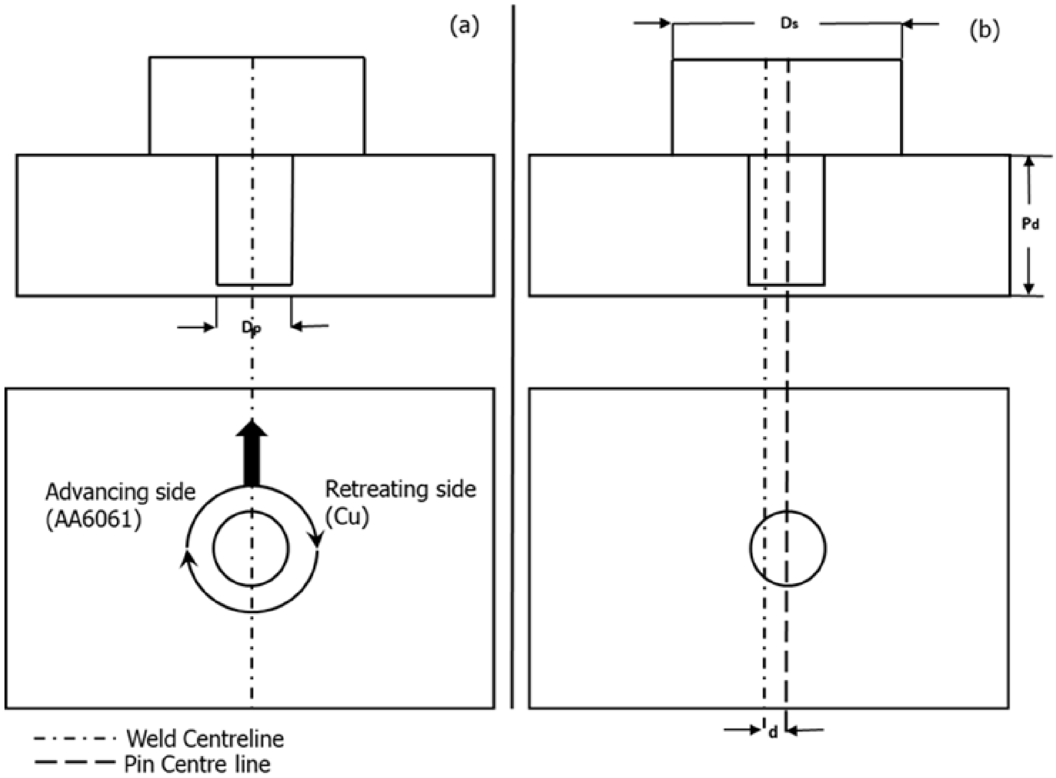

Fig. 3.4 (a) Transverse and top view showing the symmetrical location of the FSW tool at 0 mm tool offset. (b) The location at d mm tool offset.

After adopting the proposed joint configuration of placing the softer material on the AS, FSW experiments were conducted to investigate the impact of tool rotational speed and tool welding speed (ω/v ratio) on the dissimilar joint's integrity. Tables 3.3, 3.4, and 3.5 summarise the welding parameters that were used. It is worth noting that, the range of tool rotational speeds and tool welding speeds in Tables 3.3 – 3.8 were selected based on several considerations. Initially, the welding conditions necessary to produce defect-free FSW joints for similar materials i.e., aluminium-to-aluminium, copper-to-copper, and magnesium-to-magnesium were identified. These parameters served as preliminary conditions in determining the optimum process parameters for dissimilar material FSW joints.

To validate the outputs of the CEL model, a specific design of experiments was considered, as shown in Table 3.6. Unlike the previously mentioned sample size, the static gantry FSW machine was employed to butt weld 300 x 50 x 3 mm dissimilar sheets of AA6061 and commercially pure copper. The extended butt weld length was employed to ensure a stable thermal output before recording temperature results at different weldment zones. The study was also extended to explore the influence of different FSW tool designs on the dissimilar joint's quality; these welding parameters were optimised using the Taguchi technique for FSW of AA5083 to copper (Table 3.7).

Moreover, this study investigated the effect of utilising two different aluminium alloys in the FSW of aluminium and magnesium grade (AZ31B). Aluminium grades AA5083 and AA6061 were separately welded to AZ31B at different tool rotational speeds and traverse speeds (ω/v ratio) to determine the optimal parameters for producing defect-free joints (Table 3.8).

Table 3.3 Welding parameters used in the FSW experiments (AA5083 to copper)

Test No.	**Rotational speed (rpm)**	**Traverse speed (mm/min)**	**ω/ν ratio (rev/mm)**	**AS Material**
1	1000	80	12.5	AA5083
2	1000	100	10	AA5083
3	1000	120	8.3	AA5083
4	1200	80	15	AA5083
5	1200	100	12	AA5083
6	1200	120	10	AA5083
7	1400	80	17.5	AA5083
8	1400	100	14	AA5083
9	1400	120	11.7	AA5083

Table 3.4 Welding parameters used in the experiments (AA1061 to copper)

Test No.	**Rotational speed (rpm)**	**Traverse speed (mm/min)**	**ω/ν ratio (rev/mm)**	**AS Material**
1	1000	40	25	AA1061
2	1000	50	20	AA1061
3	1000	60	16.67	AA1061
4	1100	40	27.5	AA1061
5	1100	50	22	AA1061
6	1100	60	18.33	AA1061
7	1200	40	30	AA1061
8	1200	50	24	AA1061
9	1200	60	20	AA1061

Table 3.5 Welding parameters used in the experiments (AA6061 to copper)

Test No.	Rotational speed (rpm)	Traverse speed (mm/min)	ω/ν ratio (rev/mm)	AS Material
1	1000	80	12.5	AA6061
2	1000	100	10	AA6061
3	1000	120	8.3	AA6061
4	1200	80	15	AA6061
5	1200	100	12	AA6061
6	1200	120	10	AA6061
7	1400	80	17.5	AA6061
8	1400	100	14	AA6061
9	1400	120	11.7	AA6061

Table 3.6 Welding parameters of FSW of AA6061 to copper used in validating the CEL model results

Test no.	ω/ν ratio (rev/mm) *	Rotational Speed (rpm)	Backward tilt Angle (deg.)	Tool Offset, do (mm)	AS Material
1	13	1300	2.8	0	AA6061
2	14	1400	2.8	0	AA6061
3	15	1500	2.8	0	AA6061

*The welding speed was maintained constant at 100 mm/min.

Table 3.7 Welding parameters used to optimise FSW of AA5083 to copper using the Taguchi technique

Test No.	**Rotational speed (rpm)**	**Traverse speed (mm/min)**	**ω/ν ratio (rev/mm)**	**FSW tool design***	**AS Material**
1	1000	80	12.5	T	AA5083
2	1000	100	10	S	AA5083
3	1000	120	8.3	B	AA5083
4	1200	80	15	B	AA5083
5	1200	100	12	T	AA5083
6	1200	120	10	S	AA5083
7	1400	80	17.5	S	AA5083
8	1400	100	14	B	AA5083
9	1400	120	11.7	T	AA5083

*T≡ Tapered pin FSW tool design S≡ simple pin FSW tool design B≡ Larger shoulder FSW tool design.

Table 3.8 Welding parameters used in the experiments (AA5083/AA6061 to AZ31B)

Test No.	**Rotational speed (rpm)**	**Traverse speed (mm/min)**	**ω/ν ratio (rev/mm)**	**RS Material**
1	800	80	10	AA5083
2	800	100	8	AA5083
3	800	120	6.67	AA5083
4	1000	80	12.5	AA5083
5	1000	100	10	AA5083
6	1000	120	8.33	AA5083
7	800	80	10	AA6061
8	800	100	8	AA6061
9	800	120	6.67	AA6061
10	1000	80	12.5	AA6061
11	1000	100	10	AA6061
12	1000	120	8.33	AA6061

3.1.3. Metallographic examination

After the welding process, the samples for metallography were sectioned perpendicular to the welding direction using a wire cut electrical discharge machine. Standard metallographic techniques were employed to prepare the samples in accordance with ASTM E407-09 guidelines [3.15]. The samples were mechanically polished using a grit sequence of 200, 300, 500, 800, and 1200. Subsequently, a two-stage etching process was employed to enable high-resolution optical and scanning electron microscopy (SEM) analysis. To reveal the copper side macro/microstructures, a solution of 1 g $FeCl_3$, 10 mL HCl, and 100 mL distilled water was used for etching, while the AA1061, AA5083, AA6061, and AZ31B sides were etched for 60 s in a solution consisting of 1 g NaCl and 50 mL H_3PO_4 dissolved in 125 mL of ethanol, followed by a 12 s step using Wecks's tint (4 g of $KMnO_4$ and 1 g of NaOH dissolved in 100 mL of distilled water). The etched samples were then examined using high-resolution optical microscopy and SEM.

Qualitative analysis of the weldment zones' elemental composition was conducted using EDS. This analysis allowed for the interpretation of the variation in dissimilar materials content, which can be attributed to the welding conditions, such as the ω/v ratio. Additionally, EDS analysis provided detailed information about the intermixing behaviour between the dissimilar materials and identified the presence of non-equilibrium solid solutions, which have been known to degrade the joint's mechanical strength [3.2, 3.19].

XRD analysis was performed to confirm the presence of IMCs previously detected by EDS elemental analysis. The XRD scans were conducted at various locations of the weld joint with a scanning rate of 0.02 deg./step within the range of $20° < 2\theta < 100°$, using a 40-mA operating current, 40-kV voltage, and 1.5406-Å Cu Kα radiation. Furthermore, the Topas Rietveld X-ray diffraction (XRD) refinement method [3.20] was employed to study the developed phases and quantify the amount of IMCs present in the weld zone. Accurate crystallographic information of the pre-confirmed IMCs within the weldment zones was essential for the successful Rietveld quantification process. The aim of quantifying the IMC formation during dissimilar FSW was to provide additional insight into the influence of these IMCs on the joint's mechanical performance. Although the direct beneficial effects of IMCs on joint mechanical strength have been qualitatively identified [3.5-3.9], there is a lack of quantitative data and prediction of their presence relative to FSW welding parameters (i.e., ω/v ratio). Researchers [3.3-3.16] have not definitively demonstrated the negative or positive role played by IMC particles. Additionally, there is a lack of understanding regarding the evolution of these IMCs during the FSW process of dissimilar materials.

3.1.4. Mechanical testing

The Vickers hardness test was the primary method employed to evaluate the dissimilar FSW butt joints and establish the relationship between IMCs formation and joint mechanical strength. Fig. 3.5 illustrates the microhardness indentation locations measured across the top, middle and bottom of the weld cross-section, arranged in three rows at distances of 0.5, 1.5, and 2.5 mm from the top surface. All measurements were conducted using the Qness 60A+ hardness machine with a load of 300 g and a dwell time of 15 seconds. While hardness profile measurements at different depths of the cross-sectional surface of welds are commonly used to evaluate joint mechanical performance [3.19–3.23], it is important to note that hardness is not a single property but rather a complex mechanical property and an indicator of the intrinsic bonding of the dissimilar FSW joints [3.24].

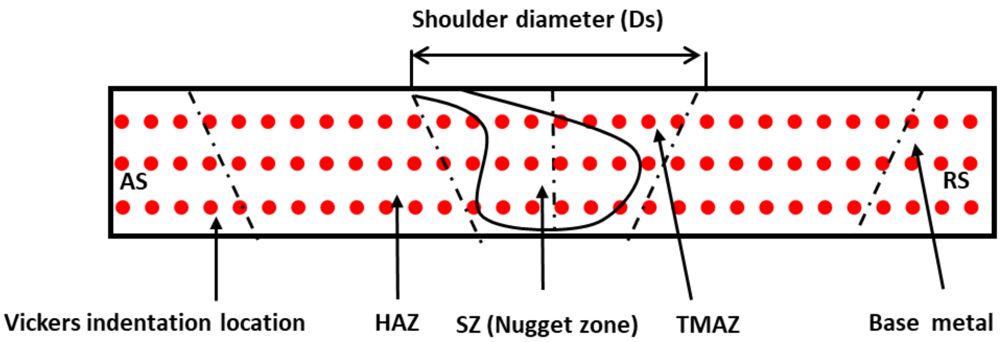

Fig. 3.5 Vickers hardness measurement positions.

Subsequently, the joint mechanical strength was further investigated by testing sub-size specimens across the weld zone of each welded sample in accordance with ASTM-E8 [3.25], as shown in Fig. 3.6 (a). An average of five tests was reported for each welding condition (Fig. 3.6 (b)). The samples were tested at a constant crosshead displacement rate of 2 mm/min using an Instron 5969 testing machine. The maximum load measured at failure for each butt joint was recorded and interpreted as the joint weld strength. This interpretation has been achieved via comparing the UTS obtained from each sub-size sample to the as-received base materials, for instance, Al in the case of Al to Copper dissimilar joints, and Mg in the case of Al to Mg joints. In addition, it's crucial to acknowledge that careful consideration was given to the post-weld thickness of each sample. Despite the distortion being relatively minimal, its impact on the overall weld strength was accounted for, ensuring that the resulting analysis and conclusions drawn were both accurate and reliably reflective of the actual welding outcomes. A selection of these measurements has also been documented in Appendix 1.

Additionally, preliminary flexural tests (3-point bend test type) were conducted to qualitatively assess the flexural behaviour of dissimilar materials FSW joints. Due to limited laboratory access during the pandemic, these tests were performed using sub-size tensile specimens, as depicted in Fig. 3.6 (a) and (b), with a span of 66.5 mm. The results are presented as a comparative analysis between different welding conditions rather than as a fully standardised evaluation. Given the absence of a widely accepted standard for flexural testing of such dissimilar joints, adaptations were made following GB/T 2653-2008, equivalent to ISO 5173:2000 [3.26], and corroborated by [3.27], as a credible approach for evaluating weld performance. Similar methodologies have been deemed acceptable in previous relevant studies [3.14, 3.28 and 3.29].

The tests were conducted at a displacement rate of 5 mm/min, and adjustments in the methodology were made to accommodate the unique attributes of the dissimilar joints, thereby ensuring a comprehensive and accurate evaluation of their flexural performance. Fig. 3.6 (c), showcasing a post-bending test macrograph of a specific dissimilar joint. It is important to highlight that these flexural tests were exploratory and not intended to serve as a fully validated mechanical characterisation method. Instead, they provide a basis for future work, where further investigation using dedicated flexural specimens and standardised methodologies would allow for a more comprehensive evaluation of dissimilar joints' flexural performance. It is also worth noting that, an average of three tests was reported for each welding condition.

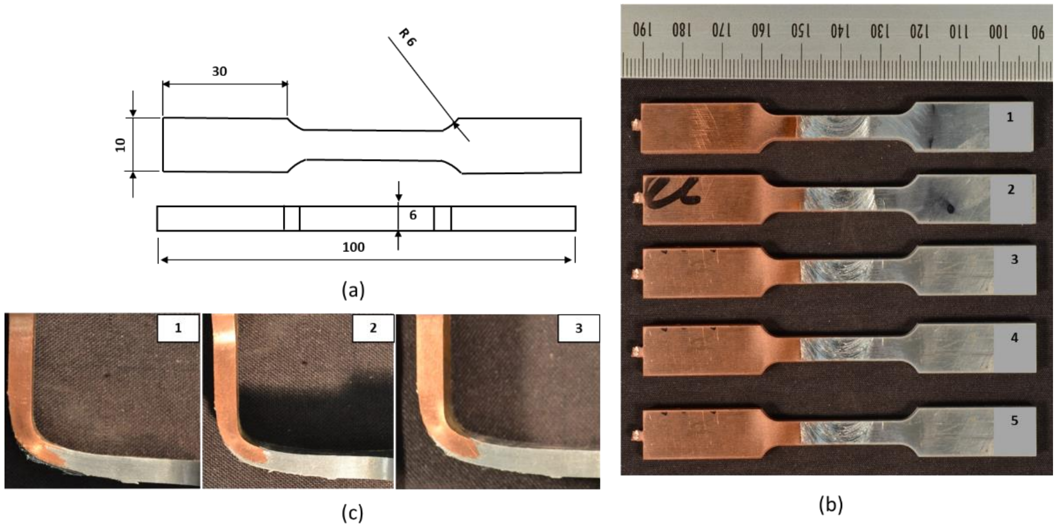

Fig. 3.6 (a) Dimensions of the tensile/ preliminary flexural sample as per ASTM E8 standards. (b) Example of tensile samples through the welding direction. (c) Post-bending test macrograph of AA5083 to copper dissimilar joint at 1000 rpm and 100 mm/min.

After conducting the aforementioned mechanical tests, the fracture surfaces were examined using high-resolution optical microscopy and SEM. The use of both types of microscopies was intended to clearly identify the fracture mode associated with each welding parameter and to quantify the chemical compositions related to each mode. To identify the significant parameters affecting the mechanical strength of dissimilar FSW joints, statistical analysis of the independent variables (ω/v ratio) and FSW tool design, along with the dependent variable of weld strength, was performed using the Minitab software environment.

3.2. Numerical methodology

This section presents the numerical modelling techniques used to simulate the FSW process and predict the formation of IMCs during welding of AA6061 to commercially pure copper. The developed model has been used to establish a novel approach for predicting IMCs formation. The temperature distribution of the weld nugget was determined using a finite element model. An Al-Cu phase diagram and the elemental concentration of copper and aluminium in the weld nugget were combined to predict the presence of several IMCs in different zones of the weldment.

3.2.1. Numerical model development

A coupled Eulerian Lagrangian (CEL) model [3.30] was utilised to simulate the FSW process of joining AA6061 to copper. Due to the complexity of the problem, CEL was deemed the most suitable modelling solution [3.30, 3.31]. CEL model is able to capture severe plastic deformation by avoiding mesh distortion during the process, where the material flows through a stationary mesh in the Eulerian domain. The Abaqus Explicit Solver environment was employed to implement and solve the model.

A geometrical model of 150 x 50 x 3 mm (Eulerian domain) was assumed, with three distinctive areas in this domain: the copper plate (RS), the aluminium plate (AS), and a 1 mm thick void layer to visualise the flash formation during the process. A fine biased seeding mesh was used along and around the FSW shoulder area, where the mesh becomes coarser towards the Eulerian domain sides. Multi-layer thermally coupled elements were assumed for the Eulerian plates. Overall, the Eulerian domain was meshed using 280,855 multi-materials thermally coupled 8-node (EC3D8RT) Eulerian elements, which equates to 307,740 nodes. Each of these elements was designed with four degrees of freedom at each node, allowing for a detailed and accurate representation of the thermal and mechanical behaviours of the materials under the extreme conditions of FSW.

Unlike the experimental setup of section 3.1.1., the Eulerian domain of the geometrical model was setup at 150 x 50 x 3 mm -after several trials-to enhance simulation accuracy by improving mesh density around the weld zone, while also reducing computational demands. However, the extraction of numerical values for comparison was meticulously carried out at the exact locations across the weld where experimental data was recorded from thermocouples (Fig. 3.3). Further, the numerical results were collected upon reaching a steady state, aligning with the experimental approach of extending workpieces length to ensure consistent state conditions during testing. It is worth mentioning that localised thermal models have been widely used to validate experimental outcomes [3.30 and 3.31].

On the other hand, A simple, featureless FSW tool with a pin diameter of 4.5 mm and shoulder diameter of 18 mm was used as a Lagrangian rigid body domain; all physical properties and boundary steps were assigned to a unique reference point. Additionally, this Lagrangian domain was constructed using 57,568 linear tetrahedral structured elements, corresponding to 10,991 nodes. This mesh configuration was crucial to accurately model the tool's interactions with the workpieces.

Unlike the CEL model reported by Al-Badour et al. [3.31], the FSW tool was assumed to rotate and traverse along the Eulerian domain in this study. The Eulerian domain was only constrained against the velocities and displacements on its sides. Fig. 3.7 (a) illustrates the typical boundary conditions for the Eulerian and Lagrangian domains, as well as the placement of the dissimilar materials, while Fig. 3.7 (b) shows the finer mesh within the shoulder area.

In terms of thermal boundary conditions, convection coefficients (h) on the AS for AA6061 and the RS for copper were assumed to be 25 W/m². Furthermore, the emissivity factors (ε) for AA6061 and copper were taken as 0.1 and 0.64, respectively. This consideration is crucial for accurately simulating the heat dissipation from the weld surfaces. To effectively model the surface-to-surface conduction between the workpieces (AA6061/copper) and the backing plate (steel), a specific conduction condition was assumed. In which, the thermal conductivity coefficients (K) of AA6061 and copper were set at 1000 W/m.K and 2000 W/m.K, respectively, to reflect their distinct heat conduction properties. The initial temperature for all model parts was assumed to be uniform and equal to 25°C.

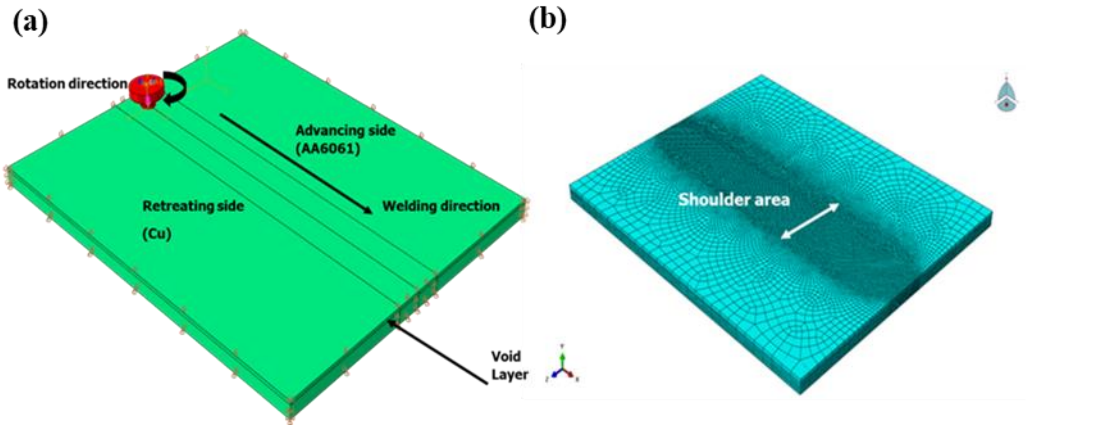

Fig. 3.7 (a) Applied boundary conditions and placement of each material. (b) Mesh in the vicinity of the FSW shoulder area.

Finally, the model was run using a dynamic, temperature-displacement explicit solver, with a time scale factor of 1000. This solver choice was instrumental in handling the complex, transient nature of the FSW process, ensuring the model's responsiveness to the rapid changes in temperature and material displacement.

3.2.2. Material properties

In order to account for the plastic deformation that occurs in the FSW zone at high temperatures and strain rates, the Johnson-Cook's constitutive mode [3.32] was employed to describe the plasticity of the dissimilar materials, as shown in Eq. (3.1). This model describes the material flow or yield stress σ_0 as a function of plastic strain, strain rate, and temperature.

$$\sigma_0 = [A + B\varepsilon_{pl}^{n}].[1 + C\ln\frac{\dot{\varepsilon_{pl}}}{\dot{\varepsilon_0}}].\ [1 - \left(\frac{T-T_{ref}}{T_{melt}-T_{ref}}\right)^{m}] \tag{3.1}$$

$* \ T_{ref} \leq \mathrm{T} \leq \ T_{melt}$

Where A is the yield stress (MPa) at a reference strain rate and temperature, B is the coefficient of strain (MPa), C and m are the Johnson-Cook’s model parameters that represent the coefficient of strain rate sensitivity and thermal softening exponent, and n is the strain hardening exponent. Table 3.9 presents these material constants for both AA6061 and copper at a reference temperature T_{ref}, T_{melt} is the material solidus temperature, ε_{pl}^{n}, $\dot{\varepsilon_{pl}}$ and $\dot{\varepsilon_0}$ are the effective plastic strain, effective plastic strain rate, and normalising strain rate, respectively.

The observed discrepancies in yield stress values between Tables 3.2 (section 3.1.2.) and 3.9 are attributed to the distinct mechanical properties of Oxygen-Free High Conductivity (OFHC) copper, for which the Johnson-Cook model parameters were specifically calculated, as opposed to the commercial copper used in the experimental work. Developing a new set of Johnson-Cook parameters for the commercial copper or AA6061 was not only a complex task but also limited by the resources available during my PhD research. Moreover, creating such data fell outside the intended scope of this study. Consequently, employing the established Johnson-Cook parameters, which have been widely recognised and utilised in material models for numerical analysis since their introduction by Cook et al. in 1983 [3.32], was considered an appropriate approach. These parameters are known for their reliability and are still extensively used in modelling the material behaviour in FSW and similar processes [3.33], [3.34].

Other material properties, such as density, thermal expansion coefficient, specific heat capacity, Poisson's ratio, and modulus of elasticity, were considered to be temperature dependent. The variation in material properties of AA6061 and copper with temperature, up to their respective melting point, is summarised in Tables 3.10 and 3.11.

Table 3.9 Johnson-Cook’s parameters [3.32].

Material	**A (MPa)**	**B (MPa)**	**C**	**n**	**m**	**Tref. (°C)**	**Tmelt. (°C)**
AA6061	324	114	0.002	0.42	1.09	25	582
Copper	90	292	0.025	0.31	1.09	25	1083

Table 3.10 Temperature dependent material properties of AA6061 in the range of 25°C–482°C [3.33].

Temp. (°C)	**Specific heat ($J\ kg^{-1}\ °C^{-1}$)**	**Thermal conductivity ($W\ m^{-1}\ °C^{-1}$)**	**Young's modulus (GPa)**	**Density (kg/m^3)**	**Coefficient of thermal expansion (10^{-6}) ($°C^{-1}$)**
25	870	140	66.94	2690	23.4
100	920	168	63.21	2690	24.6
200	960	183	56.8	2660	26.6
250	1000	196	52.0	2645	27.5
300	1040	208	47.17	2630	28.5
400	1150	219	32.67	2600	29.5
482	1280	220	20.2	2600	30.5

Table 3.11 Temperature dependent material properties of copper in the range of 25°C – 1060°C [3.34].

Temp. (°C)	**Specific heat ($J\ kg^{-1}\ °C^{-1}$)**	**Thermal conductivity ($W\ m{-}1\ °C^{-1}$)**	**Young's modulus (GPa)**	**Density ($kg\ /m^3$)**	**Coefficient of thermal expansion (10^{-6})($°C^{-1}$)**
25	384.60	398	117.2	8940	16.7
100	393.4	390	114.42	8940	17.3
200	405.13	387.3	110.32	8940	18.3
250	411.00	386	107.56	8940	18.6
350	416.00	383	99.98	8940	19.2
530	431.98	371	96.95	8940	20.4
630	440.67	364	93.25	8940	21.4
730	448.62	357	90.20	8940	22.4
930	468.14	343	87.33	8940	24.8
1060	476.19	334	84.75	8940	26.36

3.2.3. Friction coefficient

Formulating the contact condition between the FSW tool and the dissimilar materials is a complex task. There are several approaches to simulate the interaction condition between the FSW tool and the workpieces including assuming sticking boundary conditions [3.35], using the coefficient of friction as a function of pressure and slip rate [3.36], or applying Coulomb's law [3.30]. In this study, the modified friction law developed by Shokri et al. [3.37] was employed to couple the interaction between the Lagrangian (tool) and Eulerian (aluminium and copper) domains, taking into account both sticking and slipping conditions. An intermediate value of τ_{max} was selected, where -above this value- sliding conditions were no longer applicable, i.e., $\tau_{max} \neq \mu \times P_{contact}$,where μ and $P_{contact}$ are the coefficient of friction and contact pressure, respectively. The τ_{max} value was calculated from the Von-Mises relationship in Eq. (3.2) by considering that:

$$\tau_{max} = \tau_u = \alpha(\frac{\sigma_{u,Al}+\sigma_{u,Cu}}{\sqrt{3}}) \tag{3.2}$$

Where τ_u and σ_u are the ultimate shear stress and ultimate material strength and α is the material volume fraction, equal to 0.5 at the joint line. This adaptation is necessary to accurately model the plastic shear flow behaviour of the material, especially when the shear stress applied is approaching the material's shear failure stress. By selecting this intermediate τ_{max} value, a more realistic simulation of the frictional contact model, which is believed to offer a more accurate representation than models based on a slipping interface assumption can be achieved [3.37]. As a result, this has incorporated the Coulomb friction condition into all calculations, and the occurrence of elastic sliding has been assumed negligible to enhance the convergence of the simulations.

The primary parameters influencing the process are thus the friction coefficient and the critical shear stress. By adjusting the friction coefficient, the minimum stress required to initiate critical shear is altered, facilitating the material flow and rotational movement beneath the tool. Moreover, during the sticking condition where no voids were formed, an average value of 0.5 for the friction coefficient μ was assumed for the interaction between aluminium, copper, and steel (the FSW tool material).

3.3. References

[3.1] L. E. Murr, “A Review of FSW Research on Dissimilar Metal and Alloy Systems,” J. Mater. Eng. Perform., vol. 19, no. 8, pp. 1071–1089, Feb. 2010. https://doi.10.1007/s11665-010-9598-0.

[3.2] K. P. Mehta and V. J. Badheka, “A review on dissimilar friction stir welding of copper to aluminum: Process, properties, and variants,” Mater. Manuf. Process., vol. 31, no. 3, pp. 233–254, 2016. https://doi.org/10.1080/10426914.2015.1025971.

[3.3] G. K. Padhy, C. S. Wu, and S. Gao, “Friction stir based welding and processing technologies - processes, parameters, microstructures and applications: A review,” J. Mater. Sci. Technol., vol. 2, 2017. https://doi.org/10.1016/j.jmst.2017.11.029.

[3.4] P. Kah, R. Suoranta, J. Martikainen, and C. Magnus, “Techniques for joining dissimilar materials: Metals and polymers,” Rev. Adv. Mater. Sci., vol. 36, no. 2, pp. 152–164, 2014.

[3.5] Q. Z. Zhang, W. B. Gong, and W. Liu, “Microstructure and mechanical properties of dissimilar Al-Cu joints by friction stir welding,” Trans. Nonferrous Met. Soc. China (English Ed., vol. 25, no. 6, pp. 1779–1786, 2015. https://doi.org/10.1016/S1003-6326(15)63783-9.

[3.6] E. Akinlabi, D. Madyira, and S. Akinlabi, “Effect of heat input on the electrical resistivity of dissimilar friction stir welded joints of aluminium and copper,” Africon, 2011, no. September, pp. 13–15, 2011. https://doi.org/10.1109/AFRCON.2011.6071973.

[3.7] K. P. Mehta and V. J. Badheka, “Influence of tool design and process parameters on dissimilar friction stir welding of copper to AA6061-T651 joints,” Int. J. Adv. Manuf. Technol., vol. 80, no. 9–12, pp. 2073–2082, 2015. https://doi.org/10.1007/s00170-015-7176-1.

[3.8] D. Aravindkumar, “a Review on Friction Stir Welding of Dissimilar Materials Between Aluminium Alloys To Copper,” Int. J. Latest Res. Eng. Technol., vol. 2, no. 2, pp. 9–15, 2016. https://hdl.handle.net/10210/12514.

[3.9] G. Karrar, A. Galloway, A. Toumpis, H. Li, and F. Al-Badour, “Microstructural characterisation and mechanical properties of dissimilar AA5083-copper joints produced by friction stir welding,” J. Mater. Res. Technol., vol. 9, no. 5, pp. 11968–11979, 2020. https://doi.org/10.1016/j.jmrt.2020.08.073.

[3.10] A. Kostka, R. S. Coelho, and A. R. Pyzalla, “Microstructure of friction stir welding of aluminium alloy to magnesium alloy,” Scr. Mater., vol. 60, no. 11, pp. 953–956, 2009. https://doi.org/10.1016/j.scriptamat.2009.02.020.

[3.11] H. Xia, C. Tan, L. Li, and N. Ma, “In Situ SEM Observations of Fracture Behavior of Laser Welded–Brazed Al/Steel Dissimilar Joint,” J. Mater. Eng. Perform., vol. 27, no. 3, pp. 1047–1057, 2018. https://doi.org/10.1007/s11665-018-3227-8.

[3.12] N. Eslami, Y. Hischer, A. Harms, D. Lauterbach, and S. Böhm, “Optimization of process parameters for friction stir welding of aluminum and copper using the taguchi method,” Metals (Basel)., vol. 9, no. 1, pp. 6–10, 2019. https://doi.org/10.3390/met9010063.

[3.13] K. P. Mehta and V. J. Badheka, “Influence of tool pin design on properties of dissimilar copper to aluminum friction stir welding,” Trans. Nonferrous Met. Soc. China (English Ed., vol. 27, no. 1, pp. 36–54, 2017. https://doi.org/10.1016/S1003-6326(17)60005-0.

[3.14] N. Sharma, A. N. Siddiquee, and Z. A. Khan, “Friction Stir Welding Deffects in Aluminium to Copper Joining :,” vol. 9, no. 1, 2017. https://doi.org/10.1016/S1003-6326(17)60238-3.

[3.15] “ASTM E 407–09. Standard practice for micro etching Metals and alloys,” ASTM Int., 2009.

[3.16] J. Ouyang, E. Yarrapareddy, and R. Kovacevic, “Microstructural evolution in the friction stir welded 6061 aluminum alloy (T6-temper condition) to copper,” J. Mater. Process. Technol., vol. 172, no. 1, pp. 110–122, Feb. 2006. https://doi.org/10.1016/j.jmatprotec.2005.09.013.

[3.17] H. Bisadi, A. Tavakoli, M.T. Sangsaraki, and K.T. Sangsaraki, “The influences of rotational and welding speeds on microstructures and mechanical properties of friction stir welded Al5083 and commercially pure copper sheets lap joints,” Mater. Des., vol. 43, no. July 2018, pp. 80–88, 2013. https://doi.org/10.1016/j.matdes.2012.06.029.

[3.18] S. MD and A. K. Birru, “Mechanical and metallurgical properties of friction stir welded dissimilar joints of AZ91 magnesium alloy and AA 6082-T6 aluminium alloy,” J. Magnes. Alloy., vol. 7, no. 2, pp. 264–271, 2019. https://doi.org/10.1016/j.jma.2018.09.004.

[3.19] K. P. Mehta and V. J. Badheka, “Hybrid approaches of assisted heating and cooling for friction stir welding of copper to aluminum joints,” J. Mater. Process. Technol., vol. 239, pp. 336–345, 2017. https://doi.org/10.1016/j.jmatprotec.2016.08.037.

[3.20] K.H. Hestnes, B.E. Sørensen, “Quantitative Mineral Characterization of Granitic Pegmatite Using Topas Rietveld XRD Refinement Quantitative Minaral Characterisation of Grantitic,” Proceedings of the 10th International Congress for Applied Mineralogy (ICAM)January 2012. https://doi.org/10.1007/978-3-642-27682-8_40.

[3.21] R. Satish, V. Seshagiri Rao, D. Ananthapadmanaban, and B. Ravi, “Tensile Strength and Hardness Correlations with Microscopy in Friction welded Aluminium to Copper,” J. Inst. Eng. Ser. C, vol. 97, no. 1, pp. 121–126, 2016. https://doi.org/10.1007/s40032-015-0187-8.

[3.22] S. Richmire, K. Hall, and M. Haghshenas, “Design of experiment study on hardness variations in friction stir welding of AM60 Mg alloy,” J. Magnes. Alloy., vol. 6, no. 3, pp. 215–228, 2018. https://doi.org/10.1016/j.jma.2018.07.002.

[3.23] J. J. Shen, H. J. Liu, and F. Cui, “Effect of welding speed on microstructure and mechanical properties of friction stir welded copper,” Mater. Des., vol. 31, no. 8, pp. 3937–3942, 2010. https://doi.org/10.1016/j.matdes.2010.03.027.

[3.24] D. B. Sirdeshmukh, L. Sirdeshmukh, and K. G. Subhadra, “Micro- and Macro-Properties of Solids Thermal, Mechanical and Dielectric Properties”, Heidelberg: Springer Verlag, 2006. https://doi.org/10.1007/3-540-31786-4.pdf.

[3.25] American society for testing and materials (ASTM). “In: Standard test methods for tension testing of metallic materials, ASTM E8M – 09”, West Conshohocken (PA): Annual book of ASTM standards, vol. 03.01.2009.

[3.26] GB/T 2653-2008/ISO 5173:2000. “Bend test methods on welded joints”. Standardization Administration of the People’s Republic of China; 2008.

[3.27] C. W. Tan, Z. G. Jiang, L. Q. Li, Y. B. Chen, and X. Y. Chen, “Microstructural evolution and mechanical properties of dissimilar Al-Cu joints produced by friction stir welding,” Materials and Design., vol. 51, pp. 466–473, 2013. http://dx.doi.org/10.1016/j.matdes.2013.04.056.

[3.28] U. K. Singh and A. K. Dubey, “Study of Weld Characteristics in Friction Stir Welding of Dissimilar Mg-Al-Zn Magnesium Alloys under Varying Welding Conditions”, JMEPEG, 30:7690–7703, 2021. https://doi.org/10.1007/s11665-021-05893-z.

[3.29] M. S. Javadi, M.V. Ehteshamfar, H. Adibi, “A comprehensive analysis and prediction of the effect of groove shape and volume fraction of multi-walled carbon nanotubes on the polymer 3D-printed parts in the friction stir welding process”, Polymer Testing, 117, 107844, 2023. https://doi.org/10.1016/j.polymertesting.2022.107844

[3.30] B. Meyghani, M. Awang, S. S. Emamian, M. K.M. Nor, and S. R. Pedapati, “A Comparison of Different Finite Element Methods in the Thermal Analysis of Friction Stir Welding (FSW)”, Metals (Basel)., vol. 7, no. 11, pp. 450, 2017. https://doi.org/10.3390/met7100450.

[3.31] F. Al-Badour, N. Merah, A. Shuaib, and A. Bazoune, "Coupled Eulerian Lagrangian finite element modeling of friction stir welding processes", Journal of materials processing technology, vol. 213, no. 8, pp. 1433–1439, 2013. https://doi.org/10.1016/j.jmatprotec.2013.02.014.

[3.32] G. R. J. William H.Cook, "A constitutive Model and Data for Materials Subjected to Large Strains, High Starin Rates and High Temperatures", in Proceedings 7th International Symp. on Ballistics, 1983.

[3.33] V. Soundararajan, S. Zekovic, and R. Kovacevic "Thermo-Mechanical Model With Adaptive Boundary Conditions For Friction Stir Welding of Al 6061", International Journal of Machine Tools & Manufacture 45 (2005) 1577–1587. https://doi.org/10.1016/j.ijmachtools.2005.02.008.

[3.34] R.A. Smith, and Hashemi, "J. Foundations of materials science and engineering (4th ed.)", McGraw-Hill, (2006).

[3.35] X. He, F. Gu, and A. Ball, "A review of numerical analysis of friction stir welding," Progress in Materials Science, vol. 65, pp. 1–66, 2014. https://doi.org/10.1016/j.pmatsci.2014.03.003.

[3.36] N. Ponweiser, C.L. Lengauer, and K.W. Richter,"Re-investigation of phase equilibria in the system Al–Cu and structural analysis of the high-temperature phase η1-Al1−δCu", Intermetallics, vol. 19, pp. 1737–46, 2011. https://doi.org/10.1016/j.intermet.2011.07.007.

[3.37] V. Shokri, A. Sadeghi, and M. H. Sadeghi, “Thermo-mechanical modeling of friction stir welding in a Cu-DSS dissimilar joint”, Journal of Manufacturing Processes, vol. 31, pp. 46–55, 2018. https://doi.org/10.1016/j.jmapro.2017.11.004.

4. Dissimilar FSW of aluminium alloys to copper

The first part of this chapter aims to identify the welding conditions necessary to produce defect-free FSW joints for aluminium-to-aluminium and copper-to-copper materials. These parameters are subsequently employed as initial conditions to determine the optimum process parameters for dissimilar aluminium to copper FSW joints.

The second part of the chapter reports the results of a microstructural analysis conducted on dissimilar AA5083 aluminium grade to copper FSW joints. The analysis revealed the development of complex microstructures, including vortex-like patterns and lamellar structures in the thermo-mechanically affected zone. The presence of several intermetallic compounds (IMCs) in the weldment zone, such as Al_2Cu and Al_4Cu_9, was identified using X-ray diffraction (XRD) analysis, leading to an inhomogeneous hardness distribution. Moreover, the mechanical performance of dissimilar AA5083 aluminium grade to copper FSW joints was investigated, revealing the relationship between the IMCs formation and the dissimilar joint mechanical properties.

The third and final part of this chapter presents the experimental results of investigating the impact of tool rotational speed, traverse speed, and aluminium grade type on dissimilar friction stir butt welds of aluminium to copper plates.

4.1. FSW of aluminium-to-aluminium and copper-to-copper joints

This part of the study highlights the mechanical performance of defect-free butt joints made from similar grade materials using the FSW process. The welding conditions for achieving successful welds of AA6061 to AA6061, AA5083 to AA5083, and AA1061 to AA1061, as well as the optimum process parameters for producing defect-free FSW joints of copper-to-copper materials, were used as initial welding conditions to optimise the dissimilar aluminium to copper FSW process. The literature reports that successful welds of aluminium-to-aluminium materials can be obtained within the 800-1200 rpm tool rotational speed range and 80-150 mm/min tool welding speed range [4.1–4.3]. Meanwhile, defect-free joints of copper-to-copper FSW have been established within the 900-1400 rpm rotational speed range and 80-120 mm/min welding speed range [4.4–4.6]. Hence, a mutual welding condition of 1000 rpm tool rotational speed and 100 mm/min tool welding speed (10 ω/ν ratio) was considered appropriate to produce successful butt joints of aluminium-to-aluminium and copper-to-copper materials.

The mechanical evaluation of defect-free butt joints of aluminium-to-aluminium and copper-to-copper was conducted by measuring Vickers hardness across and at the middle of the weld cross-section (Fig. 4.1(a)). In the absence of IMCs formation in the weldment zone of similar FSW materials, the higher hardness values observed at the stirring zone were attributed solely to grain refinement resulting from the thermo-mechanical effect. Fig. 4.1(b) illustrates the microstructure of the stir zone (SZ) in a copper-to-copper FSW produced at 1000 rpm tool rotational speed and 100 mm/min welding speed, while Fig. 4.1(c) shows the as-received copper microstructure. It is evident that the grains are finer in the SZ and progressively increase in size towards the base metal. Similarly, Fig. 4.1(d) and Fig. 4.1(e) present the grain refinement mechanism in an AA5083-to-AA5083 FSW obtained at similar weld conditions to those of the copper-to-copper joint.

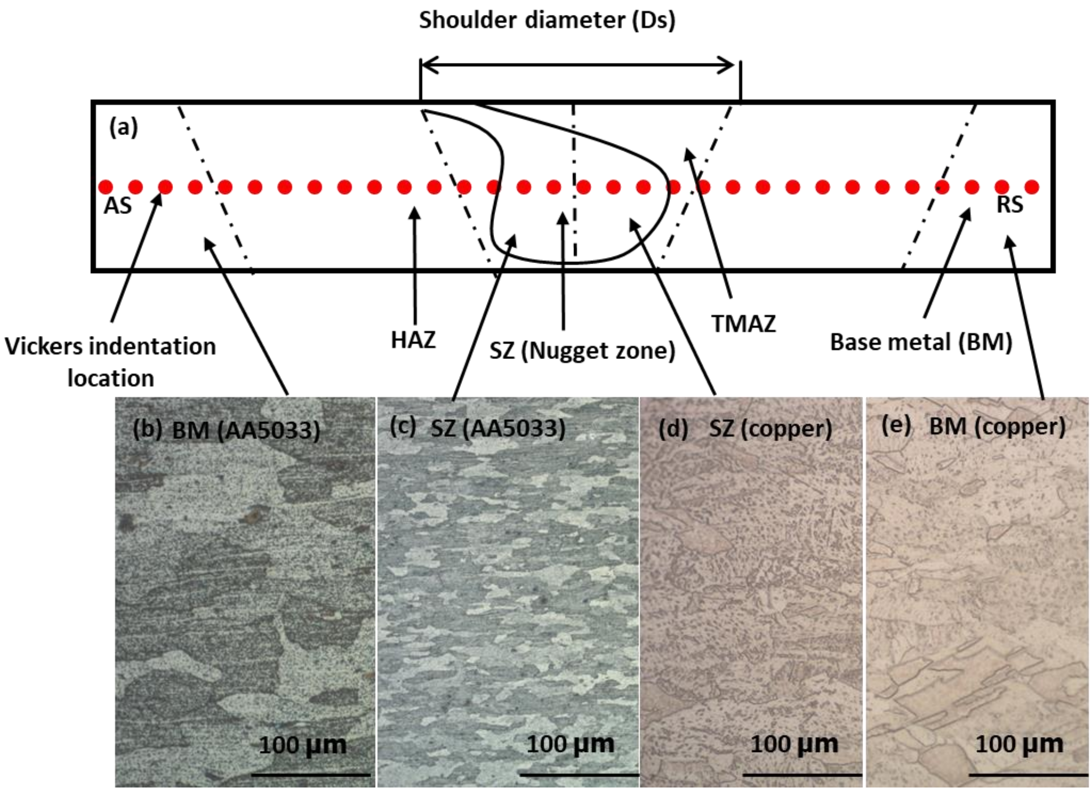

Fig. 4.1 (a) Vickers hardness measurement positions, typical microstructure of: (b) aluminium base metal, (c) aluminium-to-aluminium SZ, (d) copper-to-copper SZ, and (e) copper base metal.

Additionally, Fig. 4.2 depicts the Vickers hardness distribution profiles of similar AA5083-to-AA5083 and copper-to-copper joints. In which, the dashed lines in the figure are intended to represent the different zones within the weld, correlating to their respective hardness values. The results show a significant increase in hardness value at the SZ relative to the base metals, attributed to the plastic deformation of the workpiece caused by the FSW tool. Furthermore, grain refinement due to recrystallisation increases the hardness at the thermo-mechanically affected zone (TMAZ), while the heat-affected zone (HAZ) is mildly affected, resulting in a reduction in hardness on both sides of the HAZ.

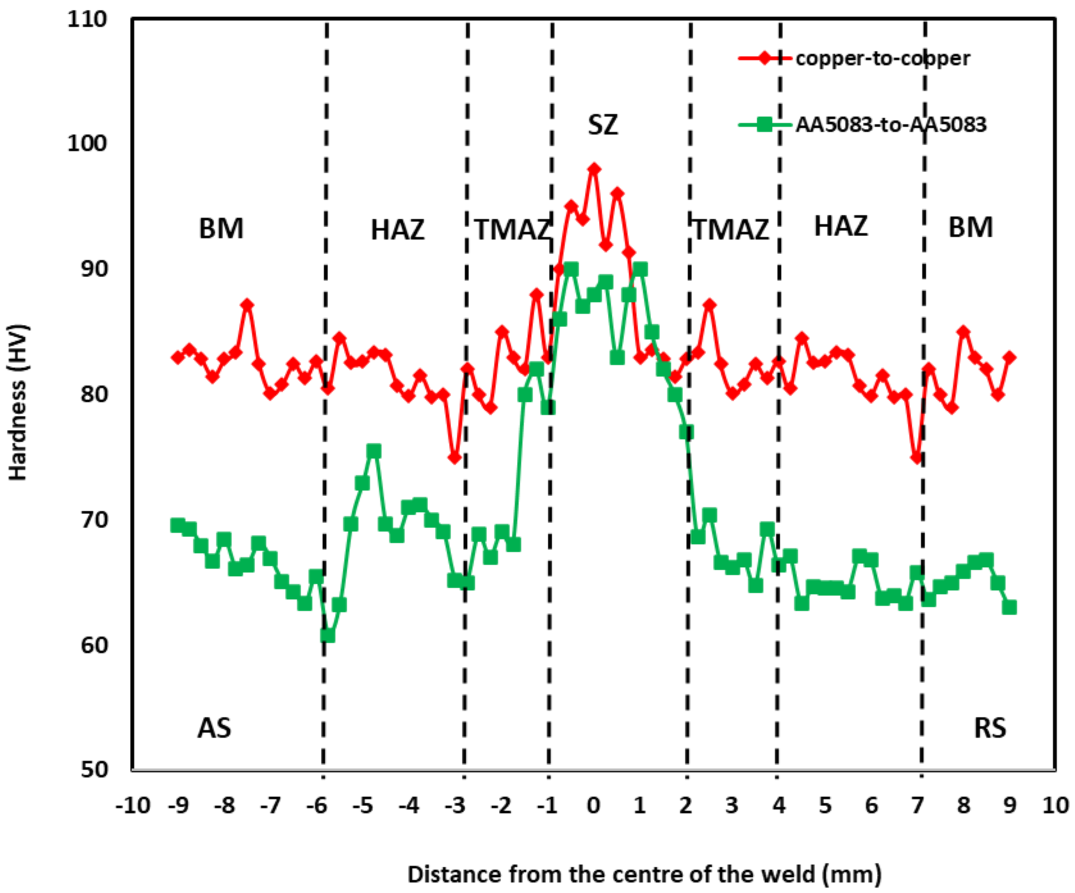

Fig. 4.2 Vickers hardness distribution at different weldment zone of copper-to-copper and AA5083 to AA5083 FSW joints.

The integrity of AA5083-to-AA5083 and copper-to-copper FSW joints was further investigated through tensile tests conducted across the weld line. Prior to these tests, care was taken to ensure that the specimens' post-weld thickness was consistent, accounting for minimal distortion as a result of the FSW process. Any excess material, or flash, resulting from the welding was carefully removed manually. This careful preparation ensured that the tensile test results would accurately reflect the quality of the weld without undue influence from variations in specimen thickness.

Fig. 4.3 illustrates the ultimate tensile strength (UTS) of AA6061 to AA6061, AA5083 to AA5083, and AA1061 to AA1061, and copper-to-copper butt joints produced by the FSW process, all at 1000 rpm tool rotational speed and 100 mm/min tool welding speed. In accordance with ASTM-E8 standards, a minimum of three tensile samples were prepared from each weld to evaluate the similar FSW joints. The labels UTS1, UTS2, and UTS3 on Fig. 4.3 represent the UTS values obtained from each individual sample, while the notation 'BM Avg. UTS' signifies the average UTS of the base metal for each material group, providing a baseline for comparison. The improvement in mechanical properties of similar joints is attributed to the optimal heat input and improved material mixing resulting from the FSW tool. The UTS of the produced welds for both aluminium-to-aluminium and copper-to-copper joints were found to be higher than the UTS of the base metal, indicating more than 100% mechanical joint efficiency.

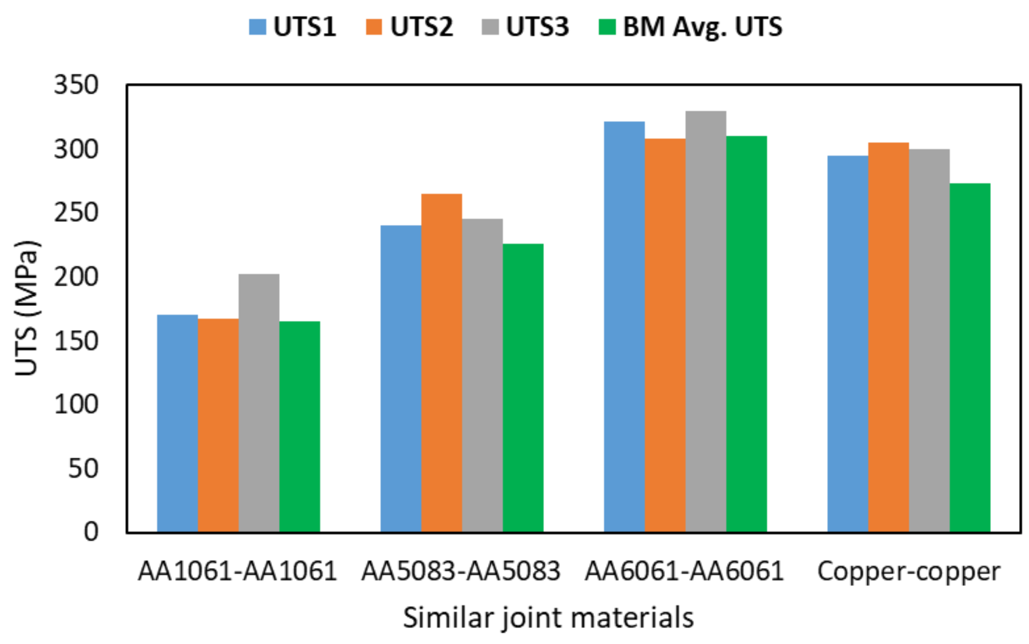

Fig. 4.3 Base metal Avg. UTS and the UTS of similar materials joints obtained at 1000 rpm and 100 mm/min (10 ω/v ratio) weld conditions.

The aforementioned mechanical analysis revealed that by using a mutual welding condition of 1000 rpm tool rotational speed and 100 mm/min tool welding speed (10 ω/v ratio), successful butt joints of aluminium-to-aluminium and copper-to-copper materials were produced. Consequently, these welding parameters were employed to set up the initial conditions required to achieve defect-free dissimilar joints between aluminium and copper.

The hypothesis is that an average range between the aluminium-to-aluminium and copper-to-copper FSW parameters is likely to result in sound weld dissimilar aluminium to copper FSW joints. This hypothesis is deemed acceptable due to the physical and chemical mismatch between aluminium and copper materials. For example, the amount of heat input required to achieve sufficient plasticity in copper-to-copper joints is higher than that required for aluminium-to-aluminium joints [4.7–4.11], necessitating consideration of an average amount of heat input to achieve successful dissimilar FSW of aluminium to copper.

Fig. 4.4 depicts the likelihood of FSW conditions for producing defect-free joints in dissimilar aluminium to copper. It is worth noting that the likelihood boundaries illustrated were informed by the mutual tool rotational speed to welding speed (ω/v) ratio, which yielded defect-free joints in similar copper-copper and aluminium-to-aluminium FSW joints, as well as the extensively documented process windows for similar materials [4.7–4.11]. This was a crucial step in determining the preliminary conditions for successful dissimilar Al to copper FSW joints, ensuring that the optimisation of the FSW process for dissimilar materials commenced from a proven baseline, thereby increasing the reliability of subsequent experimental outcomes.

Further details on the FSW experiments carried out to achieve defect-free dissimilar joints between aluminium and copper is provided in section 3.1.2.

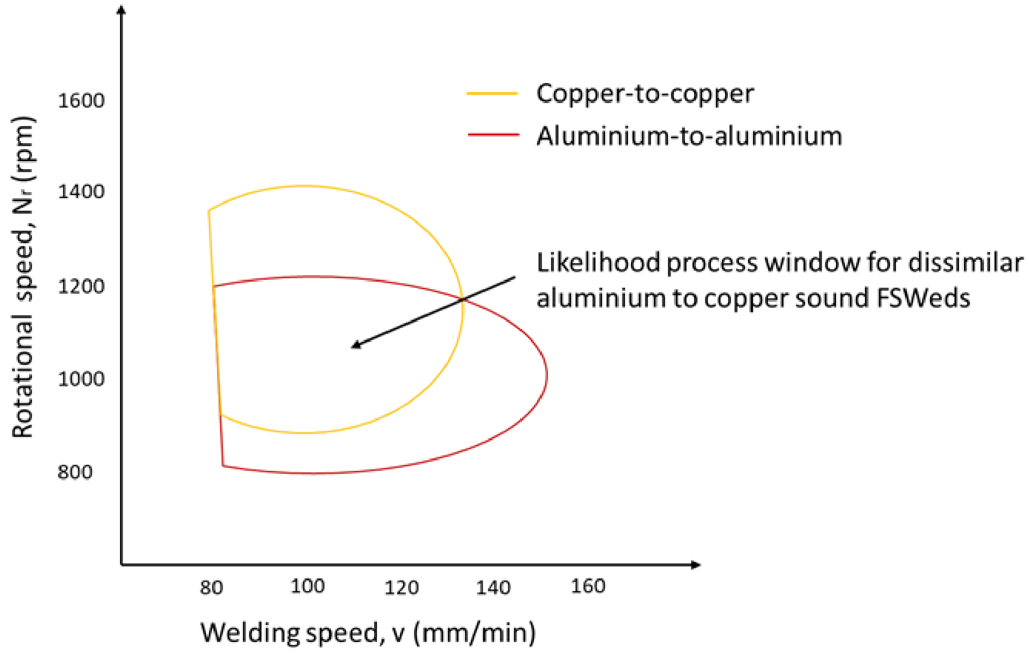

Fig. 4.4 The likelihood of FSW conditions for defect-free joints in dissimilar aluminium to copper.

4.2. Microstructural characterisation of dissimilar AA5083 to copper joints

The objective of this part is to examine the effect of tool rotational speed and tool traverse speed on dissimilar friction stir butt welds of 3 mm thick AA5083 to commercially pure copper plates. The evaluation of joint quality in relation to tool rotational and traverse speed was conducted with the aluminium placed on the AS and without introducing the complexities of tool offsetting. Three parameter sets of rotational and traverse speed were used to investigate the relationship between joint microstructure and mechanical properties, a summary of these welding parameters is provided previously in Table 3.3.

4.2.1. Weld appearance and macrostructure

Table 4.1 illustrates the typical top surface weld appearance and cross-sectional macrostructures of AA5083 to copper dissimilar metal FSW joints at different welding conditions. The symbols used for each defect type correspond to Fig. 4.5. As expected, the weld surface quality is indicative of the tendency for volumetric defects to develop [4.12]. For instance, excessive flash formation, as well as material discontinuity, will generally suggest volumetric defects [4.13]. Fig. 4.5 summarises the effect of tool rotational and traverse speed on the weld appearance and macrostructure when AA5083 was placed on the AS without tool offset. Visually acceptable welds with no surface defects were obtained at the following specific parameter sets:

- Low rotational speed level of 1000 rpm at 100 mm/min and 120 mm/min welding speeds (10 and 8.3 ω/ν ratio).
- Intermediate rotation rate level of 1200 rpm and 80 mm/min (15 ω/ν ratio).
- High rotation rate level of 1400 rpm for the two ranges of the welding speed 80, and 120 mm/min (17.5, and 11.7 ω/ν ratio), respectively.

Parameter sets outside of the above conditions resulted in an uneven surface and the formation of defects such as macro-cracks towards the retreating side (copper, Figure 4.6(a)), cavities with a defect area on the cross-section less than 0.02 mm² (Fig. 4.6(b)), voids (Fig. 4.6(c)), and tunnel defects with a defect area larger than 0.05 mm² (Fig. 4.6(d)). These types of defects have been previously reported [4.14] ,where cracks are often associated with the formation of large IMC particles, cavities, voids, and tunnel defects due to inappropriate material flow.

Table 4.1 Weld appearance and macrostructure of dissimilar joints (marks as in Fig. 4.5)

Mark	Defect	Appearance and Macrostructure	Microstructure
●	None		-
⬟	Crack	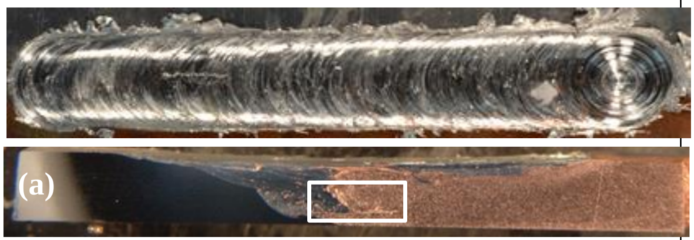	Fig. 4.6 (a)
◆	Cavity	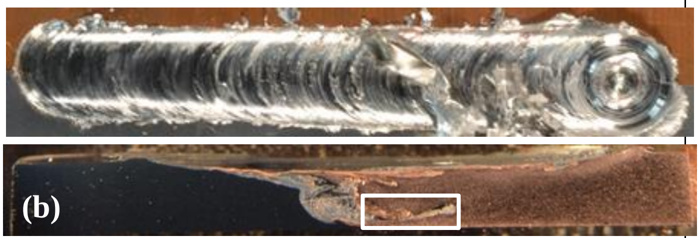	Fig. 4.6 (b)
■	Void	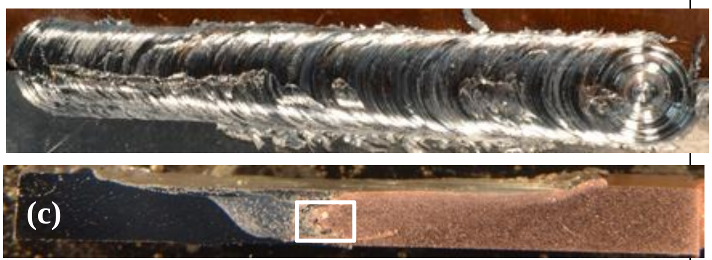	Fig. 4.6 (c)
▲	Tunnel	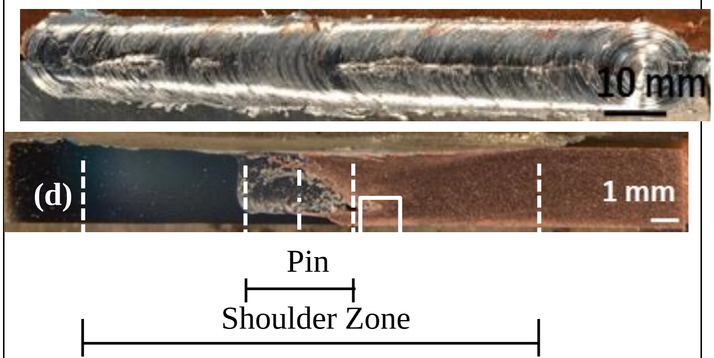	Fig. 4.6 (d)

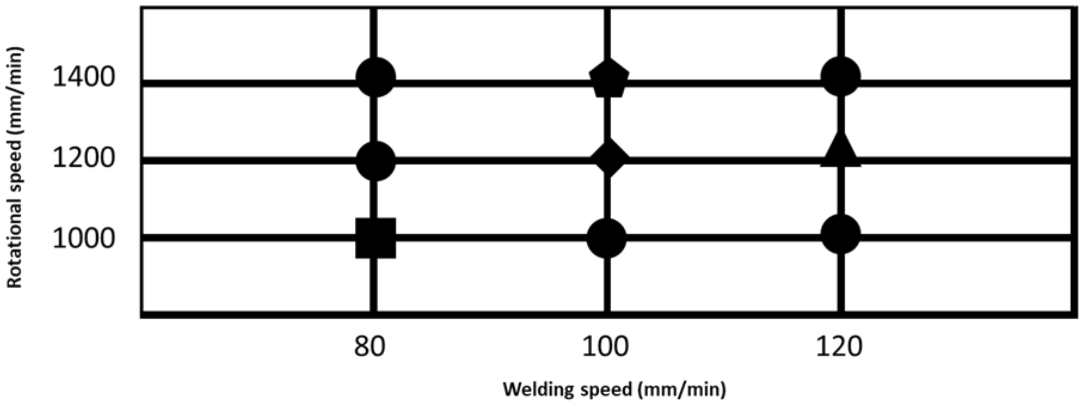

Fig. 4.5 Effect of tool rotational and traverse speed on macrostructure.

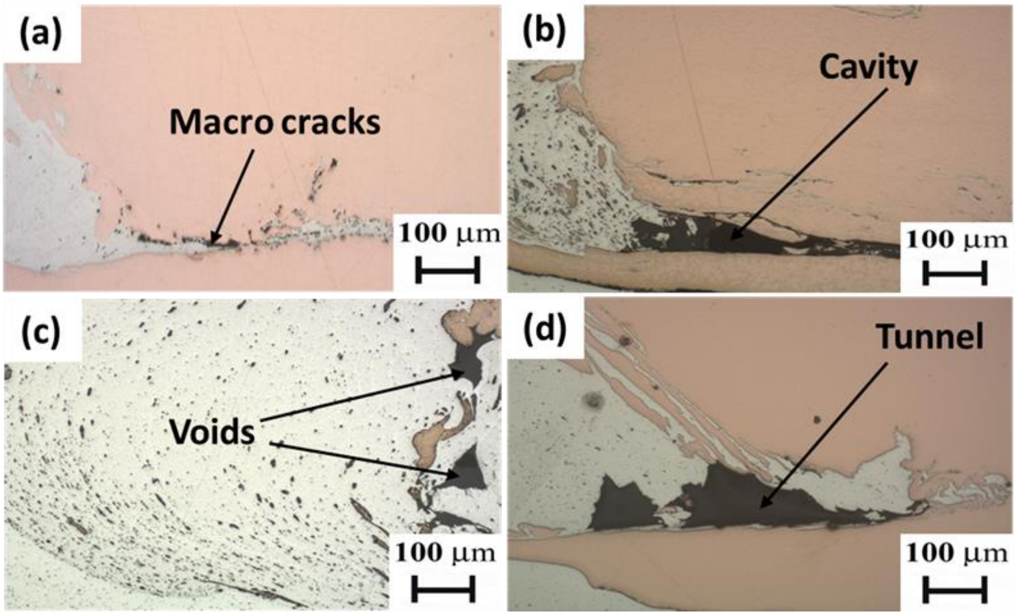

Fig. 4.6 Magnified views for different defects on regions marked in Table 4.1.

4.2.2. Microstructural analysis

The weld mechanical integrity is directly related to the SZ microstructure. A classical "onion ring" structure is commonly found in the SZ of similar material FSW joints [4.15]. In dissimilar material FSW however, a swirl-like pattern, banded or lamella structure, as well as vortex-type microstructures, are formed in the SZ, TMAZ and also in the HAZ [4.14]. Fig. 4.7 (a) represents an example of a typical cross-section of

AA5083 (AS) to copper dissimilar metal FSW joint welded at 1000 rpm and 100 mm/min. It is worth noting that, to ensure a comprehensive evaluation of such microstructures, cross-section samples were carefully extracted from the beginning, middle, and end of the weld across several joints, all welded under the same conditions. This multi-point, multi-joint sampling strategy provided a robust basis for assessing the integrity and consistency of the weld, allowing for a detailed characterisation of the microstructural evolution throughout the entire length of the weld. Towards the aluminium side (Fig. 4.7 (b&e)), relatively small copper particles were observed as regularly distributed between the aluminium interface zone and the upper surface of the SZ. Fig. 4.7 (c&f) illustrate that at the SZ, larger copper particles (fragments) were stretched and irregularly distributed along the SZ and towards the bottom of the interfacial region between the SZ and the copper side. The irregular copper particles created a lamella structure of copper and aluminium at the bottom of the TMAZ towards the copper side (Fig. 4.7 (d&g)).

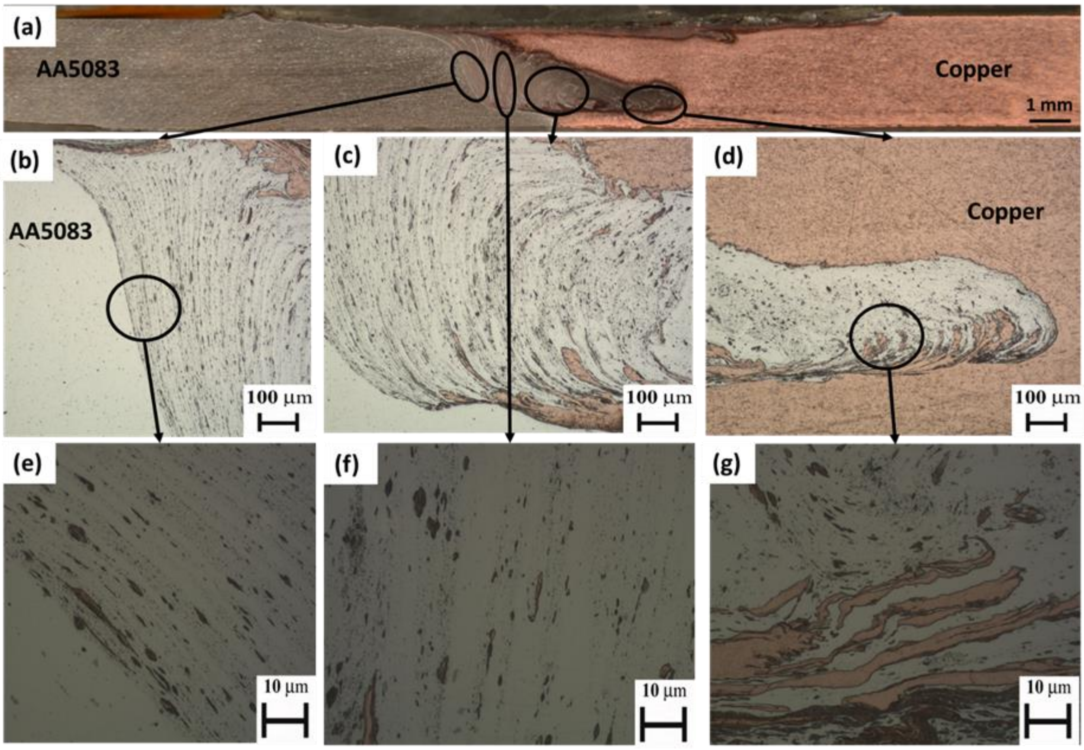

Fig. 4.7 (a) Typical cross-section of joint welded at 1000 rpm and 100 mm/min. (b&e) interface zone towards AA5083 side. (c&f) SZ. (d&g) interface zone towards the copper side.

EDS analysis was performed to reveal the variation on the aluminium and copper content at 1000 rpm, 100 mm/min i.e., 10 ω/v. It can be revealed from Fig. 4.8 (a) and Table 4.2 that good intermixing between aluminium and copper was achieved. Table 4.2 also shows the presence of different aluminium solid solutions at this low level of rotational speed. The identification of these non-equilibrium solid solutions was substantiated by cross-referencing with the Al-Cu phase diagram, which provides a theoretical framework for anticipating the phases that might form under specific compositional and thermal conditions [4.14], similar phase formations were also observed under comparable welding conditions [4.21].

Further, Fig. 4.8 (e) presents an example of how the EDS analysis was performed to capture the variation on the aluminium and copper content. Unetched microstructures for the distinctive regions from Fig. 4.8 (a): Al-SZ (rectangular i), inside the SZ (rectangular ii) as well as Cu-SZ (rectangular iii), are presented in Fig. 4.8 (b), (c) and (d), respectively. The dark shaded layers surrounding the copper particles and fragments demonstrate the formation of the Al/Cu intermixed region as shown by the arrows. This embedded layer was previously reported to accompany the formation of Al/Cu IMCs [4.16]. Moderate stirring action was observed on the copper particles and fragments, which indicates the absence of the composite-like structure under this condition. Additionally, detached copper pieces failed to react with the aluminium matrix on the AS resulting in the absence of any lamella or banded structures at the interface zone.

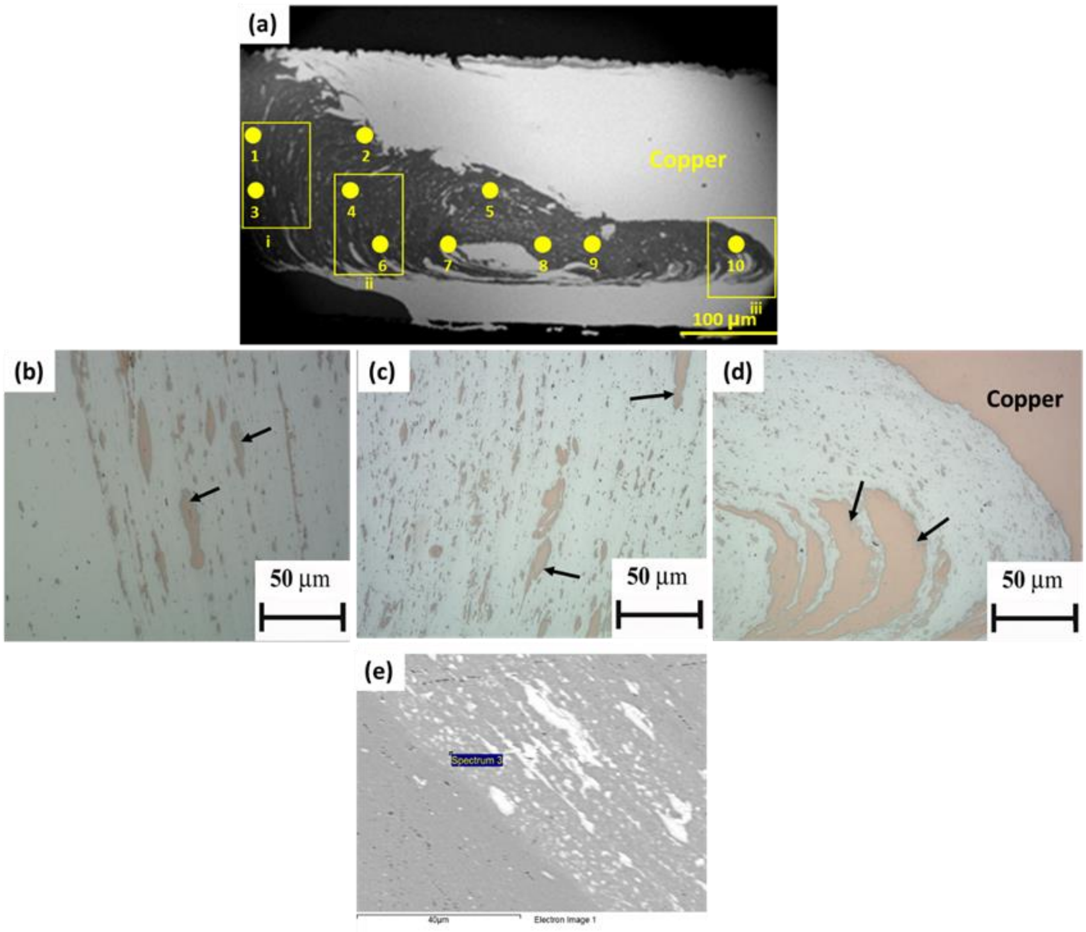

Fig. 4.8 (a) SEM image and EDS points at the weld zone of test at 100 rpm and 100mm/min. Magnified view of specific regions in Fig. 4.8 (a): (b) region i, (c) region ii, (d) region iii, (e) region i.

Table 4.2 EDS results at weld SZ of Test no. 2

Position	**Al at. %**	**Cu at. %**	**Non equilibrium solid solution**
1	75.14	24.86	-
2	62.76	37.24	-
3	90.35	9.65	Al (Cu)
4	85.84	14.16	Al (Cu)
5	61.98	38.02	-
6	68.08	31.92	-
7	67.18	32.82	-
8	79.26	20.74	-
9	37.72	62.28	-
10	35.22	64.78	-

A cross-section of an AA5083 to copper defect-free joint at a higher level of rotational speed is shown in Fig. 4.9 (a), as-welded at 1400 rpm and 80 mm/min with AA5083 on AS and no tool offset. Although three distinctive regions can still be observed across the weld joint, these regions were completely different from the example of lower welding speed, i.e., 1000 rpm. The complex structure has formed in the aluminium side of the interface and towards the SZ as shown in Fig. 4.9 (b&e). Copper fragments were detached from the RS and stirred with the aluminium matrix to create this complex structure. A higher heat input is the reason behind this complex structure, where the stirring action was insufficient to create this structure at a lower level of rotational speed. Evidence of the relationship between the heat input and the plastic stirring action was also observed inside the SZ in Fig. 4.9 (c&f) and this resulted in the swirl and vortex-like structure. Unlike others [4.17–4.19], placing the copper on the RS without tool offset produced a wider TMAZ at the Al/Cu interface as illustrated in Fig. 4.9 (d&g).

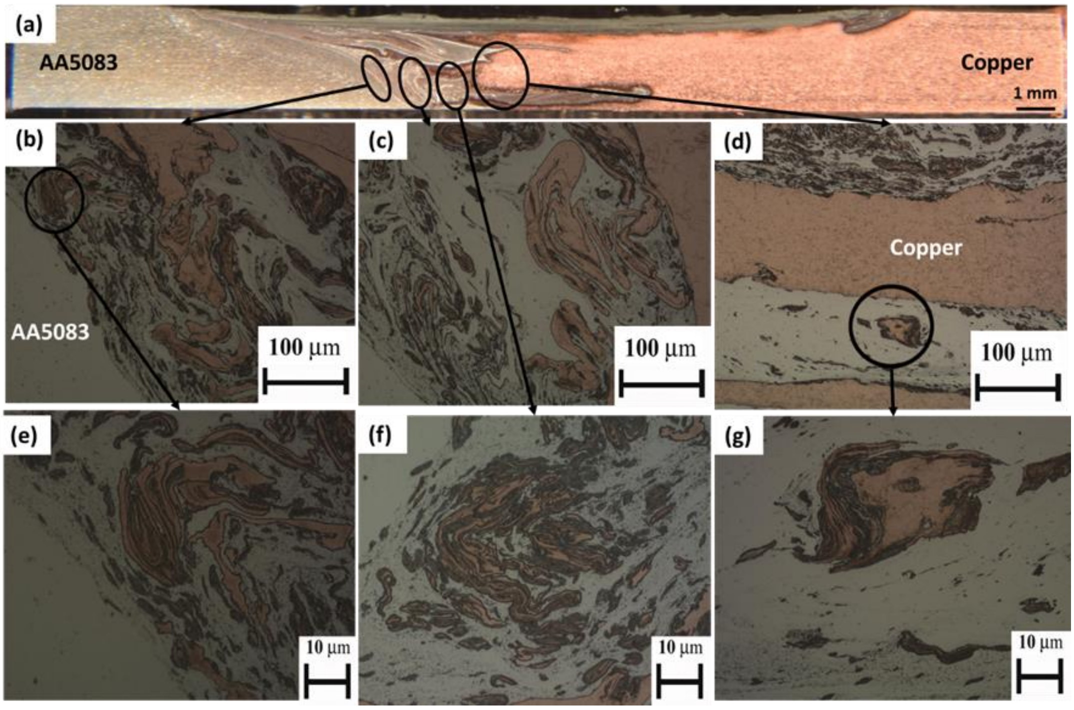

Fig. 4.9 (a) Typical cross-section of joint welded at 1400 rpm and 80 mm/min. (b&e) interface zone towards AA5083 side. (c&f) SZ. (d&g) interface zone towards copper side.

Likewise, EDS was applied at different positions on the weld zone as illustrated in Fig. 4.10 (a), where Table 4.3 summarises the elemental compositions at these points, Fig. 4.10 (e) demonstrates an example of these EDS points. Table 4.3 also shows the variation in Al/Cu contents as a result of good intermixing and the absence of non-equilibrium solid solutions. An enlarged view of rectangle (i) in Fig. 4.10 (a) is shown in Fig. 4.10 (b). A complex structure can be detected from the unetched microstructure of this region, and the chemical compositions of points 1 and 2 in Table 4.3 show slight variation in the aluminium and copper contents. The composite-like structure at the upper region of the Cu-SZ (rectangle (ii)) resulted in two different contents of Al/Cu as illustrated in Fig. 4.10 (c) and Table 4.3. The higher heat input (1400 rpm) and the tool stirring action formed similar variation in Al/Cu at the bottom of Cu-SZ as shown in Fig. 4.10 (d) of rectangle (iii). The dark shaded layers that surrounded the copper particles and accompanied the formation of Al/Cu IMCs are shown by the arrows.

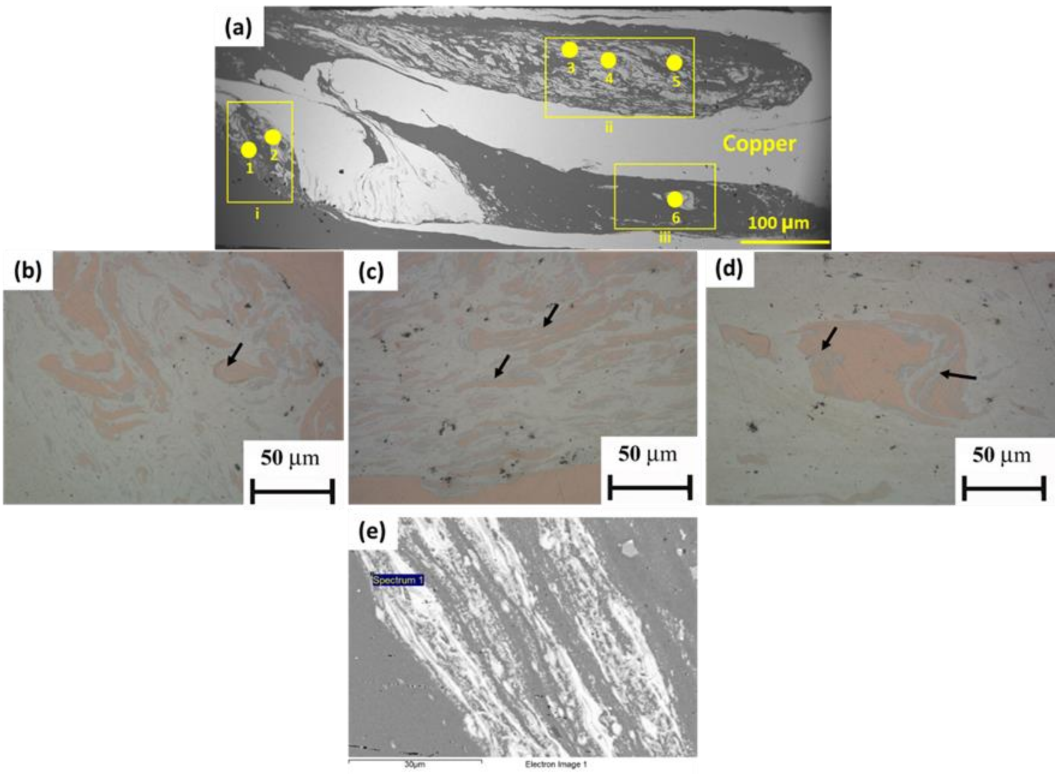

Fig. 4.10 (a) SEM image and EDS points at the weld zone at 1400 rpm and 80 mm/min. (b) Enlarge view of rectangular i in Fig. 4.1 (a). (c) Enlarge view of rectangular ii in Fig. 4.10 (a). (d) Enlarge view of rectangular (iii) in Fig. 4.10 (a). (e) Enlarge SEM image of rectangular (i) in Fig, 4.10 (a).

Table 4.3 EDS results at weld SZ condition 7

Position	**Al at. %**	**Cu at. %**
1	76.5	23.5
2	71.7	28.3
3	55.27	44.73
4	62.62	37.38
5	67.38	32.64
6	33.72	66.28

4.2.3. Interfacial elemental diffusion

The key factor to critically analysing the joint quality in FSW of dissimilar aluminium to copper is by characterising the structure of the interfacial region [4.14]. The elemental diffusion and structure are able to confirm a reliable joint [4.16]. Fig. 4.11 (a) represents a magnified view of the interfacial region between the aluminium and the SZ of test at 1200 rpm tool rotational speed and 80 mm/min tool welding speed as etched by the aluminium etching solution. Continuous layers of refined aluminium grains are clearly observed. Copper particles with different sizes are diffused along with the refined layers of aluminium as evidence of good metallurgical bonding. The resultant SZ, as shown in

Fig. 4.11 (b), elucidates that the continuous interfacial layer subsequently leads to the lamella structure that significantly improves the joint mechanical strength.

The interfacial region formed a composite-like structure as a result of increasing the heat input, as shown in Fig. 4.11 (c) of test at 1400 rpm tool rotational speed and 80 mm/min tool welding speed. It has been reported previously [4.10] that, the resultant joint strength is greatly improved by this structure. As it has been demonstrated in Fig. 4.11 (d), this composite-like structure was also dominant inside the SZ.

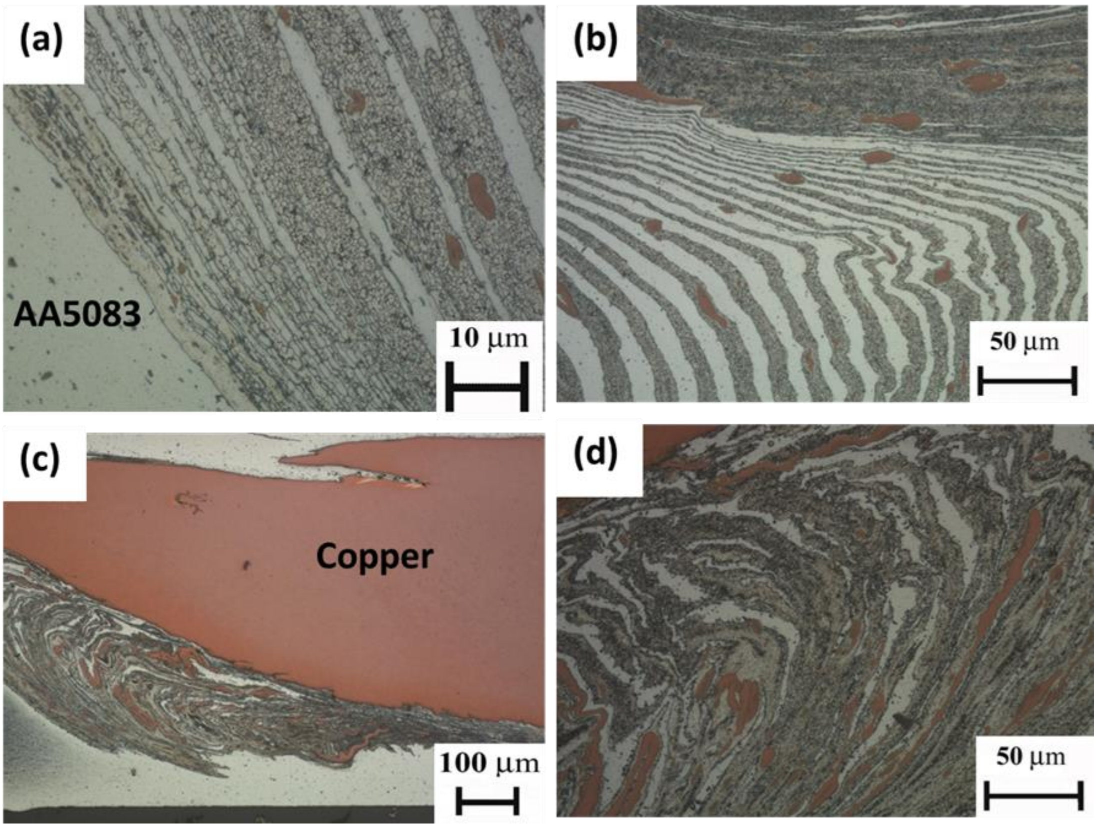

Fig. 4.11 (a) Interfacial microstructure of the joint produced at 1200 rpm and 80 mm/min. (b) Lamella structure inside the SZ at 1200 rpm and 80 mm/min. (c) Interfacial microstructure of the joint produced at 1400 rpm and 80 mm/min. (d) Composite-like structure inside the SZ at 1400 rpm and 80 mm/min.

4.2.4. Intermetallic phases

XRD analysis was performed through the cross-sections to identify the phases present in the SZ. Fig. 4.12 presents the XRD patterns of three typical defect- free joints of test no. 2, 4 and 7 of Table 3.3. The dominant IMCs on the SZ of AA5083 and copper are Al_2Cu and Al_4Cu_9, and these are confirmed from the three patterns, apart from the fact that AlCu was only detected under test no. 7. According to the above microstructure analysis of test no. 2 and 7, it can be established that the nature and quantity of IMCs are affected by the weld conditions. Peak intensity changes by varying the welding conditions, where 1000 rpm and 100 mm/min, 1200 rpm and 80 mm/min and 1400 rpm and 80 are the tool rotational speed and tool welding speed of test no. 2, 4 and 7, respectively. As observed, the peak intensity increases by increasing the tool rotational speed. It has been previously reported [4.20] that, the variation of the intensity peaks is attributed to the complex mixing between Al-Cu overall, where relatively high intensity peaks indicate a higher IMC quantity [4.18]

According to the Al-Cu phase diagram, the formation temperature Al_2Cu phase is relatively low [4.21]. Therefore, it is expected that Al_2Cu will be present in the SZ as the temperature during welding is known to reach 0.8-0.9 of the aluminium melting temperature [4.12] i.e., exceeding the formation temperature of Al_2Cu. However, the IMCs cannot be exclusively predicted on the basis of an Al-Cu phase diagram, where the chemical reactions occurring during the FSW under the thermal cycles are far from the equilibrium condition [4.21]. In the case of Al_4Cu_9, the thermo-mechanical effect of FSW explains its formation at the SZ, where the melting temperature of this IMC i.e., 1030°C [4.10] is higher than the peak temperature during FSW.

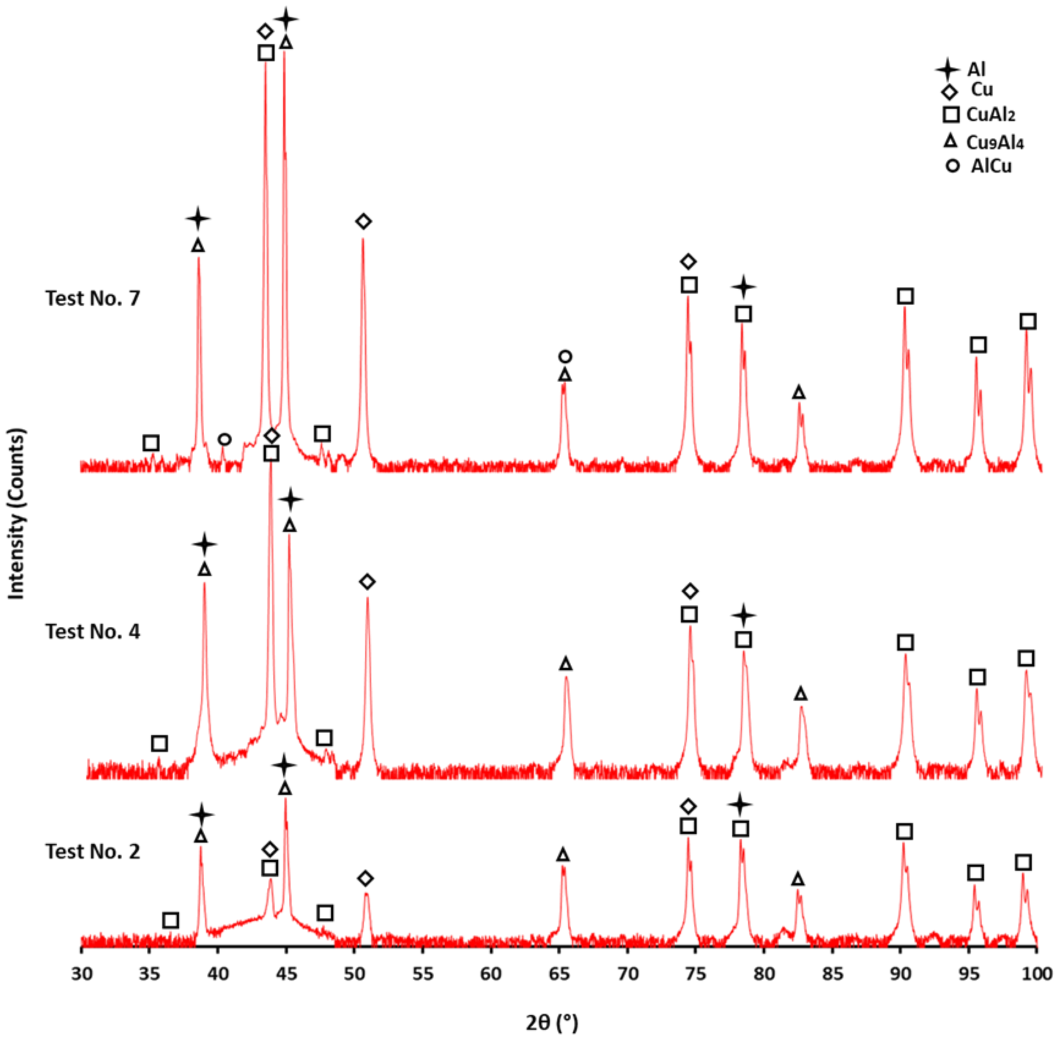

Fig. 4.12 XRD patterns acquired under tests no. 2, 4 and 7 of Table 3.3.

4.2.5. Microhardness distribution

Fig. 4.13 demonstrates the Vickers hardness distribution profiles of dissimilar joints measured across and at the middle of the weld cross-section. It is observed that the hardness value increases significantly at the SZ relative to the base metals due to the presence of the IMCs which are hard and brittle in nature [4.18] accompanied with the formation of very fine recrystallised grains and copper-rich dispersed particles.

On the other hand, the combined effect of IMC formation and grain refinement due to the recrystallisation increases the hardness at the TMAZ. The HAZ in dissimilar FSW of aluminium to copper is mildly affected by the recrystallisation; this reduces the hardness in both HAZ sides [4.14], similar effect of the recrystallisation mechanism has previously been reported in similar AA5083-to-AA5083 and copper-to-copper FSW joints (section 4.1). The hardness variations are a direct result of the heterogeneous distribution of IMCs along with the dissimilar materials (aluminium or copper) within the SZ.

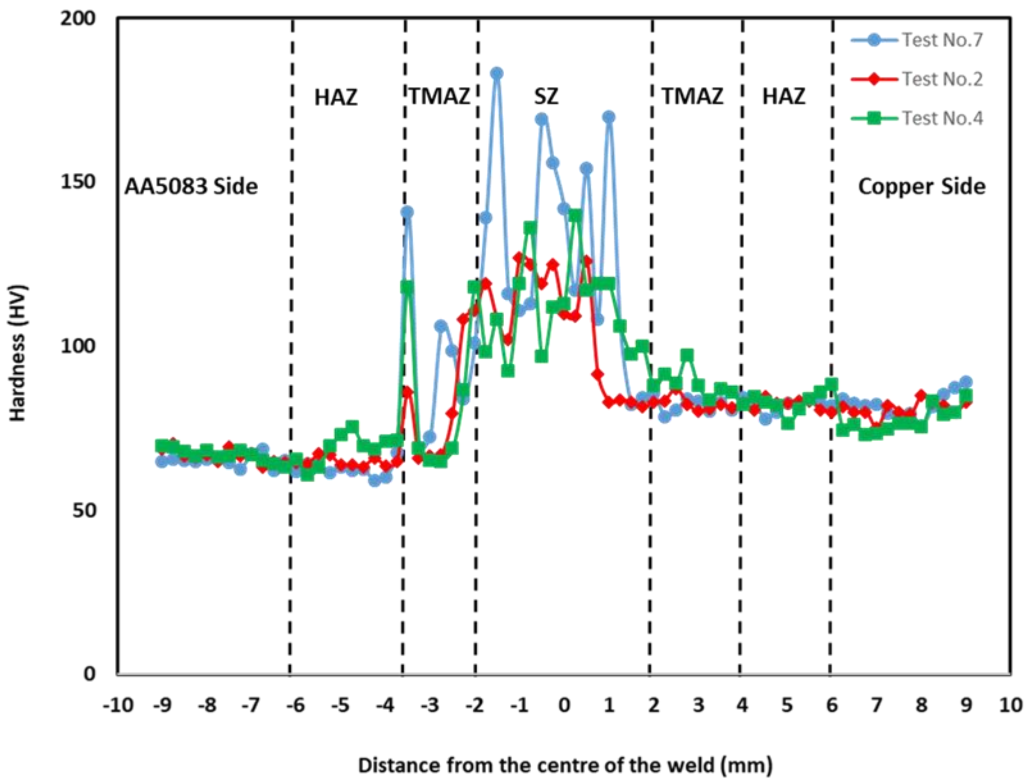

Fig. 4.13 Hardness distribution under tests no. 2, 4 and 7 of Table 3.3.

4.2.6. Joint mechanical strength

The performance of the dissimilar joints has been evaluated by assessing the tensile properties. Fig. 4.14 shows the yield strength, UTS and joint efficiency at the conditions that developed defect-free joints. Unlike other published work [4.10], [4.13], and [4.22], placing the softer material (AA5083) on the AS resulted in higher tensile strength. The error bars presented in Fig. 4.14 correspond to the standard deviation of the data, indicating the variability within the set of measurements for each sample. These bars provide insight into the consistency of the UTS values obtained from multiple tests of each joint type under the same welding conditions, thereby offering a statistical measure of the repeatability and precision of the FSW process as applied in this study. The increase in tensile properties can be directly linked to the nature and quantity of IMCs in addition to the evolved microstructure, where proper material mixing is required to enhance the joint mechanical performance [4.23]. Moreover, significant improvements in the joint tensile properties were achieved compared to other studies that placed the harder material (copper) on the AS [4.17], [4.18], and [4.24].

It is revealed from Fig. 4.14 that the effect of the tool rotational speed, in general, is higher than the effect of the welding speed, as this increases the heat input and subsequently improves the level of inter-mixing. Increasing the welding speed for the same level of tool rotational speed results in minor improvements in the joint UTS. The evolution of the composite-like structure that was produced at a higher level of tool rotational speed (1400 rpm) is the main reason for this improvement. The benefits of this structure on the joint strength have also been reported previously [4.12].

One of the most important criteria to identify the weld joint performance is by expressing the joint efficiency, i.e., the ratio of the weld tensile strength to the workpiece tensile strength, where a joint efficiency lower than 100% is generally reported during FSW of dissimilar aluminium/copper joints [4.14]. This efficiency is always relative to the lower UTS of aluminium base metal. In this work, high joint efficiency values were achieved at the conditions that yielded defect-free joints. Up to 94.8% joint efficiency was calculated at 1400 rpm and 120 mm/min, which is higher than the previously reported efficiency of 75.6% when considering the softer material on the AS [4.24].

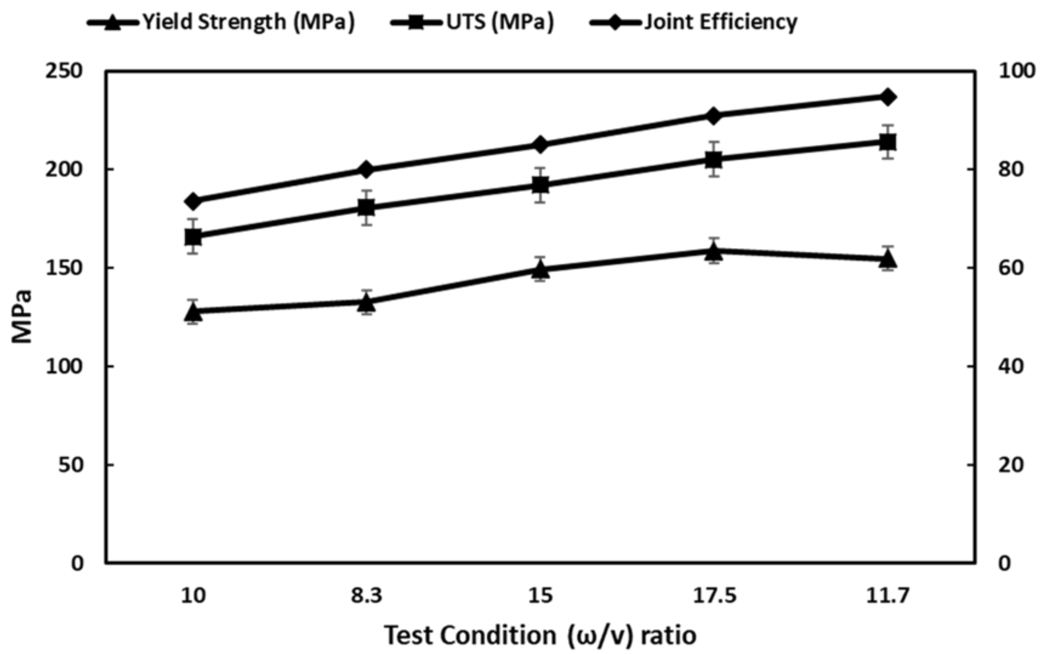

Fig. 4.14 Yield strength, UTS and joint efficiency at different welding conditions.

The typical fracture surface for three different welding conditions is shown in Fig. 4.15. Failure occurred at the AS-TMAZ at the relatively low rotational speed of 1000 rpm and 100 mm/min welding speed (Fig. 4.14 (a&d)). The failure location gradually shifted to the AS-HAZ by increasing the rotational speed as in Fig. 4.15 (b&e) and (c&f) of 1200 rpm-80 mm/min and 1400 rpm-80 mm/min, respectively. This change in failure location, shifting away from the weld zone and towards the AA5083 parent material is in full agreement with the gradual increase in joint efficiency, as displayed in Fig. 4.14.

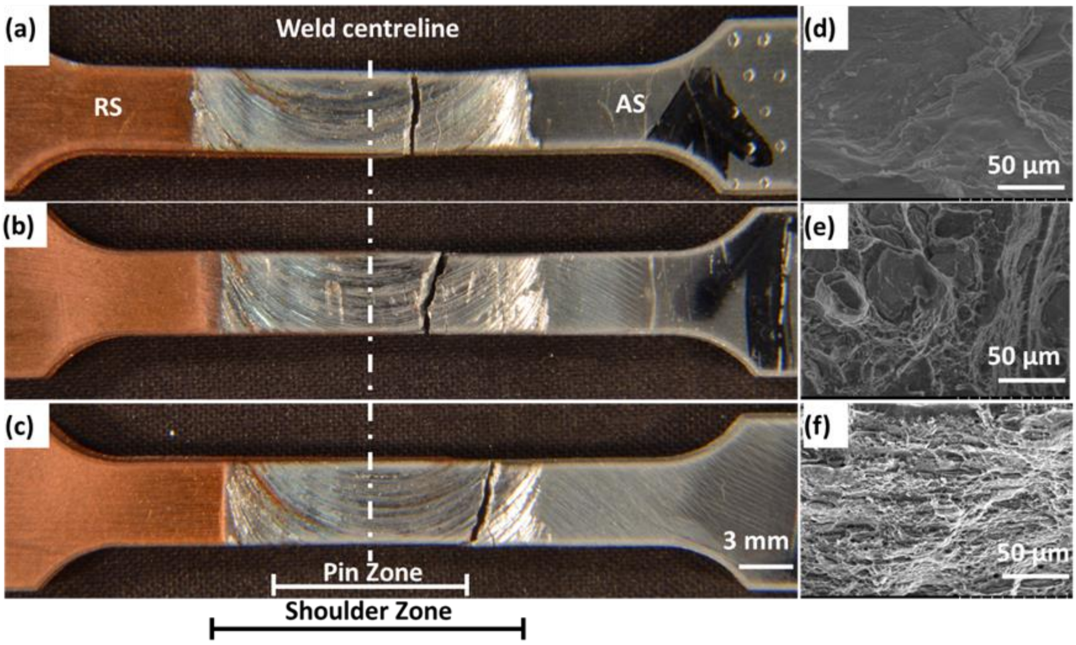

Fig. 4.15 Fractography of the welds at tests no. 2 (a&d), 4 (b&e) and 7 (c&f).

4.3. Development of processing window for dissimilar aluminium to copper joints produced by FSW

Section 4.2 of this chapter presents the experimental results of investigating AA5083 to commercially pure copper FSW joints and identifies the conditions that resulted in successful joints. Based on the results presented in section 4.2, the following key conclusions have been drawn:

- Successful weld joints between the two dissimilar materials were achieved at different rotational and traverse speeds, where the harder material (copper) was placed at the RS without any tool offset.
- An inhomogeneous microstructure was observed inside and on the interfacial zone when copper particles detached and intermixed with the aluminium matrix.

- A composite-like structure was observed at a higher level of rotational speed, while the lamella or dispersed structures were found at a low level of rotational speed.
- The predominant IMCs at the aluminium-copper joint were Al_2Cu and Al_4Cu_9.
- The volume fraction of the IMCs inside the SZ increased with increasing tool rotational speed, as confirmed by the high XRD peak intensities and higher hardness values.
- The UTS reached 203 MPa, representing a joint efficiency of 94.8% of the aluminium alloy, as a result of the composite-like structure and an excellent metallurgical bond.

Further experimental investigations were conducted to report on the effect of using different aluminium alloys on the joint quality of dissimilar aluminium to copper FSW. Aluminium grades AA1061 and AA6061 were separately welded to copper at different tool rotational speeds and traverse speeds as previously indicated in Tables 3.4 and 3.5, respectively. The optimal process parameters for achieving defect-free joints were identified through macro and microstructural analysis, as well as EDS and X-ray diffraction techniques to assess the presence and distribution of IMCs. The hardness distribution at different weld zones was also considered, allowed for the joint mechanical strength to be predicted.

Fig. 4.16 summarises the optimum process parameters that always yield defect-free joints of dissimilar aluminium to copper FSW using different aluminium grades, based on the macro/microstructural analysis. It has been observed that dissimilar FSW of aluminium to copper was influenced by the aluminium grade, in that the joint mechanical strength varied when copper was FSWed to different aluminium grade types.

It is noteworthy that Fig. 4.16 primarily reflects the successful outcomes from a series of parameters that were experimentally verified (indicated by green circles). However, it is important to acknowledge that other (ω/v) ratios inside or outside these green circles may still hold the potential for successful dissimilar FSW joints, albeit potentially with a lower likelihood of defect-free. It is also worth to highlight that the scope of this study was bounded by the resources available; for instance, the work was conducted using a uniform workpiece thickness of 3 mm. Future investigations could expand upon these findings, studying the effects of varying plate thicknesses and tool dimensions (D/t ratio) to establish a more universal set of non-dimensional process parameters. Such investigation would enhance the applicability of the FSW process across different material thicknesses and contribute to a broader understanding of the size effect in FSW.

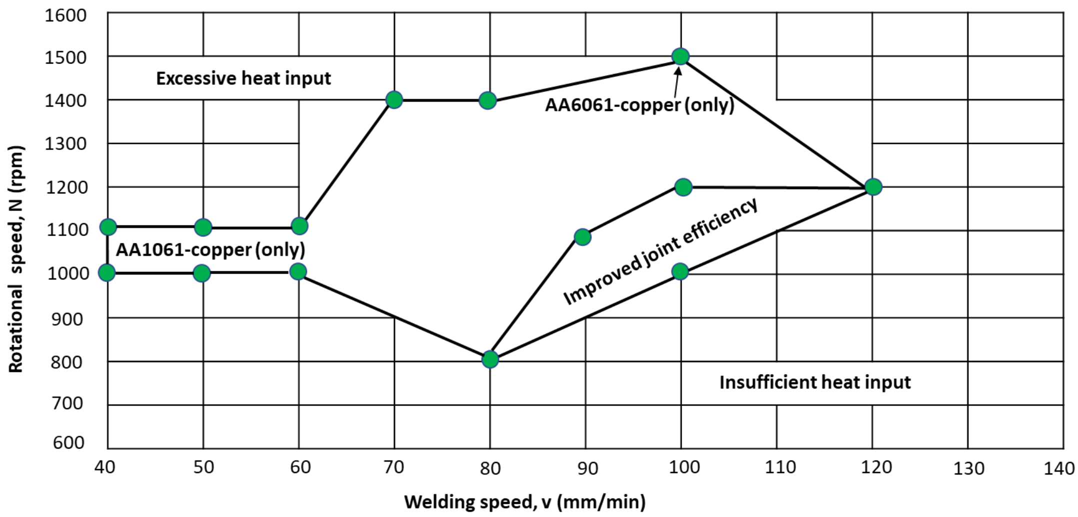

Fig. 4.16 Dissimilar aluminium to copper FSW window based on macro/microstructural analysis.

Further investigation was carried out to examine whether the mechanical performance of dissimilar aluminium to copper joints is significantly affected by using different aluminium grades on the AS. The results of the dissimilar joints' UTS and flexure stress tests are shown in Fig. 4.17 and Fig. 4.18, respectively. It is evident that the joint UTS and flexure stress were influenced by the AS aluminium grade. Specifically, a relatively higher joint UTS was obtained when using AA5083 as compared to other aluminium grades when welded to commercially pure copper. Additionally, the flexure stress of dissimilar aluminium to copper joints increased when using aluminium grade AA5083 on the AS while keeping the harder material (copper) on the RS.

Further, the inconclusiveness observed Fig. 4.17 (c) and Fig. 4.18 (c), was attributed to the relatively narrower range of tool rotational to welding speed (ω/v) ratios that were found to yield higher joints' mechanical strength, particularly for the AA6061 to copper FSW joints. This outcome underscores the significant challenge involved in achieving high mechanical performance across a broad range of ω/v ratios.

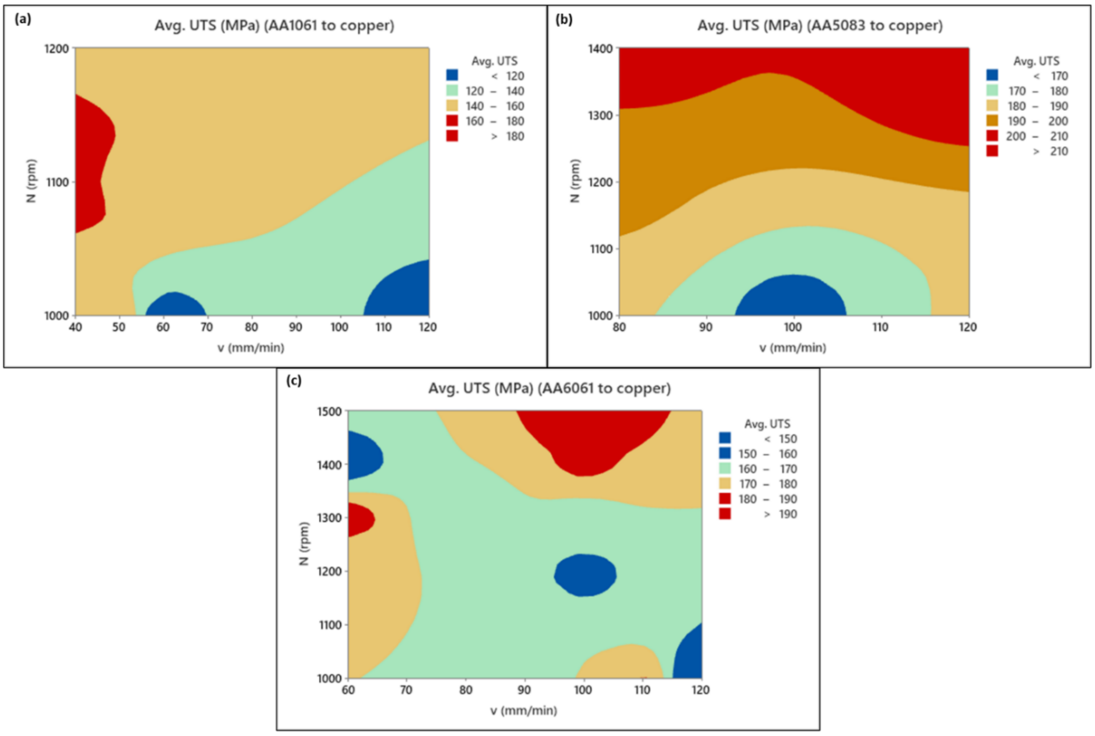

Fig. 4.17 Dissimilar joints UTS (MPa) at different welding conditions and aluminium grade types.

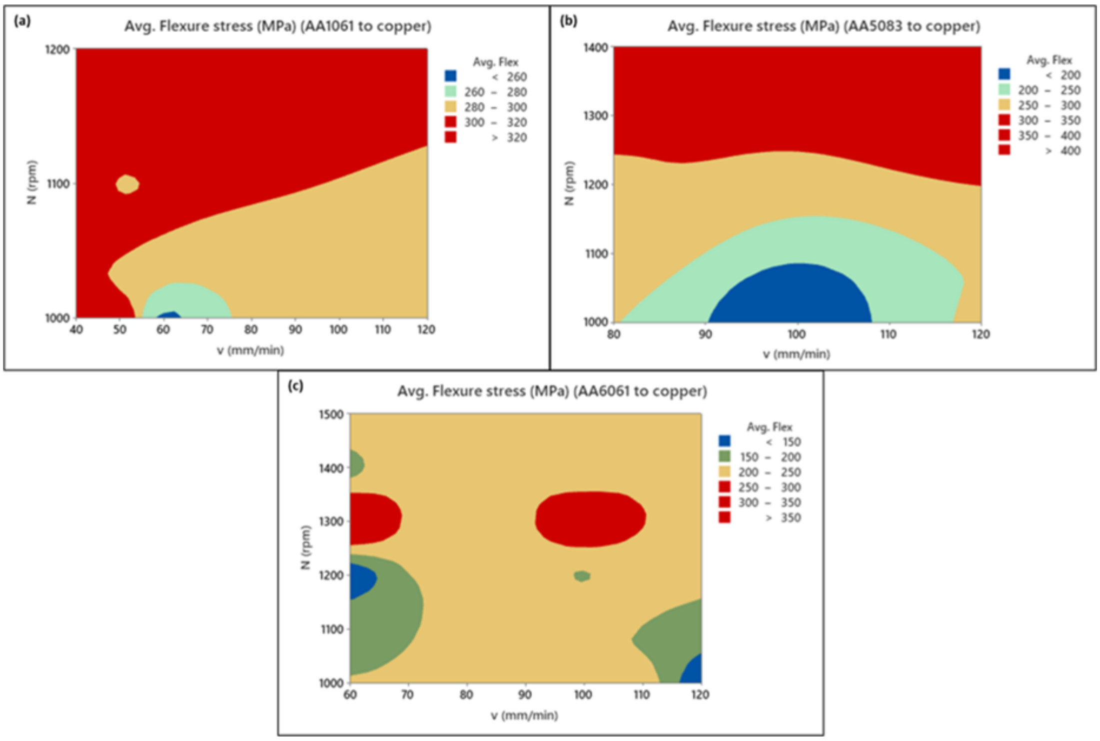

Fig. 4.18 Dissimilar joints flexure stress (MPa) at different welding conditions and aluminium grade types.

To determine whether the use of different aluminium grades on the AS has a significant impact on the dissimilar joint mechanical properties, an analysis of variance (ANOVA) test was conducted on the reported UTS, and flexure stress values shown in Fig. 4.17 and Fig. 4.18, respectively. Table 4.4 summarises the results of the ANOVA test. The null hypothesis of the ANOVA test was that there is no significant difference in the dissimilar joint mechanical strength when different aluminium grades are used on the AS. However, the p-values of both the UTS and flexure stress AS (materials) are less than 0.05, according to Table 4.4. Therefore, we have strong evidence to reject the null hypothesis and state with 95% confidence that the dissimilar aluminium to copper joint mechanical strength is impacted by the type of aluminium grade used on the AS.

Table 4.4 ANOVA test results on dissimilar aluminium to copper joint UTS and flexure stress

ANOVA of Avg. UTS (MPa)					
Source	DF	Adj SS	Adj MS	F-Value	P-Value
N (rpm)	5	4136	827.1	3.71	**0.049**
v (mm/min)	6	3952	658.6	2.95	0.08
AS (Materials)	2	5016	2508.1	11.25	**0.005**
Error	8	1784	223		
Total	21	15736			
ANOVA of Avg. Flexure stress (MPa)					
Source	DF	Adj SS	Adj MS	F-Value	P-Value
N (rpm)	5	72198	14440	7.16	**0.008**
v (mm/min)	6	23818	3970	1.97	0.185
AS (Materials)	2	65915	32957	16.33	**0.001**
Error	8	16144	2018		
Total	21	130982			

Furthermore, Table 4.4 highlights that the dissimilar aluminium to copper joint mechanical performance was also significantly influenced by the tool rotational speed, a factor that was previously discussed in Section 4.2. Ultimately, to address the variation in dissimilar joint mechanical strength between each pair of aluminium grade types, individual comparison tests were carried out. Fig. 4.19 and Fig. 4.20 depict the 95% confidence intervals of the difference in UTS and flexure stress, respectively, between each pair of aluminium grades based on the Fisher test.

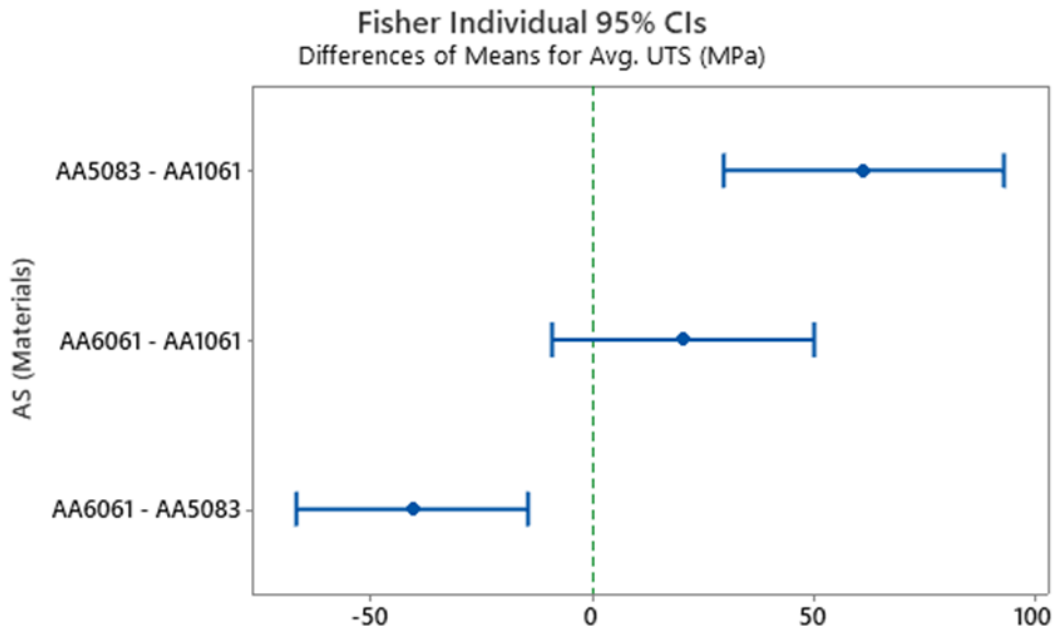

Fig. 4.19 The 95 % confidence intervals in differences of dissimilar aluminium to copper joint UTS (MPa) at each two aluminium grade type.

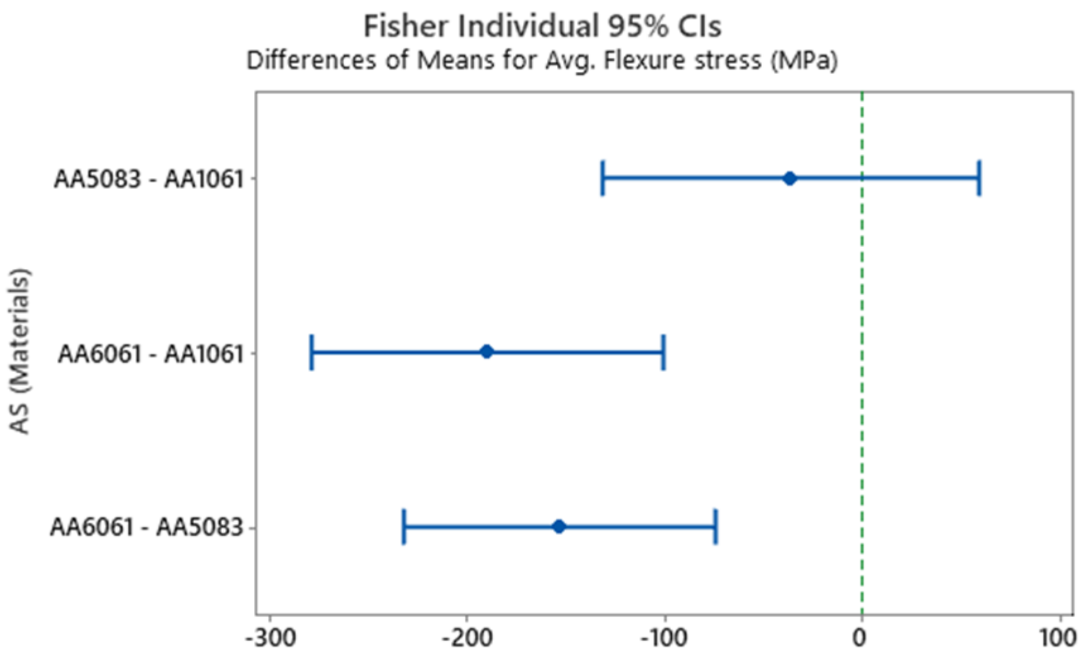

Fig. 4.20 The 95 % confidence intervals in differences of dissimilar aluminium to copper joint flexure stress (MPa) at each two aluminium grade types.

Overall, the results suggest that the selection of the appropriate aluminium grade is crucial in obtaining a strong and reliable dissimilar aluminium to copper FSW joint. Among the aluminium grades investigated in the study, AA5083 showed better joint mechanical strength than AA1061 and AA6061. The AA5083 aluminium grade is known to have a higher content of alloying elements such as magnesium, which can promote the formation of a more favourable IMC structure in the weldment zone compared to the AA1061 grade. [4.1, 4.14]. In contrast, AA1061 and AA6061 have a higher percentage of silicon and other alloying elements that lead to a coarser grain structure and reduced strength [4.1-4.3]. It has also been reported that the finer grain structure of AA5083 enhances the mechanical properties of the weld by reducing the size of the HAZ and increasing the strength of the SZ [4.25]. Additionally, the SZ of the AA5083-to-copper FSW joint was observed to have a fine equiaxed grain structure with a high density of dislocations and sub-grain boundaries, which contributed to its improved mechanical properties [4.10]. In contrast, dissimilar FSW joints of AA1061-to-copper and AA6061-to-copper exhibited an elongated grain structure with reduced dislocations and sub-grain boundaries in their SZ, leading to a weaker joint mechanical strength [4.14].

4.4. References

[4.1] L. E. Murr, “A Review of FSW Research on Dissimilar Metal and Alloy Systems,” J Mater Eng Perform, vol. 19, no. 8, pp. 1071–1089, Feb. 2010, doi: 10.1007/s11665-010-9598-0. https://doi.10.1007/s11665-010-9598-0.

[4.2] A. K. Lakshmi Narayanan, S. Malarvizhi, and V. Balasubramanian, “Developing friction stir welding window for AA2219 aluminium alloy,” Transactions of Nonferrous Metals Society of China (English Edition), vol. 21, no. 11, pp. 2339–2347, 2011, doi: 10.1016/S1003-6326(11)61018-2. https://doi.org/10.1016/S1003-6326(11)61018-2.

[4.3] H. S. Patil and S. N. Soman, "Effect of weld parameter on mechanical and metallurgical properties of dissimilar joints AA6082–AA6061 in T 6 condition produced by FSW," vol. 24, pp. 151–160, 2013. https://doi: 10.3221/IGF-ESIS.24.16.

[4.4] H. Pashazadeh, A. Masoumi, and J. Teimournezhad, "Numerical modelling for the hardness evaluation of friction stir welded copper metals," Mater Des, vol. 49, no. November 2017, pp. 913–921, 2013, https;//doi: 10.1016/j.matdes.2013.02.058.

[4.5] G. Kerrar, N. Merah, A. N. Shuaib, F. Al-Badour, and A. Bazoune, Experimental and numerical investigations of friction stir welding of aluminium to copper. 2017. https://doi: 10.1007/978-3-319-41468-3_10.

[4.6] S. Siddharth, T. Senthil Kumar, and Chandrasekar, "Development of processing windows for friction stir spot welding of aluminium Al5052 /copper C27200 dissimilar materials," Transactions of Nonferrous Metals Society of China (English Edition), vol. 27, no. 6, pp. 1273–1284, 2017. https://doi: 10.1016/S1003-6326(17)60148-1.

[4.7] E. Akinlabi, D. Madyira, and S. Akinlabi, "Effect of heat input on the electrical resistivity of dissimilar friction stir welded joints of aluminium and copper," Africon, 2011, no. September, pp. 13–15, 2011. https://doi:10.1109/AFRCON.2011.6071973.

[4.8] A. G. Wiedenhoft, H. J. de Amorim, T. de S. Rosendo, M. A. D. Tier, and A. Reguly, "Effect of Heat Input on the Mechanical Behaviour of Al-Cu FSW Lap Joints," Materials Research, vol. 21, no. 4, 2018, https://doi: 10.1590/1980-5373-mr-2017-0983.

[4.9] E. T. Akinlabi and S. A. Akinlabi, "Effect of Heat Input on the Properties of Dissimilar Friction Stir Welds of Aluminium and Copper," American Journal of Materials Science, vol. 2, no. 5, pp. 147–152, 2012. https://doi: 10.5923/j.materials.20120205.03.

[4.10] I. Galvão, J. Oliveira, A. Loureiro, and D. Rodrigues, "Formation and distribution of brittle structures in friction stir welding of aluminium and copper: influence of process parameters," Science and Technology of Welding and Joining, vol. 16, no. 8, pp. 681–689, 2011. https://doi: 10.1179/1362171811Y.0000000057.

[4.11] X. Jiang, B. P. Wynne, and J. Martin, "Variant selection in stationary shoulder friction stir welded Ti-6Al-4V alloy," Journal of Materials Science and Technology, vol. 34, no. 1, pp. 198–208, 2017. https://doi: 10.1016/j.jmst.2017.11.024.

[4.12] R. Beygi, M. Z. Mehrizi, D. Verdera, and A. Loureiro, "Influence of tool geometry on material flow and mechanical properties of friction stir welded Al-Cu bimetals," J Mater Process Technology, vol. 255, no. January, pp. 739–748, 2018. https://doi: 10.1016/j.jmatprotec.2018.01.033.

[4.13] P. Xue, B. L. Xiao, D. R. Ni, and Z. Y. Ma, "Enhanced mechanical properties of friction stir welded dissimilar Al-Cu joint by intermetallic compounds," Materials Science and Engineering A, vol. 527, no. 21–22, pp. 5723–5727. 2010, https://doi: 10.1016/j.msea.2010.05.061.

[4.14] Sharma N, Khan ZA, Siddiquee AN, "Friction stir welding of aluminum to copper—An overview," Transactions of Nonferrous Metals Society of China (English Edition), vol. 27, no. 10, pp. 2113–2136, 2017. https://doi: 10.1016/S1003-6326(17)60238-3.

[4.15] C. Genevois, M. Girard, B. Huneau, X. Sauvage, and G. Racineux, "Interfacial Reaction during Friction Stir Welding of Al and Cu," Metallurgical and Materials Transactions A, vol. 42, no. 8, pp. 2290–2295, Aug. 2011. https://doi: 10.1007/s11661-011-0660-9.

[4.16] P. Xue, D. R. Ni, D. Wang, B. L. Xiao, and Z. Y. Ma, "Effect of friction stir welding parameters on the microstructure and mechanical properties of the dissimilar Al–Cu joints," Materials Science and Engineering: A, vol. 528, no. 13–14, pp. 4683–4689, May 2011. https://doi: 10.1016/j.msea.2011.02.067.

[4.17] S. Shankar, P. Vilaça, P. Dash, S. Chattopadhyay, and S. Hloch, "Joint strength evaluation of friction stir welded Al-Cu dissimilar alloys," Measurement, vol. 146, no. July, pp. 892–902, 2019. https://doi: 10.1016/j.measurement.2019.07.019.

[4.18] H. J. Liu, J. J. Shen, L. Zhou, Y. Q. Zhao, C. Liu, and L. Y. Kuang, "Microstructural characterisation and mechanical properties of friction stir welded joints of aluminium alloy to copper," no. January 2011. https://doi: 10.1179/1362171810Y.0000000007.

[4.19] I. Galvão, R. M. Leal, A. Loureiro, and D. M. Rodrigues, "Material flow in heterogeneous friction stir welding of aluminium and copper thin sheets," Science and Technology of Welding and Joining, vol. 15, no. 8, pp. 654–660, 2010. https:// doi: 10.1179/136217110X12785889550109.

[4.20] F. Bakhtiari Argesi, A. Shamsipur, and S. E. Mirsalehi, “Dissimilar Joining of Pure Copper to Aluminium Alloy via Friction Stir Welding,” Acta Metallurgica Sinica (English Letters), vol. 5, 2018. https://doi: 10.1007/s40195-018-0741-5.

[4.21] J. Ouyang, E. Yarrapareddy, and R. Kovacevic, “Microstructural evolution in the friction stir welded 6061 aluminium alloy (T6-temper condition) to copper,” J Mater Process Technology, vol. 172, no. 1, pp. 110–122, Feb. 2006. https://doi: 10.1016/j.jmatprotec.2005.09.013.

[4.22] A. Regensburg, R. Schürer, M. Weigl, and J. Bergmann, “Influence of Pin Length and Electrochemical Platings on the Mechanical Strength and Macroscopic Defect Formation in Stationary Shoulder Friction Stir Welding of Aluminium to Copper,” Metals (Basel), vol. 8, no. 2, p. 85, 2018. https://doi: 10.3390/met8020085.

[4.23] N. Kumar, W. Yuan, and R. S. Mishra, “Introduction,” Friction Stir Welding of Dissimilar Alloys and Materials, pp. 1–13, 2015. https://doi: 10.1016/B978-0-12-802418-8.00001-1.

[4.24] C. W. Tan, Z. G. Jiang, L. Q. Li, Y. B. Chen, and X. Y. Chen, “Microstructural evolution and mechanical properties of dissimilar Al-Cu joints produced by friction stir welding,” Mater Des, vol. 51, pp. 466–473, 2013. https://doi: 10.1016/j.matdes.2013.04.056.

[4.25] G. Karrar, A. Galloway, A. Toumpis, H. Li, and F. Al-Badour, “Microstructural characterisation and mechanical properties of dissimilar AA5083-copper joints produced by friction stir welding,” J. Mater. Res. Technol., vol. 9, no. 5, pp. 11968–11979, 2020. https://doi.org/10.1016/j.jmrt.2020.08.073.

5. Prediction and validation of IMCs formation during FSW of AA6061 to commercially pure copper

The subsequent discussion presents a novel approach for predicting the formation of IMCs during FSW of AA6061 to commercially pure copper. The approach is based on three related criteria: the thermal outputs from a finite element model, the use of an Al-Cu phase diagram, and a microstructure and property evaluation to accurately predict the IMCs present in the different zones of the weldment.

The methodology developed in this chapter was applied to butt-weld dissimilar metals of AA6061 and commercially pure copper using the FSW process. The results showed that the highest ultimate tensile strength of 194.5 MPa was achieved at a tool rotational speed of 1500 rpm, traverse speed of 100 mm/min, and a zero-tool offset. The chapter's findings provide a valuable contribution to the optimisation of FSW process parameters to achieve better mechanical performance of dissimilar metal joints.

5.1. Thermal model validation

Detailed information on the experimental setup used to produce defect-free joints of dissimilar AA6061 to commercially pure copper FSW joints is provided in section 3.1.1 of this study. The coupled Eulerian Lagrangian (CEL) modelling approach, which was used to simulate the FSW process and predict the formation of intermetallic compounds (IMCs) during the welding of AA6061 to commercially pure copper, is also discussed in detail in section 3.2. Consequently, the nodal temperature history from the CEL model is compared quantitatively to the experimental data at distances of 11 mm and 13 mm from the weld centreline and towards both the AA6061 (AS) and copper (RS) sides (as shown in Fig. 3.4). To ensure a high degree of accuracy, care is taken by running the model exactly at the same welding parameters in test no. 2 (Table 3.6) of 1400 rpm, 100 mm/min and 0 mm tool offset. Fig. 5.1 (a) and (b) reveal the experimental temperature measurements recorded by thermocouples and the CEL model temperature history towards AS and RS, respectively.

It is crucial to acknowledge that presenting numerical and experimental data on a single plot may not accurately represent the obtained results due to differences in the dimensions of the experimental setup and the CEL model. To mitigate this, the results have been segregated into two subfigures (a) and (b), to enhance the clarity and accuracy of the validation process. Additionally, the experimental setup was designed with an extended length to ensure the achievement of steady-state thermal conditions. This methodological approach was reflected in the numerical analysis by implementing a refined mesh around the weld zone, thus providing a more accurate simulation of the actual welding process. It is also worth noting that, the temperature measurements obtained via thermocouples were not isolated; rather, they were consistently replicated across three iterations of the welding process under identical conditions to ensure the reliability of the data.

Notably, the higher temperature differences between the AS and RS observed in Fig. 5.1 (a) and (b) using the CEL model have been substantiated in previous literature [5.1], which is indicative of the model's robustness in capturing the thermal trends observed during the FSW of dissimilar materials. Hence, the CEL with a modified friction law results in good agreement with the experimental data. It is also observed that the AS (AA6061) temperature is lower than the RS (copper) due to the fact that copper dissipated heat more rapidly than aluminium. This asymmetric behaviour of the temperature distribution was previously reported in a separate publication [5.2].

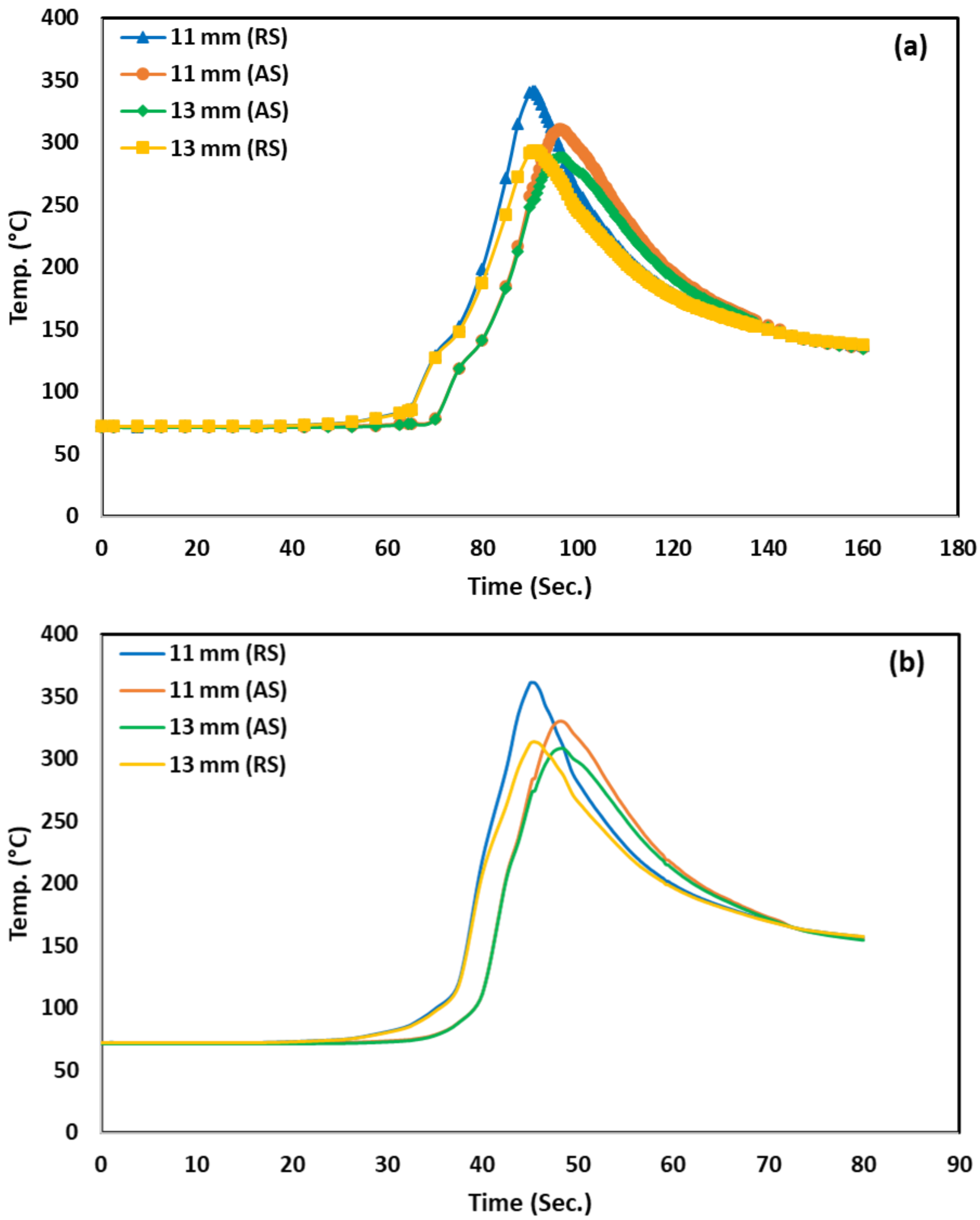

Fig. 5.1 (a) Measured temperature of 1400 rpm, 100 mm/min and 0 mm tool, at different positions from the pin centre toward both the AS (AA6061) and the RS (copper). (b) Calculated temperature history towards AS and RS.

In the dissimilar FSW of aluminium to copper, the formation of IMCs is related to the welding parameters, i.e., frictional heat input (ω/v) ratio and tool offset. The formation of these IMCs greatly affects the joint quality in terms of mechanical strength, morphology, and defect formation [5.3] , [5.4], and [5.5]. Thus, any attempts to control or inhibit the IMC evolution along the weld joint will significantly improve the joint quality. Hence, a qualitative analysis for the IMC formation based on the CEL model results together with the Al-Cu binary system is presented. The effect of rotational speed (ω/v ratio), material placement, tool pin offset and the peak temperature are all considered in this analysis. The qualitative description for the IMC formation in FSW of aluminium to copper, based on the work of Shailesh et al. [5.6], has been modified and developed herein for use on aluminium to copper. Fig. 5.2 shows the material volumes of AA6061 and copper in the case of 0 mm tool offset (b), d mm tool offset (c). Where the total volume swept by the tool is given by Eq. (5.1), The volume of copper swept by the pin (V_{Cu}) can be expressed by Eq. (5.3), hence the ratio of copper swept volume over the total volume can be determined from Eq. (5.4).

$$V_{total} = \pi R_P^2 l \tag{5.1}$$

$$\cos\theta = \frac{d}{R_p} \tag{5.2}$$

$$V_{Cu} = \left\{R_P^2 \cos^{-1}\frac{d}{R_p} - d(R_P^2 - d^2)^{1/2}\right\} l \tag{5.3}$$

$$\frac{V_{Cu}}{V}(Cu.at\%) = \left\{\cos^{-1}\frac{d}{R_p} - d/R_P(1 - d^2/R_P^2)^{1/2}\right\}/\pi \tag{5.4}$$

* l ≡The cylindrical section height or length.

* R_P ≡The tool pin radius.

* V_{cu} ≡The swept copper volume by the FSW tool pin as per Fig. 5.2.

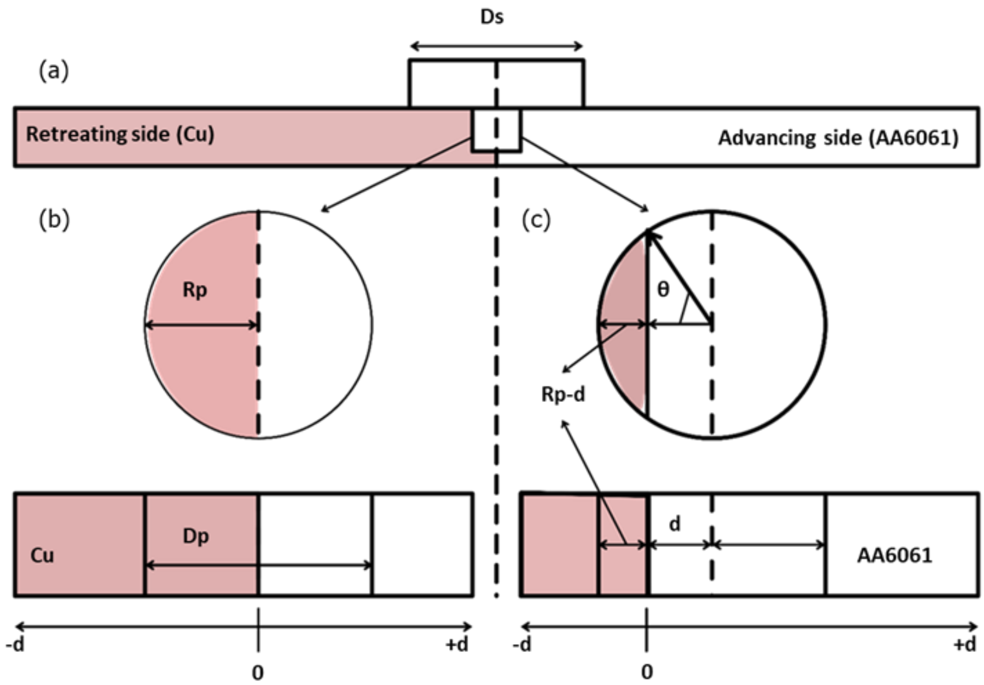

Fig. 5.2 Schematic of the material volume at different tool offsets (adapted from [5.6]).

Fig. 5.2 and Eq. 5.4 demonstrate that the tool offset affects the volume fraction of the total weld nugget, a prerequisite for IMC formation. Table 5.1, which summarises the predicted Al-Cu phases at different tool offsets towards both AA6061 and copper side, is constructed based on the Al-Cu equilibrium phase diagram, allowing the predicted phases to be determined based on the volume fraction of aluminium and copper (Fig. 5.3). Itis important to note that continuous cooling transformation (CCT) curves were not incorporated into this analysis. The phase diagram presented if Fig 5.3 serves as a tool for predicting the phases at equilibrium conditions, which are the primary concern in the context of the temperatures and compositions utilised in the experiments. The simplification is that the thermal history of the materials during the FSW process did not traverse the critical cooling rates that would necessitate the use of CCT curves for an accurate phase determination. Consequently, the phase diagram provides a sufficient theoretical framework for predicting the resultant phases under the specified welding parameters and material states [5.4].

Table 5.1 Predicted phases at different tool offset.

Case	$\boldsymbol{d}$ $(\boldsymbol{mm})$	$\boldsymbol{at.\%Cu}$	$\boldsymbol{at.\%AA6061}$	**Predicted Phases**
0.5 mm towards AA6061	+0.5	35.97	64.03	Al_2Cu
1 mm towards AA6061	+1.0	10.96	89.04	Al(Cu)
0 mm offset	0	50.00	50.00	AlCu
0.5 mm towards Cu	-0.5	64.03	35.97	Al_4Cu_9
1.5 mm towards Cu	-1.5	89.04	10.96	Cu(Al)

The generic approach to control the IMC formation at the weld nugget is by positioning the tool in a way that keeps the compositions of aluminium to copper within the comfort zone, i.e., reduced possibility of IMC formation below the resulting temperature during FSW of AA6061 to copper [5.7]. Thus, the third aspect of this qualitative analysis is the temperature profile at the weld nugget. Fig. 5.4 (a) exhibits the top view of the temperature distribution at the welding stage in Kelvin at 0 mm tool offset. The same figure also shows that the peak temperature predicted by the CEL model is always lower than the aluminium melting temperature and within the plasticised zone. Fig. 5.4 (b) and (c) present cross-sectional views of the temperature profiles at 1400 rpm- 100 mm/min and 0 mm tool offset as well as 1500 rpm- 100 mm/min and 0 mm tool offset. As observed, the calculated temperature within the weldment zone is affected by the tool rotational speed, where increasing the rotational speed increases the heat input and thus the temperature.

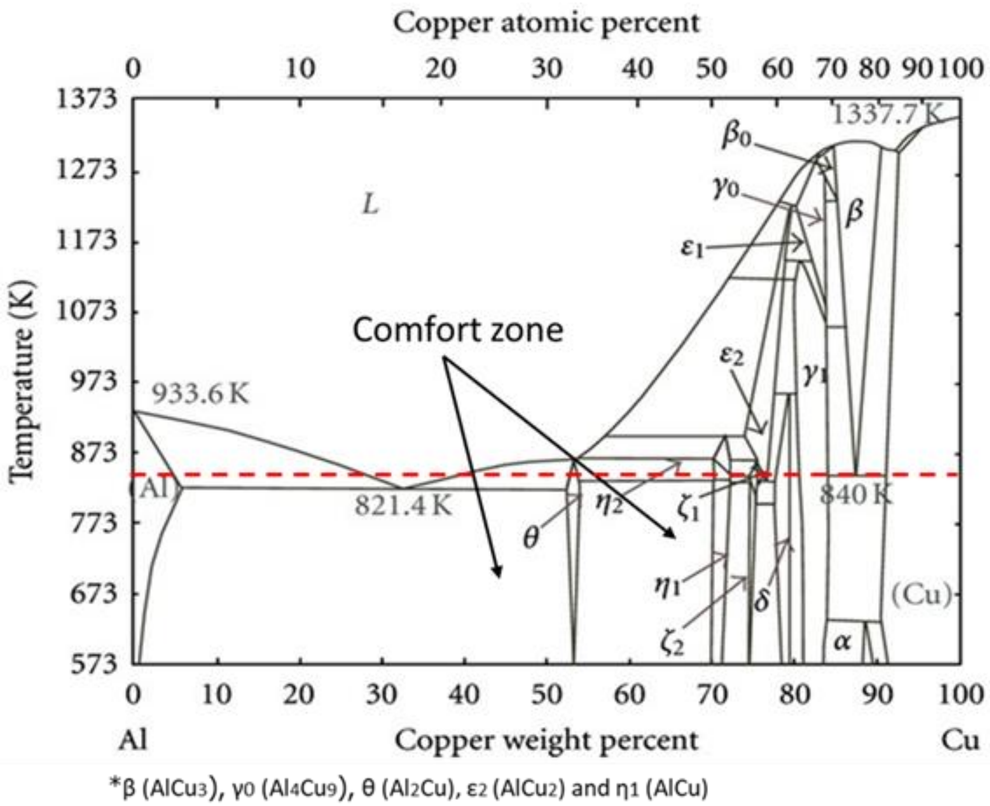

Fig. 5.3 Al-Cu equilibrium phase diagram (adapted from [5.8]).

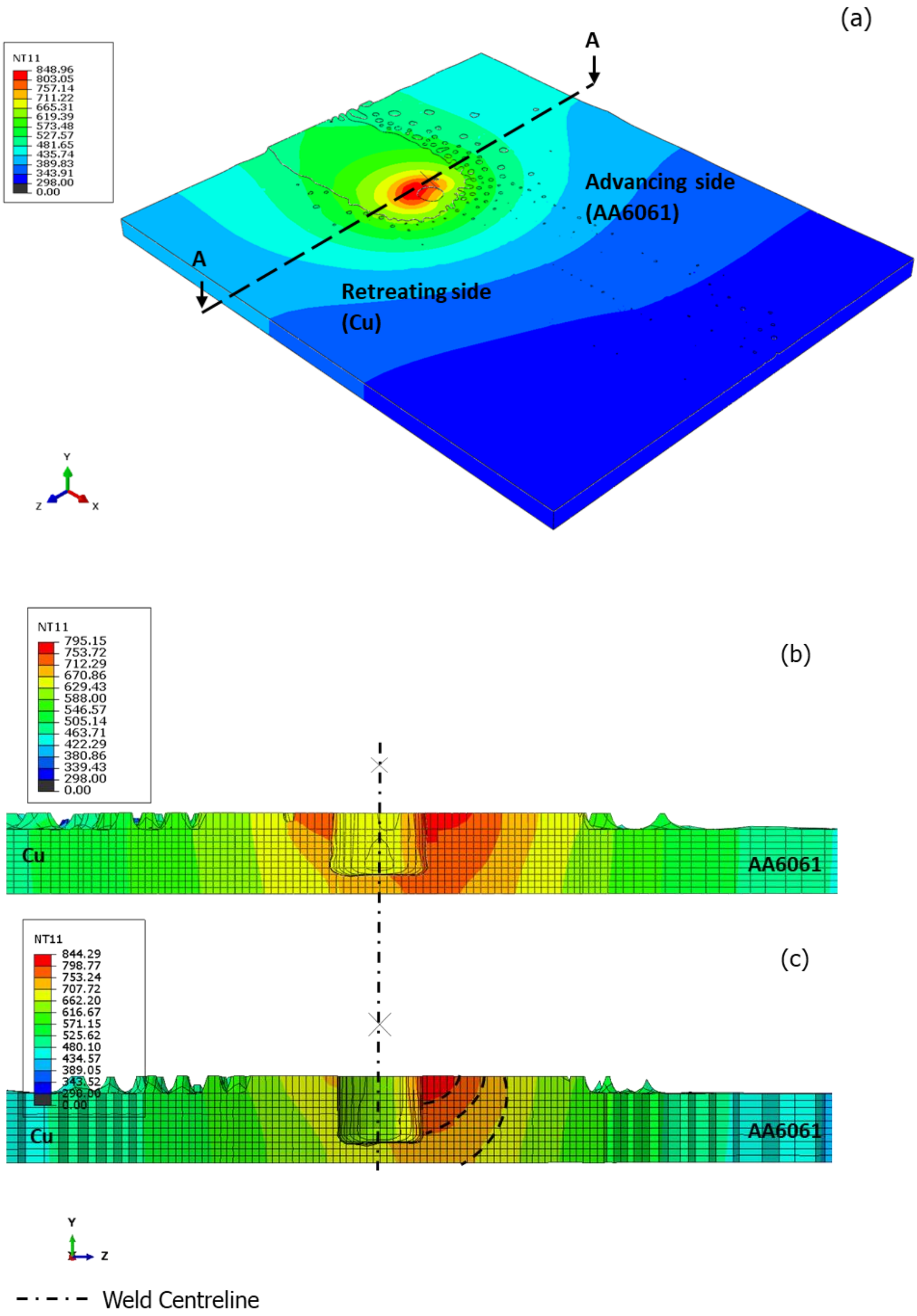
(a)
A
A
Advancing side
(AA6061)
Retreating side
(Cu)
NT11
848.96
803.05
757.14
711.22
665.31
619.39
573.48
527.57
481.65
435.74
389.83
343.91
298.00
0.00
(b)
NT11
795.15
753.72
712.29
670.86
629.43
588.00
546.57
505.14
463.71
422.29
380.86
339.43
298.00
0.00
Cu
AA6061
(c)
NT11
844.29
798.77
753.24
707.72
662.20
616.67
571.15
525.62
480.10
434.57
389.05
343.52
298.00
0.00
Cu
AA6061
Weld Centreline

Fig. 5.4 (a) Top view of temperature profile at 1400 rpm and 100 mm/min, (b) cross-section view of temperature profile at 1400 rpm and 100 mm/min, (c) cross-section view of temperature profile at 1500 rpm and 100 mm/min.

5.2. Weld quality in the AA6061 - copper interface region

The weld quality of the AA6061-copper joint can be generally assessed when its cross-sectional macro features and microstructures are examined from the corresponding optical images. Fig. 5.5 (a) shows a macrograph of the dissimilar materials joint of test no. 1 of Table 3.6, at 1300 rpm rotational speed and 100 mm/min welding speed. Figs. 5.5 (b) and (c) show optical micrographs of the weldment at the interface region and the weld nugget, respectively. Close examination of Fig. 5.5 (c) reveals a degree of void formation at the weld nugget which is related to the irregular distribution of copper particles. Inadequate material flow, due to a suboptimal ω/ν ratio, is the main reason for the resultant voids [5.9].

Fig. 5.5 (b) and Table 5.2 show the EDS analysis applied at different positions on the joint interface. The effective concentration of AlCu IMC was dominant with different Al/Cu contents in agreement with the calculations presented in section 5.1.

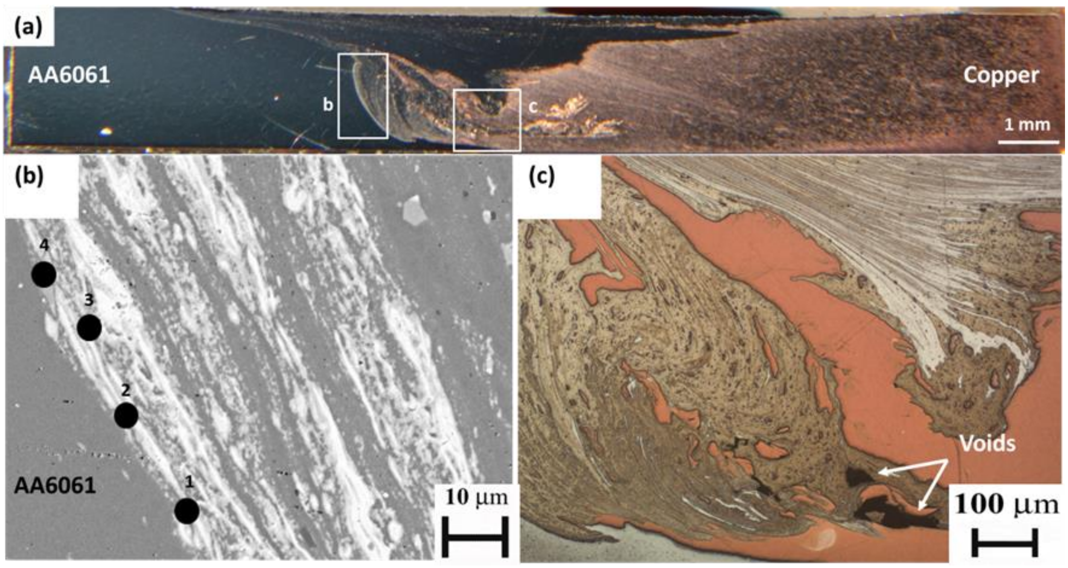

Fig. 5.5 (a) Typical cross-section of joint welded at 1300 rpm and 100 mm/min. (b) interface zone towards AA6061 side. (c) weld nugget.

Table 5.2 EDS results at weld nugget at 1300 rpm and 100 mm/min

Spectrum	Al at. %	Cu at. %	Probable Phase	Predicted Phases
1	55.27	44.73	AlCu	AlCu
2	50.68	49.32	AlCu	AlCu
3	62.62	37.38	Al_2Cu	AlCu
4	33.72	66.28	Al_4Cu_9	AlCu

Defect free joints were obtained at the higher rotational speeds of 1400 rpm and 1500 rpm (test nos. 2 and 3 of Table 3.6). Distinctive regions were observed across the weld joint. Towards the aluminium side (Fig. 5.6 (a & b)), relatively large copper particles were identified; these were irregularly distributed between the aluminium interface zone and the upper weld nugget surface. At the bottom of the aluminium interface zone, copper particles (fragments) were stretched and regularly distributed along the stir zone (SZ), as shown in Fig. 5.6 (c). Evidence of the intermixing between aluminium and copper particles was also observed at the weld nugget and towards the copper side (Fig. 5.6 (d)). Unlike other researchers [5.10, 5.11], placing the softer material (AA6061) on the AS with 0 mm tool offset resulted in defect free joints when a suitable ω/ν ratio was selected.

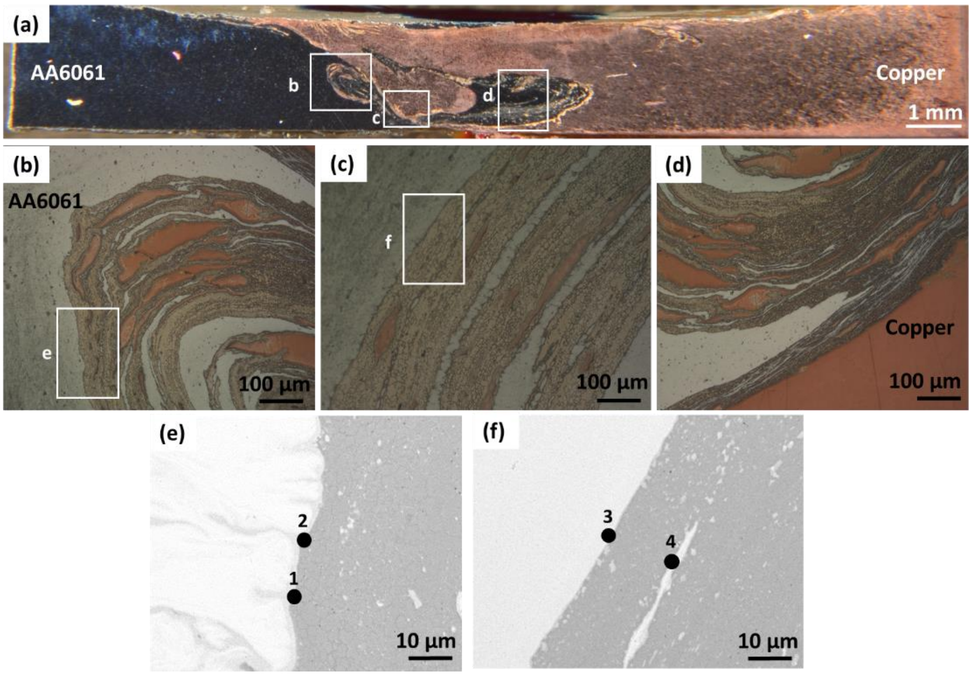

Fig. 5.6. (a) Typical cross-section of joint welded at 1400 rpm and 100 mm/min. (b) interface zone towards AA6061 side. (c) weld nugget. (d) interface zone towards copper side. (e) EDS points of rectangle e. (f) EDS points of rectangle f.

EDS analysis was performed at the interface zone to validate the developed approach of predicting the IMC formation (section 5.1). Figs. 5.6 (e) and (f), and Table 5.3 show that, the newly generated layer close to the aluminium side is identified as AlCu according to the effective concentration of Al/Cu content (points 1 and 2). The possible IMC phases of points 3 and 4 are identified as Al_2Cu and Al_4Cu_9, respectively. This interface zone contains three different IMCs. The effective concentration of aluminium to copper under this non-equilibrium condition allows the AlCu phase to be formed first, i.e., lowest Gibbs free energy [5.12]. The Al_2Cu and Al_4Cu_9 phases formed later as a result of the diffusion kinetics, where the presence of these IMCs was determined further by XRD analysis.

Table 5.3 EDS results at weld nugget test no. 2 and 3 of Table 3.6

			Test no. 2			**Test no. 3**	
Spectrum	Al at. %	Cu at. %	Probable Phase	Al at. %	Cu at. %	Probable Phase	Predicted Phases
1	53.18	46.82	AlCu	53.12	46.88	AlCu	AlCu
2	55.60	44.40	AlCu	50.66	49.34	AlCu	AlCu
3	62.62	37.38	Al_2Cu	71.70	28.30	Al_2Cu	AlCu
4	35.22	64.78	Al_4Cu_9	37.72	62.28	Al_4Cu_9	AlCu

Comparatively small copper particles were detected as regularly distributed along the aluminium interfacial zone (Fig. 5.7 (a, b, & c)) of test no.3 (1500 rpm and 100 mm/min). Sufficient heat input generated by the relatively higher rotational speed of 1500 rpm is the reason behind this enhanced thermo-mechanical effect and the regular dispersion of copper particles in the aluminium. Towards the copper side, refined aluminium grains were intermixed with the copper particles, thus resulting in a wider copper thermo-mechanical affected zone (TMAZ) (Fig. 5.7 (d)).

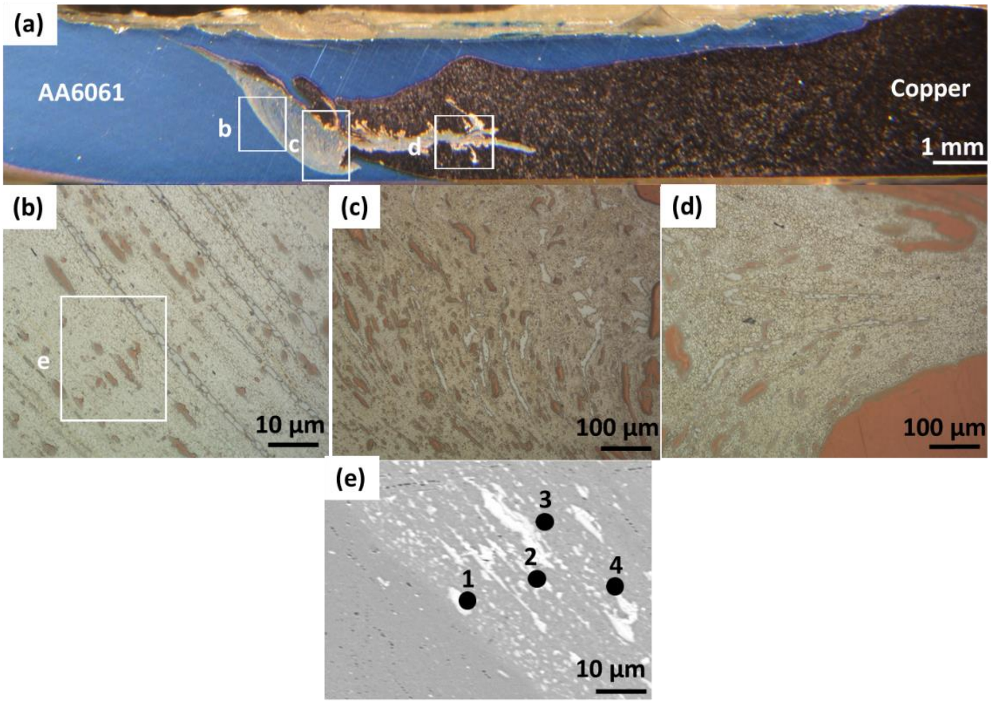

Fig. 5.7 (a) Typical cross-section of a joint welded at 1500 rpm and 100 mm/min. (b) interface zone towards the AA6061 side. (c) weld nugget. (d) interface zone towards the copper side. (e) EDS points of rectangle e.

According to the results of Table 5.3, points 1 and 2 in Fig. 5.7 (e), the AlCu IMC phase is identified close to the aluminium side. Al_2Cu and Al_4Cu_9 are the possible phases as per Fig. 5.7 (e) points 3-4, and Table 5.3. This is in agreement with the calculations presented in section 5.1 and supports the findings of test no.2.

5.3. Intermetallic phases at the weld nugget zone

For phase identification, XRD analysis was conducted across the weld nugget on defect-free joints of tests 2 and 3 (Table 3.6). The extracted XRD patterns (Fig.5.8) revealed that the dominant IMCs in the weld zone of pure copper to AA6061 were AlCu, Al_2Cu and Al_4Cu_9; this is in agreement with the EDS analysis and predictions discussed previously (section 5.2). However, the Al-Cu phase diagram cannot be solely used to reliably predict the formation of IMCs. Based on the temperatures estimated using finite element analysis (FEA) during FSW of copper to AA6061, it was found to be in the range of 80-90% of AA6061 melting point. This temperature range is beyond the formation temperature of AlCu and Al_2Cu phases, and lower than the one needed to form Al_4Cu_9 (1030°C). Despite the low peak temperature during FSW, Al_4Cu_9 formation is related to the process's thermo-mechanical effect as reported in previous publications [5.6].

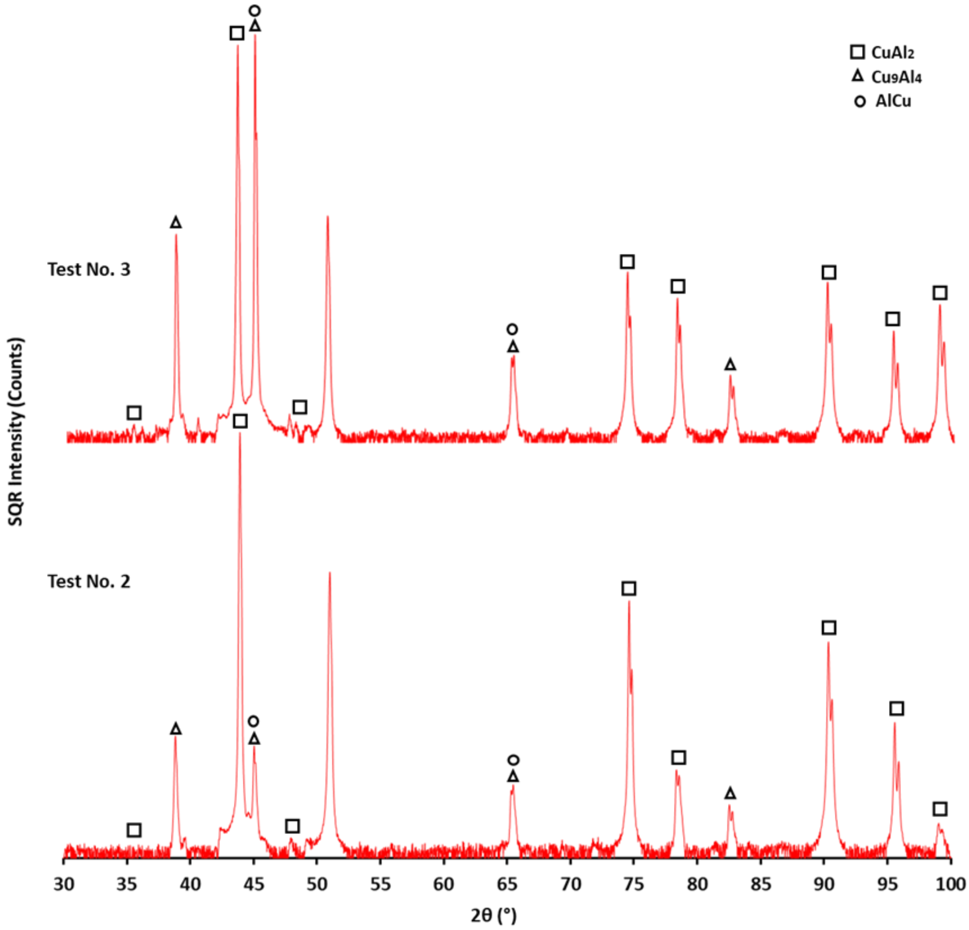

Fig. 5.8 XRD patterns acquired under tests no. 2 and 3 of Table 3.6.

The peak intensity increases proportionally with the tool rotational speed. Qualitatively, it has been previously noted that high intensity peaks indicate higher IMC quantity [5.13]. Table 5.4 shows the results of quantifying the IMC volume fractions in the weld nugget considering the Topas Rietveld refinement method [5.14] on the XRD patterns of test no. 2 and 3 of Table 3.6. The developed method provides evidence of the increase in the IMCs volume as a result of increasing the tool rotational speed, where 1400 rpm and 1500 rpm are the tool rotational speeds of test no. 2 and 3, respectively.

Table 5.4 Quantitative analysis of the IMCs at different welding conditions (vol.%)

Test no. (Table 3.6)	Al_2Cu	AlCu	Al_4Cu_9
2	15.00	5.00	1.00
3	13.00	4.00	2.00

5.4. Joint mechanical strength

Fig. 5.9 (a) and (b) present the microhardness measurement locations across the weld nugget and the distribution profile, respectively. The measurements were taken at the middle of the sheet thickness with a step size measurement of 0.7 mm. As predicted, the hardness within the SZ increases significantly as compared to the base metals. This increase is due to the combined effects of grain refinement, the presence of hard and brittle IMCs [5.9] and the evolution of copper-rich dispersed particles. Similarly, the TMAZ hardness was found to be higher as compared to the base metals due to the combined effect of IMC formation and grain refinement [5.15]. The variations in hardness within the SZ are a result of the varied distribution of IMCs in the softer materials (aluminium or copper).

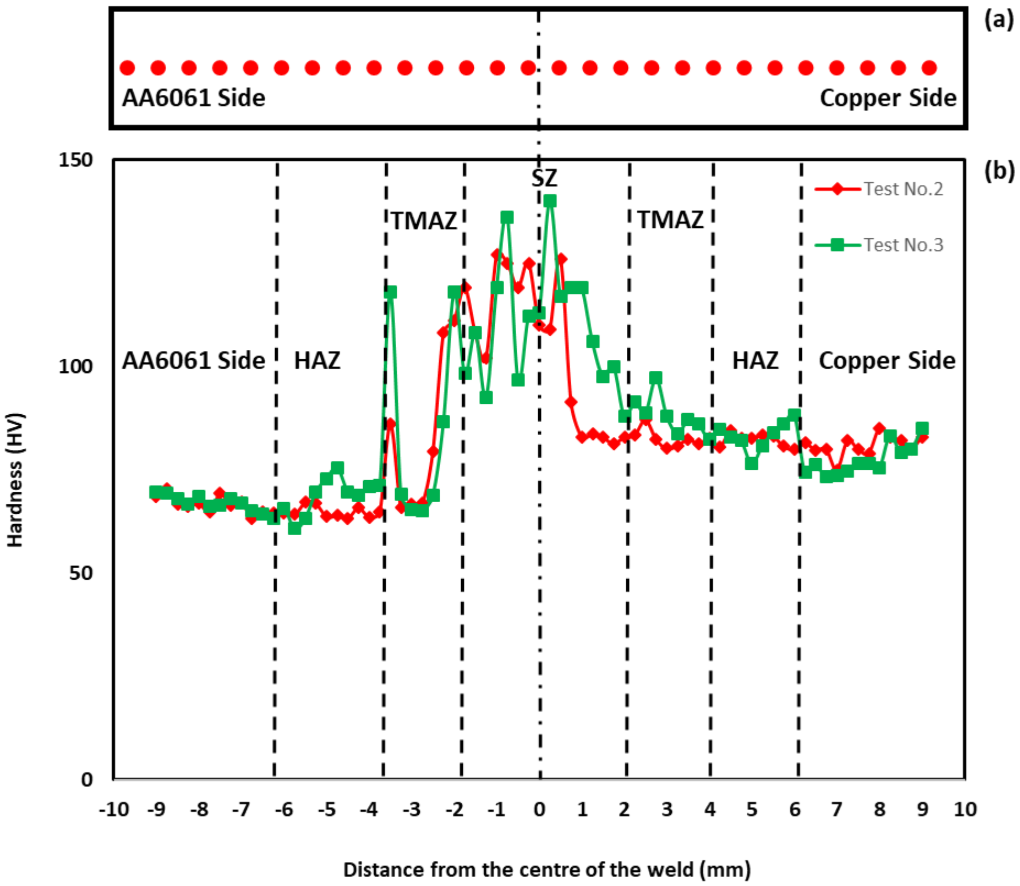

Fig. 5.9 (a) Vickers hardness measurement positions. (b) Vickers hardness variation at tests no. 2 and 3 of Table 3.6.

For assessing the impact of tool rotational speed on joint integrity, tensile tests across the weld line of dissimilar joints (AA6061 to copper) generated at the three welding conditions listed in Table 3.6, were conducted. The results are shown in Fig.5.10, where the increased tool rotational speed (1300 to 1500 rpm) resulted in a joint strength increase, as well as higher modulus of elasticity, by 7.0%. This enhancement in mechanical properties is known to be driven by the heat input increase and improved material mixing [5.16]. Moreover, the joint strength enhancement is directly linked to the distribution, nature, and quantity of IMCs.

Unlike other published work [5.17, 5.18], that placed the softer material on the RS, placing the AA6061 on the AS in this work resulted in a higher tensile strength of 194.5 MPa (92.0% joint efficiency). Further, FSWed joints at test no. 3 (1500 rpm and 100 mm/min) of higher tensile strength, experienced ductile fracture behaviour with different dimples sizes (Fig. 5.11). All the failures occurred at the TMAZ towards the AA6061 side.

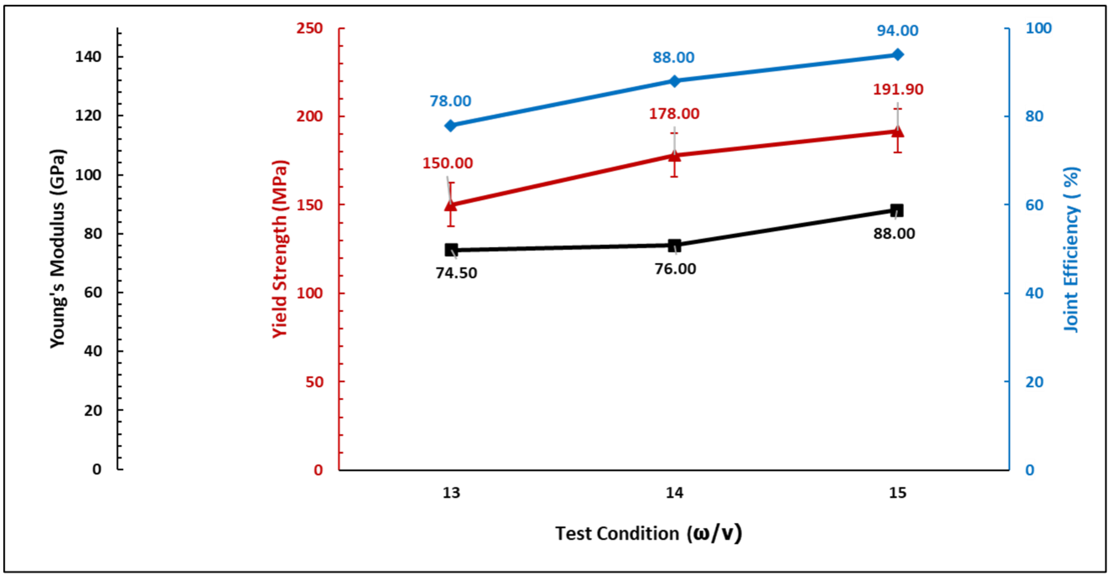

Fig. 5.10 Yield strength, Young's modulus, and joint efficiency at the different (ω/v) ratio.

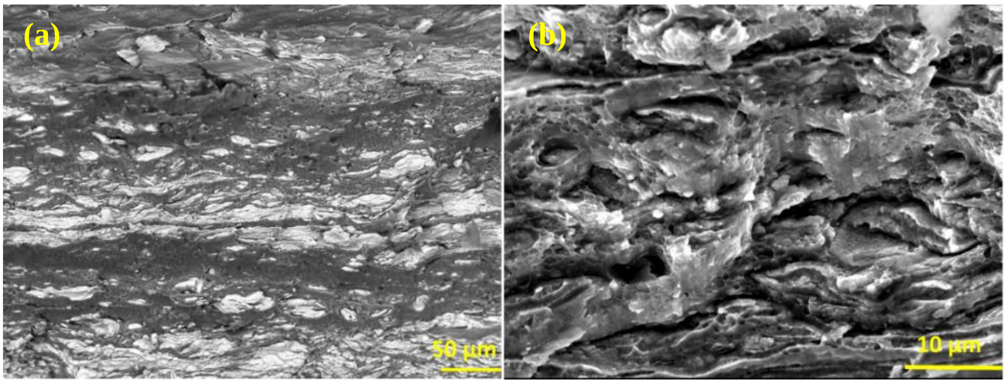

Fig. 5.11 SEM image of the fracture surface at weld test no. 3 of Table 3.6.

In summary, this part of the study focused on investigating the FSW of AA6061 to commercially pure copper through a combination of experimental and numerical approaches. The aim was to identify the conditions that would yield defect-free joints. Based on the findings, the following conclusions can be drawn:

- The formation of IMCs in FSW of AA6061 to copper has been predicted and validated with the experimental results.
- The predominant intermetallic compound phases in the aluminium-copper dissimilar joint were AlCu, Al_2Cu, and Al_4Cu_9.
- A defect-free weld joint between the two dissimilar materials has been obtained at 1400 rpm and 1500 rotational speeds and 100 mm/min traverse speed, where the softer material (AA6061) was placed at the advancing side without any tool offset.
- Improvements in the UTS were found to be controlled by the relatively regular distribution of IMCs together with the evolution of the composite like structure.

5.5. References

[5.1] F. Al-Badour, N. Merah, A. Shuaib, and A. Bazoune, “Coupled Eulerian Lagrangian finite element modelling of friction stir welding processes,” Journal of Materials Processing and Technology, vol. 213, no. 8, pp. 1433–1439, 2013. https://doi.org/10.1016/j.jmatprotec.2013.02.014.

[5.2] X. He, F. Gu, and A. Ball, “A review of numerical analysis of friction stir welding,” Progress in Materials Science, vol. 65, pp. 1–66, 2014. https://doi.org/10.1016/j.pmatsci.2014.03.003.

[5.3] I. Galvão, J. C. Oliveira, A. Loureiro, and D. M. Rodrigues, “Intermetallic Formation and distribution of brittle structures in friction stir welding of aluminium and copper: Influence of shoulder geometry,” Intermetallic (Barking), vol. 22, pp. 122–128, 2012, doi: 10.1016/j.intermet.2011.10.014. https://doi.org/10.1016/j.intermet.2011.10.014.

[5.4] N. Kumar, W. Yuan, and R. S. Mishra, “Introduction,” Friction Stir Welding of Dissimilar Alloys and Materials, pp. 1–13, 2015. https://doi.org/10.1016/B978-0-12-802418-8.00001-1

[5.5] Z. Y. Ma, A. H. Feng, D. L. Chen, and J. Shen, “Recent Advances in Friction Stir Welding/Processing of Aluminium Alloys: Microstructural Evolution and Mechanical Properties,” Critical Reviews in Solid State and Materials Sciences, vol. 8436, pp. 1–65, 2017. https://doi.org/10.1080/10408436.2017.1358145.

[5.6] S. N. Pandya and J. Menghani, "Optimum heat source position offset in welding of dissimilar Al-Cu metals using a theoretical approach," Mater Today Proc, vol. 5, no. 13, pp. 26974–26980, 2018 https://doi.org/10.1016/j.matpr.2018.08.187.

[5.7] P. Xue, D. R. Ni, D. Wang, B. L. Xiao, and Z. Y. Ma, "Effect of friction stir welding parameters on the microstructure and mechanical properties of the dissimilar Al–Cu joints," Materials Science and Engineering: A, vol. 528, no. 13–14, pp. 4683–4689, May 2011. https://doi.org/10.1016/j.msea.2011.02.067.

[5.8] K. Raza, M. Shamir, M. K. A. Qureshi, A. S. Shaikh, and M. Zain al-Abedin, "On the friction stir welding, tool design optimization, and strain rate-dependent mechanical properties of HDPE–ceramic composite joints," Journal of Thermoplastic Composite Materials, vol. 31, no. 3, pp. 291–310, 2018. https://doi.org/10.1177/0892705717697779.

[5.9] N. Sharma, Z. A. Khan, and A. N. Siddique, "Friction stir welding of aluminium to copper—An overview," Transactions of Nonferrous Metals Society of China (English Edition), vol. 27, no. 10, pp. 2113–2136, 2017. https://doi.org/10.1016/S1003-6326(17)60238-3.

[5.10] J. Ouyang, E. Yarrapareddy, and R. Kovacevic, "Microstructural evolution in the friction stir welded 6061 aluminium alloy (T6-temper condition) to copper," J Mater Process Technology, vol. 172, no. 1, pp. 110–122, Feb. 2006. https://doi.org/10.1016/j.jmatprotec.2005.09.013.

[5.11] I. Galvão, J. Oliveira, A. Loureiro, and D. Rodrigues, "Formation and distribution of brittle structures in friction stir welding of aluminium and copper:

influence of process parameters," Science and Technology of Welding and Joining, vol. 16, no. 8, pp. 681–689, 2011. https://doi.org/10.1179/1362171811Y.0000000057

[5.12] G. Wang, C. Zhao, X. Qi, J. Tang, and C. Liang, "Gibbs free energy calculation of Al-Cu alloy using Thermo-Calc software for microstructure simulation," Adv Mat Res, vol. 472–475, pp. 256–259, 2012. https://doi.org/10.4028/www.scientific.net/AMR.472-475.256.

[5.13] D.A. Kumar, "a Review on Friction Stir Welding of Dissimilar Materials Between Aluminium Alloys to Copper," International Journal of Latest Research in Engineering and Technology, vol. 2, no. 2, pp. 9–15, 2016. https://hdl.handle.net/10210/12514

[5.14] K.H. Hestnes, B.E. Sørensen, "Quantitative Mineral Characterization of Granitic Pegmatite Using Topas Rietveld XRD Refinement Quantitative Minaral Characterisation of Grantitic," Proceedings of the 10th International Congress for Applied Mineralogy (ICAM)January 2012. https://doi.org/10.1007/978-3-642-27682-8_40.

[5.15] V. Shokri, A. Sadeghi, and M. H. Sadeghi, "Thermomechanical modelling of friction stir welding in a Cu-DSS dissimilar joint," J Manufacturing Process, vol. 31, pp. 46–55, 2018. https://doi.org/10.1016/j.jmapro.2017.11.004.

[5.16] K. P. Mehta and V. J. Badheka, "A review on dissimilar friction stir welding of copper to aluminium: Process, properties, and variants," Materials and Manufacturing Processes, vol. 31, no. 3, pp. 233–254, 2016. https://doi.org/10.1080/10426914.2015.1025971.

[5.17] C. Genevois, M. Girard, B. Huneau, X. Sauvage, and G. Racineux, “Interfacial Reaction during Friction Stir Welding of Al and Cu,” Metallurgical and Materials Transactions A, vol. 42, no. 8, pp. 2290–2295, Aug. 2011. https://doi.org/10.1007/s11661-011-0660-9.

[5.18] M. N. Fenoël, R. Taillard, G. Ji, and D. Goran, “Multiscale study of interfacial intermetallic compounds in a dissimilar Al 6082-T6/Cu friction-stir weld,” Materials Trans A Physics Metallurgy Science, vol. 43, no. 12, pp. 4655–4666, 2012. https://doi.org/10.1007/s11661-012-1277-3.

6. Optimisation of FSW parameters using the Taguchi technique for dissimilar joining of AA5083 to copper

The following discussion details the outcomes of optimising the process parameters of FSW of aluminium grade AA5083 to copper. The effects of welding speed, tool rotational speed, and tool design were considered throughout the optimisation process. The Taguchi design of experiments (DoE) was used to identify the significant parameters that affect the mechanical strength of FSW joints and to reduce the number of experiments required to maximise joint efficiency. The analysis of variance (ANOVA) statistical method was also considered to verify that the identified process parameters significantly affect the mechanical properties of dissimilar AA5083 to copper FSW joints.

The optimal combination of process parameters for achieving the highest ultimate tensile strength (UTS) was determined to be a tool rotational speed of 1200 rpm, a tool welding speed of 120 mm/min, and the use of a simple FSW tool (FSWT) design (S). On the other hand, the highest flexure stress values for dissimilar AA5083 to copper FSW joints were obtained at a tool rotational speed of 1400 rpm, a tool welding speed of 100 mm/min, and by employing a relatively larger shoulder FSWT design (B).

6.1. Taguchi approach and orthogonal array selection

The optimisation process for dissimilar aluminium-to-copper FSW process involves various welding parameters, each with its own positive or negative impact on the mechanical strength of the joint [6.1, 6.2]. Fig. 6.1 is an adopted cause-and-effect diagram that illustrates the impact of different FSW parameters on the joint quality characteristics, such as hardness, UTS, flexure stress, electrical resistance, and thermal conductivity. Based on the results obtained in chapters 4 and 5, it was determined that the rotational speed of the FSW tool and the welding speed (ω/v ratio) significantly affect the quality of dissimilar aluminium-to-copper FSW joints. However, FSWT design has also been shown to influence the mechanical strength of dissimilar aluminium-to-copper FSW joints [6.3–6.6]. Consequently, the objective of this part is to optimise the process parameters for dissimilar AA5083 to copper FSW by utilising the robust elimination process of the Taguchi method. The three welding parameters considered in this optimisation are the tool rotational speed (Nr) in rpm, tool welding speed (v) in mm/min, and FSWT design. The obtained process parameters are then less sensitive to changes in any remaining, uncontrolled parameters, such as environmental conditions, user input, and other factors.

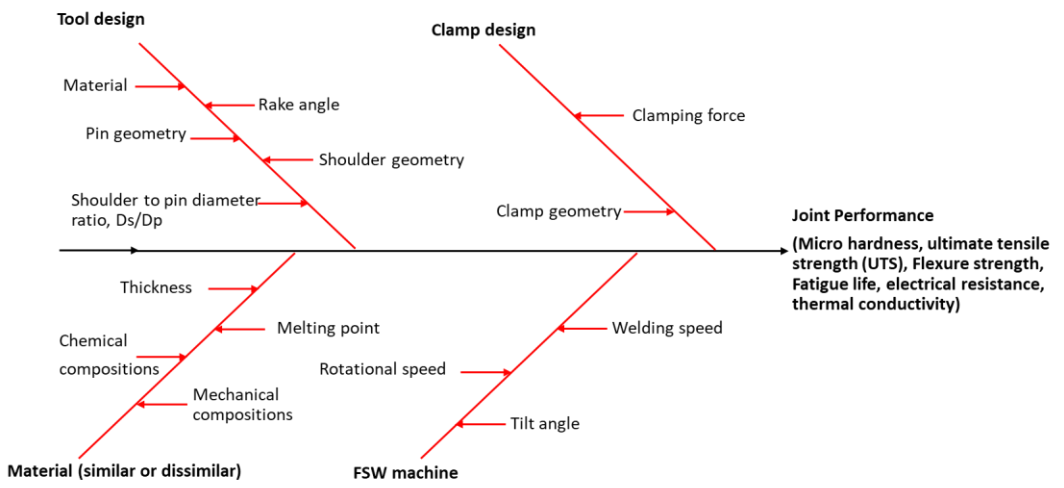

Fig. 6.1 Dissimilar aluminium-to-copper cause-and-effect diagram (adopted from [6.7]).

The application of the Taguchi method's elimination process necessitates the use of a specific orthogonal array (OA) design, which enables the identification of the overall process parameters while minimising the number of experiments required [6.7, 6.8]. Through several preliminary trials conducted in this study, it was established that Nr (rpm), ν (mm/min), and FSWT design all have a significant impact on the quality of dissimilar AA5083 to copper FSW joints. Accordingly, an L9 (3^3) OA (Table 3.7) was designed to include these three process parameters, with each parameter having three levels. Table 6.1 provides a summary of the dissimilar AA5083 to copper FSW parameters and their corresponding levels, based on the information outlined previously in Table 3.7 (section 3.1.2). The UTS and flexure (bending) stress of dissimilar AA5083 to copper FSW joints were selected as characteristic properties, allowing for independent evaluation of the effects of the Nr (rpm), ν (mm/min), and FSWT design.

Table 6.1 Dissimilar AA5083 to copper FSW parameters and their corresponding levels

Symbol	Process parameters	Units	Levels		
			1	2	3
N_r	Rotational speed	rpm	1000	1200	1400
ν	Welding speed	mm/min	80	100	120
FSWT	Tool design	-	S	T	B

*S≡ simple FSWT design, T≡ tapered FSWT design, and B≡ larger shoulder FSWT design.

The larger-the-better signal-to-noise (S/N) ratio method [6.9] was employed to determine the significant order of effect and percentage contribution of each factor on dissimilar AA5083 to copper FSW joint's UTS and flexure stress. To achieve this, 9 mean values of UTS were calculated based on a minimum of five samples for each set of welding conditions, 9 mean values of flexure stress, the mean values were derived from at least three samples, along with 9 corresponding equivalent S/N ratios were generated using Eq. 6.1 [6.9]. This facilitated a statistical analysis aimed at maximising the response values of UTS and flexure stress. Consequently, the highest S/N ratio was used to identify the optimal level for each process parameter (Nr (rpm), ν (mm/min), and FSWT design). Additionally, the ANOVA method [6.10] was applied to confirm the significant impact of the selected process parameters on the mechanical strength of the dissimilar joints. The analysis revealed that the FSWT design, Nr (rpm), and ν (mm/min) were ranked in order of significance, from highest to lowest, with regards to their influence on the mechanical strength of dissimilar AA5083 to copper FSW joints. Ultimately, the predicted optimal levels resulting from the ANOVA method were confirmed through repeated experiments on dissimilar AA5083 to copper FSW joints.

$$\text{S/N ratio for the larger-the-better} = -10 \log 1/n(\sum \frac{1}{R^2}) \tag{6.1}$$

Where: n= No. of observations

R = Observed data for each response

6.2. The impact of FSW process parameters on the mechanical performance of dissimilar AA5083 to copper FSW joints

Table 6.2 provides a summary of the mean values obtained for the UTS and flexure stress of the dissimilar AA5083 and copper FSW joints, using the L9 (3^3) OA as previously presented in Table 3.7 of section 3.1.2. The table also displays the corresponding S/N ratios calculated according to Eq. 6.1. To ensure a high level of confidence, a minimum of five samples of ASTM tensile strength were taken into account when calculating the mean values for each quality characteristic factor i.e., UTS and flexure stress. These samples were extracted from welds that were consistently defect-free, highlighting the effectiveness of the selected FSW parameters. The consistency in weld quality and the mechanical properties from multiple plates welded under the same conditions confirm the high level of repeatability achieved with the identified FSW parameters. This uniformity across samples and welds substantiates the reliability of the process parameters in yielding defect-free joints with predictable mechanical strengths.

Table 6.2 Dissimilar AA5083 to copper FSW joints' UTS, flexure stress, and the corresponding S/N ratios

Exp. No	Input parameters			Mean of UTS (MPa)	S/N ratio (UTS)	Mean of Flexure (MPa)	S/N ratio (Flexure)
	Nr (rpm)	ν (mm/min)	FSWT				
1	1000	80	T	109.32	40.57	140.86	42.80
2	1000	100	S	205.35	45.62	254.40	47.14
3	1000	120	B	235.39	47.24	328.62	50.16
4	1200	80	B	237.95	47.33	236.47	51.07
5	1200	100	T	148.75	47.01	364.93	46.81
6	1200	120	S	264.46	48.25	223.58	47.30
7	1400	80	S	194.33	44.87	263.71	48.25
8	1400	100	B	229.35	43.25	375.80	52.16
9	1400	120	T	72.92	37.06	255.40	47.97

Fig. 6.2 (a) illustrates the impact of FSW process parameters on the UTS of the joints. As anticipated, the UTS of dissimilar AA5083 to copper FSW joints was influenced by the FSW parameters i.e., Nr (rpm), ν (mm/min), and FSWT design. It was observed that

increasing the tool rotational speed initially led to an increase in the joint UTS, followed by a decrease. Conversely, an adverse effect on UTS was observed with increasing tool welding speed. Previous studies [6.11–6.15] have reported that aluminium grade AA5083 to copper FSW joints exhibited a variety of intermetallic compounds (IMCs), such as Al_2Cu, AlCu, and Al_4Cu_9. The evolution of these IMCs was found to be controlled by the tool rotational speed and tool welding speed. The presence of a composite-like structure and higher levels of IMCs in the stir zone contributed at an appropriate ω/ν ratio to the enhancement of joint UTS. Fig. 6.2 (a) also demonstrates that the highest joint UTS was achieved when employing a simple FSWT design and an appropriate ω/ν ratio. On the other hand, it was found that the tapered FSWT design had a negative impact on joint UTS.

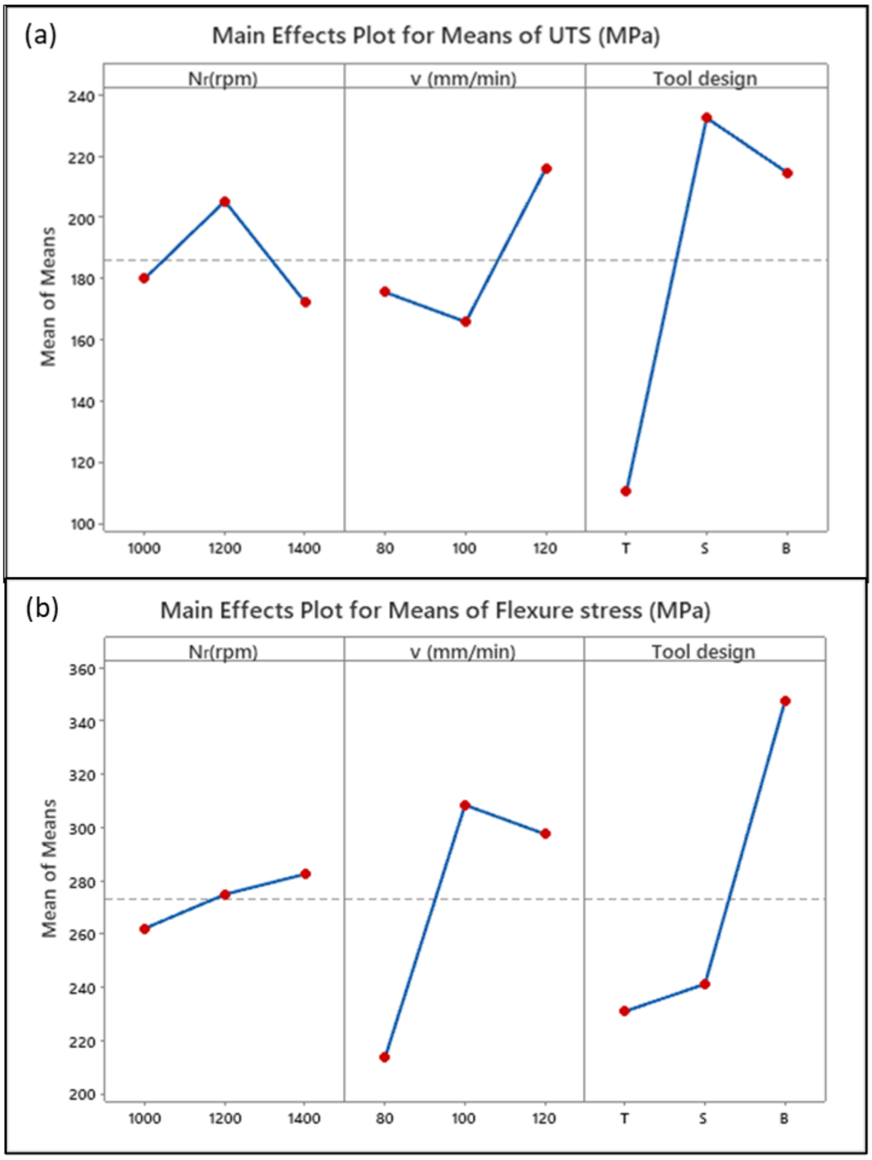

Fig. 6.2 The influence of FSW parameters on dissimilar AA5083 to copper FSW joints: (a) UTS (MPa) and (b) flexure stress (MPa).

In contrast, the flexure stress of dissimilar AA5083 to copper FSW joints exhibited a different behaviour. It was observed that increasing the tool rotational speed had a positive effect on flexure stress, while, unlike the UTS, the flexure stress initially increased and then decreased as the tool welding speed was increased (Fig. 6.2 (b)). While the presence of a composite-like structure at an appropriate ω/v ratio significantly enhanced the UTS of the dissimilar AA5083 to copper joints, the highest flexure stress in these joints was achieved at different levels of the ω/ν ratio. Additionally, it was notable that a larger shoulder FSWT design substantially enhanced the flexure stress of the joints.

6.3. Selection of optimum FSW process parameters for dissimilar AA5083 to copper FSW joints

To further investigate the effect of FSW process parameters on the mechanical performance of dissimilar AA5083 to copper FSW joints, the mean S/N ratios were obtained using Minitab software tool [6.16] and Eq. 6.1. Table 6.3 and Fig. 6.3 (a) present the mean S/N ratios for the UTS values of dissimilar AA5083 to copper FSW joints. Higher S/N ratios indicate the minimal variation between the desired output and the measured output [6.8, 6.15]. According to Table 6.3 and Fig. 6.3 (a), the highest mean S/N ratio for the UTS of dissimilar AA5083 to copper FSW joints was achieved with the following parameters: Nr of 1200 rpm (level 2), ν of 120 mm/min (level 3), and a simple FSWT design (level 2). Consequently, the predicted optimal FSW process parameters for achieving the highest UTS, as determined by the Taguchi method, can be represented as Nr(2)- ν(3)- FSWT(2). The corresponding level values are highlighted in bold in Table 6.3.

Table 6.3 Mean S/N ratio for dissimilar AA5083 to copper FSW joints' UTS (MPa)

Symbol	Process Parameters	Mean S/N ratio				
		Level 1	Level 2	Level 3	Max-min	Rank
Nr	Rotational speed (rpm)	44.48	**45.86**	43.39	2.47	3
v	Welding speed (mm/min)	44.26	43.23	**46.25**	3.02	2
FSWT	Tool design	40.29	**47.06**	46.37	6.77	1

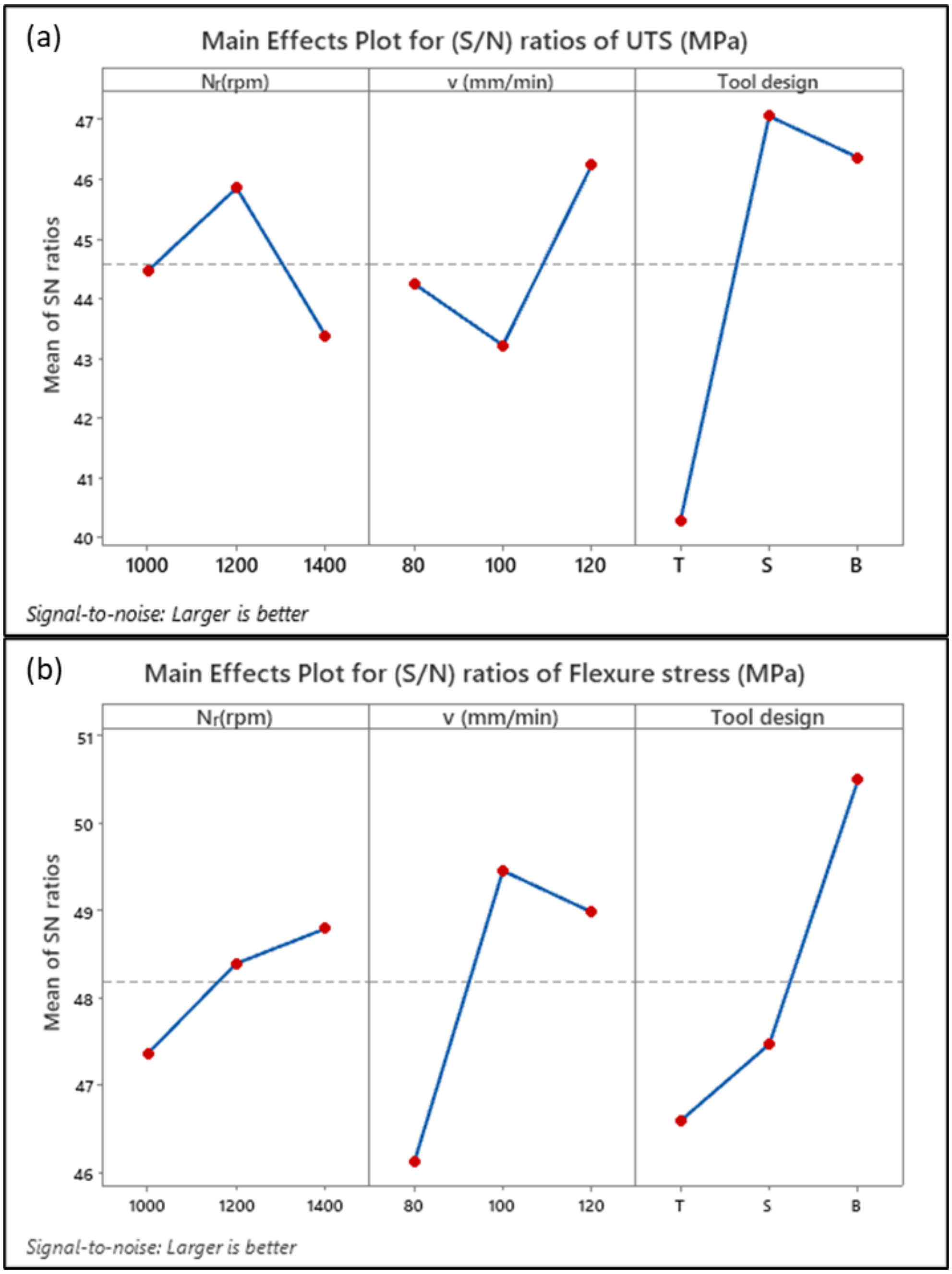

Fig. 6.3 Mean effect plots: (a) UTS S/N ratio and (b) flexure stress S/N ratio.

Similarly, Table 6.4 and Fig. 6.3 (b) display the obtained S/N ratios response for the flexure stress of dissimilar AA5083 to copper FSW joints using Eq. 6.1. According to Fig. 6.3 (b), the estimated optimal FSW process parameters for maximising the flexure stress were identified as follows: Nr at 1400 rpm (level 3), ν at 100 mm/min (level 2), and employing the relatively larger shoulder FSWT design (level 3). Alternatively, the predicted optimal FSW parameters for achieving the highest flexure stress of dissimilar AA5083 to copper FSW joints' can also be represented as Nr(3)- v(2)- FSWT(3).

Table 6.4 Mean S/N ratio for dissimilar AA5083 to copper FSW joints' Flexure stress (MPa)

Symbol	Process Parameters	Mean S/N ratio				
		Level 1	Level 2	Level 3	Max-min	Rank
Nr	Rotational speed (rpm)	47.37	48.4	**48.79**	1.43	3
v	Welding speed (mm/min)	46.16	**49.46**	48.98	3.34	2
FSWT	Tool design	46.59	47.47	**50.49**	3.9	1

6.4. Confirmation test

This part presents the results of the confirmation tests conducted to validate the predicted optimal levels of FSW parameters that led to the highest mechanical strength in dissimilar AA503 to copper joints, as obtained in section 6.3. The predicted S/N ratio parameter ($\varepsilon_{predicted}$) [6.8] was used to estimate and verify the response values under the obtained optimum FSW parameters, as described in Eq. (6.2):

$$\varepsilon_{predicted} = \sum_{i=1}^{x}(\varepsilon_0 - \varepsilon_{li}) \tag{6.2}$$

Where:

ε_l = Total mean S/N ratio

ε_0 = Mean S/N ratio at optimal level

x= No. of input process parameters

Tables 6.5 and 6.6 showcase the results of the confirmation tests conducted at the Taguchi predicted optimal FSW parameters for the UTS and flexure stress of the dissimilar AA5083 to copper FSW joints, respectively. Initially, the FSW conditions were set at Nr(1), v(2), and FSWT(2), corresponding to a tool rotational speed of 1000 rpm, a tool welding speed of 100 mm/min, and a simple FSWT design. It is evident from Tables 6.5 and 6.6 that both the UTS and flexure stress of the dissimilar AA5085 and copper FSW joints have significantly improved when the Taguchi predicted optimal levels of FSW parameters were employed. Specifically, the dissimilar AA5083 to copper FSW joints' UTS exhibited a 27.3% increase compared to the UTS obtained with the initial set of FSW parameters (Fig. 6.4 (a)). Similarly, the flexure stress of dissimilar AA5083 to copper FSW joints was enhanced by 35.2% under the optimum levels of FSW parameters (Fig. 6.4 (b)).

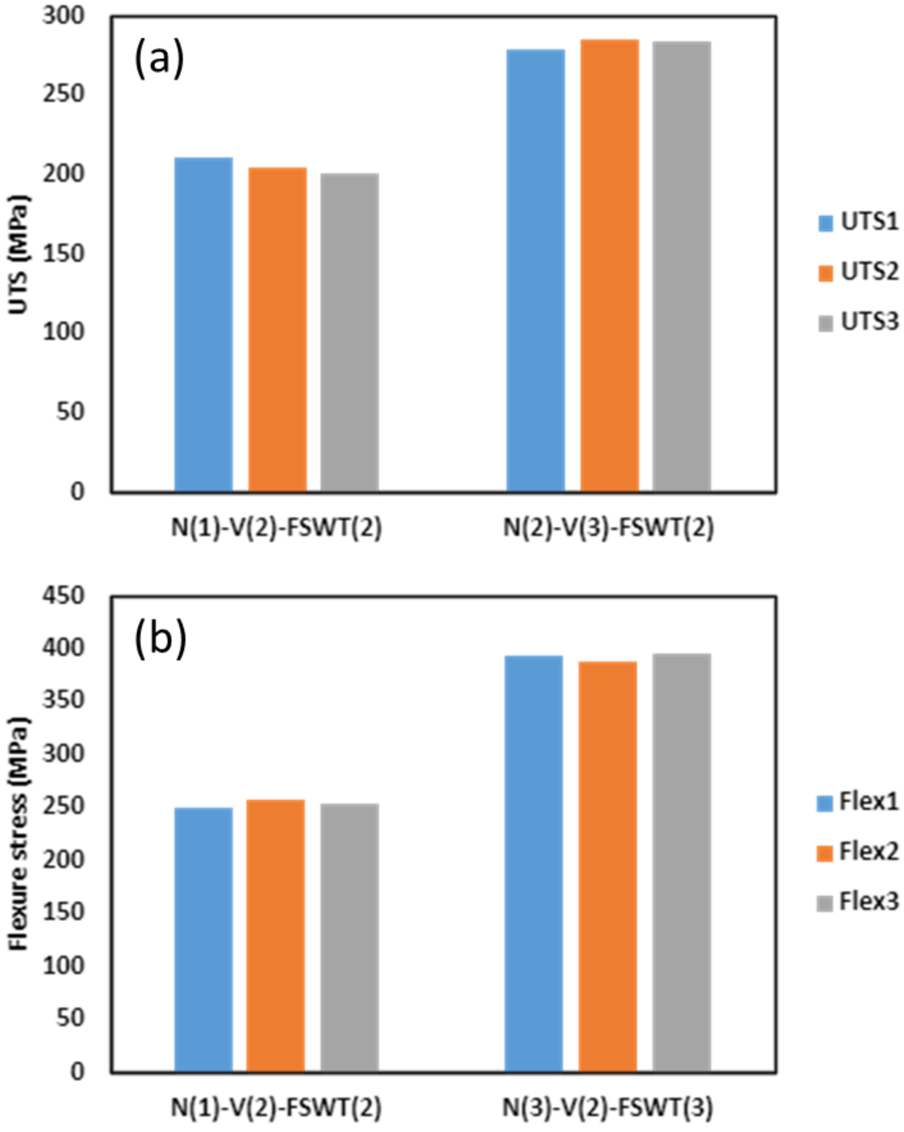

*UTS1, UTS2, and UTS3 are the UTS (MPa) measured at three different locations of each weld.

*Flex1, Flex2, and Flex3 are the flexure stress (MPa) measured at three different locations of each weld.

Fig. 6.4 Comparison between dissimilar AA5083 to copper FSW joints' mechanical performance at the initial conditions and the optimum levels of (a) UTS (MPa) and (b) flexure stress (MPa).

Moreover, it is worth noting that the S/N ratios at the optimal FSW parameters have also shown significant improvements. The S/N ratio for the dissimilar AA5083 to copper FSW joints' UTS increased by 4.53, while the S/N ratio for the flexure stress increased by 5.41, as indicated in Tables 6.5 and 6.6, respectively. This increase in the S/N ratio signifies a reduction in the variation difference between the desired output and the measured output [6.13]. It is also important to acknowledge that these optimal parameters for UTS and flexure stress were achieved under different welding conditions. As a result, when applying these parameters in practical scenarios, it may be necessary to reach a compromise that considers the specific application for which the weld is intended. This compromise is pivotal in configuring the welding process to meet the specific performance criteria dictated by the operational demands of the welded assembly.

Table 6.5 Conformation test results of dissimilar AA5083 to copper FSW joints' UTS (MPa)

Symbol	Initial Process Parameters	Optimal process parameters	
		Prediction	Experiment
Level	Nr(1)-v(2)-FSWT(2)	Nr(2)-v(3)-FSWT(2)	Nr(2)-v(3)-FSWT(2)
UTS (MPa)	205.35		282.5
S/N (dB)	45.62	50.21	50.15
Improvement in S/N (dB)	4.53		
% Increase in UTS (MPa)	27.3		

Table 6.6 Conformation test results of dissimilar AA5083 to copper FSW joints' flexure stress (MPa)

Symbol	Initial Process Parameters	Optimal process parameters	
		Prediction	Experiment
Level	N r(1)-v(2)-FSWT(2)	N r(3)-v(2)-FSWT(3)	N r(3)-v(2)-FSWT(3)
Flexure stress (MPa)	254.4		392.5
S/N (dB)	47.14	52.45	52.55
Improvement in S/N (dB)	5.41		
% Increase in Flexure stress (MPa)	35.2		

6.5. ANOVA for dissimilar AA5083 to copper FSW joint' UTS and Flexure stress

The ANOVA technique was employed to validate the significance of the identified process parameters (Nr (rpm), ν (mm/min), and FSWT design), on the mechanical properties of the dissimilar AA5083 to copper FSW joints. Additionally, the ANOVA results provide insights into the significant levels of each welding parameter. Tables 6.7 and 6.8 present the ANOVA results obtained for the UTS and flexure stress of dissimilar AA5083 to copper FSW joints, respectively.

According to Table 6.7, it was observed that the FSWT design had the most significant influence on the UTS of the dissimilar joints, followed by Nr (rpm) and ν (mm/min). The respective contributions of FSWT design, Nr (rpm), and ν (mm/min) to the dissimilar AA5083 to copper FSW joints' UTS were found to be 76.03%, 12.87%, and 8.4%, respectively.

Table 6.7 ANOVA test results of dissimilar AA5083 to copper FSW joints' UTS (MPa)

Source	Degree of Freedom	Sum of Squares	Mean of Squares	% Contribution
Nr (rpm)	2	9.20	4.60	8.40
ν (mm/min)	2	14.10	7.05	12.87
FSWT design	2	83.29	41.64	76.03
Residual Error	2	2.95	1.47	-
Total	8	109.55	-	-

Table 6.8 ANOVA test results of dissimilar AA5083 to copper FSW joint' flexure stress (MPa)

Source	Degree of Freedom	Sum of Squares	Mean of Squares	% Contribution
Nr (rpm)	2	3.25	1.625	5.34
ν (mm/min)	2	19.58	9.788	32.19
FSWT design	2	25.14	12.568	41.33
Residual Error	2	12.87	6.432	-
Total	8	60.83	-	-

Similarly, the flexure stress of dissimilar AA5083 to copper FSW joints was mostly influenced by the FSWT design, followed by Nr (rpm) and ν (mm/min). However, in contrast to the contribution of the identified FSW parameters to the UTS of dissimilar AA5083 to copper FSW joints, the flexure stress response values were found to be less affected by the FSWT design and more susceptible to the tool rotational speed (Nr rpm). The estimated percentages of contribution for the FSWT design and Nr (rpm) to the flexure stress were 41.33% and 32.19%, respectively. Moreover, Tables 6.7 and 6.8 demonstrate that both the UTS and flexure stress of the dissimilar AA5083 to copper FSW joints were less influenced by the tool welding speed (ν mm/min).

6.6. Modelling of dissimilar AA5083 to copper FSW joints' UTS and flexure stress

This part provides the results of applying a linear regression analysis model to accurately predict the mechanical performance of dissimilar AA5083 to copper FSW joints, based on the most significant process parameters obtained in section 6.5. The Minitab software tool [6.16] was utilised to develop predictive mathematical models for the characteristics factors of the dissimilar AA5083 to copper FSW joints i.e., UTS (MPa) and flexure stress (MPa), as functions of the FSWT design, Nr (rpm), and ν (mm/min).

According to the ANOVA results, the optimal parameters for achieving the highest values of UTS and flexure stress in the dissimilar FSW of AA5083 to commercially pure copper can be represented by Eq. 6.3 and Eq. 6.4, respectively. Consequently, the predictive equations obtained from the regression analysis are described in Eq. 6.5 and Eq. 6.6. It is noteworthy that the interaction effect between the tool rotational speed and tool welding speed (ω/ν ratio) was also investigated in this analysis, as it has been previously established that the dissimilar AA5083 to copper FSW process is influenced by the combined effect of these parameters [6.13–6.19].

$$\text{UTS (predicted)} = Nr^{(2)} + v^{(3)} + FSWT^{(2)} - 2\text{TUTS} \quad (6.3)$$

$$\text{Flexure stress (predicted)} = Nr^{(3)} + v^{(2)} + FSWT^{(3)} - 2\text{TFlex} \quad (6.4)$$

where:

$Nr^{(2)}, v^{(3)},$ and $FSWT^{(2)}$ represent the average UTS stress at 1200 rpm (level 2), 120 mm/min (level 3), and simple FSWT design (level 2).

$Nr^{(3)}, v^{(2)},$ and $FSWT^{(3)}$ represent the average flexure stress at 1400 rpm (level 3), 100 mm/min (level 2), and larger FSWT design (level 3).

TUTS and TFlex represent the overall mean of UTS and flexure stress in MPa, respectively.

$$UTS\ (MPa) = 1960 - 1.75Nr - 19.9v + 82.2FSWT + 0.0180Nr * v \quad (6.5)$$

$$Flexure\ stress\ (MPa) = -687 + 0.5Nr + 7.4v + 54.1FSWT - 0.0041Nr * v$$

(6.6)

Moreover, the coefficient of determination (R_2) [6.10] was calculated to assess the relationship between the independent FSW process parameters (Nr (rpm), ν (mm/min), and FSWT design) and the dependent variables (UTS (MPa) and flexure stress (MPa)) of the dissimilar AA5083 to copper FSW joints. It was found that the developed regression models for dissimilar AA5083 to copper FSW joints' UTS and flexure stress exhibited high R_2 values of 86.12% and 84.24%, respectively. This means that the independent variables (Nr (rpm), ν (mm/min), and FSWT design) can explain a significant amount of the variation in the dependent variables (UTS (MPa) and flexural stress (MPa)).

Residual plots were also used to evaluate the significance of the coefficients obtained from the regression models of Eq. 6.5 and Eq. 6.6. The residual plot illustrates the disparity between observed values and predicted values, plotted against the predicted values. A widely accepted criterion [6.10, 6.16] is that the residuals should exhibit random scattering around zero when the model accurately fits the data. However, if the residuals do not demonstrate random scattering, it suggests that the model may not fit the data well, and the significance of the coefficients might be compromised [6.10]. Figs. 6.5 (a) and (b) demonstrate that the residual errors in the regression models for UTS (MPa) and flexure stress (MPa) displayed a tendency to follow a normal distribution, as indicated by the straight line pattern [6.10]. This observation suggests that the regression models provided a good fit to the data. Additionally, there was sufficient evidence against the null hypothesis for the obtained coefficients of the FSWT design in the two models (p-value $<< 0.5$), hence, dissimilar AA5083 to copper FSW joints' UTS (MPa) and flexure stress (MPa) were significantly affected by the FSWT design. Summaries of the UTS (MPa) and flexural stress (MPa) linear regression models are presented in Tables 6.9 and 6.10, respectively.

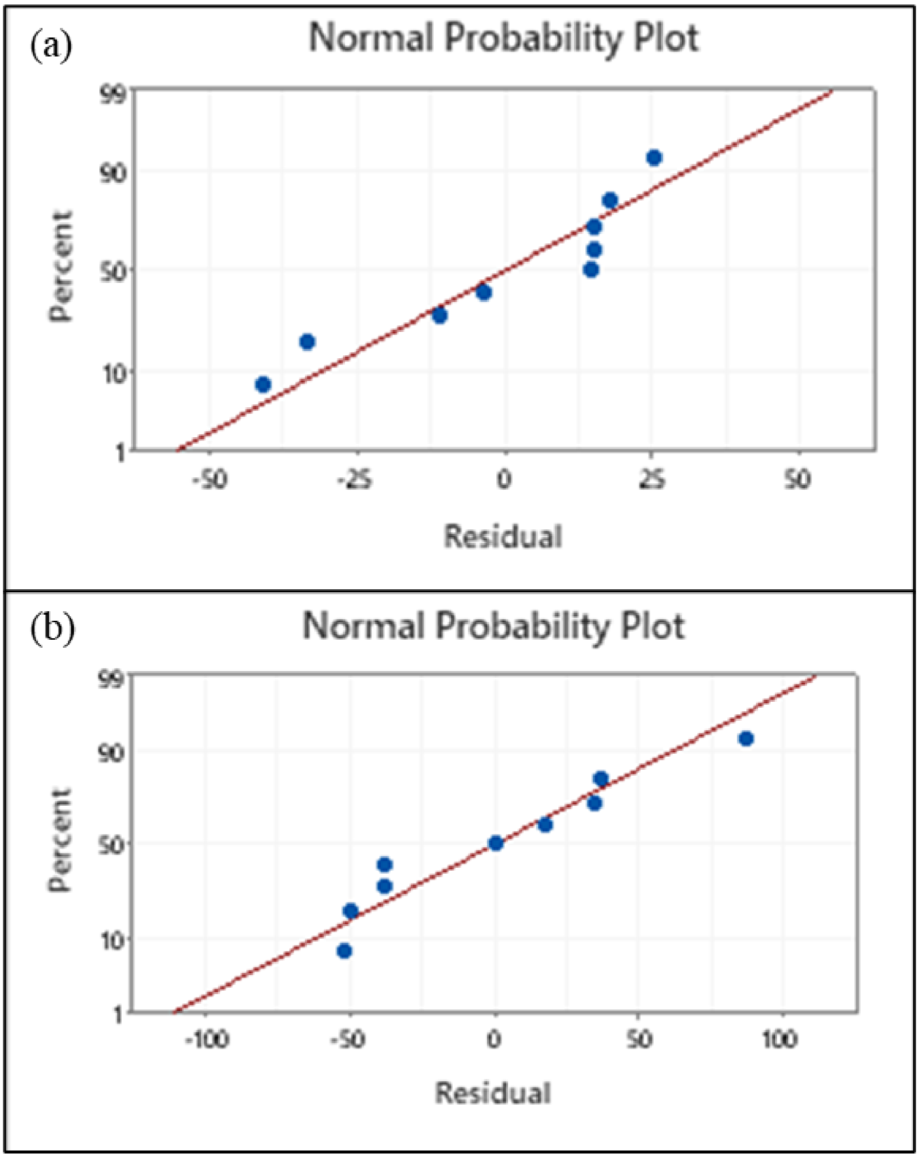

Fig. 6.5 Normality plots of residuals for responses (a) UTS (MPa) and (b) flexure stress (MPa).

Table 6.9 Summary of dissimilar AA5083 to copper FSW joint's UTS (MPa) regression model

Model Summary

S	R-sq	R-sq(adj)	R-sq(pred)
34.0266	86.12%	72.24%	36.41%

Coefficients

Term	Coef	SE Coef	T-Value	P-Value	VIF
Constant	1960	1287	1.52	0.203	
Nr (rpm)	-1.75	1.13	-1.55	0.196	93.35
V (mm/min)	-19.9	13.6	-1.46	0.217	134.89
FSWT design	82.2	35.8	2.29	0.03	2.7
Nr *v	0.018	0.0115	1.57	0.192	237.28

Table 6.10 Summary of dissimilar AA5083 to copper FSW joint's flexure stress (MPa) regression model

Model Summary

S	R-sq	R-sq(adj)	R-sq(pred)
34.0266	84.24%	69.43%	33.95%

Coefficients

Term	Coef	SE Coef	T-Value	P-Value	VIF
Constant	-687	1433	-0.48	0.657	
Nr (rpm)	0.5	1.26	0.4	0.71	93.35
V (mm/min)	7.4	15.1	0.49	0.649	134.89
FSWT design	54.1	39.9	1.36	0.047	2.7
Nr *v	-0.0041	0.0128	-0.32	0.766	237.28

Furthermore, contour plots were employed to analyse the combined effect of the tool rotational speed to welding speed ratio (ω/ν ratio) on the UTS and flexure stress of the dissimilar AA5083 to copper FSW joints. As shown in Fig. 6.6 (a), the highest values of dissimilar AA5083 to copper FSW joints' UTS can be obtained at different levels of the (ω/ν ratio). This means that there is no single combination of tool rotational speed and welding speed that will result in the highest UTS for all dissimilar AA5083 to copper FSW joints. Therefore, an appropriate combination of FSW tool rotational speed and welding speed must be considered to achieve better mechanical strength, similar findings have previously been discussed in section 4.2.1.

On the other hand, the flexural stress of dissimilar AA5083 to copper FSW joints was found to increase with increasing tool rotational speed. However, the highest level of flexural stress can only be obtained at specific ω/ν ratios. This means that the optimal combination of tool rotational speed and welding speed for maximising flexural strength will also depend on a specific ω/ν ratio. It is worth to note that the results presented in Fig. 6.6.(a) and (b) were derived from experiments conducted using a simple FSW tool design.

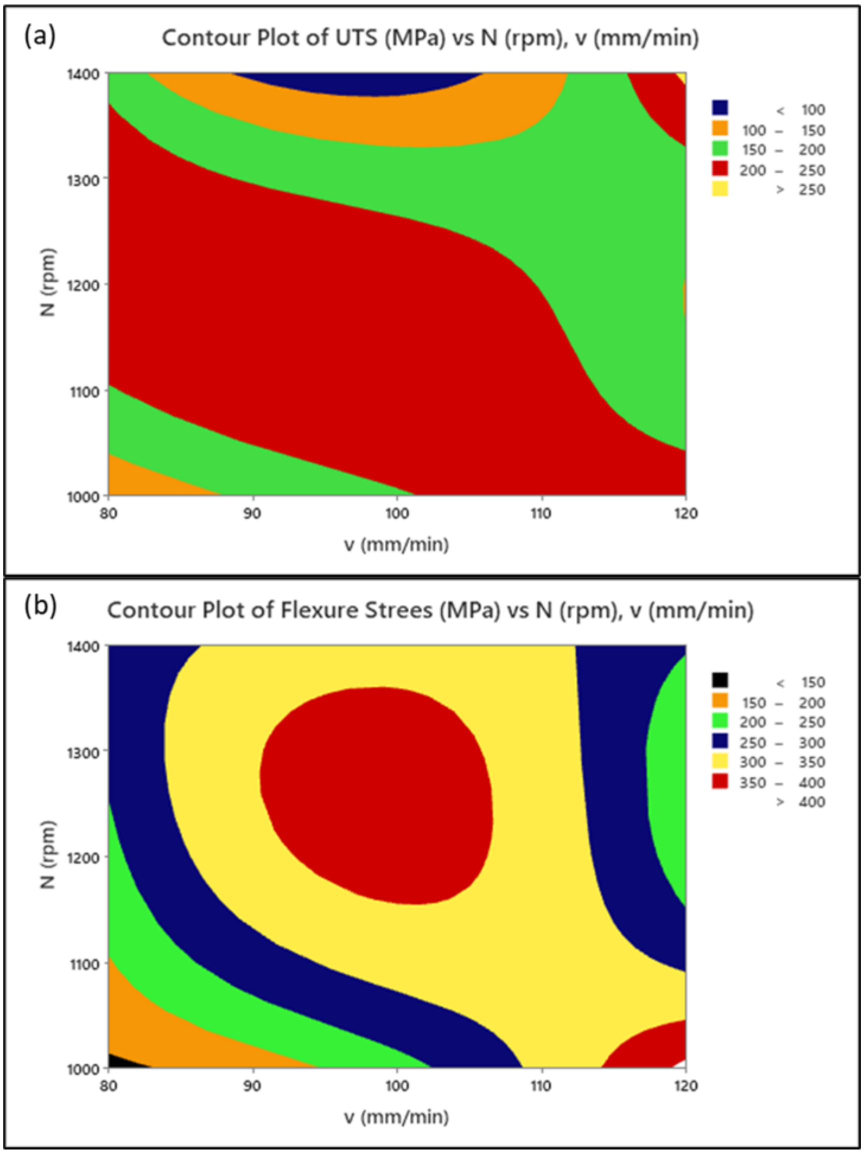

Fig. 6.6 Contour plots of dissimilar joints' characteristics factors (a) UTS (MPa) vs rotational and welding speeds, (b) flexure stress (MPa) vs rotational and welding speeds.

In summary, the following key conclusions can be drawn from the optimisation results presented in this chapter:

- Successful weld joints between AA5083 and commercially pure copper were achieved by placing the softer material (AA5083) on the advancing side at different levels of FSW tool rotational speed, tool welding speed, and FSWT design.
- The significant order of effect on AA5083 to copper FSW joints' UTS and flexure stress, from high to low, was found to be ranked as FSWT design, tool rotational speed, and tool welding speed. FSWT design was found to have the principal effect on dissimilar AA5083 to copper FSW joint' mechanical strength.
- The optimum FSW parameters for achieving the highest values of dissimilar AA5083 to copper FSW joints' UTS were identified as follows: Nr of 1200 rpm (level 2), ν of 120 mm/min (level 3), and simple FSWT design (level 2).
- The highest values of dissimilar AA5083 to copper FSW joints' flexure stress were obtained with the following parameters: Nr of 1400 rpm (level 3), ν of 100 mm/min (level 2), and larger shoulder FSWT design (level 3).
- By applying the Taguchi optimisation method, it was proved that dissimilar AA5083 to copper FSW joints' UTS at the predicted optimum levels increased by 27.3% compared to the joints' UTS using the initial sets of FSW parameters. On the other hand, dissimilar AA5083 to copper FSW joints' flexure stress enhanced by 35.2% under the optimum levels of FSW parameters.

- A good agreement between predicted and observed values of dissimilar AA5083 to copper FSW joints' UTS and flexure stress was achieved by using the linear regression analysis.
- Overall, these findings highlight the effectiveness of the optimisation approach in achieving improved mechanical performance in dissimilar AA5083 to copper FSW joints.

6.7. References

[6.1] L. E. Murr, "A Review of FSW Research on Dissimilar Metal and Alloy Systems," J Mater Eng Perform, vol. 19, no. 8, pp. 1071–1089, Feb. 2010. https://doi.org/10.1007/s11665-010-9598-0.

[6.2] D. A. Kumar, "a Review on Friction Stir Welding of Dissimilar Materials Between Aluminium Alloys to Copper," International Journal of Latest Research in Engineering and Technology, vol. 2, no. 2, pp. 9–15, 2016.

[6.3] S. Siddharth and T. S. Kumar, "Study of tool Penetration Behaviour in Dissimilar Al5083 /C10100 Friction Stir Spot Welds," Procedia Eng, vol. 173, pp. 1439–1446, 2017. https://doi.org/10.1016/j.proeng.2016.12.209.

[6.4] M. Shiraly, M. Shamanian, M. R. Toroghinejad, M. A. Jazani, and S. Sadreddini, "The Influence of Tool Geometry on the Mechanical Behaviour of FSSWed Al/Cu ARBed Composite," Transactions of the Indian Institute of Metals, vol. 70, no. 8, pp. 2205–2211, 2017. https://doi.org/10.1007/s12666-017-1044-7.

[6.5] W. M. Syafiq, M. Afendi, R. Daud, M. N. Mazlee, M. S. Abdul Majid, and Y. S. Lee, "Mechanical properties of friction stir welded butt joint of steel/aluminium alloys: Effect of tool geometry," J Phys Conf Ser, vol. 908, no. 1, pp. 0–7, 2017. https://doi.org/10.1088/1742-6596/908/1/012061.

[6.6] K. P. Mehta and V. J. Badheka, "Influence of tool pin design on properties of dissimilar copper to aluminium friction stir welding," Transactions of Nonferrous Metals Society of China (English Edition), vol. 27, no. 1, pp. 36–54, 2017. https://doi.org/10.1016/S1003-6326(17)60005-0.

[6.7] D. Devaiah, K. Kishore, and P. Laxminarayana, "Parametric Optimization of Friction Stir Welding Parameters Using Taguchi Technique for Dissimilar Aluminium Alloys," vol. 07, no. December, pp. 44–49, 2016.

[6.8] L. N. Harris, "Taguchi techniques for quality engineering, Philip J. Ross, Mcgraw-hill book company, 1988," Qual Reliab Eng Int, vol. 5, no. 3, pp. 249–249, Jul. 1989. https://doi.org/10.1002/qre.4680050312.

[6.9] T. Menten and M. Phadke, "Quality Engineering Using Robust Design," Technometrics, vol. 33, no. 2, p. 236, May 1991. https://doi.org/10.2307/1269049.

[6.10] D. C. Montgomery, "Design and analysis of experiments", John wiley & sons, Eighth Ed. 2022.

[6.11] G. Karrar, A. Galloway, A. Toumpis, H. Li, and F. Al-Badour, "Microstructural characterisation and mechanical properties of dissimilar AA5083-copper joints produced by friction stir welding," Journal of Materials Research and Technology, vol. 9, no. 5, pp. 11968–11979, 2020. https://doi.org/10.1016/j.jmrt.2020.08.073.

[6.12] X. Li, D. Zhang, C. Qiu, and W. Zhang, "Microstructure and mechanical properties of dissimilar pure copper/1350 aluminium alloy butt joints by friction stir welding," Transactions of Nonferrous Metals Society of China, vol. 22, no. 6, pp. 1298–1306, Jun. 2012. https://doi.org/10.1016/S1003-6326(11)61318-6.

[6.13] I. Galvão, J. Oliveira, A. Loureiro, and D. Rodrigues, "Formation and distribution of brittle structures in friction stir welding of aluminium and copper: influence of process parameters," Science and Technology of Welding and Joining, vol. 16, no. 8, pp. 681–689, 2011. https://doi.org/10.1179/1362171811Y.0000000057.

[6.14] F. Bakhtiari Argesi, A. Shamsipur, and S. E. Mirsalehi, "Dissimilar Joining of Pure Copper to Aluminium Alloy via Friction Stir Welding," Acta Metallurgica Sinica (English Letters), vol. 5, 2018. https://doi.org/10.1007/s40195-018-0741-5.

[6.15] N. Eslami, Y. Hischer, A. Harms, D. Lauterbach, and S. Böhm, "Optimization of process parameters for friction stir welding of aluminium and copper using the Taguchi method," Metals (Basel), vol. 9, no. 1, pp. 6–10, 2019. https://doi.org/10.3390/met9010063.

[6.16] MINITAB™ Statistical software Release 19.

7. Influence of aluminium alloy grade on dissimilar FSW of aluminium to magnesium AZ31B

Aluminium grades AA5083 and AA6061 were separately welded to magnesium AZ31B at different tool rotational speeds (ω) and traverse speeds (ν). The optimal process parameters for achieving defect-free joints were identified by examining the joints microstructure, as well as assessing the presence and distribution of intermetallic compounds (IMCs) using energy dispersive spectroscopy (EDS) and X-ray diffraction (XRD) techniques. Additionally, the hardness distribution of different weld zones allowed for the joint mechanical strength to be predicted. The chapter also explores the combined impact of dissimilar joints' microstructure and IMCs formation on the dissimilar aluminium to magnesium FSW joints' mechanical strength.

It has been found that the dissimilar aluminium to magnesium FSW process was influenced by the aluminium grade, in that the highest joint mechanical strength was achieved when magnesium grade AZ31B was friction stir welded to the harder aluminium grade (AA6061). Placing the AZ31B on the advancing side (AS) with no tool offset, 1000 rpm tool rotational speed and 100 mm/min traverse speed, delivered defect-free joints. Additionally, several IMCs such as Al_3Mg_2 and $Al_{12}Mg_{17}$ were identified at the weld nugget of the dissimilar joints, the presence of which resulted in higher hardness values at the weld nugget compared to the parent metals.

7.1. Weld appearance and macro/microstructure

The analysis of weld quality aimed to identify the process parameters that led to the formation of defect-free joints. To track the formation of volumetric defects, the typical appearance of the top surface weld and the macrostructures of AA5083 to AZ31B and AA6061 to AZ31B dissimilar FSW joints under different welding parameters were considered as per Table 3.8 section 3.1.2. The microstructure of the weld joint was examined using high-resolution optical microscopy to detect possible weld defects i.e. micro-voids and cracks. Fig. 7.1 (a) illustrates a representative cross-section of an AA5083 to AZ31B (AS) dissimilar FSW joint welded at 1000 rpm and 100 mm/min (test no. 5 of Table 3.8). Towards the AZ31B side (Fig. 7.1 (b)), relatively larger magnesium particles were observed to be irregularly distributed between the AZ31B interface zone and the bottom surface of the stir zone (SZ).

Further, Fig. 7.1 (a) reveals that under these parameters (10 ω/v ratio), the irregular distribution of these larger magnesium particles led to the formation of macro/micro-cracks in the SZ and towards the AA5083 interface zone (Fig. 7.1 (c)). Previous reports [7.1–7.3] have indicated that the formation of larger IMCs particles and improper material flow can result in crack defects in dissimilar aluminium to AZ31B FSW joints.

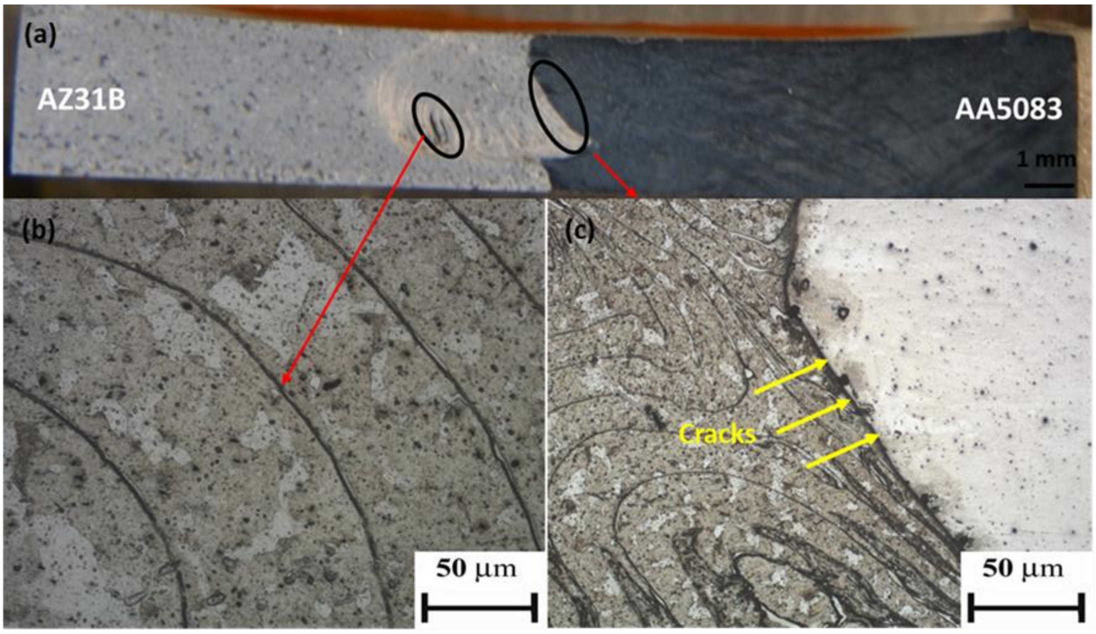

Fig. 7.1 (a) Typical cross-section of AA5083 to AZ31B FSW joint welded at 1000 rpm and 100 mm/min. (b) SZ and interface zone towards AZ31B side. (c) interface zone towards the AA5083 side.

In contrast to the dissimilar FSW joint between AA5083 and AZ31B, defect-free joints between AA6061 and AZ31B were consistently achieved under conditions that led to crack formation when considering the AA5083 aluminium grade. Fig. 7.2 (a) presents a typical cross-section of a defect-free dissimilar AA6061 to AZ31B FSW joint, as-welded at 1000 rpm and 100 mm/min (10 ω/ν ratio), with AZ31B placed on the AS and zero tool offset (test no. 11 of Table 3.8). The presence of irregular aluminium particles resulted in the formation of a lamella structure consisting of magnesium and aluminium in the SZ and towards the AZ31B interface zone (Fig. 7.2 (b)). This structure, which was suppressed in dissimilar AA5083 to AZ31B FSW joints under similar welding conditions (10 ω/ν ratio), demonstrates the influence of the aluminium alloy grade on the dissimilar aluminium to AZ31B FSW process.

Additionally, a complex structure was observed in the AA6061 side of the interface zone and towards the SZ (Fig. 7.2 (c)). This complex structure was formed as aluminium fragments detached from the retreating side (RS) and mixed with the magnesium matrix during the stirring process. The appropriate heat input for the dissimilar joints between AA6061 and AZ31B accounts for the formation of this complex structure [7.4–7.6]. It has been previously suggested [7.7-7.9] that the stirring action alone is inadequate to generate this structure at a lower rotational speed.

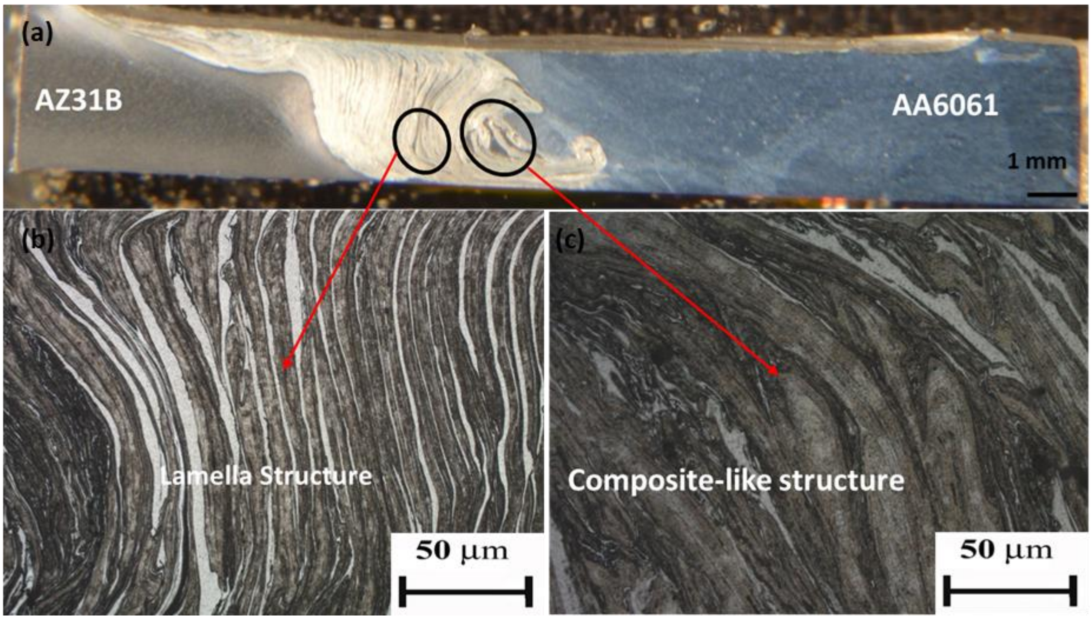

Fig. 7.2 (a) Typical cross-section of AA6061 to AZ31B FSW joint welded at 1000 rpm and 100 mm/min. (b) SZ. (c) interface zone towards the AA6061 side.

7.2. Dissimilar aluminium to magnesium FSW joints' interfacial zone

The impact of aluminium grade on dissimilar aluminium to magnesium FSW joints was corroborated through an analysis of the interfacial zone of these dissimilar joints. Widely acknowledged studies [7.10-7.12] suggest that the interfacial structure of dissimilar aluminium to magnesium FSW joints is a crucial determinant of the mechanical performance of the resulting joint. Microstructural examination from section 7.2 elucidates that aluminium (Al) to magnesium (Mg) FSW joints were influenced by the aluminium grade. Consequently, AA5083 to AZ31B FSW joints were consistently produced at a lower rotational speed of 800 rpm and a welding speed of 100 mm/min (test no. 2 of Table 3.8).

A detailed view of the lamella structure, predominant in the AA5083 to AZ31B interfacial zone, is displayed in Fig. 7.3 (a). According to the EDS results, the elemental distribution along the interface was also found to be susceptible to the welding conditions (ω/ν ratio) as well as the aluminium grade. Table 7.1 summarises the elemental compositions as applied on the points as demonstrated in Fig. 7.3 (b). The variation in Al/Mg and the diffusion of aluminium particles along the layers of magnesium resulted in a good metallurgical bonding.

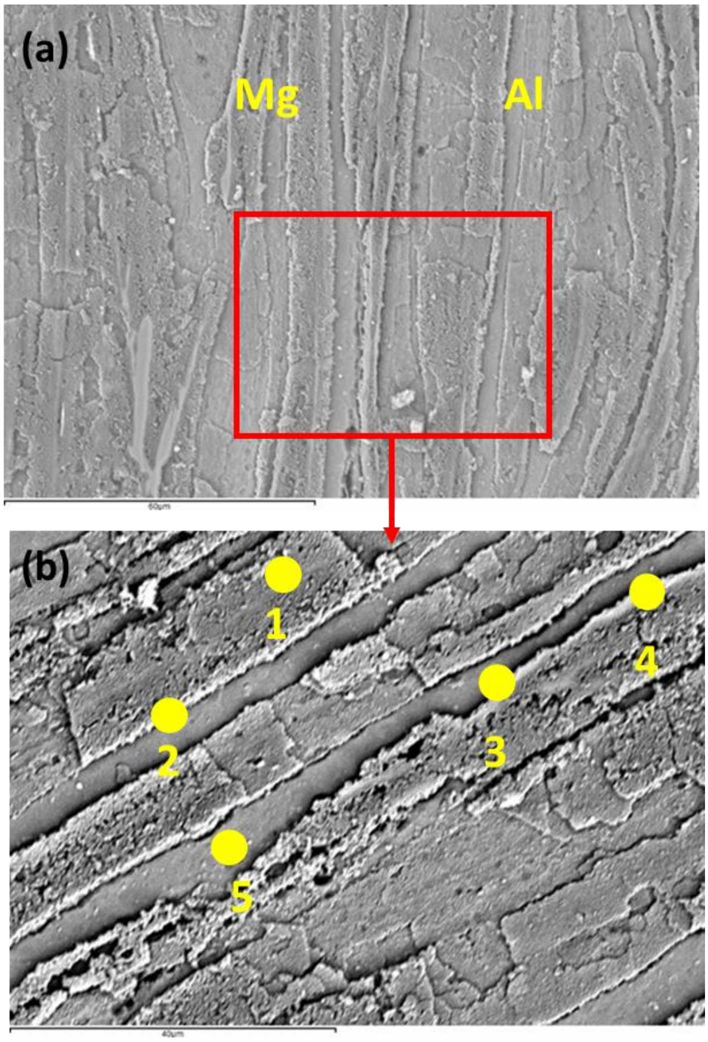

Fig. 7.3 (a) AA5083 to AZ31B interfacial microstructure of the joint produced at 800 rpm and 100 mm/min. (b) Lamella structure inside the SZ at 800 rpm and 100 mm/min and the EDS positions.

Table 7.1 EDS results at SZ of AA5083 to AZ31B (Fig. 7.3 (b))

Position	Al at. %	Mg at. %	Possible phases
1	9.64	90.36	Mg+γ
2	55.27	44.73	$Al_{12}Mg_{17}$
3	62.76	37.24	Al_3Mg_2
4	62.62	37.38	Al_3Mg_2
5	88.26	11.74	Al+β

On the other hand, the relatively higher heat input required to friction stir weld AA6061 to AZ31B resulted in a composite-like structure at the interface zone and towards the aluminium side. Fig. 7.4 (a) shows a typical interface zone of an AA6061 to AZ31B FSW joint produced at a rotational speed of 1000 rpm and a welding speed of 100 mm/min (test no. 11 of Table 3.8). Fig. 7.4 (a) also presents the EDS analysis conducted at various points along the interface zone, and the elemental compositions at these points are summarised in Table 7.2. The chemical compositions of points 1 to 4 in Table 7.2 reveal a moderate variation in the Al/Mg contents at the detected composite-like structure (Fig. 7.4(b)). It has been claimed [7.1-7.4] that the mechanical strength of dissimilar aluminium to magnesium FSW joints is significantly improved by the presence of a composite-like structure inside the SZ and towards the interfacial zone. Therefore, AA6061 to AZ31B FSW joints are likely to have better mechanical performance due to the formation of this complex structure.

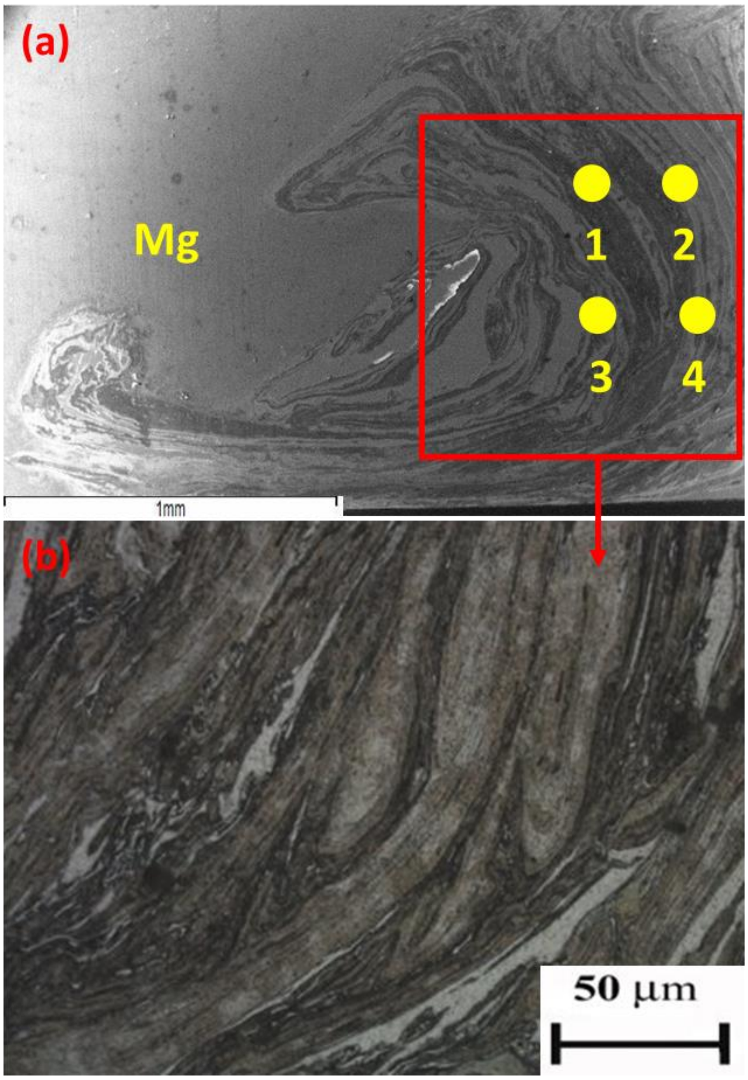

Fig. 7.4 (a) AA6061 to AZ31B interfacial microstructure and the EDS positions of the joint produced at 1000 rpm and 100 mm/min. (b) Composite-like structure inside the SZ at 1000 rpm and 100 mm/min

Table 7.2 EDS results towards the RS (AA6061) of AA6061 to AZ31B (Fig. 7.4 (a))

Position	Al at. %	Mg at. %	Possible phases
1	63.5	36.5	Al_3Mg_2
2	52.3	47.7	$Al_{12}Mg_{17}$
3	54.4	45.6	$Al_{12}Mg_{17}$
4	62.9	37.1	Al_3Mg_2

Overall, Fig. 7.5 demonstrates, based on the above macro/microstructural investigations, the optimum process conditions that consistently resulted in a defect-free joint of dissimilar aluminium to AZ31B FSW using different aluminium grades i.e., AA5083 and AA6061. It has been established that dissimilar FSW of aluminium to AZ31B is affected by the aluminium grade, in that the joint microstructure (and thus the joint mechanical performance) was influenced when AZ31B was friction stir welded to different aluminium grade types at various ω/ν ratios. Although Fig 7.5 highlights the parameters that were empirically tested and found to -consistently- result in defect-free joints of aluminium to AZ31B, it also provides a visual guide to the anticipated challenges when operating outside of these proven parameters, thus highlighting the likelihood of encountering issues such as excessive or insufficient heat input.

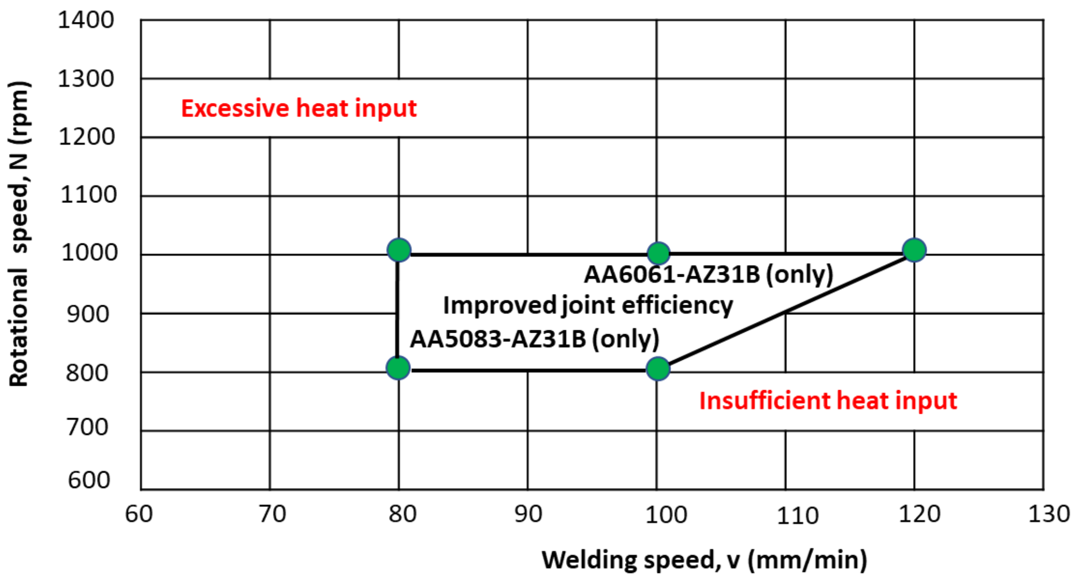

Fig. 7.5 Dissimilar aluminium to AZ31B FSW process window based on macro/microstructural analysis.

7.3. Intermetallic phases at the weld nugget

XRD analysis conducted across the dissimilar aluminium to magnesium FSW joints revealed the formation of several IMCs such as Al_3Mg_2 and $Al_{12}Mg_{17}$ at the weld nugget. It was observed that the intensity peaks of these IMCs, indicating the quantity of IMCs present at the weld nugget, varied with the aluminium grade. Fig. 7.6 illustrates the XRD patterns of two typical defect-free joints: AA5083 to AZ31B and AA6061 to AZ31B (tests no. 2 and 11 in Table 3.8, respectively). Although both patterns indicate that the dominant IMCs in the SZ were Al_3Mg_2 and $Al_{12}Mg_{17}$, the intensity peaks of the IMCs were relatively higher in the AA6061 to AZ31B SZ.

The previous investigation of microstructure in section 7.2 of tests no. 2 and 11 in Table 3.8 demonstrates that the elemental distribution of Al/Mg contents at the interfacial zone and towards the SZ was influenced by the welding parameters. Concurrently, the XRD analysis revealed that the relatively higher rotational speed required to achieve a defect-free joint of AA6061 to AZ31B (1000 rpm) resulted in an increase in the peak intensity of the detected IMCs, which is consistent with previous research findings [2]. Therefore, it is worth noting that the variation in intensity peaks resulted in a complex mixture of aluminium and magnesium within the weld zones.

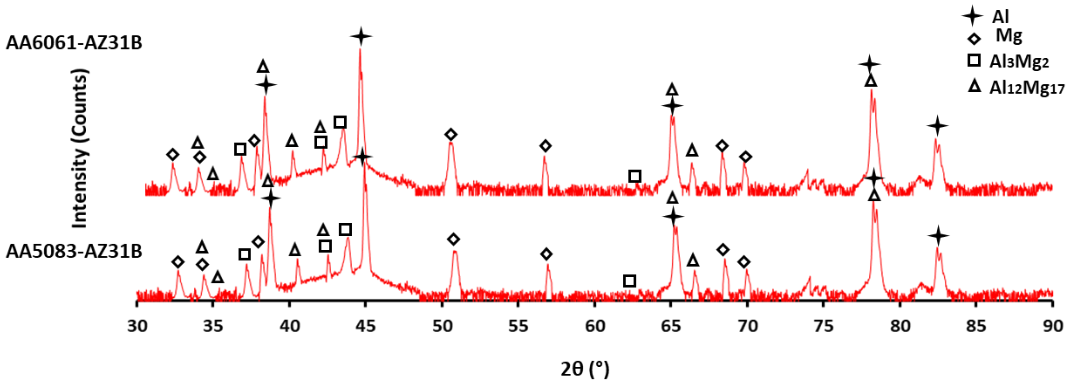

Fig. 7.6 XRD patterns acquired under tests no. 2 (AA5083 to AZ31B), 11 (AA6061 to AZ31B) of Table 3.8.

7.4. Dissimilar aluminium to AZ31B FSW joints' mechanical strength

The evaluation of dissimilar aluminium to AZ31B FSW joints involved the measurement of Vickers hardness distribution across and at the middle of the weld cross-section, as depicted in Fig. 7.7 (a). It was observed, as shown in Fig. 7.7 (b), that the hardness values significantly increased at the SZ compared to the base metals. This increase was attributed to the presence of hard and brittle IMCs such as Al_3Mg_2 and $Al_{12}Mg_{17}$ [7.1, 7.3]. Additionally, the high hardness values in the thermo-mechanically affected zone (TMAZ) were associated with the presence of very fine recrystallised grains, dispersed aluminium-rich particles, and the formation of a lamella and/or composite-like structure at this interfacial zone.

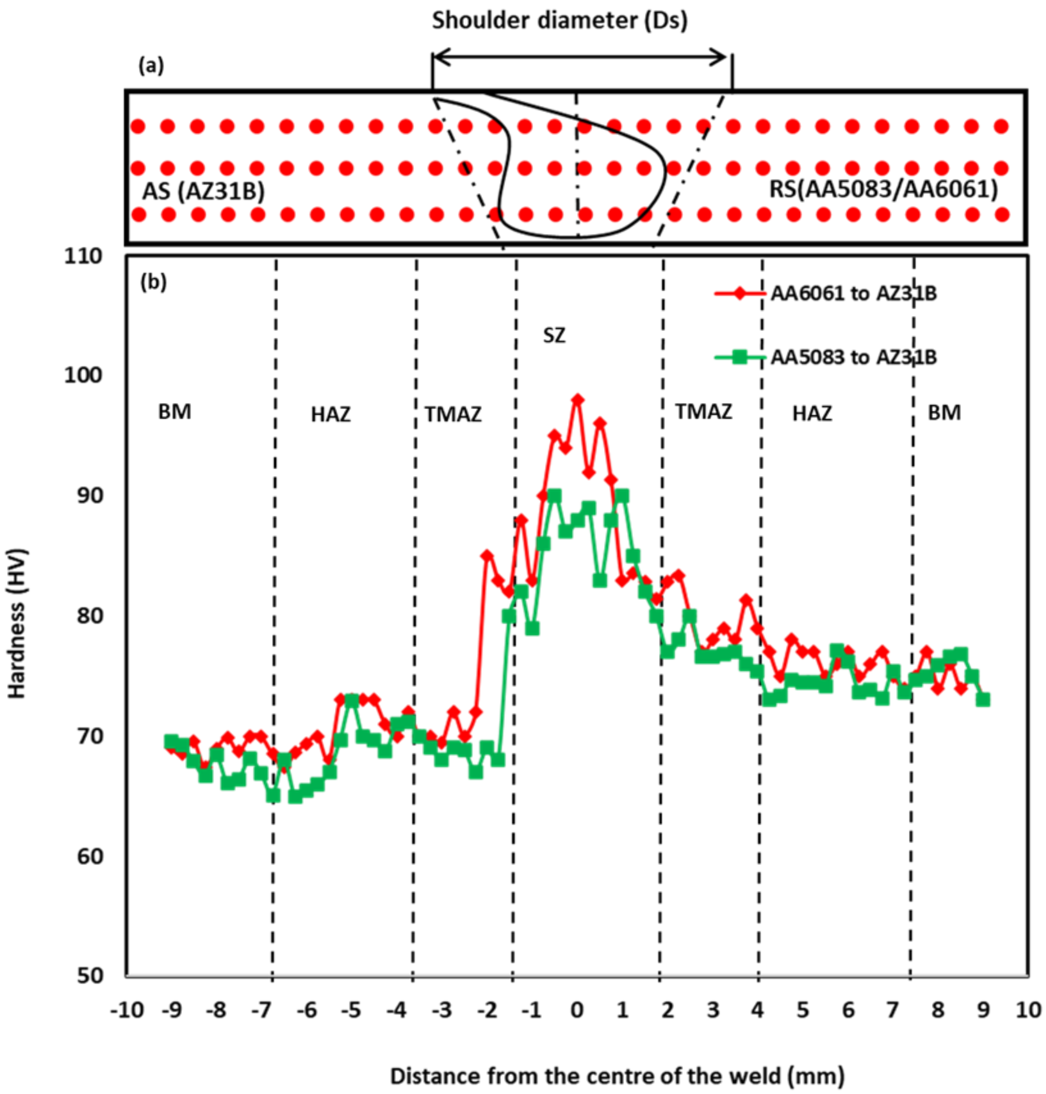

*BM≡ base metal. *HAZ≡ heat affected zone.

Fig. 7.7 (a) Hardness measurements points at the weld cross-section. (b) Hardness distribution under tests no. 2 (AA5083 to AZ31B) and 11 (AA6061 to AZ31B) of Table 3.8.

To confirm the influence of aluminium grade types on dissimilar aluminium to AZ31B friction stir welded joints, further mechanical investigations were conducted. Each dissimilar aluminium to AZ31B FSW joint was evaluated by testing sub-size specimens across the weld zone of each welded sample in accordance with ASTM-E8 [7.13]. Table

7.3 provides a summary of the obtained means of ultimate tensile strength (UTS) for dissimilar AA5083 to AZ31B and AA6061 to AZ31B FSW joints under the conditions that resulted in defect-free joints. A minimum of three ASTM-E8 tensile strength samples were analysed to calculate the mean UTS at each welding condition, ensuring a high level of confidence. Remarkably, an overall joint mechanical efficiency of up to 91% was achieved by placing the softer material (AZ31B) on the AS.

It is worth noting that some discrepancies in the UTS values may be attributed to the formation of IMCs at the interface of aluminium and magnesium, known to form brittle phases such as Al_3Mg_2 and $Al_{12}Mg_{17}$, which can have a significant impact on mechanical performance. These IMCs were qualitatively observed through XRD analysis (as shown previously in Fig. 7.6), and their brittle nature may lead to variations in joint strength, especially at certain weld zones where the concentration of IMCs could differ. While further quantification of these IMCs, including their exact distribution, would provide additional insights into the mechanical discrepancies, this was beyond the core objectives of this study. Nonetheless, the presented results are deemed acceptable and consistent with the scope and objectives of this research, serving as a foundation for future studies in the field.

Table 7.3 Dissimilar AA5083/AA6061 to AZ31B FSW joints' UTS (MPa)

Exp. No	**Input parameters**			**UTS1 (MPa)**	**UTS2 (MPa)**	**UTS3 (MPa)**	**UTS Avg. (MPa)**
	Nr (rpm)	ν (mm/min)	RS (Material)				
1	800	80	AA5083	190.85	310.50	250.67	250.67
2	800	100	AA5083	260.74	300.67	270.34	277.25
3	800	120	AA5083	320.55	215.45	264.38	266.79
4	1000	80	AA5083	200.35	255.34	230.43	228.71

5	1000	100	AA5083	280.75	210.44	240.65	243.95
6	1000	120	AA5083	220.32	190.54	290.15	233.67
7	800	80	AA6061	245.48	334.82	280.14	286.81
8	800	100	AA6061	230.22	360.74	330.45	307.14
9	800	120	AA6061	223.56	350.67	320.13	298.12
10	1000	80	AA6061	242.43	370.26	338.78	317.16
11	1000	100	AA6061	260.89	390.13	360.44	337.15
12	1000	120	AA6061	255.12	377.25	334.87	322.41

Furthermore, Fig. 7.8 (a) illustrates the influence of FSW process parameters on the UTS of dissimilar AA5083/AA6061 to AZ31B FSW joints. As anticipated, the UTS of the joints was affected by the FSW parameters, including tool rotational speed, tool welding speed, and the aluminium grade on the RS. Specifically, the UTS of dissimilar AA6061 to AZ31B joints was relatively higher compared to dissimilar AA5083 to AZ31B joints. This improvement in UTS for dissimilar AA6061 to AZ31B joints was attributed to the combined presence of a composite-like structure and relatively larger amounts of IMCs in the SZ. Figs. 7.8 (a) and (b) demonstrate that the UTS of dissimilar aluminium to AZ31B FSW joints consistently increased with higher tool rotational speed. However, the UTS of the joints exhibited an increase followed by a decrease as the tool welding speed was increased, highlighting the dual impact of tool rotational and welding speeds, which has been extensively discussed in Chapters 4,5, and 6.

Moreover, the analysis of variance (ANOVA) technique was employed to further verify the significant influence of the aluminium grade type on dissimilar aluminium to AZ31B FSW joints' UTS. By utilising, Table 7.4, it was determined that there was insufficient evidence to reject the null hypotheses for the tool rotational speed and tool welding speed. This indicates that there was no significant difference in the UTS of dissimilar joints when considering the proposed levels of tool rotational speeds (800-1000 rpm), tool welding speeds (80-120 mm/min), and similar aluminium grade at the RS as outlined in Table 7.3. However, there was enough evidence to reject the null hypothesis regarding the consideration of two different aluminium grades on the RS. Therefore, it can be concluded that the UTS of dissimilar aluminium to AZ31B joints was significantly affected by the aluminium grade.

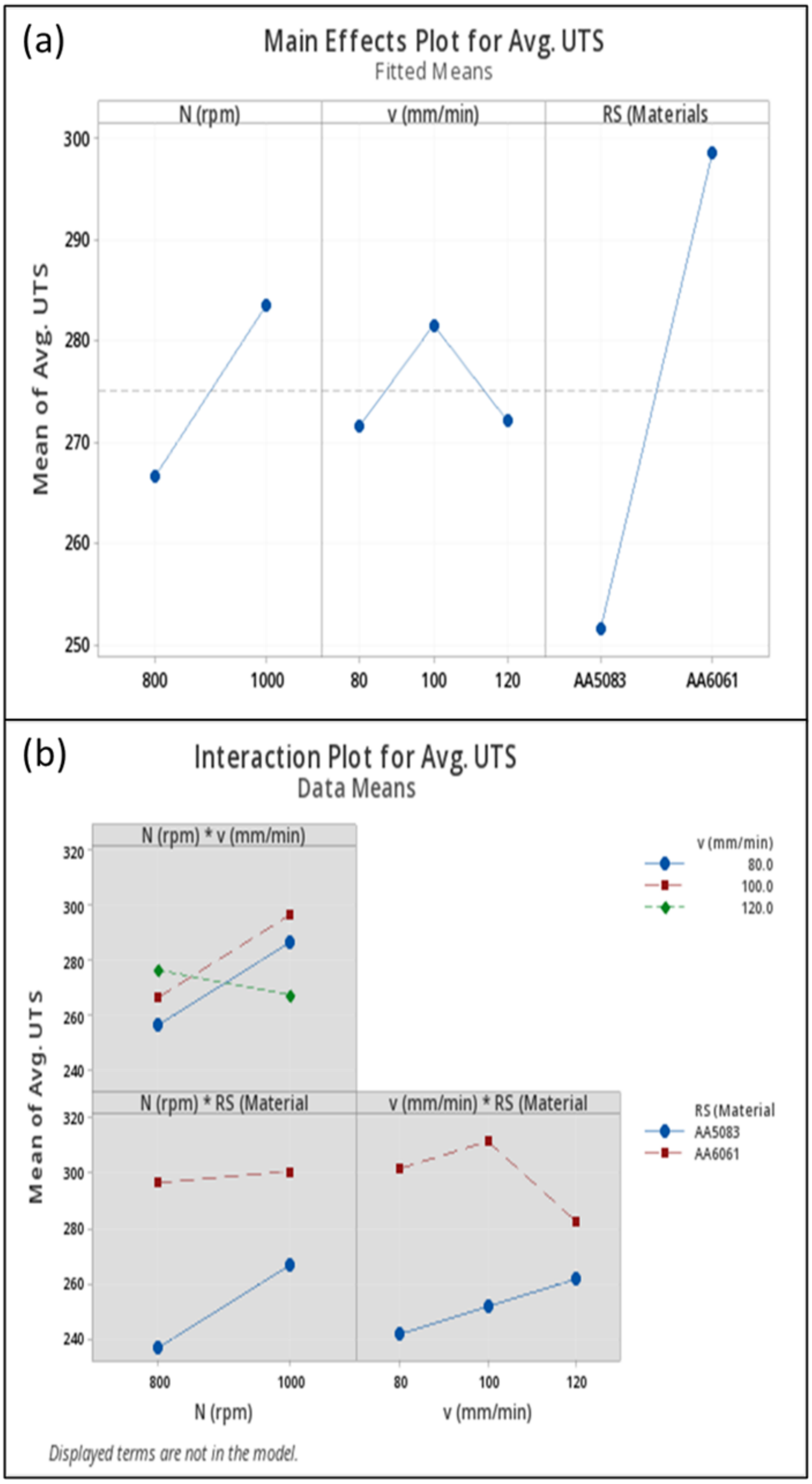

Fig. 7.8 (a) Influence of FSW parameters on dissimilar joints' UTS (MPa) and (b) Interaction plots effect on Avg. UTS (MPa).

Table 7.4 ANOVA test results of the UTS (MPa)

ANOVA results					
Source	**DF**	**Adj SS**	**Adj MS**	**F-Value**	**P-Value**
N (rpm)	1	867	867	1.71	0.232
v (mm/min)	2	254	127	0.25	0.785
RS (Materials)	1	6627	6627	13.07	**0.009**
Error	7	3549	507		
Total	11	11297			

In summary, the following key conclusions can be drawn from the investigation results presented in this chapter:

- Defect-free joints of two aluminium alloys (AA5083 and AA6061) to AZ31B were achieved by placing the softer material (AZ31B) on the AS, without implementing any tool offset.
- The dissimilar FSW of aluminium to AZ31B was influenced by the aluminium alloy grade, with AA6061 to AZ31B defect-free joints requiring higher heat input compared to AA5083 to AZ31B FSW joints.
- The joint mechanical strength was significantly improved by the composite-like structure at the SZ; as a result, a joint mechanical efficiency of 91% of the AZ31B magnesium alloy was achieved.

7.5. References

[7.1] U. Singarapu, K. Adepu, and S. R. Arumalle, “Influence of tool material and rotational speed on mechanical properties of friction stir welded AZ31B magnesium alloy," Journal of Magnesium and Alloys, vol. 3, no. 4, pp. 335–344, 2015. https://doi.org/10.1016/j.jma.2015.10.001.

[7.2] B. Fu, G. Qin, F. Li, X. Meng, J. Zhang, and C. Wu, "Friction stir welding process of dissimilar metals of 6061-T6 aluminium alloy to AZ31B magnesium alloy," J Mater Process Technology, vol. 218, pp. 38–47, 2015. https://doi.org/10.1016/j.jmatprotec.2014.11.039.

[7.3] S. Ramaiyan, S. Kumar, V. Santhanam, P. Muthuguru, and T. Pin, "Effect of Scroll Pin Profile and Tool Rotational Speed on Mechanical Properties of Submerged Friction Stir Processed AZ31B Magnesium Alloy," 2018.

[7.4] G. Karrar, A. Galloway, A. Toumpis, H. Li, and F. Al-Badour, "Microstructural characterisation and mechanical properties of dissimilar AA5083-copper joints produced by friction stir welding," Journal of Materials Research and Technology, vol. 9, no. 5, pp. 11968–11979, 2020. https://doi.org/10.1016/j.jmrt.2020.08.073.

[7.5] M. Shiraly, M. Shamanian, M. R. Toroghinejad, M. A. Jazani, and S. Sadreddini, "The Influence of Tool Geometry on the Mechanical Behaviour of FSSWed Al/Cu ARBed Composite," Transactions of the Indian Institute of Metals, vol. 70, no. 8, pp. 2205–2211, 2017. https://doi.org/10.1007/s12666-017-1044-7.

[7.6] F. Badkoobeh, H. Mostaan, M. Rafiei, H. R. Bakhsheshi-Rad, and F. Berto, "Friction stir welding/processing of mg-based alloys: A critical review on advancements and challenges," Materials, vol. 14, no. 21, 2021. https://doi.org/10.3390/ma14216726.

[7.7] G. K. Padhy, C. S. Wu, and S. Gao, "Friction stir based welding and processing technologies - processes, parameters, microstructures and applications: A review," J Mater Sci Technol, vol. 2, 2017. https://doi.org/10.1016/j.jmst.2017.11.029.

[7.8] K. P. Mehta and V. J. Badheka, "A review on dissimilar friction stir welding of copper to aluminum: Process, properties, and variants," Materials and Manufacturing Processes, vol. 31, no. 3, pp. 233–254, 2016. https://doi.org/10.1080/10426914.2015.1025971.

[7.9] Z. Y. Ma, A. H. Feng, D. L. Chen, and J. Shen, "Recent Advances in Friction Stir Welding/Processing of Aluminum Alloys: Microstructural Evolution and Mechanical Properties," Critical Reviews in Solid State and Materials Sciences, vol. 8436, pp. 1–65, 2017. https://doi.org/10.1080/10408436.2017.1358145.

[7.10] C. Genevois, M. Girard, B. Huneau, X. Sauvage, and G. Racineux, "Interfacial Reaction during Friction Stir Welding of Al and Cu," Metallurgical and Materials Transactions A, vol. 42, no. 8, pp. 2290–2295, Aug. 2011. https://doi.org/10.1007/s11661-011-0660-9.

[7.11] Z. Sun, C. S. Wu, and S. Kumar, "Determination of heat generation by correlating the interfacial friction stress with temperature in friction stir welding," J Manuf Process, vol. 31, pp. 801–811, 2018. https://doi.org/10.1016/j.jmapro.2018.01.010.

[7.12] M. N. Avettand-Fenoël, R. Taillard, G. Ji, and D. Goran, "Multiscale study of interfacial intermetallic compounds in a dissimilar Al 6082-T6/Cu friction-stir weld," Metall Mater Trans A Phys Metall Mater Sci, vol. 43, no. 12, pp. 4655–4666, 2012. https://doi.org/10.1007/s11661-012-1277-3.

[7.13] American society for testing and materials (ASTM). In: Standard test methods for tension testing of metallic materials, ASTM E8M – 09, vol. 03.01. West Conshohocken (PA): Annual book of ASTM standards.

8. Conclusions and future work

The forthcoming discussion presents the conclusions drawn from the research conducted on the FSW process of dissimilar aluminium to copper materials, along with future research prospects. The investigation involved experimental and numerical methods to evaluate the weld quality through metallurgical and mechanical analyses. Finite Element (FE) methods were utilised as an auxiliary tool, supplementing the experimental work to simulate the FSW process and facilitating the prediction of IMCs formation. This inclusion of FE methods provided valuable insights into how various FSW process parameters influence the formation of IMCs and the overall characteristics of the weld.

The Taguchi design of experiments (DoE) was utilised to identify the significant parameters affecting the mechanical strength of dissimilar aluminium grade AA5083 to copper FSW joints and reduce the number of required experiments for maximising joint efficiency. Furthermore, the study examined the influence of using two different aluminium alloys (AA5083 and AA6061) on joint quality in FSW of aluminium to magnesium grade (AZ31B).

8.1. Dissimilar FSW of aluminium alloys to copper

The comprehensive analysis presented in the literature review (Chapter 2) has emphasised that dissimilar aluminium to copper FSW defect-free joints can be achieved by positioning the harder material (copper) on the advancing side (AS). These studies have indicated that placing copper on the AS promotes effective mixing between aluminium and copper due to the easier flow of the softer material (aluminium).

However, in order to achieve defect-free joints, tool offsetting towards either the retreating side (RS) or AS was typically necessary. The reported ranges of tool offsets varied widely, rendering this method impractical for industrial applications. Alternatively, researchers reported success in obtaining defect-free joints by placing the softer material (aluminium) on the AS, requiring minimal or no tool offset.

Despite the advantages of placing aluminium on the AS for joint mechanical properties, limited research has been conducted on this configuration. Additionally, the relationship between the microstructure of intermetallic compounds (IMCs) and mechanical properties requires further investigation. The study evaluated the influence of tool rotational and traverse speeds on dissimilar AA5083 to copper FSW joint quality when placing aluminium on the AS without introducing tool offsetting. The conclusions derived from the experimental investigation are as follows:

- Successful weld joints were obtained between dissimilar AA5083 to copper materials at different tool rotational and traverse speeds, with copper placed on the RS without tool offset.
- Dissimilar AA5083 to copper defect-free joints produced by FSW were achieved at the specific following parameters:
  - ➢ Low rotational speed level of 1000 rpm at 100 mm/min and 120 mm/min welding speeds (10 and 8.3 ω/ν ratio).
  - ➢ Intermediate rotation rate level of 1200 rpm and 80 mm/min (15 ω/ν ratio).
  - ➢ High rotation rate level of 1400 rpm for the two ranges of the welding speed 80, and 120 mm/min (17.5, and 11.7 ω/ν ratio).

- An inhomogeneous microstructure was observed inside and on the interfacial zone, when copper particles detached and intermixed with the aluminium matrix.
- At higher level of rotational speeds, a composite-like structure was observed, while lamella or dispersed structures were found at lower level of rotational speeds.
- The predominant IMCs at the aluminium-copper joint were Al_2Cu and Al_4Cu_9.
- The volume fraction of the IMCs inside the stir zone increased by increasing the tool rotational speed as confirmed by the high XRD peak intensities and higher hardness values.
- The ultimate tensile strength (UTS) reached 203 MPa, representing a joint efficiency of 94.8% of the aluminium alloy as a result of the composite like structure and of an excellent metallurgical bond.
- Overall, dissimilar aluminium to copper FSW joint was influenced by the aluminium grade, in that the joint mechanical strength was varied when copper was friction stir welded to different aluminium grade types. Among the aluminium grades investigated in the study, AA5083 showed better joint mechanical strength than AA1061 and AA6061.

8.2. Prediction and validation of IMCs formation during FSW of AA6061 to commercially pure copper

A novel approach for predicting and validating the formation of IMCs during FSW of AA6061 to copper was presented, along with their effect on mechanical properties. Numerically, the work built upon the previously reported coupled Eulerian Lagrangian

(CEL) model approach, which assumed the FSW tool to rotate and traverse along the Eulerian domain. A modified friction law was adopted to describe the interaction between the Lagrangian (the FSW tool) and Eulerian (aluminium and copper) domains, resulting in good agreement with experimental data.

The temperature distribution within the weld nugget, obtained through finite element modelling, combined with an Al-Cu phase diagram and elemental concentration of copper and aluminium, allowed the prediction of several IMCs present in different weldment zones. The following conclusions were derived from this investigation:

- The formation of IMCs in FSW of AA6061 to copper has been predicted and validated with the experimental results.
- The predominant intermetallic compound phases in the aluminium-copper dissimilar joint were AlCu, Al_2Cu, and Al_4Cu_9.
- A defect free weld joint between the two dissimilar materials has been obtained at 1400 rpm and 1500 rotational speeds and 100 mm/min traverse speed, where the softer material (AA6061) was placed at the AS without any tool offset.
- Improvements in the UTS were found to be controlled by the relatively regular distribution of IMCs together with the evolution of the composite like structure.
- The highest UTS of 194.5 MPa was achieved at 1500 rpm tool rotational speed, 100 mm/min traverse speed and a zero-tool offset.

8.3. Optimisation of FSW parameters using the Taguchi technique for dissimilar joining of AA5083 to copper

A detailed parametric analysis was conducted to optimise the process parameters for dissimilar FSW of AA5083 to copper. The study considered the impact of rotational speed (Nr rpm), welding speed (ν mm/min), tool and FSW tool (FSWT) design throughout the optimisation process. The Taguchi DoE was applied to identify the significant parameters affecting the mechanical strength in dissimilar AA5083 to copper FSW joints and reduce the number of required experiments for maximising joint efficiency. Statistical analysis methods (ANOVA) were employed to verify the significant effects of the obtained process parameters on the dissimilar AA5083 to copper FSW joints' mechanical properties. The key conclusions derived from the optimisation results are as follows:

- Successful weld joints between AA5083 and commercially pure copper were achieved by placing the softer material (AA5083) on the AS at different levels of tool rotational speed, tool welding speed, and FSWT design.
- The order of significance in terms of impact on the joint UTS, from high to low, was as follows: FSWT design, tool rotational speed, and tool welding speed.
- Optimum FSW parameter for achieving highest values of dissimilar joints' UTS was found as: Nr of 1200 rpm (level 2), ν of 120 mm/min (level 3), and simple FSWT design (level 2).
- The highest values of dissimilar AA5083 to copper FSW joints' flexure stress were obtained with the following parameters: Nr of 1400 rpm (level 3), ν of 100 mm/min (level 2), and larger shoulder FSWT design (level 3).
- By applying the Taguchi optimisation method, it was demonstrated that the UTS of dissimilar joints increased by 27.3% and flexure stress enhanced by 35.2% compared to initial sets of FSW parameters.

- Linear regression analysis showed that the predicted values of the UTS and flexure stress of dissimilar AA5083 to copper FSW joints were in good agreement with the actual values.

8.4. Influence of aluminium alloy grade on dissimilar FSW of aluminium to AZ31B

Moreover, the study investigated the influence of different aluminium grades (AA5083 and AA6061) on dissimilar FSW of aluminium to magnesium AZ31B. The following conclusions were drawn:

- Placing the softer material (AZ31B) at the AS consistently produced defect-free FSW joints between dissimilar aluminium to AZ31B materials, without the need for tool offset.
- Dissimilar FSW between aluminium and AZ31B was influenced by the aluminium grade, with higher joint mechanical strength achieved when AZ31B was joined to the harder aluminium grade (AA6061).
- Several IMCs, including Al_3Mg_2 and $Al_{12}Mg_{17}$, were identified in the weld nugget, resulting in higher hardness values compared to the parent metals.
- The dissimilar joint's mechanical performance significantly improved due to the composite-like structure in the weld nugget, resulting in a joint mechanical efficiency of 91% for the AZ31B magnesium alloy.

In summary, this thesis presents substantial advancements in the FSW of dissimilar aluminium to copper and dissimilar aluminium to magnesium materials, aligning closely with the initial aims and objectives set out in Chapter 1. The comprehensive research undertaken, encompassing both experimental and numerical methods, has significantly contributed to the state-of-the-art in FSW research.

Key achievements include:

- Dissimilar FSW of aluminium alloys to copper: The study successfully demonstrated that defect-free joints in dissimilar aluminium to copper FSW are achievable by placing the softer material (aluminium) on the advancing side (AS), without the need for tool offset. This finding challenges the conventional practice and provides a more practical approach for industrial applications.
- Influence of aluminium alloy grades: The research also highlighted that the choice of aluminium grade significantly impacts the joint quality in dissimilar FSW, with AA5083 exhibiting superior mechanical strength compared to other grades.
- Prediction and validation of IMC formation: A novel approach for predicting and validating IMC formation in FSW of AA6061 to copper was introduced. This approach, combining numerical models with experimental results, provides a predictive insight into the microstructural evolution during welding, enhancing the understanding of material behaviour.
- Optimisation using Taguchi method: The application of the Taguchi method for optimising process parameters in dissimilar FSW of AA5083 to copper underscores the effectiveness of this statistical approach in refining welding conditions to maximise joint efficiency.
- FSW of aluminium to AZ31B: The research extended to explore the impact of aluminium alloy grades on the quality of joints in dissimilar FSW of aluminium

to AZ31B. The findings affirm that placing the softer material (AZ31B) at the AS consistently yields high-quality joints.

Each of these findings represents a significant stride forward in FSW research, providing new insights and methodologies that enhance the understanding and practical application of this welding technique. The outcomes of this thesis not only meet but, in many cases, exceed the initial objectives, positioning this research as a noteworthy contribution to the field of FSW.

8.5. Future work

The detailed experimental and numerical investigations conducted in this thesis have advanced the state of the art in the field of FSW of dissimilar materials. The research opens up several prospects for further work, including:

- Exploring the effects of FSW process parameters on dissimilar FSW of other metal combinations. This could include steel with Copper-Nickel, aluminium to steel, or dissimilar aluminium alloys. These investigations could be carried out in various applications, such as tube-tube sheet heat exchangers or the automobile industry.
- The potential application of Non-Destructive Testing (NDT) techniques, including Ultrasonic, X-Ray, or Computed Tomography (CT) scans, represents a promising direction for future research to assess the integrity of FSW joints. Although these methods were not incorporated into the current study due to budgetary limitations and the focus on extensive microstructural analysis, their capability to provide a further evaluation of weld quality is acknowledged. In subsequent work, it would be advantageous to integrate these NDT techniques

to offer a more in-depth understanding of the welds. Their use could significantly enrich the quality assessment, providing a multi-faceted evaluation that complements the microstructural analysis and further refines the characterisation of FSW joints.

- Future investigations into the FSW process should consider incorporating advanced characterisation techniques such as Electron Backscatter Diffraction (EBSD) to more accurately quantify the formation of IMCs. While the present study employed a mathematical transformation to highlight differences in peak intensities across various welding conditions, investigating the IMC distribution may benefit from the enhanced resolution and analytical capabilities that EBSD provides. Recognising the limitations of the current study, the application of EBSD would be an invaluable addition to future work, offering a more definitive validation of the Topas method and enabling precise quantification of IMCs.
- Extending the CEL model to predict features such as tool wear, void formation, and residual stresses. This could be done by combining the model with experimental results.
- Further utilising the Taguchi DoE method to optimise the distribution of IMCs, electrical resistance, thermal conductivity, and fatigue life in dissimilar aluminium to copper FSW joints.
- Investigating the FSW process window for achieving defect-free joints by consistently placing the softer material on the AS. This could be done by conducting more experiments and identifying the optimal process parameters for different combinations of materials. A key avenue for advancement would be the development of a non-dimensional process window, i.e., incorporating

the plate thickness to tool diameter (D/t) ratio. This ratio is a critical factor that influences the heat generation and material flow during welding and is thus expected to have a significant impact on the quality of the joint. By understanding the influence of the D/t ratio, it will be possible to apply the FSW process more flexibly and accurately across different material thicknesses and tool sizes, enhancing the robustness of the technique for dissimilar material welding.

- Studying the dynamic response of the FSW tool and workpiece during the joining process and establishing correlations between FSW conditions and dissimilar joint quality. This could be done using numerical simulations and/or experimental measurements.

Appendix 1

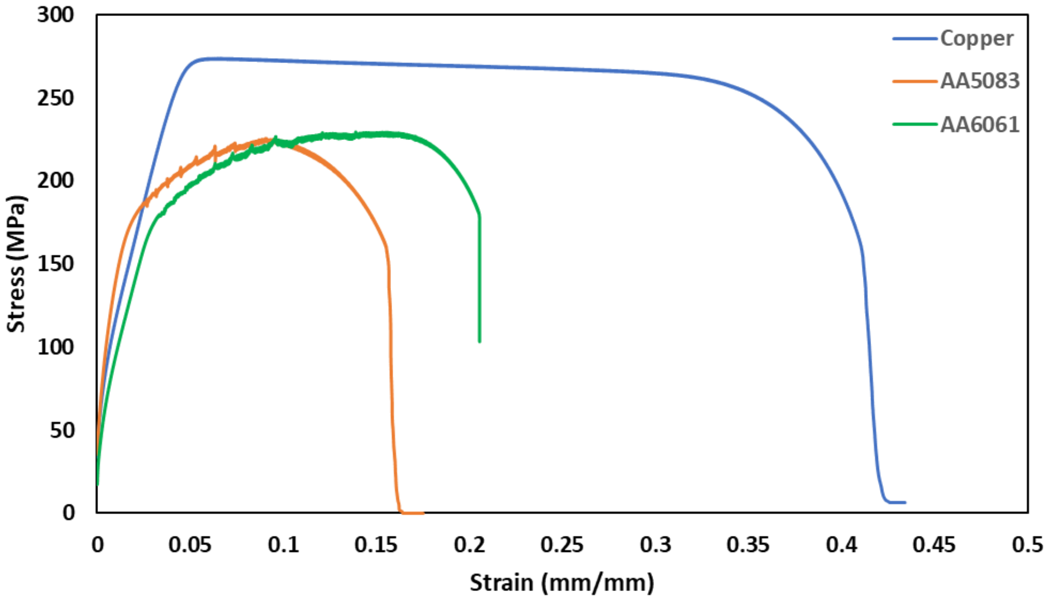

Typical Stress-Strain curves of sample base metals materials.

Samples of experimental BM test data

BM			**Tensile stress at Yield (Offset 0.2 %) [MPa]**	**Modulus (Automatic Young's) [GPa]**	**UTS (MPa)**
	Width (mm)	Thickness (mm)			
Copper	5.1	2.86	257.26	114.14	273.81
AA5083	5.08	2.88	166.07	73.42	166.07
AA1061	5.03	2.92	163.97	67.56	163.97

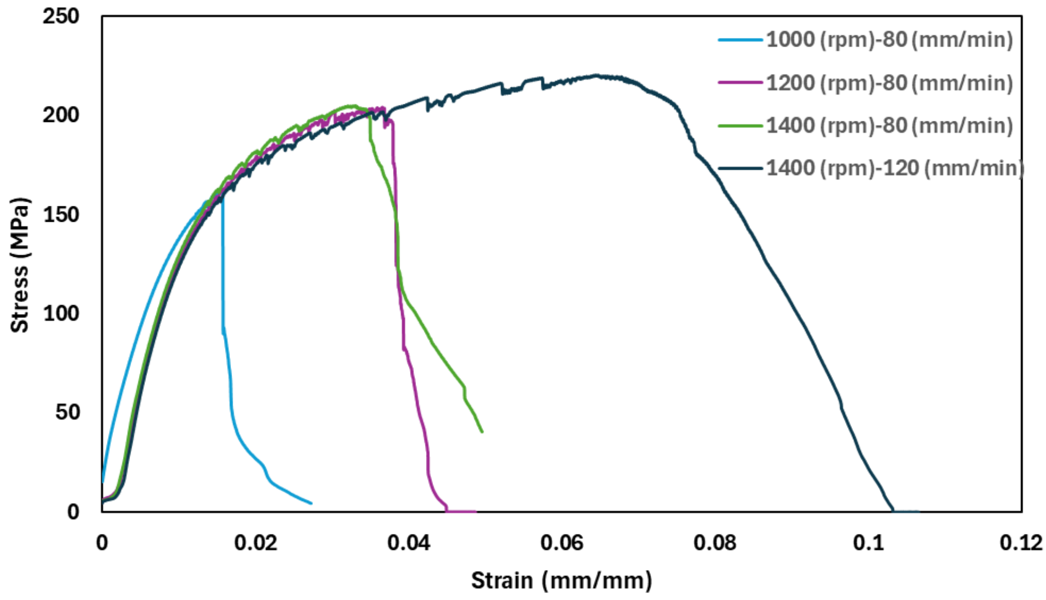

Typical Stress-Strain curves at different welding conditions of AA5083 to copper

Samples of experimental FSW test data with post-weld measurements of AA5083 to Copper

Input parameters		**Post-weld measurement**		**Tensile stress at Yield (Offset 0.2 %) [MPa]**	**Modulus (Automatic Young's) [GPa]**	**UTS (MPa)**
Nr (rpm)	ν (mm/min)	Width (mm)	Thickness (mm)			
1000	80	5.02	2.95	143.45	48.72	163.11
1200	80	5.07	2.65	147.87	99.14	204.23
1400	80	5.05	2.50	155.26	103.88	205.04
1400	120	5.04	2.73	159.55	29.61	220.49

Appendix 2

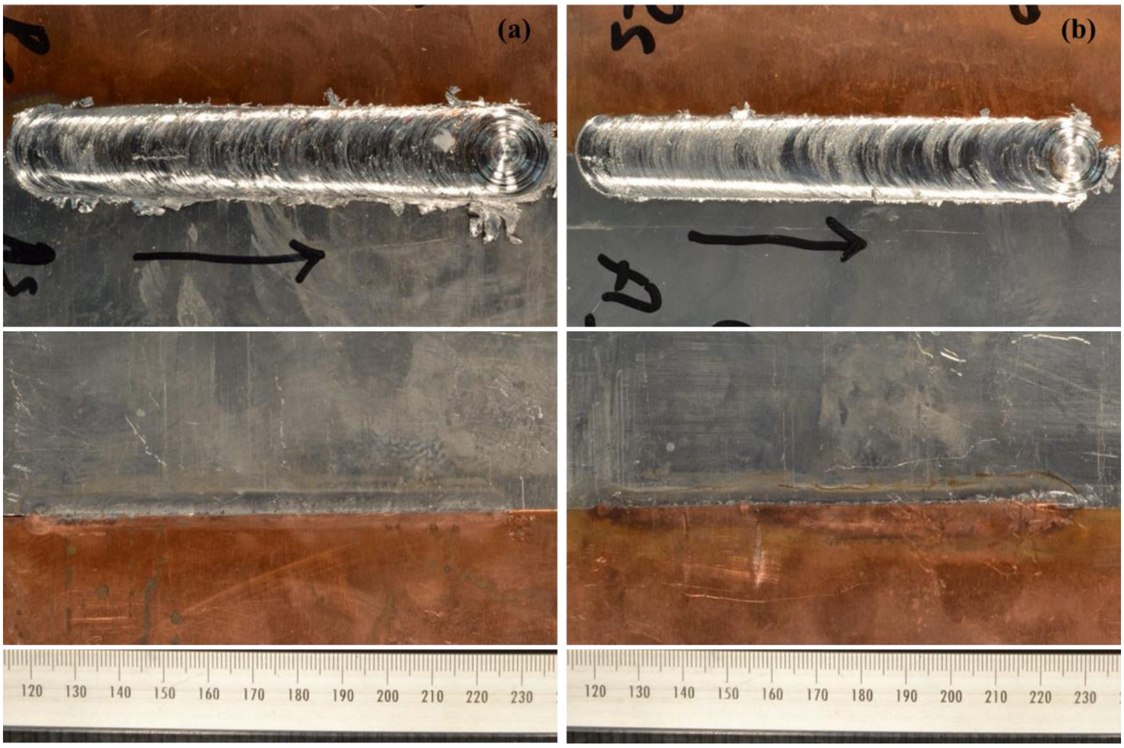

Macrographic comparison of FSW joints at different welding conditions: (a) Front and back views of the weld produced at 1000 rpm and 120 mm/min. (b) Front and back views of the weld produced at 1000 rpm and 100 mm/min.

Appendix 4 – Viva Notes

The viva for this PhD took place on Monday the 28th of August 2023 at the University of Strathclyde, Glasgow.

- **Date:** 28/08/2023
- **Time:** 0915 – 1530
- **Place:** Bell Room, Level 8, James Weir Building, University of Strathclyde
- **External Examiner:** Prof. Duncan Camilleri, University of Malta
- **Internal Examiner:** Dr Tugrul Comlekci, University of Strathclyde
- **Convener:** Dr Reda Felfel, University of Strathclyde
- **Outcome:** Pass – minor corrections

The author expresses sincere gratitude to Dr. Tugrul Comlekci and Prof. Duncan Camilleri for their invaluable discussions and constructive feedback, which have significantly enhanced the quality of this thesis. Special thanks are also extended to Dr. Reda Felfel for his pivotal role as the convener on the day of the viva, coordinating the proceedings with exceptional guidance and support.